BST
BioScience Trends

IRCA
BSSA

IACMHR

www.biosciencetrends.com

BioScience Trends is one of a series of peer-reviewed journals of the International Research and Cooperation Association for Bio & Socio-Sciences Advancement (IRCA-BSSA) Group and is published bimonthly by the International Advancement Center for Medicine & Health Research Co., Ltd. (IACMHR Co., Ltd.) and supported by the IRCA-BSSA and Shandong University China-Japan Cooperation Center for Drug Discovery & Screening (SDU-DDSC).

BioScience Trends devotes to publishing the latest and most exciting advances in scientific research. Articles cover fields of life science such as biochemistry, molecular biology, clinical research, public health, medical care system, and social science in order to encourage cooperation and exchange among scientists and clinical researchers.

BioScience Trends publishes Original Articles, Brief Reports, Reviews, Policy Forum articles, Case Reports, News, and Letters on all aspects of the field of life science. All contributions should seek to promote international collaboration.

Editorial Board

BioScience Trends

Editorial and Head Office

Pearl City Koishikawa 603, 2-4-5 Kasuga, Bunkyo-ku,
Tokyo 112-0003, Japan

Tel: +81-3-5840-8764, Fax: +81-3-5840-8765
E-mail: office@biosciencetrends.com
URL: www.biosciencetrends.com

CONTENTS *Volume 10, Number 5, 2016*

CONTENTS   (*Continued*)

Commentary

Guide for Authors

Copyright

Advance in studies on traditional Chinese medicines to treat infection with the hepatitis B virus and hepatitis C virus

Jufeng Xia[1], Yoshinori Inagaki[1], Peipei Song[2], Tatsuo Sawakami[1], Norihiro Kokudo[1], Kiyoshi Hasegawa[1], Yoshihiro Sakamoto[1], Wei Tang[1,*]

[1] *Hepato-Biliary-Pancreatic Surgery Division, Department of Surgery, Graduate School of Medicine, The University of Tokyo, Tokyo, Japan;*
[2] *Graduate School of Frontier Sciences, The University of Tokyo, Kashiwa-shi, Chiba, Japan.*

Summary   **Traditional Chinese medicine (TCM), as a type of complementary and alternative medicine (CAM), is a sophisticated and time-honored form of healthcare in China. Many TCMs are widely used to treat hepatitis B and hepatitis C in countries like China, Japan, and South Korea. Since conventional clinical preparations like interferon-α cause obvious dose-dependent adverse reactions and drug resistance, TCMs and related bioactive compounds have garnered increasing attention from physicians and medical researchers. Thus far, a number of TCMs and compounds have been used to inhibit the hepatitis B virus (HBV) or hepatitis C virus (HCV) *in vitro*, *in vivo*, and even in clinical trials. The current review summarizes TCMs and related compounds that have been used to inhibit HBV or HCV. Most of these medicines are derived from herbs. HepG2.2.15 cells have been used to study HBV *in vitro* and Huh7.5 cells have been similarly used to study HCV. Ducks have been used to study the anti-HBV effect of new medication *in vivo*, but there are few animal models for anti-HCV research at the present time. Thus far, a number of preclinical studies have been conducted but few clinical trials have been conducted. In addition, a few chemically modified compounds have displayed greater efficacy than natural products. However, advances in TCM research are hampered by mechanisms of action of many bioactive compounds that have yet to be identified. In short, TCMs and related active compounds are a CAM that could be used to treat HBV and HCV infections.**

Keywords: Traditional Chinese medicine, active compounds, HBV, HCV, clinical trials

1. Introduction

Hepatitis is a type of inflammation occurring in the liver. Acute hepatitis can be self-limiting and progress to chronic hepatitis or it can lead to acute liver failure in rare instances (*1*). Chronic hepatitis may progress to fibrosis, cirrhosis, or liver cancer. Hepatitis viruses are the most common cause of hepatitis around the world.

Address correspondence to:
Dr. Wei Tang, Hepato-Biliary-Pancreatic Surgery Division, Department of Surgery, Graduate School of Medicine, the University of Tokyo, Hongo 7-3-1, Bunkyo-ku, Tokyo 113-8655, Japan.
E-mail: tang-sur@h.u-tokyo.ac.jp

There are 5 major hepatitis viruses, types A, B, C, D, and E. These five types are of great significance because of their morbidity and mortality and their potential for causing outbreaks and spreading extensively (*2*). Types B and C cause chronic liver disease in hundreds of millions of people worldwide, especially in Africa and Central and East Asia, and these 2 types are the most common cause of cirrhosis and liver cancer (*3*). Although a few antivirals have been used to inhibit the hepatitis B virus, they also lead to obvious dose-dependent adverse reactions and drug resistance (*4*). Interferon-α (IFN-α) was the world's first medication to treat chronic hepatitis B virus (HBV) infection (*5*). However, IFN-α does not yield satisfactory therapeutic outcomes and it leads to several adverse reactions such as flu-like syndrome, fatigue, drowsiness, and low blood counts (*6*). Lamivudine, also called 3TC, was a major

Table 1. Extracts in and formulations of TCMs to treat HBV

Common name	Composition	Research stages	Tested in	Anti-HBV activity	Combination
Aqueous extract of *B. nivea*	*Boehmeria nivea* (Linn.) Gaudich	Cell experiment	HepG2.2.15 cells	Inhibits HBsAg, HBeAg, and HBV DNA	-
Ethanol extract of Hu-Zhang	*Polygonum cuspidatum*	Cell experiment	HepG2.2.15 cells	Inhibits HBsAg and HBeAg	-
Aqueous extract of *S. media*	*Stellaria media* (L.) Vill.	Cell experiment	HepG2.2.15 cells	Inhibits HBsAg and HBeAg	-
Ethyl acetate extract	*Ligularia atroviolacea*	Cell experiment	HepG2.2.15 cells	Inhibits HBsAg	-
Aqueous extract of *R. Astragali*	*Radix Astragali*	Cell experiment and animal experiment	HepG2.2.15 cells and duck	Inhibits HBeAg, HBV DNA, and DHBV DNA	-
Ethanol extract of *O. javanica*	*Oenanthe javanica*	Cell experiment and animal experiment	HepG2.2.15 cells and duck	Inhibits HBsAg, HBeAg, and DHBV DNA	-
Xiao-Chai-Hu-Tang	*Scutellariae radix et al.*	Cell experiment	HepA2 cells	Inhibits HBV DNA	-
Qizhu granules	*Astragalus et al.*	Clinical trial	Patients	Inhibits HBV DNA and HBeAg	Lamivudine
Fu-Zheng-Jie-Du-Tang	*Cuscuta chinensis* Lam. *et al.*	Clinical trial	Patients	Inhibits HBsAg and increases IFN-γ	-
Cinobufacini	*Bufo Bufo gargarizans* Cantor	Cell experiment and clinical trial	HepG2.2.15 cells and patients	Inhibit HBsAg, HBeAg, HBcrAg, and HBV DNA	IFN-2α 2b

medication to treat HBV infection, but its therapeutic outcomes are also accompanied by a number of adverse reactions and it leads to drug resistance with long-term administration (*7*). Recently, the most common therapy for chronic hepatitis C virus (HCV) has been IFN-α plus ribavirin. Both markedly inhibit the virus. However, both also cause various adverse reactions as well. Adverse reactions to IFN-α have previously been mentioned. Ribavirin is a major ribonucleic analog that is used to suppress HCV, but it often leads to a series of adverse reactions such as anemia, pain, fever, and trouble breathing (*8,9*). Besides these adverse events, most antivirals are costly. Therefore, novel drugs are urgently needed to treat HBV and HCV infection. Accordingly, alternative and complementary medicines (ACM) are being increasingly used.

Traditional Chinese medicine (TCM), as a type of ACM, is a sophisticated and time-honored form of healthcare in China (*10*). Many TCMs are widely used to treat hepatitis B in China and a number of other countries (*11*). In China, TCM is used as CAM treatment and accounts for 30-50% of all medications used, with a low cost and low level of toxicity (*12*). In the US, the 2002 National Health Interview Survey (NHIS) revealed that 19% of adults used some form of herbal medicine within the previous year (*13*). TCMs are complicated mixtures of active compounds. Although the active compounds in TCMs have not been fully isolated and identified, a few have been found to be potential antivirals (*14*). Bioactive compounds

extracted from natural products have characteristics similar to chemically synthesized medications and they can be easily assimilated and metabolized by the human body (*15*). Moreover, TCMs can be obtained from various organisms without the need for laborious or industrial chemosynthesis. Thus, TCMs could be a good candidate for antiviral development. Over the past few years, TCMs have garnered increasing attention from investigators searching for effective antiviral compounds.

2. Extracts in and formulations of TCMs to treat HBV

The effects of major extracts in and formulations of TCM to treat HBV infection, including *Boehmeria nivea* (Linn.) Gaudich, *Polygonum cuspidatum*, Stellaria media (L.) Vill., *Ligularia atroviolacea*, *Radix Astragali*, *Oenanthe javanica*, Xiao-Chai-Hu-Tang, Qizhu granules, Fu-Zheng-Jie-Du-Tang, and cinobufacini, are summarized here. Research has mainly focused on cell experiments, animal experiments, and clinical trials. Anti-HBV activities of these formulations in preclinical experiments and clinical trials are listed in Table 1.

Boehmeria nivea (Linn.) Gaudich is a type of perennial ratoon herbal plant, the root of which is used in TCM and possesses a number of pharmacological characteristics. A recent study found that the expression of hepatitis B virus surface antigen (HBsAg) and hepatitis B virus envelope antigen (HBeAg) decreased

in HepG2.2.15 cells treated with the *Boehmeria nivea* extract. Moreover, the concentration of HBV DNA detected in HepG2.2.15 cells in culture medium decreased significantly after treatment (*16*).

Polygonum cuspidatum, also known as Hu-Zhang in China, is a type of TCM herb. *P. cuspidatum* which has a wide range of pharmacological effects, has been used to treat hot flashes, heart disease, cancer, and liver disease. An ethanol extract and resveratrol isolated from *P. cuspidatum* were found to be able to inhibit HBV at 10 μg/mL *in vitro* (*17*).

Stellaria media (L.) Vill. is a TCM that has been used for hundreds years in China to mainly treat skin diseases, arthritis, and bronchitis. A study in HepG2.2.15 cells reported that 30 μg/mL of *S. media* effectively decreased the expression of HBsAg 27.92% and the expression of HBeAg 25.35% after administration for 6 days (*18*).

Ligularia, also known as leopard plant, is a group of herbaceous perennial plants that is mainly distributed in the inland areas. *Ligularia atroviolacea* has been traditionally used as an herbal medicine to treat hepatitis B, asthma, hemoptysis, and pulmonary tuberculosis. Shi *et al*. reported that an ethyl acetate extract of *L. atroviolacea* inhibited the secretion of HBsAg in HepG2.2.15 cells (*19*).

Radix Astragali is the dried root of *Astragalus membranaceus* (Fisch.) Bunge and *Astragalus mongholicus* Bunge (Fabaceae). Extracts of *R. Astragali* have been found to markedly decrease the concentration of HBeAg and HBV DNA in 116 clinical blood samples after 2 months of treatment and to inhibit levels of duck hepatitis B virus (DHBV) DNA in models of duck viral hepatitis B (*20*).

The TCM *Oenanthe javanica* has been used to treat inflammation for many years in China. Han's research group used the HepG2.2.15 cell line and a model of DHBV infection to evaluate the anti-HBV effects of an ethanol extract of *O. javanica*. Results indicated that *O. javanica* suppressed HBsAg and HBeAg *in vitro* and that it also inhibited DHBV replication in duck models (*21*).

Xiao-Chai-Hu-Tang (XCHT) has been widely used to treat various liver diseases in Asian countries. It consists of 7 different constituents, with *Scutellariae radix* accounting for most of its therapeutic effect. A study by Tseng *et al*. indicated that XCHT might inhibit HBV viral gene expression and DNA replication by regulating hepatic transcriptional machinery *in vitro* (*22*).

Qizhu granules (QZG) are a TCM consisting of several herbs such as *Astragalus*. In a clinical trial, 103 patients with chronic hepatitis B were divided into 2 groups. All patients received lamivudine. The treatment group also received QZG. After 1 year of treatment, the treatment group tested positive for HBV DNA at the same rate as the control group, but the level of secreted HBeAg in the treatment group differed significantly from that in the control group (*23*). Thus, the authors

contended that a combination of lamivudine and QZG would have therapeutic efficacy.

Several systematic reviews of TCM have reported that Fu-Zheng-Jie-Du-Tang (FZJDT) is able to inhibit HBV. FZJDT consists of a number of herbs, such as *Cuscuta chinensis* Lam., *Eucommia ulmoides* Oliver, and *Poria cocos* (Schw.) Wolf. He *et al*. designed a clinical trial in which three hundreds of patients infected with HBV were divided into a treatment group and control group. After 52 weeks of treatment, the treatment group had a more marked decrease in the mean concentration of serum HBsAg than the control group did. The treatment group had a significant increase in IFN-γ, suggesting that FZJDT was able to modulate host immune function (*24*).

Cinobufacini, also known as Hua-Chan-Su, is a water-soluble extract made from toad skin (*Bufo bufo gargarizans* Cantor). Cinobufacini has long been used in China as an anti-tumor agent, an analgesic, an anti-inflammatory, and an anti-microbial. In a cell experiment, cinobufacini was reported to inhibit HBV replication by suppressing serum levels of HBsAg, HBeAg, hepatitis B core-related antigen (HBcrAg), and HBV DNA (*25*). Results of a clinical trial by Yu *et al*. suggested that cinobufacini combined with IFN-2α 2b significantly inhibited HBV replication (*26*).

3. Bioactive compounds in TCMs to treat HBV

Although TCMs have facilitated drug development and clinical treatment, the full potential of those medicines has yet to tapped because of their complex composition and varying quality (*27*). Over the past few years, rapid and substantial advances have been made in development of TCMs with the increasing emergence of novel theories, methods, techniques, and instruments (*28*). Numerous bioactive compounds have been discovered in TCMs and their functions have been studied. A few bioactive compounds isolated from TCM have been reported to possess anti-HBV activity (*29,30*). The current review identified recent studies on bioactive compounds in TCMs with anti-HBV activity. These compounds have been found to be effective and warrant intensive study in the treatment of hepatitis B (Table 2). The results of the studies in question have been classified into 4 findings: *i*) inhibiting the secretion of HBsAg, HBeAg, and/or HBcrAg; *ii*) inhibiting HBV DNA; *iii*) inhibiting both *i*) and *ii*); and *iv*) inhibiting HBV proliferation *via* other pathways.

i) Inhibiting the secretion of HBsAg, HBeAg, and/or HBcrAg. A study by Dai *et al*., isolated 13 bioactive compounds from the TCM *Viola diffusa* Ging, and results suggested that 2β-hydroxy-3,4-seco-friedelolactone-27-oicacid,2β, 28β-dihydroxy-3,4-seco-friedelolactone-27-oicacid, and 2β,30β-dihydroxy-3,4-seco-friedelolactone-27-lactone suppressed HBsAg and HBeAg in HepG2.2.15 cells (*31*). The rhizome of *Cyperus rotundus*

Table 2. Bioactive compounds in TCMs to treat HBV

Compounds	Herbs	Tested in	Anti-HBV activity	IC$_{50}$	Mechanism
2β,30β-dihydroxy-3,4-seco-friedelolactone-27-lactone	*Viola diffusa Ging*	HepG2.2.15	Inhibits HBsAg and HBeAg	33.7 μM/26.2 μM	Unclear
Sesquiterpenoid	*Cyperus rotundus*	HepG2.2.15	Inhibits HBsAg and HBeAg	46.6 μM/162.5 μM	Unclear
Swermacrolactone	*Swertia*	HepG2.2.15	Inhibits HBsAg and HBeAg	0.02 μM/0.02 μM	Unclear
Piperine	*Piper longum Linn.*	HepG2.2.15	Inhibits HBsAg and HBeAg	0.13 mM/0.16 mM	Unclear
Gentiocrucine	*Swertia macrosperma*	HepG2.2.15	Inhibits HBsAg and HBeAg	3.14 mM/3.35 mM	Unclear
1,2,4,6-tetra-O-galloyl-β-D-glucose	*Phyllanthus emblica L.*	HepG2.2.15	Inhibits HBsAg and HBeAg	6.25 μg/mL/3.13 μg/mL	Unclear
Bufalin and cinobufagin	*Bufo bufo gargarizans Cantor*	HepG2.2.15	Inhibits HBsAg and HBeAg	-	Unclear
Aserythrocentaurin	*Swertia delavayi*	HepG2.2.15	Inhibits HBV DNA	0.05 mM	Unclear
Dehydroandrographolide	*Andrographis paniculata*	HepG2.2.15	Inhibits HBV DNA	22.6 μM	Unclear
Menisdaurin	*Saniculiphyllum guangxiense*	HepG2.2.15	Inhibits HBV DNA	0.32 mM	Unclear
Chrysophanol 8-O-β-D-glucoside	*Rheum palmatum L.*	HepG2.2.15	Inhibits HBsAg, HBeAg, and HBV DNA	36.98 ± 2.28 μg/mL	Suppress DNA polymerase
Wogonin	*Scutellaria radix*	HepG2.2.15 and duck model	Inhibits HBsAg, HBeAg, HBV DNA, and DHBV DNA	4 μg/mL	Suppress DNA polymerase
Vanitaracin A	Fungus	HepG2.2.15	Inhibits entry of HBV	0.61 ± 0.23 μM	Block NTCP
Saponin	*Hydrocotyle sibthorpioides*	HepG2.2.15 and duck model	Inhibits HBsAg, HBeAg, HBV DNA, and DHBV DNA	56.9 μM	Suppress core,s1,s2, and X gene
Cepharanthine hydrochloride	*Stephania cepharantha Hayata.*	HepG2.2.15	Inhibits HBV proliferation	31.89 ± 5.77 μM	Inhibit Hsc70

is a well-known TCM with a number of formulations that is used to treat hepatitis. Thirty-seven sesquiterpenoids were isolated from the fraction of *C. rotundus* using liquid chromatography-mass spectrometry (LC-MS). Six of those sesquiterpenoids may contribute to the anti-HBV activity of *C. rotundus* (*32*). Plants of the genus Swertia (Gentianaceae), annual or perennial herbs, are thought to have hepatoprotective activity but whether they contained anti-HBV compounds was unclear. A study by Wang *et al.* found 3 new secoiridoids, swermacrolactones A-C, that were able to inhibit the expression of HBsAg and HBeAg in HepG2.2.15 cells with a 50% inhibitory concentration (IC$_{50}$) of 0.02 and 0.02 mM, respectively (*33*). *Piper longum* Linn., a slender aromatic climber that is widely distributed in the world's tropical and subtropical areas, is used as a TCM. Recently, 11 active compounds were extracted from P. longum Linn. and 4 of those compounds were found to significantly inhibit the secretion of HBsAg and HBeAg in HepG2.2.15 cells (34). *Swertia macrosperma* is a congeneric species of *Swertia mileensis* (Gentianaceae) that has been listed in the Chinese Pharmacopoeia (1977-2010 editions) because of

its therapeutic effect on hepatitis B. In a recent study, 5 bioactive compounds, gentiocrucines A-E, were isolated from *S. macrosperma* and *S. angustifolia*, and those compounds were found to inhibit both the secretion of HBsAg and HBeAg in HepG2.2.15 cells, with an IC$_{50}$ of 3.14 and 3.35 mM (*35*). A polyphenolic compound, 1,2,4,6-tetra-O-galloyl-β-D-glucose, was isolated from *Phyllanthus emblica* L. (Euphorbiaceae), and treatment with that TCM decreased levels of both HBsAg and HBeAg in the supernatant of cultured HepG2.2.15 cells (*36*). Unlike the TCMs derived from herbs as have been mentioned thus far, bufalin and cinobufagin are active compounds that are derived from an animal source, the skin of *Bufo bufo* gargarizans Cantor (Bufonidae) (37). A chemiluminescent enzyme immunoassay revealed that bufalin and cinobufagin effectively decreased the concentration of HBsAg, HBeAg, and HBcrAg in HepG2.2.15 cells in culture medium (*27*).

ii) Inhibiting HBV DNA. Fifteen active compounds were isolated from *Swertia delavayi* using silica gel, Sephadex LH-20, and Rp-18 column chromatography (*38*). Six of those compounds, aserythrocentaurin,

Table 3. Extracts in and formulations of TCMs to treat HCV

Common name	Composition	Research stages	Tested in	Anti-HCV activity	Combination
Extract of *A. annua*	*Artemisia annua*	Animal experiment	BALB/c mice	Increases antibody levels	HCV/NS3 DNA vaccine
EtOAc extract of *G. Chinese*	*Galla chinensis*	Cell experiment	_	Inhibits HCV proliferation	_
Actinobacteria extract	*Termite*	Cell experiment	MDBK cells	Inhibits BVDV proliferation	_
Xiao-Chai-Hu-Tang	*Radix Bupleuri et al.*	Cell experiment and clinical trial	Phase II trial	Decreases HCV titer	_

erythrocentaurindimethylacetal, swertiakoside A, 2'-O-acetylswertiamarin, 1,5,8-trihydroxy-3-methoxyxanthone, and isovitexinm, markedly inhibited HBV DNA replication, with an IC_{50} of 0.05-1.46 mM. *Andrographis paniculata*, a well-known TCM described as Chuan-Xin-Lian in all editions of the Chinese Pharmacopoeia, is widely used to suppress inflammation (*39*). Two compounds, dehydroandrographolide and andrographolide, isolated from *A. paniculata* were reported to inhibit HBV DNA replication with an IC_{50} of 22.6 and 54.1 μM. *Saniculiphyllum guangxiense*, also known as Bian-Dou-Ye-Cao, was little known since it was rarely collected or observed (*40*). Recently, 8 active compounds were isolated from *S. guangxiense*, and one, menisdaurin, significantly inhibited HBV DNA replication with an IC_{50} of 0.32 mM.

iii) Inhibiting the secretion of HBsAg, HBeAg, and HBV DNA. The herb *Rheum palmatum* L. is a TCM that has been reported to be able to inhibit herpes simplex virus (HSV) and coxsackie virus (*41*). Chrysophanol 8-O-β-D-glucoside, an active compound isolated from *R. palmatum* L., significantly inhibited HBV DNA replication and expression of viral antigens, with an IC_{50} of 36.98 ± 2.28 μg/mL. An endogenous HBV DNA polymerase activity assay suggested that chrysophanol 8-O-β-D-glucoside might inhibit HBV DNA by suppressing DNA polymerase activity. Similarly, an active constituent, wogonin, from *Scutellaria radix* also was found to inhibit HBV DNA by inactivating DNA polymerase (*42*). In HepG2.2.15 cells, wogonin effectively inhibited HBV antigen expression and DNA replication with an IC_{50} of 4 μg/mL after 9 days of treatment. Wogonin decreased DHBV DNA, with an IC_{50} of 0.57 μg/mL, in ducks infected with DHBV.

iv) Inhibiting HBV proliferation *via* other pathways. A new tricyclic polyketide, vanitaracin A, was part of a secondary metabolite pool extracted from a fungus, and vanitaracin A specifically inhibited HBV (*43*). Vanitaracin A did not directly block the process of HBV replication. Instead, it interacted with sodium taurocholate cotransporting polypeptide (NTCP), an HBV entry receptor, and it disrupted its bile acid transport activity (*44*). Vanitaracin A was similarly found to inhibit proliferation of the hepatitis D virus (HDV). *Hydrocotyle sibthorpioides* (Apiaceae) is a

TCM used to treat inflammation and hepatitis B in China. An active compound, saponin, was isolated from *H. sibthorpioides*, and a study suggested that saponin would be able to decrease antigens in a culture medium containing HepG2.2.15 cells and that it would be able to inhibit DHBV DNA replication in ducks infected with HBV by suppressing the activity of core, s1, s2, and X gene promoters in the HBV genome (*45*). Lamivudine-resistant strains of HBV have emerged with the widespread clinical use of lamivudine. Recently, two research teams respectively reported that cepharanthine hydrochloride and oxymatrine inhibited HBV proliferation by inhibiting heat stress cognate 70 (Hsc70), which is a host protein used for HBV replication (*46,47*).

4. Extracts in and formulations of TCMs to treat HCV

The ways in which major extracts in and formulations of TCMs, including *Artemisia annua*, *Zingiberaceae*, *Galla Chinese*, and Xiao-Chai-Hu-Tang, inhibit HCV infection are summarized here. Research has mainly focused on cell experiments and clinical trials. Anti-HCV activities of these extracts in and formulations in preclinical experiments and clinical trials are listed in Table 3.

Artemisia annua, the dried aerial section of *A. annua* L. of the *Compositae* family, is a TCM that is used clinically to treat a fever or malaria and to enhancing immunity. Results of a study by Bao *et al.* suggested that an extract of *A. annua*, when used as an adjuvant of HCV/Nonstructural protein 3 (NS3) DNA vaccine, increased antibody levels *in vivo* and promoted IFN-γ secretion by increasing a Th1-type cellular immune response (*48*). *Galla chinensis*, also called Wu-Bei-Zi, is a TCM that is commonly used to treat dysentery, bleeding, coughing, sweating, and rectal prolapse. An ethyl acetate (EtOAc) extract of *G. Chinese* was found to inhibit HCV proliferation by inhibiting NS3 protease, which is a 70-kDa cleavage product of the HCV polyprotein that acts as a serine protease (*49*). In addition to drugs derived from herbs, drugs derived from animals also can inhibit HCV activity. Extracts from termite-associated bacteria were reported to inhibit bovine viral diarrhea virus (BVDV), which is used as a surrogate model for *in vitro* antiviral studies of HCV (*50*).

Table 4. Bioactive compounds in TCMs to treat HCV

Compounds	Herbs	Tested in	Anti-HBV activity	IC$_{50}$	Mechanism
Grosheimol and cynaropicrin	*Cynara cardunculus* L.	Huh7/Scr cells, Huh7.5.1 Cl.2 cells	Inhibits HCV entry	1.0 µM and 1.3 µM	Unclear
Delphinidin	*Tea*	Huh-7, HEK 293T	Inhibits HCV entry	3.7 ± 0.8 µM	Impairing HCV attachment to the cell surface
Saikosaponin b2	*Bupleurum kaoi root*	HuH7.5, S29 cells	Inhibits HCV entry	16.13 ± 2.41 µM	Neutralizing particles and preventing attachment
Oleanolic acid derivative	*Glycyrrhiza species*	293T cells	Inhibits HCV entry	1.4 µM	Inhibits HCV attachment to host cell CD81 receptor
Ursolic acid	*Ligustrum lucidum*	HepG2 cells	Inhibits HCV proliferation	3.1 µg/mL	Suppressing NS5B polymerase
Aqueous extract	*Fructus Ligustri Lucidi*	HeLa cells	Inhibits HCV proliferation	10 µg/mL	Suppressing NS5B polymerase
Vitisin B	Grapevine root	Huh7.5 cells and rats	Inhibits HCV proliferation	3 nM	Suppressing NS3 protease
3-Deacetyl-3-cinnamoyl-azadirachtin	*Azadirachta indica*	-	Inhibits HCV proliferation	-	Suppressing NS3 protease
Honokiol	*Magnolia*	Huh7.5.1 cells	Inhibits HCV proliferation	1.2 µM	Suppressing NS3, NS5A, NS5B
Pheophorbide A and pyropheophorbide	*Morinda citrifolia*	Huh7.5 cells	Inhibits HCV proliferation	0.2 µg/mL and	Suppressing RNA replication
Silybin B	*Silybum marianum*	Huh7.5.1 cells	Inhibits HCV proliferation	0.3 µg/mL	Inhibiting HCV core proteins and drug-metabolizing enzymes

Xiao-Chai-Hu-Tang (XCHT) is a formula consisting of 7 herbs that has been used to treat liver diseases in East Asia. In a phase II trial, XCHT was found to decrease levels of HCV (*51*). However, the investigators cited several limitations of their trial, such as sampling bias, inter-observer variability, slow accrual, and a high drop-out rate. Trial results also indicated that XCHT caused interstitial pneumonitis.

5. Bioactive compounds in TCMs to treat HCV

A number of bioactive compounds contained in TCMs have been found to act as HCV inhibitors. The current review identified recent studies on bioactive compounds in TCMs with anti-HCV activity. These compounds have been found to be effective and warrant intensive study in the treatment of hepatitis C (Table 4). The results of the studies in question have been classified into 3 findings: *i*) inhibiting HCV entry; *ii*) inhibiting NS protein; and *iii*) other activities.

i) Inhibiting HCV entry. Entry is the first step

for HCV to infect host cells. HCV entry into host hepatocytes is a complicated and multistep process that involves the HCV envelope glycoproteins E1 and E2 and several host factors like CD81 (*52*). Thus far, several active compounds from TCM have been found to be able to interrupt the interaction between the HCV envelope proteins and receptors of host cells. *Cynara cardunculus* L. was used by Egyptians to treat diverse symptoms of hepatitis, such as jaundice and ascites. Two compounds isolated from *C. cardunculus* L., grosheimol and cynaropicrin, were studied for their anti-HCV activity (*53*). Results indicated that these compounds inhibited HCV by suppressing HCV entry into host cells and that they blocked cell-free infection and cell-cell transmission. Calland *et al.* found that the flavonoids delphinidin and epigallocatechin-3-gallate (EGCG) (EGCG is found in green tea) inhibited HCV entry by changing the viral particle structure that facilitated HCV attachment to the host cell surface (*54*). Similarly, a study by Lin *et al.* identified an active compound called saikosaponin b2, which was isolated from the TCM

Bupleurum kaoi root, as an inhibitor of HCV entry (*55*). Saikosaponin b2 played a role in neutralizing viral particles, inhibiting viral attachment, and suppressing viral fusion. In addition to these natural products, many derivatives of natural active compounds are found in TCMs. A study by Yu *et al.* found that oleanolic acid slightly inhibited HCV entry with an IC_{50} of 10 μM. Hydroxylation at the C-16 position markedly increased the anti-HCV effect of oleanolic acid with an IC_{50} of 1.4 μM. Chemical modified oleanolic acid inhibited HCV entry by interrupting the interaction between HCV envelope protein E2 and the receptor CD81 in host cells (*56*).

ii) Inhibiting NS protein. HCV contains a series of nonstructural (NS) proteins such as NS2, NS3, NS4A, NS4B, NS5A, and NS5B (*57*). These proteins act as proteases, replicating viral RNA, or cofactors with other NS proteins. A study by Wozniak *et al.* found that the natural compound ursolic acid, isolated from *Ligustrum lucidum*, inhibited HCV proliferation by suppressing NS5B viral RNA polymerase (*58*). Similarly, another study found that an aqueous extract from Fructus *Ligustri Lucidi blocked* HCV entry by inhibiting NS5B viral RNA polymerase (*59*). Except for NS5B polymerase, NS3 viral proteases have seldom been studied. Lee *et al.* reported that vitisin B, a resveratrol tetramer isolated from grapevine root, was able to inhibit HCV replication by binding to and suppressing NS3 *in vitro* and *in vivo*. A combination of vitisin B and sofosbuvir (an inhibitor of NS5B polymerase) had synergistic anti-HCV activity (*60*). Ashfaq *et al.* found that 3-Deacetyl-3-cinnamoyl-azadirachtin, isolated from *Azadirachta indica*, inhibited HCV by binding with NS3 protease and neutralizing it (*61*). A study by Lan *et al.* revealed that honoliol, a compound derived from *Magnolia*, was able to block HCV infection by inhibiting NS3, NS5A, and NS5B (*62*). According to that study, a combination of honoliol and interferon-α displayed synergistic anti-HCV activity.

iii) Other activities. In addition to inhibiting HCV entry, compounds also inhibit viral infection after entry. Ratnoglik *et al.* found that pheophorbide A and pyropheophorbide, two active compounds isolated from *Morinda citrifolia*, inhibited HCV infection by interrupting viral RNA replication and viral protein production (*63*). Silybin B, a silymarin isolated from *Silybum marianum*, inhibited HCV infection in 2 ways (*64*). Silybin B was reported to inhibit HCV by decreasing HCV core proteins and it was also reported to increase antiviral efficacy by inhibiting major drug-metabolizing enzymes (CYP2C9, CYP3A4/5, and UDP-glucuronsyltransferases).

6. Adverse reactions

Although TCMs and related compounds have been reported to be able to improve the efficacy of monotherapy or combination therapy for HBV and HCV, the adverse reactions caused by TCMs have not been discussed in-depth. A few studies have reported that some TCMs attenuate the adverse effects of chemotherapy or radiotherapy and produce fewer or no adverse reactions, but other studies have suggested that TCMs may cause obvious adverse reactions (*65-67*). Kansui, the root of *Euphorbia kansui T.N. Liou ex T.P. Wang*, has been used as a remedy for edema, ascites, and asthma. According to one study, however, kansui affected cardiac and hepatic function and it affected the histomorphology of the heart, liver, and kidneys in rats (*68*). The authors of a review concluded that the major adverse reactions to TCMs were gastrointestinal symptoms including abdominal bloating or pain, epigastric discomfort, and stomach disorder, followed by diarrhea, headaches, nausea, breast distension or pain, abnormal vaginal bleeding, and dizziness (*69*). In a randomized controlled trial, Li *et al.* reported that Tongxinluo Capsules, a TCM used to treat coronary disease and angina pectoris, caused an adverse reaction in the form of stomachaches in the treatment group (*70*). Berberine, an active compound extracted from the herb *Berberis*, may induce the onset of competitive junctional rhythm, causing a loss of atrioventricular synchronization, and reduce chronotropic competence with the onset of symptoms upon exertion (*71*). In fact, the present evidence of adverse reactions and toxicity is insufficient. There are a few obstacles to evaluating adverse reactions: *i*) experimental data is limited to pharmacokinetics and inaccurate clinical research, *ii*) only a few studies have documented target organ toxicity, and *iii*) the evidence is not sufficient to elucidate the biochemical mechanisms responsible for the biological activities of TCMs. Thus, further studies are needed to study the pharmacokinetics and features of TCMs and their active compounds, and comprehensive and accurate data should be collected through clinical trials. Furthermore, mechanisms causing adverse reactions to TCMs need to be explored in depth.

7. Conclusion

Hepatitis is a severe liver disease leading to chronic hepatitis, acute liver failure, or hepatocellular carcinoma. Two pathogens that predominantly cause hepatitis are HBV and HCV. Conventional medications cause adverse effects and are costly, so TCMs and related bioactive compounds are garnering attention as CAM. This review has summarized the TCMs and active compounds used to treat HBV and HCV. Several points have become evident from this review: *i*) HepG2.2.15 is a generally accepted cell line for anti-HBV research *in vitro*; *ii*) ducks are used as animal model for DHBV infection to study anti-HBV activity *in vivo*; *iii*) Hun7.5 is a cell line that is often used in anti-HCV research *in vitro*; *iv*) there are few animal models for anti-HCV research *in vivo*; *v*) in addition to

TCMs and compounds derived from herbs, compounds derived from animals are also used to inhibit HCV infection and have yielded desired results; *vi*) a few therapies combining compounds and medications have yielded satisfactory results; *vii*) thus far, few clinical trials have been conducted on active compounds; *viii*) limited basic studies thus far have yet to elucidate the mechanisms of antiviral action of TCMs; *ix*) several chemically modified bioactive compounds have displayed more effective antivirus activity than natural products. Several steps need to be taken in future work on treatments for HBV and HCV infections. More bioactive compounds from TCMs need to be explored, new animal models need to be created for anti-HCV research, novel chemically modified bioactive compounds need to be developed, clinical trials need to be conducted, and the molecular mechanisms of action of TCMs need to be elucidated.

Acknowledgements

References

1. Yoshio S, Kanto T. Host-virus interactions in hepatitis B and hepatitis C infection. J Gastroenterol. 2016; 51:409-420.
2. El-Serag HB. Epidemiology of viral hepatitis and hepatocellular carcinoma. Gastroenterology. 2012; 142:1264-1273.
3. Nishida N, Kudo M. Clinical features of vascular disorders associated with chronic hepatitis virus infection. Dig Dis. 2014; 32:786-790.
4. Kovari H, Sabin CA, Ledergerber B, Ryom L, Worm SW, Smith C, Phillips A, Reiss P, Fontas E, Petoumenos K, De Wit S, Morlat P, Lundgren JD, Weber R. Antiretroviral drug-related liver mortality among HIV-positive persons in the absence of hepatitis B or C virus coinfection: The data collection on adverse events of anti-HIV drugs study. Clin Infect Dis. 2013; 56:870-879.
5. Lu J, Zhang S, Liu Y, Du X, Ren S, Zhang H, Ma L, Chen Y, Chen X, Shen C. Effect of Peg-interferon alpha-2a combined with Adefovir in HBV postpartum women with normal levels of ALT and high levels of HBV DNA. Liver Int. 2015; 35:1692-1699.
6. Palacios-Alvarez I, Roman-Curto C, Mir-Bonafe JM, Canueto J, Usero-Barcena T, Fernandez-Lopez E. Autoimmune response as a side effect of treatment with interferon-alpha in melanoma: Does this have prognostic implications? Int J Dermatol. 2015; 54:e91-93.
7. Gualdesi MS, Brinon MC, Quevedo MA. Intestinal permeability of lamivudine (3TC) and two novel 3TC prodrugs. Experimental and theoretical analyses. Eur J Pharm Sci. 2012; 47:965-978.
8. Zhang Y, Lu H, Ji H, Li Y. Inflammatory pseudotumor of the liver: A case report and literature review. Intractable Rare Dis Res. 2015; 4:155-158.
9. Ali AH, Carey EJ, Lindor KD. Current research on the treatment of primary sclerosing cholangitis. Intractable Rare Dis Res. 2015; 4:1-6.
10. Takayama S, Iwasaki K. Systematic review of traditional Chinese medicine for geriatrics. Geriatr Gerontol Int. 2016; doi: 10.1111/ggi.12803.
11. Tsai DS, Huang MH, Chang YS, Li TC, Peng WH. The use of Chinese herbal medicines associated with reduced mortality in chronic hepatitis B patients receiving lamivudine treatment. J Ethnopharmacol. 2015; 174:161-167.
12. Song PP, Gao JJ, Kokudo N, Tang W. Standardization of traditional Chinese medicine and evaluation of evidence from its clinical practice. Drug Discov Ther. 2011; 5:261-265.
13. Kennedy J. Herb and supplement use in the US adult population. Clin Ther. 2005; 27:1847-1858.
14. Xia JF, Gao JJ, Inagaki Y, Kokudo N, Nakata M, Tang W. Flavonoids as potential anti-hepatocellular carcinoma agents: Recent approaches using HepG2 cell line. Drug Discov Ther. 2013; 7:1-8.
15. Larson EC, Hathaway LB, Lamb JG, Pond CD, Rai PP, Matainaho TK, Piskaut P, Barrows LR, Franklin MR. Interactions of Papua New Guinea medicinal plant extracts with antiretroviral therapy. J Ethnopharmacol. 2014; 155:1433-1440.
16. Wei J, Lin L, Su X, Qin S, Xu Q, Tang Z, Deng Y, Zhou Y, He S. Anti-hepatitis B virus activity of leaf extracts in human HepG2.2.15 cells. Biomed Rep. 2014; 2:147-151.
17. Peng W, Qin R, Li X, Zhou H. Botany, phytochemistry, pharmacology, and potential application of *Polygonum cuspidatum Sieb.et* Zucc.: A review. J Ethnopharmacol. 2013; 148:729-745.
18. Ma L, Song J, Shi Y, Wang C, Chen B, Xie D, Jia X. Anti-hepatitis B virus activity of chickweed [*Stellaria media* (L.) Vill.] extracts in HepG2.2.15 cells. Molecules. 2012; 17:8633-8646.
19. Shi SY, Zhou HH, Huang KL, Li HB, Liu SQ, Zhao Y. Application of high-speed counter-current chromatography for the isolation of antiviral eremophilenolides from *Ligularia atroviolacea*. Biomed Chromatogr. 2008; 22:985-991.
20. Tang LL, Sheng JF, Xu CH, Liu KZ. Clinical and experimental effectiveness of Astragali compound in the treatment of chronic viral hepatitis B. J Int Med Res. 2009; 37:662-667.
21. Han YQ, Huang ZM, Yang XB, Liu HZ, Wu GX. *In vivo* and *in vitro* anti-hepatitis B virus activity of total phenolics from *Oenanthe javanica*. J Ethnopharmacol. 2008; 118:148-153.
22. Tseng YP, Wu YC, Leu YL, Yeh SF, Chou CK. *Scutellariae radix* suppresses hepatitis B virus production in human hepatoma cells. Front Biosci (Elite Ed). 2010; 2:1538-1547.
23. Zhu YF, Gu XB, Guo XY, Yan ZH, Pu YC, Tu KW, Hua Z, Pei H. Effect of compound qizhu granule on cellular immunity of chronic hepatitis B patients. Zhongguo Zhong Xi Yi Jie He Za Zhi. 2014; 34:1178-1181. (in Chinese)
24. He J, Zhou D, Tong G, Xing Y, Chen Y, Zhang X, Zhan B, Gao H, Zhou X, Xiong Y, Liu X, Peng L, Qiu M, Zheng Y. Efficacy and safety of a chinese herbal formula (invigorating kidney and strengthening spleen) in chronic hepatitis B virus carrier: Results from a multicenter, randomized, double-blind, and placebo-controlled trial. Evid Based Complement Alternat Med. 2013;

2013:961926.

25. Cui X, Inagaki Y, Xu H, Wang D, Qi F, Kokudo N, Fang D, Tang W. Anti-hepatitis B virus activities of cinobufacini and its active components bufalin and cinobufagin in HepG2.2.15 cells. Biol Pharm Bull. 2010; 33:1728-1732.

26. Yu Q, Xi Q. Observation on the effect of cinobufacini and IFN-α 2b treating chronic hepatitis B. Capital Medicine. 2011; 16:48-49.

27. Zhao XL, Han JX. The connotation of the Quantum Traditional Chinese Medicine and the exploration of its experimental technology system for diagnosis. Drug Discov Ther. 2013; 7:225-232.

28. Zhou G, He YP. Problems in quality standard research of new traditional Chinese medicine compound. Zhongguo Zhong Yao Za Zhi. 2014; 39:3389-3391. (in Chinese)

29. Li L, Bonneton F, Chen XY, Laudet V. Botanical compounds and their regulation of nuclear receptor action: The case of traditional Chinese medicine. Mol Cell Endocrinol. 2015; 401:221-237.

30. Huang H, Peng X, Zhong C. Idiopathic pulmonary fibrosis: The current status of its epidemiology, diagnosis, and treatment in China. Intractable Rare Dis Res. 2013; 2:88-93.

31. Dai JJ, Tao HM, Min QX, Zhu QH. Anti-hepatitis B virus activities of friedelolactones from *Viola diffusa* Ging. Phytomedicine. 2015; 22:724-729.

32. Xu HB, Ma YB, Huang XY, Geng CA, Wang H, Zhao Y, Yang TH, Chen XL, Yang CY, Zhang XM, Chen JJ. Bioactivity-guided isolation of anti-hepatitis B virus active sesquiterpenoids from the traditional Chinese medicine: Rhizomes of *Cyperus rotundus*. J Ethnopharmacol. 2015; 171:131-140.

33. Wang HL, Geng CA, Ma YB, Zhang XM, Chen JJ. Three new secoiridoids, swermacrolactones A-C and anti-hepatitis B virus activity from *Swertia macrosperma*. Fitoterapia. 2013; 89:183-187.

34. Jiang ZY, Liu WF, Zhang XM, Luo J, Ma YB, Chen JJ. Anti-HBV active constituents from *Piper longum*. Bioorg Med Chem Lett. 2013; 23:2123-2127.

35. Wang HL, He K, Geng CA, Zhang XM, Ma YB, Luo J, Chen JJ. Gentiocrucines A-E, five unusual lactonic enamino Ketones from *Swertia macrosperma* and *Swertia angustifolia*. Planta Medica. 2012; 78:1867-1872.

36. Xiang YF, Ju HQ, Li S, Zhang YJ, Yang CR, Wang YF. Effects of 1,2,4,6-tetra-O-galloyl-beta-D-glucose from *P. emblica* on HBsAg and HBeAg secretion in HepG2.2.15 cell culture. Virol Sin. 2010; 25:375-380.

37. Nakata M, Kawaguchi S, Oikawa A, Inamura A, Nomoto S, Miyai H, Nonaka T, Ichimi S, Fujita-Yamaguchi Y, Luo C, Gao B, Tang W. An aqueous extract from toad skin prevents gelatinase activities derived from fetal serum albumin and serum-free culture medium of human breast carcinoma MDA-MB-231 cells. Drug Discov Ther. 2015; 9:417-421.

38. Cao TW, Geng CA, Ma YB, He K, Zhou NJ, Zhou J, Zhang XM, Chen JJ. Chemical constituents of *Swertia delavayi* and their anti-hepatitis B virus activity. Zhongguo Zhong Yao Za Zhi. 2015; 40:897-902. (in Chinese)

39. Chen H, Ma YB, Huang XY, Geng CA, Zhao Y, Wang LJ, Guo RH, Liang WJ, Zhang XM, Chen JJ. Synthesis, structure-activity relationships and biological evaluation of dehydroandrographolide and andrographolide derivatives as novel anti-hepatitis B virus agents. Bioorg Med Chem Lett. 2014; 24:2353-2359.

40. Geng CA, Huang XY, Lei LG, Zhang XM, Chen JJ. Chemical constituents of *Saniculiphyllum guangxiense*. Chem Biodivers. 2012; 9:1508-1516.

41. Li Z, Li LJ, Sun Y, Li J. Identification of natural compounds with anti-hepatitis B virus activity from *Rheum palmatum* L. ethanol extract. Chemotherapy. 2007; 53:320-326.

42. Guo Q, Zhao L, You Q, Yang Y, Gu H, Song G, Lu N, Xin J. Anti-hepatitis B virus activity of wogonin *in vitro* and *in vivo*. Antiviral Res. 2007; 74:16-24.

43. Matsunaga H, Kamisuki S, Kaneko M, Yamaguchi Y, Takeuchi T, Watashi K, Sugawara F. Isolation and structure of vanitaracin A, a novel anti-hepatitis B virus compound from *Talaromyces sp.* Bioorg Med Chem Lett. 2015; 25:4325-4328.

44. Kaneko M, Watashi K, Kamisuki S, *et al*. A novel tricyclic polyketide, vanitaracin A, specifically inhibits the entry of hepatitis B and D viruses by targeting sodium taurocholate cotransporting polypeptide. J Virol. 2015; 89:11945-11953.

45. Huang Q, Zhang S, Huang R, Wei L, Chen Y, Lv S, Liang C, Tan S, Liang S, Zhuo L, Lin X. Isolation and identification of an anti-hepatitis B virus compound from *Hydrocotyle sibthorpioides Lam*. J Ethnopharmacol. 2013; 150:568-575.

46. Zhou YB, Wang YF, Zhang Y, Zheng LY, Yang XA, Wang N, Jiang JH, Ma F, Yin DT, Sun CY, Wang QD. *In vitro* activity of cepharanthine hydrochloride against clinical wild-type and lamivudine-resistant hepatitis B virus isolates. Eur J Pharmacol. 2012; 683:10-15.

47. Gao LM, Han YX, Wang YP, Li YH, Shan YQ, Li X, Peng ZG, Bi CW, Zhang T, Du NN, Jiang JD, Song DQ. Design and synthesis of oxymatrine analogues overcoming drug resistance in hepatitis B virus through targeting host heat stress cognate 70. J Med Chem. 2011; 54:869-876.

48. Bao LD, Ren XH, Ma RL, Wang Y, Yuan HW, Lv HJ. Efficacy of Artemisia annua polysaccharides as an adjuvant to hepatitis C vaccination. Genet Mol Res. 2015; 14:4957-4965.

49. Duan D, Li Z, Luo H, Zhang W, Chen L, Xu X. Antiviral compounds from traditional Chinese medicines *Galla Chinese* as inhibitors of HCV NS3 protease. Bioorg Med Chem Lett. 2004; 14:6041-6044.

50. Padilla MA, Rodrigues RA, Bastos JC, Martini MC, Barnabe AC, Kohn LK, Uetanabaro AP, Bomfim GF, Afonso RS, Fantinatti-Garboggini F, Arns CW. Actinobacteria from Termite Mounds Show Antiviral Activity against Bovine Viral Diarrhea Virus, a Surrogate Model for Hepatitis C Virus. Evid Based Complement Alternat Med. 2015; 2015:745754.

51. Deng G, Kurtz RC, Vickers A, Lau N, Yeung KS, Shia J, Cassileth B. A single arm phase II study of a Far-Eastern traditional herbal formulation (sho-sai-ko-to or xiao-chai-hu-tang) in chronic hepatitis C patients. J Ethnopharmacol. 2011; 136:83-87.

52. Lyu J, Imachi H, Fukunaga K, Yoshimoto T, Zhang H, Murao K. Roles of lipoprotein receptors in the entry of hepatitis C virus. World J Hepatol. 2015; 7:2535-2542.

53. Elsebai MF, Koutsoudakis G, Saludes V, Perez-Vilaro G, Turpeinen A, Mattila S, Pirttila AM, Fontaine-Vive F, Mehiri M, Meyerhans A, Diez J. Pan-genotypic Hepatitis C Virus Inhibition by Natural Products Derived from the Wild Egyptian Artichoke. J Virol. 2016; 90:1918-1930.

54. Calland N, Sahuc ME, Belouzard S, *et al*. Polyphenols

Inhibit Hepatitis C Virus Entry by a New Mechanism of Action. J Virol. 2015; 89:10053-10063.

55. Lin LT, Chung CY, Hsu WC, Chang SP, Hung TC, Shields J, Russell RS, Lin CC, Li CF, Yen MH, Tyrrell DL, Richardson CD. Saikosaponin b2 is a naturally occurring terpenoid that efficiently inhibits hepatitis C virus entry. J Hepatol. 2015; 62:541-548.

56. Yu F, Wang Q, Zhang Z, *et al*. Development of oleanane-type triterpenes as a new class of HCV entry inhibitors. J Med Chem. 2013; 56:4300-4319.

57. Zhu SL, Wang L, Cao ZY, Wang J, Jing MZ, Xia ZC, Ao F, Ye LB, Liu S, Zhu Y. Inducible CYP4F12 enhances Hepatitis C virus infection *via* association with viral nonstructural protein 5B. Biochem Biophys Res Commun. 2016; 471:95-102.

58. Wozniak L, Skapska S, Marszalek K. Ursolic Acid--A Pentacyclic Triterpenoid with a Wide Spectrum of Pharmacological Activities. Molecules. 2015; 20:20614-20641.

59. Kong L, Li S, Han X, Xiang Z, Fang X, Li B, Wang W, Zhong H, Gao J, Ye L. Inhibition of HCV RNA-dependent RNA polymerase activity by aqueous extract from *Fructus Ligustri Lucidi*. Virus Res. 2007; 128:9-17.

60. Lee S, Yoon KD, Lee M, *et al*. Identification of a resveratrol tetramer as a potent inhibitor of hepatitis C virus helicase. Br J Pharmacol. 2016; 173:191-211.

61. Ashfaq UA, Jalil A, Ul Qamar MT. Antiviral phytochemicals identification from *Azadirachta indica* leaves against HCV NS3 protease: An in silico approach. Nat Prod Res. 2015;1-4.

62. Lan KH, Wang YW, Lee WP, Lan KL, Tseng SH, Hung LR, Yen SH, Lin HC, Lee SD. Multiple effects of Honokiol on the life cycle of hepatitis C virus. Liver Int. 2012; 32:989-997.

63. Ratnoglik SL, Aoki C, Sudarmono P, Komoto M, Deng L, Shoji I, Fuchino H, Kawahara N, Hotta H. Antiviral activity of extracts from *Morinda citrifolia* leaves and chlorophyll catabolites, pheophorbide a and pyropheophorbide a, against hepatitis C virus. Microbiology and Immunology. 2014; 58:188-194.

64. Althagafy HS, Graf TN, Sy-Cordero AA, Gufford BT, Paine MF, Wagoner J, Polyak SJ, Croatt MP, Oberlies NH. Semisynthesis, cytotoxicity, antiviral activity, and drug interaction liability of 7-O-methylated analogues of flavonolignans from milk thistle. Bioorg Med Chem. 2013; 21:3919-3926.

65. Yu M, Zhao Y. Cantharis by photosynthetic bacteria biotransformation: Reduced toxicity and improved antitumor efficacy. J Ethnopharmacol. 2016; 186:151-158.

66. Wang Z, Li J, Ji Y, An P, Zhang S, Li Z. Traditional herbal medicine: A review of potential of inhibitory hepatocellular carcinoma in basic research and clinical trial. Evid Based Complement Alternat Med. 2013; 2013:268963.

67. Li D, Lu L, Zhang J, Wang X, Xing Y, Wu H, Yang X, Shi Z, Zhao M, Fan S, Meng A. Mitigating the effects of Xuebijing injection on hematopoietic cell injury induced by total body irradiation with gamma rays by decreasing reactive oxygen species levels. Int J Mol Sci. 2014; 15:10541-10553.

68. Shen J, Wang J, Shang EX, Tang YP, Kai J, Cao YJ, Zhou GS, Tao WW, Kang A, Su SL, Zhang L, Qian DW, Duan JA. The dosage-toxicity-efficacy relationship of kansui and licorice in malignant pleural effusion rats based on factor analysis. J Ethnopharmacol. 2016; 186:251-256.

69. Xu LW, Jia M, Salchow R, Kentsch M, Cui XJ, Deng HY, Sun ZJ, Kluwe L. Efficacy and side effects of chinese herbal medicine for menopausal symptoms: A critical review. Evid Based Complement Alternat Med. 2012; 2012:568106.

70. Li S, Qi T. 36 Cases report of the tongxinluo capsule combined with western medicine on CSX. Yunan Tradit Chin Med. 2009; 30:15-16.

71. Cannillo M, Frea S, Fornengo C, Toso E, Mercurio G, Battista S, Gaita F. Berberine behind the thriller of marked symptomatic bradycardia. World J Cardiol. 2013; 5:261-264.

Advances in the study of oncofetal antigen glypican-3 expression in HBV-related hepatocellular carcinoma

Min Yao[1,2,*], Li Wang[3,*], Miao Fang[2], Wenjie Zheng[2], Zhizhen Dong[4], Dengfu Yao[2,**]

[1] *Department of Immunology, Medical School of Nantong University, Nantong, China;*
[2] *Research Center of Clinical Medicine, Affiliated Hospital of Nantong University, Nantong, China;*
[3] *Department of Medical Informatics, Medical School of Nantong University, Nantong, China;*
[4] *Department of Diagnostics, Nantong University Hospital, Nantong, China.*

Summary   **Early specific diagnosis and effective treatment of hepatocellular carcinoma (HCC) are crucial. Expression of membrane-associated heparan sulfate proteoglycan glypican-3 (GPC-3) was recently found to increase as part of the malignant transformation of hepatocytes, and this increase is especially marked in patients with hepatitis B virus (HBV) infection, periportal cancerous embolus, or extra-hepatic metastasis. According to data from basic and clinical studies, the oncofetal antigen GPC-3 is a highly specific diagnostic biomarker of HCC and an indicator of its prognosis, and GPC-3 is also a promising target molecule for HCC gene therapy since it may play a crucial role in cell proliferation, metastasis, and invasion and it may mediate oncogenesis and oncogenic signaling pathways. This review summarizes recent advances in the use of oncofetal antigen GPC-3 to diagnose HBV-related HCC, estimate its prognosis, and its targeted therapy.**

Keywords: Glypican-3, hepatocellular carcinoma, HBV infection, diagnosis, prognosis, targeted therapy

1. Introduction

Hepatocellular carcinoma (HCC) is one of the most common malignancies worldwide. Its incidence is still increasing with a multi-factorial, multi-step, complex process, and very poor prognosis (*1,2*). The development and progression of HCC occurs within the context of a chronic, persistent infection with the hepatitis B virus (HBV) or hepatitis C virus (HCV) along with alcohol and aflatoxin B1 intake (*3,4*). Most patients with HCC soon die because of its rapid progression. Hepatic resection, radio-frequency ablation, and transplantation are potential treatments for HCC, but the options are rather limited. HCC can become resistant to radiotherapy or chemotherapy, it has a higher rate of recurrence and

a considerably shorter 5-year survival after surgery, and it readily metastasizes (*5,6*). Therefore, HCC needs to be diagnosed early and effective treatments need to be identified (*7,8*).

All glypicans share a structure characterized by a conserved pattern of 14 cysteine residues that may form intra-molecular disulphide linkages (*9*), and glypicans play important roles in cellular growth, differentiation, and migration. Glypican-3 (GPC-3) belongs to a family of heparan sulfate proteoglycans with 6 sub-types (GPC$_{1-6}$). In this family, the proteoglycans are linked to the exocytoplasmic surface of the plasma membrane by a glycosyl-phosphatidylinositol anchor (*10*). The GPC-3 gene is located on the X human chromosome (Xq26) and it encodes a 70-kDa core protein that can be cleaved by furin to generate a 40 kDa N-terminal- and a 30 kDa C-terminal-protein containing two heparan sulfate glycan chains. Serine^{560} is predicted to be a cleavage site in GPC-3, allowing GPC-3 to bind Wnt, Hedgehog (Hh), and fibroblast growth factor-2 through its core protein and/or the HS chains (*11,12*). GPC-3 contributes to cell migration, invasion, angiogenesis, and apoptosis, possibly through its interactions with the Wnt, Hh, bone morphogenetic protein-7, and insulin-

like growth factor (IGF) signaling pathways (*13-15*). Abnormal expression of hepatic GPC-3 is associated with HCC progression (*16*). The current review focuses on recent advances in the use of oncofetal antigen GPC-3 to diagnose HCC, estimate its prognosis, and treat the disease.

2. GPC-3 as a promising marker of HCC

2.1. *Dynamic expression of GPC-3*

Hepatocyte oncogenesis may be induced by GPC-3 *via* activation of the IGF-II pathway, *via* regulation of zinc fingers and homeoboxes 2, or *via* expression of AFP regulator 2 during liver regeneration. Dynamic changes in hepatic GPC-3, GPC-3 mRNA, and serum GPC-3 expression were investigated in a rat model of hepatocarcinogenesis induced by 2-fluorenylacetamide (2-FAA), and results indicated that GPC-3 has value in diagnosing the early stages of HCC. Positive GPC-3 staining in the liver cytoplasm revealed the morphological stages of granule-like degeneration, atypical hyperplasia (a precancerous stage), and malignant transformation of hepatocytes. A previous study by the current authors found that the level of GPC-3 mRNA expression in the liver was 100%, expression of GPC-3 in the liver was 100%, and expression of GPC-3 in serum was 77.8% in patients with HCC; the level of GPC-3 mRNA expression in the liver was 100%, expression of GPC-3 in the liver was 100%, and expression of GPC-3 in serum was 66.7% in patients with precancerous lesions; the level of GPC-3 mRNA expression in the liver was 83.3%, expression of GPC-3 in the liver was 83.3%, and expression of GPC-3 in serum was 38.9% in patients with degenerated hepatocytes; and GPC-3 was not detected in the control group (*17*). Expression of GPC-3 mRNA in the liver was closely correlated with expression of total RNA in the liver, the level of GPC-3 protein in the liver, and the level of GPC-3 in serum, indicating that abnormal expression of GPC-3 mRNA or protein (which are associated with the malignant transformation of hepatocytes) should be a promising molecular marker for early diagnosis of HCC (*18*).

2.2. *Diagnosis and differential diagnosis*

Although many markers for diagnosis of HCC have been used in clinical practice (*19,20*), only a few markers such as HS-GGT (*21*), AFP-L3 (*22*), and Wnt3a (*23*) have sufficient sensitivity and specificity. The level of circulating AFP is a routine marker for diagnosis of HCC. However, an elevated AFP level results in a higher false positive rate in patients with benign liver diseases, greatly hampering the differential diagnosis (Figure 1) (*24,25*). Circulating GPC-3 increases in patients with HCC, which implies that
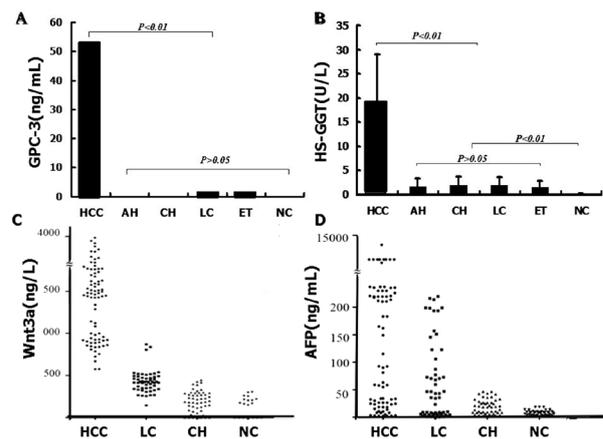
Figure 1 Comparative analysis of 4 markers for HCC diagnosis. (A), the levels of GPC-3 expression in patients with different liver diseases; **(B)**, the levels of HS-GGT expression in patients with different liver diseases; **(C)**, the levels of Wnt3a expression in patients with different liver diseases; and **(D)**, the levels of total AFP expression in patients with different liver diseases. HCC, hepatocellular carcinoma; GPC-3: glypican-3; AFP, total α-fetoprotein; HS-GGT, hepatoma-specific γ-glutamyl transferase.

GPC-3 may be very valuable in diagnosing HCC and monitoring its progression. Serum GPC-3 is superior to AFP in terms of specificity, positive or negative predictive value, and the accuracy with which it diagnoses HCC. Moreover, GPC-3 is also superior to AFP in formulating a treatment strategy and predicting the survival of patients with HCC. Yao M *et al.* found that serum GPC-3 was detectable in 52.8% of patients with HCC with a specificity of 97.1%, and only 1.4% to 2.0% of patients had other liver diseases (*26*). AFP is not accurate at diagnosing HCC because of its higher false positive rate (14.3% to 35.0%) in benign liver diseases. AFP-L3 has a sensitivity of 53.3% and a specificity of 88.9%. Serum GPC-3 levels could be used to differentiate HCC from non-malignant chronic liver disease and other liver cancers. Although serum GPC-3 has a higher level of specificity at diagnosing HCC, the combination of circulating levels of GPC-3, positive GPC-3 mRNA, and AFP significantly improves the accuracy of HCC diagnosis (*27-29*).

3. GPC-3 in relation to disease stage and prognosis

Clinical studies have reported that GPC-3 is specifically over-expressed in HCC and that it is a valuable marker for diagnosis of HCC and estimation of its prognosis (*17,24*). GPC-3 promotes the growth of HCC by stimulating canonical Wnt signaling. There is increasing evidence indicating that the structural requirements for GPC3 activity are cell type-specific, and its core protein is processed by a furin-like convertase. GPC-3 is expressed like a carcinoembryonic antigen, it stains dark brown deep within HCC tissues, and it is found in the cytoplasm and cell membrane (*30*). Immunohistochemistry has revealed oncofetal GPC-

3 expression in the cytoplasm and cell membrane at levels of 70-100% in HCC or hepatoblastoma, 6%-75% in fibrolamellar carcinoma or high-grade dysplasia, and 0-10% in cholangiocarcinoma (*31,32*).

3.1. Clinical staging

Wang *et al.* found that 80.6% of patients with HCC tested positive for GPC-3, 41.7% of their para-cancerous tissues tested positive, and none of the tissues distant from the cancer tested positive. The intensity of GPC-3 in HCC is significantly higher than that in surrounding tissues (*33*). Hepatic GPC-3 expression gradually increases in different stages, with dark staining in the advanced stage. A previous study by the current authors staged 69 specimens of cancerous tissue in accordance with the clinical staging criteria of the IUAC for HCC, and 11 specimens had stage I carcinoma (15.9%, 11 of 69), 19 had stage II (27.6%, 19 of 69), and 39 had stage III or IV (56.5%, 39 of 69). High levels of GPC-3 expression were noted in 45.5% of stage I HCC tissue specimens while low levels were noted in 54.5%, high levels were noted in 52.6% of stage II specimens while low levels were noted in 47.4%, and high levels were noted in 100% of stage III or IV specimens while low levels were noted in 0% (33).

GPC-3 is a developmentally-regulated oncofetal protein that is a clinically relevant biomarker for diagnosis of HCC and is one of the first transcripts to appear during the hepatocyte malignant transformation; about 50% of high-grade dysplastic macro-nodules in the cirrhotic liver express GPC-3 (*34,35*). GPC-3 can provide a molecular signature of early HCC since it is expressed in all HCC tissues and not expressed in any of the dysplastic nodules. Thus, GPC-3 should be a specific biomarker for diagnosis of HCC. An examination of hepatic fine needle aspirates (FNA) found that GPC-3 immunoreactivity was from 83% to 90% in cases of HCC, whereas there was no reaction in any benign lesions or metastatic carcinomas (*36,37*). The usefulness of GPC-3 when examining specimens is as an aid to distinguish HCC from metastatic tumors and benign liver lesions.

3.2. Monitoring metastasis

Metastasis occurs as cancerous cells enter the circulation and eventually grow into a lethal tumor in distant organs (*38*). GPC-3 mRNA from peripheral blood mononuclear cells (PBMC) is of value in monitoring HCC with extra-hepatic metastasis. Hepatic and blood GPC-3 mRNA are associated with extra-hepatic metastasis of HCC (*39*). Metastasis is the final stage in tumor progression and is thought to be responsible for up to 90% of deaths from HCC as cancerous cells enter the circulation and eventually grow into a lethal tumor in distant organs, reflecting inherent differences within the disseminating

cells of distinct tumors (*2*). Amplification of fragments of the GPC-3 gene and verification of its identity by sequencing has revealed GPC-3 mRNA in most cancerous tissues or circulating PBMCs from patients with HCC but not in tissues distant from the cancer or cells from benign liver diseases (*26*).

Transcription of the GPC-3 gene in circulating PBMCs was associated with extra-hepatic metastasis of HCC. GPC-3 mRNA was expressed in 74.8% of primary and recurrent HCC but only in 3.2% of normal livers according to Northern blotting (*31*). The expression of GPC-3 mRNA was low or absent in the normal liver, focal nodular hyperplasia, and liver cirrhosis. Fragments of the GPC-3 gene were amplified and the identity of the gene was verified with DNA sequencing, but the gene was not found in tissue distant from the cancer or cells from benign liver diseases. Circulating GPC-3 mRNA is related to the TNM stage, periportal cancerous embolus, and extra-hepatic metastasis ($p < 0.001$) (*18*). Interestingly, a higher level of GPC-3 mRNA expression was found in patients with stage I-II HCC, HBV infection, and a small tumor, and GPC-3 is highly expressed in early and small HCC, and especially in patients with periportal cancer embolus (100%) or extra-hepatic metastasis (100%) (*32*), suggesting that up-regulation of circulating GPC-3 mRNA could be a more sensitive and specific biomarker with which to monitor the metastasis of HCC (*18*).

3.3. Prognostic value

The prognosis for HCC remains poor because of its late diagnosis and high rate of recurrence after surgery. New findings regarding the use of circulating GPC-3 as a marker have recently been reported, with GPC-3 displaying prognostic value in patients with HCC and HBV-associated cirrhosis after liver transplantation (*40-42*). GPC-3-positive patients had lower 5-year survival and disease-free survival rates than GPC-3-negative patients (38.2% vs. 75.4%; 30.8% vs. 69.7%) (*33*). Multivariate Cox regression analysis revealed that GPC-3 is an independent risk factor for the 5-year survival ($p = 0.031$) and disease-free survival rates ($p = 0.047$). Together with tumor differentiation, the Milan criteria, and preoperative AFP, GPC-3 is a potential indicator of a poor prognosis after liver transplantation in patients with HCC and HBV-associated cirrhosis (*43,44*).

Early detection of HCC and monitoring its recurrence after surgery would improve prognosis and justify screening programs for at-risk populations, such as chronic carriers of HBV and individuals with cirrhotic HCV (*3,6*). Basic and clinical studies have indicated that GPC-3 is a specific indicator of the prognosis for HCC (*45*). As expected, the over-expression of hepatic GPC-3 was significantly related to the 5-year survival of 69 patients with HCC ($p < 0.001$). Cox regression univariate analysis indicated that

certain HCC clinical prognostic factors, such as liver cirrhosis ($p = 0.007$) and HBV infection ($p = 0.014$), were significantly correlated with the 5-year survival rate. All of these factors were entered in multivariable analysis. A high level of GPC-3 expression ($p < 0.001$), liver cirrhosis ($p = 0.008$), and HBV infection ($p = 0.006$) were all identified as independent predictive factors for worse outcomes from HCC (46). Kaplan-Meier survival curves indicated that patients with HCC and high levels of GPC-3 expression had a significantly shorter survival time than those with low levels or no GPC-3 expression (33).

4. GPC-3 as a novel target for HCC therapy

Molecularly targeted therapy offers an effective option for non-surgical management of HCC that is highly chemo-resistant or that fails to respond to medication (5,7). However, molecular therapy remains a challenge mainly due to lack of specific targets. Use of the GPC-3 antigen as a target for HCC has been investigated with siRNA (47), vaccines (48,49), T lymphocytes (50-52), and anti-GPC-3 antibodies *in vitro* and *in vivo* (53,54). Some advances on the use of GPC-3 as the novel target for HCC therapy have been made (55). Of these, antibody-based therapy is the most clinically advanced. Given that GPC-3 increases in early, high-grade dysplastic macronodules and since a significant proportion of overt HCC is immunoreactive to anti-GPC-3, a therapeutic mAb (GC33, aa524-563) in the C-terminal portion of GPC-3 has been generated in MRL/lpr mice against a GST-fusion protein fragment, indicating that the antibodies are cytotoxic and significantly inhibit HCC growth both *in vitro* and *in vivo* (56).

4.1. *Studies in vitro*

The over-expression of hepatic GPC-3 plays an important role in HCC transformation, proliferation, and metastasis (18). Therefore, GPC-3 should be a specific molecular target for HCC therapy. Intervening in gene transcription with specific short hairpin RNA (shRNA) or microRNA (miRNA) inhibits cell proliferation *via* apoptosis *in vitro* (47,57,58). Silencing the GPC-3 gene with specific shRNA inhibits HCC cell proliferation, with inhibition of 71.1% in cells transfected with shRNA and 80.1% in cells transfected with shRNA and treated with sorafenib (100 μmol/L). A total of 65.6% of the cells were arrested in the G1 phase. Cell apoptosis increased significantly to 66.8% in comparison to cells that were not transfected with shRNA (6.9%) (59). By up-regulating key molecules (cyclin D1, β-catenin, and GSK3β) in the Wnt/β-catenin signaling pathway, oncofetal GPC-3 stimulates cell proliferation, suggesting that the GPC-3 gene should be a novel therapeutic target for HCC, but further studies
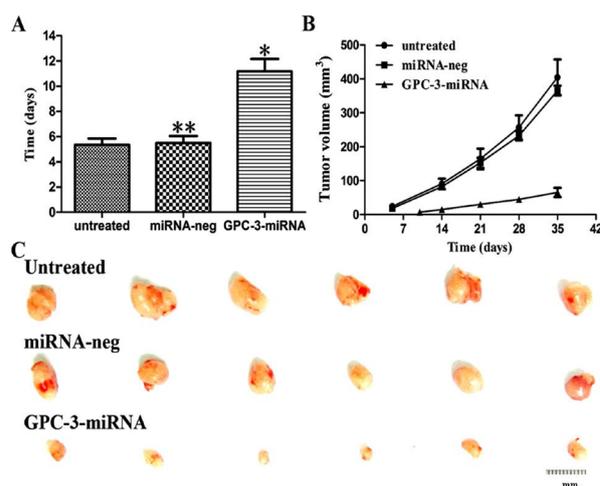
Figure 2 Silencing *GPC-3* inhibited tumor development when a liver cancer cell line was xenografted to nude mice. (A), the time for a tumor to develop after nude mice were injected with stable HepG2 cells; **(B)**, the tumor volume in different groups ($n = 6$); **(C)**, the dissected tumor and its actual size. Scale bar, 100μm. *$p < 0.05$; **$p < 0.01$.

should focus on the combination of miRNA and multi-targeting strategies for HCC therapy (60).

4.2. *Studies in vivo*

Xenograft models are commonly used in tumor studies because of their convenience, high success rate, short latent period, and ease of monitoring. Besides anti-GPC-3 antibodies, siRNA targeting GPC-3 has also displayed therapeutic efficacy in a model of HCC (54,61). Tumor formation and growth are significantly inhibited by miRNA in a model of HepG2-cell-induced HCC in nude mouse in comparison to the same mice not treated with miRNA (Figure 2, unpublished data). Immunohistochemical analysis indicated that down-regulation of GPC-3 with miRNA significantly ($p < 0.01$) decreases expression of β-catenin, p-GSK3β, and cyclin D1. β-catenin and GSK3β are known to play an important role in regulating metabolism, transcription, embryonic development, and other processes and to also play a key role in the Wnt/β-catenin-induced phosphorylation of GSK3β, which results in the dissolution of the complex responsible for β-catenin degradation (62,63). A therapeutic intervention targeting GPC-3 is a promising approach for the clinical management of HCC.

5. Conclusion

In conclusion, HCC is one of the most common malignancies worldwide, and treatment outcomes generally remain poor (64,65). The GPC-3 gene is located upstream of the Wnt signaling pathway, which is involved in tumor development and progression, and GPC-3 is up-regulated in HBV-related liver malignancies. Activation of several key signaling

molecules regulates the expression of inflammation response- or cancer related-genes. An interesting finding is that GPC-3 levels and HBV infection have been identified as independent predictive factors for worse outcomes of HCC, that is, patients with HCC and higher levels of GPC-3 expression have a shorter survival time than those with lower levels or no expression. GPC-3 is specifically expressed in HCC but not in benign liver diseases. This means that GPC-3 is both a promising diagnostic or independent prognostic factor and also a therapeutic target for HCC. Further work should explore the combination of specific siRNA plus multi-targeting strategies in HCC therapy.

Acknowledgements

References

1. Chen W, Zheng R, Baade PD, Zhang S, Zeng H, Bray F, Jemal A, Yu XQ, He J. Cancer statistics in China, 2015. CA Cancer J Clin. 2016; 66:115-132.
2. Bruix J, Gores GJ, Mazzaferro V. Hepatocellular carcinoma: Clinical frontiers and perspectives. Gut. 2014; 63:844-885.
3. Riviere L, Ducroux A, Buendia MA. The oncogenic role of hepatitis B virus. Recent Results Cancer Res. 2014; 193:29-74.
4. El-Serag HB. Epidemiology of viral hepatitis and hepatocellular carcinoma. Gastroenterol. 2012; 142:1264-1273.
5. Bruix J, Reig M, Sherman M. Evidence-based diagnosis, staging, and treatment of patients with hepatocellular carcinoma. Gastroenterol. 2016; 150:835-853.
6. El-Serag HB. Hepatocellular carcinoma. N Engl J Med. 2011; 365:1118-1127.
7. Jain S, Singhal S, Lee P, Xu R. Molecular genetics of hepatocellular neoplasia. Am J Transl Res. 2010; 2:105-118.
8. Maluccio M, Covey A. Recent progress in understanding, diagnosing, and treating hepatocellular carcinoma. CA Cancer J Clin. 2012; 62:394-399.
9. Filmus J, Capurro M. The role of glypican-3 in the regulation of body size and cancers. Cell Cycle. 2008; 7:2787-2790.
10. Theocharis AD, Skandalis SS, Tzanakakis GN, Karamanos NK. Proteoglycans in health and disease: Novel roles for proteoglycans in malignancy and their pharm- acological targeting. FEBS J. 2010; 277:3904-3923.
11. Gao W, Kim H, Feng M, Phung Y, Xavier CP, Rubin JS, Ho M. Inactivation of Wnt signaling by a human antibody that recognizes the heparan sulfate chains of glypican-3 for liver cancer therapy. Hepatol. 2014; 60:576-587.
12. Dong Z, Yao M, Wang L, Yang JL, Yao DF. Down-regulating glypican-3 expression: Molecular-targeted therapy for hepatocellular carcinoma. Mini Rev Med Chem. 2014; 14:1183-1193.
13. Magistri P, Leonard SY, Tang CM, Chan JC, Lee TE, Sicklick JK. The glypican 3 hepatocellular carcinoma marker regulates human hepatic stellate cells *via* Hedgehog signaling. J Surg Res. 2014; 187:377-385
14. Lai JP, Sandhu DS, Yu C, *et al.* Sulfatase 2 up-regulates glypican 3, promotes fibroblast growth factor signaling, and decreases survival in hepatocellular carcinoma. Hepatol. 2008; 47:1211-1222.
15. Cheng W, Tseng CJ, Lin TT, Cheng I, Pan HW, Hsu HC, Lee YM. Glypican-3 -mediated oncogenesis involves the insulin-like growth factor-signaling pathway. Carcinogen. 2008; 29:1319-1326.
16. Baghy K, Tátrai P, Regős E, Kovalszky I. Proteoglycans in liver cancer. World J Gastroenterol. 2016; 22:379-393.
17. Yao M, Yao DF, Bian YZ, Zhang CG, Qiu LW, Wu W, Sai WL, Yang JL, Zhang HJ. Oncofetal antigen glypican-3 as a promising early diagnostic marker for hepatocellular carcinoma. HBPD Int. 2011; 10:289-294.
18. Wang L, Yao M, Dong Z, Zhang Y, Yao DF. Circulating specific biomarkers in diagnosis of hepatocellular carcinoma and its metastasis monitoring. Tumour Biol. 2014; 35:9-20.
19. Abd El Gawad IA, Mossallam GI, Radwan NH, Elzawahry HM, Elhifnawy NM. Comparing prothrombin induced by vitamin K absence-II (PIVKA-II) with the oncofetal proteins glypican-3, alpha fetoprotein and carcinoembryonic antigen in diagnosing hepatocellular carcinoma among Egyptian patients. J Egypt Natl Canc Inst. 2014; 26:79-85.
20. Huang TS, Shyu YC, Turner R, Chen HY, Chen PJ. Diagnostic performance of alpha-fetoprotein, lens culinaris agglutinin-reactive alpha-fetoprotein, des-gamma carboxyprothrombin, and glypican-3 for the detection of hepatocellular carcinoma: A systematic review and meta-analysis protocol. Syst Rev. 2013; 2:37.
21. Yao DF, Jiang D, Huang Z, Lu JX, Tao QY, Yu ZJ, Meng XY. Abnormal expression of hepatoma specific gamma-glutamyl transferase and alteration of gamma-glutamyl transferase gene methylation status in patients with hepato- cellular carcinoma. Cancer. 2000; 88:761-769.
22. Wu CS, Lee TY, Chou RH, Yen CJ, Huang WC, Wu CY, Yu YL. Development of a highly sensitive glycan microarray for quantifying AFP-L3 for early prediction of hepatitis B virus-related hepatocellular carcinoma. PLoS One. 2014; 9:e99959.
23. Pan LH, Yao M, Zheng WJ, Gu JJ, Yang XL, Qiu LW, Cai Y, Wu W, Yao DF. Abnormality of Wnt3a expression as novel specific biomarker for diagnosis and differentiation of hepatocellular carcinoma. Tumour Biol, 2016; 37:5561-5568.
24. Liu XF, Hu ZD, Liu XC, Cao Y, Ding CM, Hu CJ. Diagnostic accuracy of serum glypican-3 for hepatocellular carcinoma: A systematic review and meta-analysis. Clin Biochem. 2014;47:196-200.
25. Enan ET, El-Hawary AK, El-Tantawy DA, Abu-Hashim MM, Helal NM. Diagnostic role of glypican 3 and CD34 for differentiating hepatocellular carcinoma from nonmalignant hepatocellular lesions. Ann Diagn Pathol. 2013; 17:490-493.
26. Yao M, Yao DF, Bian YZ, Wu W, Yan XD, Yu DD, Qiu LW, Yang JL, Zhang HJ, Sai WL, Chen J. Values of circulating GPC-3 mRNA and alpha-fetoprotein in detecting patients with hepatocellular carcinoma. HBPD

Int. 2013; 12:171-179.

27. Wang SK, Zynger DL, Hes O, Yang XJ. Discovery and diagnostic value of a novel oncofetal protein: Glypican 3. Adv Anat Pathol. 2014; 21:450-460.

28. Li B, Liu H, Shang HW, Li P, Li N, Ding HG.Li P, Li N, Ding HG. Diagnostic value of glypican-3 in alpha fetoprotein negative hepatocellular carcinoma patients. Afr Health Sci. 2013; 13:703-709.

29. Lagana SM, Salomao M, Bao F, Moreira RK, Lefkowitch JH, Remotti HE. Utility of an immunohistochemical panel consisting of glypican-3, heat-shock protein-70, and glutamine synthetase in the distinction of low-grade hepatocellular carcinoma from hepatocellular adenoma. Appl Immunohistochem Mol Morphol. 2013; 21:170-176.

30. Li L, Jin R, Zhang X, Lv F, Liu L, Liu D, Liu K, Li N, Chen D. Oncogenic activation of glypican-3 by c-Myc in human hepatocellular carcinoma. Hepatol. 2012; 56:1380-1390.

31. Zaakook M, Ayoub M, Sinna EA, El-Sheikh S. Role of glypican-3 immunocyto- chemistry in differentiating hepatocellular carcinoma from metastatic carcinoma of the liver utilizing fine needle aspiration cytology. J Egypt Natl Canc Inst. 2013; 25:173-180.

32. Nassar A, Cohen C, Siddiqui MT. Utility of glypican-3 and survivin in differentiating hepatocellular carcinoma from benign and preneoplastic hepatic lesions and metastatic carcinomas in liver fine-needle aspiration biopsies. Diagn Cytopathol. 2009; 37:629-635.

33. Wang L, Pan L, Yao M, Cai Y, Dong ZZ, Yao DF. Expression of oncofetal antigenglypican-3associates significantly with poor prognosis in HBV-related hepatocellular carcinoma. Oncotarget. 2016; 7:42150-42158.

34. Li J, Gao JZ, Du JL, Wei LX. Prognostic and clinicopathological significance of glypican-3 overexpression in hepatocellular carcinoma: A meta-analysis. World J Gastroenterol. 2014; 20:6336-6344.

35. Xiao WK, Qi CY, Chen D, Li SQ, Fu SJ, Peng BG, Liang LJ. Prognostic significance of glypican-3 in hepatocellular carcinoma: A meta-analysis. BMC Cancer. 2014; 14:104.

36. Kandil D, Leiman G, Allegretta M, Trotman W, Pantanowitz L, Goulart R, Evans M. Glypican-3 immunocytochemistry in liver fine-needle aspirates: A novel stain to assist in the differentiation of benign and malignant liver lesions. Cancer. 2007; 111:316-322.

37. Ibrahim TR, Abdel-Raouf SM. Immunohistochemical study of glypican-3 and HepPar-1 in differentiating hepatocellular carcinoma from metastatic carcinomas in FNA of the liver. Pathol Oncol Res. 2015; 21:379-387.

38. Geramizadeh B, Seirfar N. Diagnostic value of arginase-1 and glypican-3 in differential diagnosis of hepatocellular carcinoma, cholangiocarcinoma and metastatic carcinoma of liver. Hepat Mon. 2015; 15:e30336.

39. Wang Y, Shen Z, Zhu Z, Han R, Huai M. Clinical values of AFP, GPC3 mRNA in peripheral blood for prediction of hepatocellular carcinoma recurrence following OLT: AFP, GPC3 mRNA for prediction of HCC. Hepat Mon. 2011; 11:195-199.

40. Cui X, Li Z, Gao PJ, Gao J, Zhu JY. Prognostic value of glypican-3 in patients with HBV-associated hepatocellular carcinoma after liver transplantation. HBPD Int. 2015; 14:157-163.

41. Wang YL, Zhu ZJ, Teng DH, Yao Z, Gao W, Shen ZY. Glypican-3 expression and its relationship with recurrence

of HCC after liver transplantation. World J Gastroenterol. 2012; 18:2408-2414.

42. Chen IP, Ariizumi S, Nakano M, Yamamoto M. Positive glypican-3 expression in early hepatocellular carcinoma predicts recurrence after hepatectomy. J Gastro-enterol 2014; 49:117-125.

43. Jeon Y, Kim H, Jang ES, Hong S, Kim JW, Yoon YS, Cho JY, Han HS, Jeong SH. Expression profile and prognostic value of glypican-3 in post-operative South Korean hepatocellular carcinoma patients. APMIS. 2016; 124:208-215.

44. Feng J, Zhu R, Chang C, Yu L, Cao F, Zhu G, Chen F, Xia H, Lv F, Zhang S, Sun L. CK19 and glypican 3 expression profiling in the prognostic indication for patients with HCC after surgical resection. PLoS One. 2016; 11:e0151501.

45. Liu X, Wang SK, Zhang K, Zhang H, Pan Q, Liu Z, Pan H, Xue L, Yen Y, Chu PG. Expression of glypican 3 enriches hepatocellular carcinoma development- related genes and associates with carcinogenesis in cirrhotic livers. Carcinogen. 2015; 36:232-242.

46. Haruyama Y, Yorita K, Yamaguchi T, Kitajima S, Amno J, Ohtomo T, Ohno A, Kondo K, Kataoka H. High preoperative levels of serumglypican-3 containing N-terminal subunit are associated with poor prognosis in patients with hepato- cellular carcinoma after partial hepatectomy. Int J Cancer. 2015; 137:1643-1651.

47. Maurel M, Jalvy S, Ladeiro Y, Combe C, Vachet L, Sagliocco F, Bioulac-Sage P, Pitard V, Jacquemin-Sablon H,Zucman-Rossi J, Laloo B, Grosset CF. A functional screening identifies five microRNAs controlling glypican-3: Role of miR-1271 down-regulation in hepatocellular carcinoma. Hepatol. 2013; 57:195- 204.

48. Kawashima I, Kawashima Y, Matsuoka Y, Fujise K, Sakai H, Takahashi M, Yoshikawa T, Nakatsura T, Ishihara T, Ohno T. Suppression of postsurgical recurrence of hepatocellular carcinoma treated with autologous formalin-fixed tumor vaccine, with special reference to glypican-3. Clin Case Rep. 2015; 3:444- 447.

49. Sawada Y, Yoshikawa T, Ofuji K, *et al.* Phase II study of the GPC3-derived peptide vaccine as an adjuvant therapy for hepatocellular carcinoma patients. Oncoimmunol. 2016; 5:e1129483.

50. Iwama T, Uchida T, Sawada Y, Tsuchiya N, Sugai S, Fujinami N, Shimomura M, Yoshikawa T, Zhang R, Uemura Y, Nakatsura T. Vaccination with liposome-coupled glypican-3 derived epitope peptide stimulates cytotoxic T lymphocytes and inhibits GPC3-expressing tumor growth in mice. Biochem Biophys Res Commun. 2016; 469:138-143.

51. Sayem MA, Tomita Y, Yuno A, Hirayama M, Irie A, Tsukamoto H, Senju S, Yuba E, Yoshikawa T, Kono K, Nakatsura T, Nishimura Y. Identification of glypican-3 -derived long peptides activating both CD8+ and CD4+ T cells; prolonged overall survival in cancer patients with Th cell response. Oncoimmunol. 2015; 5:e1062209.

52. Dargel C, Bassani-Sternberg M, Hasreiter J, *et al.* T cells engineered to express a T-cell receptor specific for glypican-3 to recognize and kill hepatoma cells *in vitro* and in mice. Gastroenterol. 2015; 149:1042-1052.

53. Gao W, Kim H, Ho M. Human monoclonal antibody targeting the heparan sulfate chains of glypican-3 inhibits HGF-mediated migration and motility of hepato- cellular carcinoma cells. PLoS One. 2015; 10:e0137664.

54. Hanaoka H, Nagaya T, Sato K, Nakamura Y, Watanabe

R, Harada T, Gao W, Feng M, Phung Y, Kim I, Paik CH, Choyke PL, Ho M, Kobayashi H. Glypican-3 targeted human heavy chain antibody as a drug carrier for hepato-cellular carcinoma therapy. Mol Pharm. 2015; 12:2151-2157.

55. Wang L, Yao M, Pan LH, Qian Q, Yao DF. Glypican-3 as special biomarker or promising target molecule for primary liver cancer. HBPD Int. 2015; 14:361-366.

56. Feng M, Ho M. Glypican-3 antibodies: A new therapeutic target for liver cancer. FEBS Lett. 2014; 588:377-382.

57. Huang N, Lin J, Ruan J, Su N, Qing R, Liu F, He B, Lv C, Zheng D, Luo R. MiR-219-5p inhibits hepatocellular carcinoma cell proliferation by targeting glypican-3. FEBS Lett. 2012; 586:884-891.

58. Miao HL, Lei CJ, Qiu ZD, Liu ZK, Li R, Bao ST, Li MY. MicroR-NA-520c-3p inhibits hepatocellular carcinoma cell proliferation and invasion through induction of cell apoptosis by targeting glypican-3. Hepatol Res. 2014; 44:338-348.

59. Yu D, Dong Z, Yao M, Wu W, Yan MJ, Yan XD, Qiu LW, Chen J, Sai WL, Yao DF. Targeted glypican-3 gene transcription inhibited the proliferation of human hepatoma cells by specific short hairpin RNA. Tumour Biol. 2013; 34:661-668.

60. Yao M, Wang L, Qiu L, Qian Q, Yao D. Encouraging microRNA-based thera- peutic strategies for hepatocellular carcinoma. Anticancer Agents Med Chem. 2015; 15:453-460.

61. Yao M, Wang L, Dong Z, Qian Q, Shi Y, Yu DD, Wang SY, Zheng WJ, Yao DF. Glypican-3 as an emerging molecular target for hepatocellular carcinoma gene therapy. Tumour Biol. 2014; 35:5857-5868.

62. Gao W, Tang Z, Zhang YF, Feng M, Qian M, Dimitroy DS, Ho M. Immunotoxin targeting glypican-3 regresses liver cancer *via* dual inhibition of Wnt signalling and protein synthesis. Nat Commun. 2015; 6:6536.

63. Capurro M, Martin T, Shi W, Filmus J. Glypican-3 binds to Frizzled and plays a direct role in the stimulation of canonical Wnt signaling. J Cell Sci 2014; 127:1565-1575.

64. Tagliamonte M, Petrizzo A, Tornesello ML, Ciliberto G, Buonaguro FM, Buonaguro L. Combinatorial immunotherapy strategies for hepatocellular carcinoma. Curr Opin Immunol. 2016; 39:103-113.

65. Inagaki Y, Tang W, Zhang L, Du GH, Xu WF, Kokudo N. Novel aminopeptidase N (APN/CD13) inhibitor 24F can suppress invasion of hepatocellular carcinoma cells as well as angiogenesis. Biosci Trends. 2010; 4:56-60.

Review

Status of and prospects for bronchoscopic lung volume reduction for patients with severe emphysema

Hang Yu, Lijie Wang, Zhen Wu, Zhen Yang*

Department of Respiratory Medicine, Chinese PLA General Hospital, Beijing, China.

Summary   Bronchoscopic lung volume reduction (BLVR) is a minimally invasive treatment for severe emphysema, providing treatment options for patients who are unable to undergo lung volume reduction surgery (LVRS) or lung transplantation. Current BLVR techniques include bronchoscopic volume reduction with valve implants, use of a lung volume reduction coil (LVRC), bronchoscopic thermal vapor ablation (BTVA), biological lung volume reduction (BioLVR), and use of airway bypass stents (ABS). To date, several randomized controlled trials of these bronchoscopic therapies have been conducted in patients with emphysema, and bronchoscopic volume reduction with valve implants remains the best approach thus far. Recent studies indicate that BLVR may be of great value in improving lung function, exercise capacity, and quality of life and that BLVR has the potential to replace conventional surgery for patients with severe emphysema. Optimal patient selection and the proper selection of the BLVR technique in accordance with patient characteristics are crucial to the success of BLVR. More multicenter, prospective, randomized controlled trials need to be conducted in the future to optimize the current selection strategy and evaluate the safety, efficiency, and long-term benefit of BLVR techniques.

Keywords: Bronchoscopic lung volume reduction, chronic obstructive pulmonary disease, emphysema, endobronchial valve

1. Introduction

Chronic obstructive pulmonary disease (COPD) is a severe chronic respiratory disease characterized by progressive development and airflow limitation that is not fully reversible, and COPD seriously affecting the mobility and quality of life of patients (*1*). COPD is a serious global public health problem because of its high mortality and high morbidity; globally, COPD patients numbered about 65 million in 2005 and COPD resulted in about 300 million deaths. By 2020, this ailment will be among the world's top three major causes of death (*2,3*). Emphysema is a key pathology and type of COPD. Chronic airway inflammation causes a reduction in lung tissue elasticity; without

that elasticity, the bronchial and alveolar walls are destroyed (emphysema), leading to airway collapse, hyperinflation, and gas trapping (*4*). When emphysema is severe, traditional medical treatments include bronchodilators and anti-inflammatory drugs are ineffective; patients suffer decreased lung function and a severely diminished quality of life, and they eventually die from respiratory failure.

Surgery to treat severe COPD and emphysema has been performed for many years, including lung volume reduction surgery (LVRS) and lung transplantation. In 1957, Mueller first proposed the use of LVRS to treat emphysema (*5*). LVRS involves removing tissue affected by emphysema, thereby reducing ineffective ventilation and improving lung ventilation while the remaining lung enlarges. Pulmonary vascular resistance decreased and right ventricular function improves. Thus, LVRS is effective in reducing difficulty breathing and improving lung function and quality of life (*6*). The National Emphysema Treatment Trial (NETT) found that LVRS was effective, but only did patients with low exercise capacity and predominantly upper

lobe emphysema benefit from LVRS (*7*). NETT also found that the wide use of LVRS was limited in clinical contexts because of the physical condition the patient had to be in, surgical trauma, a postoperative mortality rate of up to 7.9% in the next 90 days, an incidence of pulmonary complications as high as 29.8%, and an incidence of cardiovascular complications as high as 20.8%. Whether lung transplantation may improve lung function, pulmonary activity, quality of life, and long-term survival for patients with emphysema appears inconclusive, and such an option cannot be widely promoted due to the vast shortage of donors, surgical trauma, major problems after transplant rejection, and infection (*8,9*). Therefore, surgery has limited ability to meet clinical needs, and a new, minimally invasive, and effective treatment is needed to eliminate the bottleneck limiting current techniques and approaches.

Bronchoscopic lung volume reduction (BLVR) originated in 2001 and developed rapidly afterwards as a new option to treat severe emphysema (*10*). BLVR techniques are categorized as blocking and non-blocking techniques and their use is based on the type of emphysema and interlobular collateral ventilation. Blocking BLVR involves reversible implantation of one-way valves, while non-blocking involves use of a lung volume reduction coil (LVRC), bronchoscopic thermal vapor ablation (BTVA), biological lung volume reduction (BioLVR), or use of airway bypass stents (ABS). This paper aims to provide an overview of the status of and progress in BLVR research according to the current literature. The latest and most investigated BLVR techniques are summarized in Table 1.

2. Blocking BLVR – Valve Implantation

2.1. *Endobronchial valves and intrabronchial valves*

One-way valve implantation for treatment of severe emphysema was first reported in 2003 (*11*). Currently, two types of valves are used, the endobronchial valves (EBVs) (Zephyr; Pulmonx, Inc., Neuchatel, Switzerland) and intrabronchial valves (IBVs) (Spiration; Olympus, Tokyo, Japan). A one-way valve is held in place by a coated (a silicone membrane for EBVs and polyurethane film for IBVs) self-expanding NiTi retainer. The two types of valve function differently because of their structure. An IBV has anchors that hold an umbrella-shaped valve in place in an airway. The valve closes to allow trapped air and mucus to escape the damaged lung and it opens to block breath from entering the damaged lung. Since the IBV has to be anchored, it depends on the wall of the airway. An EBV is a duckbill valve that fits snugly in an airway with the bill pointed away from the damaged lung. Air and mucus can pass through the valve to escape the damaged lung during expiration, but the close of the valve during inspiration blocks air from entering the

damaged lung. In contrast to the IBV, the EBV depends less on the airway wall. Either valve is placed using bronchoscopy to prevent gas from entering during inhalation while not affecting the exhalation of gas and secretions. This reduces lung hyperinflation, resulting in a reduction in lung volume, while the blocked portion undergoes relatively normal lung tissue recruitment. Valve implantation is a reversible procedure, and either type of valve can be removed at any time using a bronchoscope.

EBVs are the most widely studied and widely used valves. Early studies were based on observational studies and indicated that EBV implantation was safe, but most studies have found that EBV implantation has little benefit (*11-17*). A series of early studies indicated that EBV implantation substantially benefited patients in whom the target lobe collapsed and in whom target lung volume reduction (TLVR) was achieved, but TLVR was achieved in only 24.9% of patients (*11-15*). Post-procedure quality of life and exercise capacity improved to some extent for patients with no significant collapse of the target lobe, the difference was not statistically significant (*16,17*). Although the target lobe does not collapse, EBV implantation reduces physiological dead space and it improves the efficiency of ventilation; increased ventilation allows more air to healthy lungs and reduces dynamic hyperinflation, so patients receive a slight benefit. These early studies proved that collapse of the target lung is the ultimate goal of EBV implantation.

In those early studies, EBVs were usually implanted in one lung or both lungs. Wan *et al.* (*17*) found that patients undergoing EBV implantation in one lung had more benefits than those receiving implants in both lungs. Unilateral implantation differed significantly from LVRS, which requires treatment of both lungs to have an obvious benefit. Theoretically, expansion of the opposite lung can lead to collapse of the target lung after unilateral implantation of an EBV. In the study by Wan *et al.*, post-operative complications increased when both lungs were treated. In light of these findings, EBV implantation is almost always performed unilaterally.

The Endobronchial Valve for Emphysema Palliation Trial, or VENT, was the first and largest randomized controlled trial (RCT) of valve implantation to treat emphysema; the trial was conducted separately in the US and Europe (*18,19*). In US VENT study by Sciurba *et al.*, an EBV was implanted in 214 patients with emphysema, and results indicated that the forced expiratory volume in 1 second (FEV_1) increased by 4.3% over the previous procedure in 6 months, compared to a decrease of 2.5% in the control group ($p = 0.005$). Similar differences were observed in the 6-minute walk test (6MWT) and health-related quality of life measured with the St. George's Respiratory Questionnaire (SGRQ), and the modified Medical Research Council (mMRC) Dyspnea scale (*18*). In the

European VENT study, respiratory symptom scores on the SGRQ also improved significantly after 6 months for patients receiving an EBV in comparison to the control group (*19*). Results of the VENT study indicated that EBV implantation is effective in treating patients with severe emphysema, but the clinical improvements were not significant. In order to improve the effectiveness of EBV implantation, a retrospective study of the VENT results and a series of studies examined the characteristics of patients receiving EBVs and those studies described a series of predictive factors as will now be described.

2.2. Factors predicting the success of valve treatment

2.2.1. TLVR

A retrospective study of the VENT results indicated that there was a significant correlation between TLVR and the success of EBV implantation (*20*). Improvements in the BODE index (more than 1 point) were observed in 67% of patients with a TLVR > 50%, 37% of patients with a TLVR of 20-50%, and 41% of patients with a TLVR < 20% ($p = 0.011$ for intergroup differences). The study also indicated that a TLVR of more than 350 mL was an independent predictor of the success of EBV implantation. A long-term-survival study ($n = 19$) indicated that 5 patients who developed atelectasis in the target lobe survived 6 years after EBV implantation while 8 of 14 patients with no atelectasis died (*21*). Another study ($n = 33$) indicated that patients with atelectasis in the target lobe after EBV implantation had a better long-term survival (*22*).

The importance of TLVR in IBV implantation has been indicated. Unlike complete occlusion of the target lobe with an implanted EBV, IBV implantation involves incomplete occlusion of more than one lobe in bilateral lungs in the hopes of achieving TLVR with no increase in post-procedure complications. However, two multicenter studies of IBV implantation found that the volume of the patient's target lobe and lung function decreased slightly and exercise capability did not improve significantly after IBV implantation (*23,24*). An RCT involving 277 patients found that incomplete bilateral occlusion did not achieve a satisfactory TLVR (TLVR is only about 200 mL), and the treatment group displayed no significant improvement according to their SGRQ scores (*25*). Eberhardt *et al*. compared the use of implanted IBVs in complete unilateral occlusion and incomplete bilateral occlusion (*26*). In 7 of 11 patients, complete occlusion resulted in collapse of the target lobe; in 11 patients with incomplete occlusion, none had atelectasis. Lung function, exercise capability, and quality of life after IBV implantation differed significantly in the two groups of patients. Therefore, incomplete bilateral occlusion with an implanted IBV has been abandoned, and new strategies for IBV

implantation need to be developed for the technique to be effective.

2.2.2. Fissure integrity

In addition to the surgical technique and anatomical abnormalities, collateral channels of ventilation can affect the collapse of the target lobe. Both normal individuals and patients with emphysema have interalveolar channels (pores of Kohn), bronchiole-alveolar channels (canals of Lambert), and interbronchiolar channels (channels of Martin). The existence of these channels means that an EBV must block all segments of the target lobe (*27-30*). Interlobular collateral ventilation is main factor influencing TLVR and determining the success of EBV implantation. This collateral ventilation is the inevitable result of emphysema damaging the interlobular fissure. Therefore, integrity of the interlobular fissure is likely to be a predictor of the success of EBV implantation.

A retrospective analysis of the VENT results confirmed this theory. Six months after EBV implantation, patients with complete interlobular fissures (defined as more than 90% completeness of the fissure between the target and adjacent lobes on the cross-sectional, sagittal, or coronal plane on MDCT) had a significant improvement in lung function (*19*). Recently, an RCT known as the BeLieVeR-HIFi study implanted valves in patients with intact interlobular fissures on CT ($n = 25$) and the study compared those patients to a control group who received sham valve implantation ($n = 25$) (*31*). After 3 months, the FEV_1 in the group receiving a valve increased by a mean of 24.8% (median 8.77%) compared to 3.9% (median 2.88%) in the control group ($p = 0.0326$). A clinically significant improvement (improvement in $FEV_1 \geq 15\%$) was noted in 39% of patients and in only 4% of the control group ($p = 0.0044$).

2.2.3. Direct measurement of collateral ventilation

Current methods for the assessment of fissure integrity are mainly based on visual assessment by imaging experts using high-resolution reconstructed CT images (*18,19,31*). The assessments are heavily influenced by the level of experience of the experts and they are highly subjective, and often there is disagreement between imaging experts (*32*). With the development of computer technology, automated analysis can improve the efficiency and accuracy of inspections of the interlobular fissure, but it still cannot replace the role of imaging experts (*33,34*). In the BeLieVeR-HIFi study, 4 patients with a complete interlobular fissure according to imaging experts failed to benefit from EBV implantation (*31*).

The Chartis Pulmonary Assessment System (Pulmonx, Inc., Neuchatel, Switzerland) is a direct method to determine whether interlobular collateral ventilation (CV) exists in the target lobe. A catheter with a balloon at its tip is placed in the bronchus of

Table 1. Summary of reported trials on bronchoscopic lung volume reduction

Device/year (Ref.)	Design	No. of patients treated	Emphysema phenotype: hetero, homo, or both	Procedure unilateral or bilateral	Follow-up duration	ΔFEV₁ (95% CI)	ΔRV (95% CI)	Δ6MWT distance (95% CI)	ΔSGRQ, total score (95% CI)
EBV									
Klooster, 2015 (39)	Prospective RCT; Single center	34	hetero	unilateral	6 months	216 mL** (128 to 304) 26.5%** (16.3 to 36.4)		92 m** (64 to 120)	-17.4* (-24.8 to -10.0)
Davey, 2015 (31)	Double-blind, sham-controlled RCT; Single center	25	hetero	unilateral	3 months	0.06 L* (0.02 to 0.38) 8.77%* (2.27 to 35.85)	-0.26 L (-1.07 to -0.16) -6.58% (-18.60 to 2.94)	25 m* (7 to 64)	-4.40 (-16.93 to 6.76)
Herth, 2013 (36)	Non-randomized prospective trial; Multicenter	51 (patients with no CV)	hetero	unilateral	30 days	0.14 ± 0.20 L** 16 ± 22%**	4.49 ± 1.22 L	24 ± 57 m	-10 ± 13
Herth, 2012 (19)	Prospective RCT; Multicenter	44 (Complete fissure), 67 (Incomplete fissure)	hetero	unilateral	12 months	15 ± 29%* 0 ± 23%		13 ± 35% 5 ± 30%	0 ± 15 -1 ± 14
Sciurba, 2010 (18)	Prospective RCT; Multicenter	220	hetero	unilateral	6 months	4.3%** (1.4 to 7.2) 34.5 mL** (10.8 to 58.3)		2.5%* (-1.1 to 6.1) 9.3 m* (-0.5 to 19.1)	-2.8* (-4.7 to -1.0)
IBV									
Wood, 2014 (25)	prospective, adaptive, double-blind RCT; Multicenter	142	hetero	bilateral	6 months	-0.07 ± 0.17 L -2.11 ± 5.49%	0.31 ± 1.00 L 12.57 ± 51.11%	-24.02 ± 69.81 m	2.15 ± 16.36
Ninane, 2012 (24)	Single-blinded sham-controlled RCT; Multicenter	37	hetero	bilateral	3 months	0.99 ± 0.35 L to 0.90 ± 0.34 L	4.65 ± 1.30 L to 4.86 ± 1.35 L	337 ± 106 m to 344 ± 18 m	-4.3 ± 16.2
Eberhardt, 2012 (26)	RCT; Single center	11 (unilateral), 11 (bilateral)	hetero	unilateral (11) bilateral (11)	30 days 30 days	267 ± 154 mL# 13 ± 140 mL	-546 ± 1307 mL -61 ± 990 mL	47.8 ± 55.7 m# -25.0 ± 81.5 m	-12.2 ± 13.4# -0.3 ± 9.8
Sterman, 2010 (23)	Prospective, open enrollment case series; Multicenter	91	hetero	bilateral	12 months	0.87 ± 0.25 L to 0.85 ± 0.33 L	4.74 ± 1.06 L to 4.71 ± 1.27 L	338 ± 95 m to 358 ± 92 m	-9.5 ± 14.4#
LVRC									
Sciurba, 2016 (67)	Prospective, assessor-blinded RCT; Multicenter	158	both	bilateral	12 months	3.8%** (-6.3 to 16.1)	-0.41 L** (0.57 to -0.25)	10.3 m* (-33.0 to 45.0)	-8.1* (-10.2 to -6.0)
Deslee, 2016 (66)	Prospective, open-label, superiority RCT; Multicenter	50	both	bilateral	6 months	0.06 L* (0.02 to 0.11) 9%** (4 to 14)	-0.52 L* (-0.74 to -0.31) -9%** (-12 to -5)	36% improvement ≥ 54 m* 18 m (-6 to 43)	-11.1* (-15.9 to -6.2)
Klooster, 2014 (63)	Prospective, open-label, cohort trial; Single center	10	homo	bilateral	6 months	0.58 (0.45 to 0.93) to 0.69 (0.56 to 1.02) L#	5.04 (4.14 to 6.57) to 4.44 (3.57 to 5.68) L##	289 (160 to 485) m to 350 (192 to 520) m##	63 (45 to 79) to 48 (25 to 68) #
Deslee, 2014 (62)	Prospective, open-label feasibility study, Multicenter	60	hetero	bilateral	12 months	0.11 ± 0.30 L# 16.0 ± 35.5%#	-0.71 ± 0.81 L# -13.8 ± 12.7%##	51.4 ± 76.1 m#	-11.1 ± 13.3##

* $p < 0.05$ compared to control, ** $p < 0.01$ compared to control, # $p < 0.05$ compared to baseline, ## $p < 0.01$ compared to baseline, Δ, change; ABS, airway bypass stents; BioLVR, biological lung volume reduction; BTVA, bronchoscopic thermal vapor ablation; EBV, endobronchial valve; FEV, forced expiratory volume over 1 second; IBV, intrabronchial valve; LVRC, lung volume reduction coil; RV, residual volume; SGRQ, St. George's Respiratory Questionnaire; 6MWT, 6-min walk test; CV, collateral ventilation.

Table 1. Summary of reported trials on bronchoscopic lung volume reduction (continued)

Device/year (Ref.)	Design	No. of patients treated	Emphysema phenotype: hetero, homo, or both	Procedure unilateral or bilateral	Follow-up duration	ΔFEV_1 (95% CI)	ΔRV (95% CI)	Δ6MWT distance (95% CI)	ΔSGRQ, total score (95% CI)
Shah, 2013 (64)	Prospective RCT; Multicenter	23	both	bilateral	90 days	14.2%* (6.8 to 21.6)	-0.51 L* (-0.73 to -0.30)	51.2 m** (27.7 to 74.7)	-8.1* (-13.8 to 2.4)
Slebos, 2012 (61)	Prospective, cohort pilot study; Single center	16	hetero	unilateral (12) bilateral (4)	6 months	14.9 ± 17%##	-11.4 ± 9%##	84.4 ± 73.4 m##	-14.9 ± 12.1##
BTVA Herth, 2016 (72)	Prospective, parallel-group, open-label RCT; Multicenter	45	hetero	unilateral	6 months	130.8 mL** (63.6 to 198.0) 11.0 ± 16.2%**	-302.5 mL* (-542.6 to -62.4)	30.5 m (-1.5 to 62.4)	-9.7 ± 14.4**
Snell, 2012 (69)	Two open-label, single-arm studies; Multicenter	44	hetero	unilateral	6 months	140.8 ± 26.3 mL##	-406 ± 112.9 mL##	46.5 ± 15.0 m##	-14.0 ± 2.4##
BioLVR Come, 2015 (78)	Prospective, open-label RCT; Multicenter	59	hetero	bilateral	3 months (n = 34)	110 mL** (18 to 211)			-11* (-18 to -1)
					6 months (n = 21)	100 mL* (0 to 370)		31.0 m* (0 to 41.3)	-12** (-22 to -5)
Kramer, 2012 (76)	Single-arm, prospective study; Multicenter	20	both	bilateral	6 months	335 ± 438 mL## 31.2 ± 36.6%##	-485 ± 981 mL -7.1 ± 19.3%	11.8 ± 57.5 m	-8.0 ± 17.2
Herth, 2011 (74)	Non-controlled, open-label, pilot study; Multicenter	21	hetero	unilateral	6 months	0.105 ± 0.201 L# 10.0 ± 19.8%#		24.6 ± 58.9 m	-7.5 ± 14.4#
Refaely, 2009 (75)	Open-label, non-randomized, phase 2 study; Multicenter	17	homo	bilateral	6 months	13.8 ± 20.26%##		2.6 ± 38.25 m	-12.2 ± 12.38##
ABS Shah, 2011 (81)	Double-blind, sham-controlled RCT; Multicenter	208	homo	bilateral	Day 1	3.1 ± 6%**	-17.9 ± 38%*		57 ± 13 to
					1 month	0.7 ± 4%	-6.8 ± 29%	302 ± 88 m to 314 ± 95 m	50 ± 15**
					6 months	-0.15 ± 7%	-5.6 ± 32%	302 ± 88 m to 281 ± 109 m	57 ± 13 to 56 ± 16

*$p < 0.05$ compared to control, **$p < 0.01$ compared to control, #$p < 0.05$ compared to baseline, ##$p < 0.01$ compared to baseline, Δ, change; ABS, airway bypass stents; BioLVR, biological lung volume reduction; BTVA, bronchoscopic thermal vapor ablation; EBV, endobronchial valve; FEV₁, forced expiratory volume over 1 second; IBV, intrabronchial valve; LVRC, lung volume reduction coil; RV, residual volume; SGRQ, St. George's Respiratory Questionnaire; 6MWT, 6-min walk test; CV, collateral ventilation.

the target lobe. The balloon is inflated to occlude the airway and the airflow can be measured. If the airflow gradually decreases during measurement, CV is absent (*35*). A multicenter study reported that the accuracy of CV assessment by Chartis system was 75%. Moreover, 1 month after valve placement, patients with no CV had an improvement of 16% in FEV_1 whereas patients with CV experienced only an increase of 1% in FEV_1 ($p = 0.0013$) (*36*). However, the existence of CV cannot be determined by the Chartis system in about 10% of patients because of the anatomy of the airway and excessive airway secretions. At this time, a means of high-resolution CT to assess CV is still needed (*37*).

Only a few studies have compared CT and Chartis at evaluating collateral ventilation. A retrospective study ($n = 33$) indicated that CT was comparable to Chartis in predicting if a TLVR of more than 350 mL ($p = 0.55$) could be achieved in the target lobe; CT had an accuracy of 78.8% and Chartis had an accuracy of 75.8% (*34*). A retrospective study by Gompelmann *et al*. indicated that the Chartis system had an accuracy of 74% and CT had an accuracy of 77% (*38*).

Recently, a single-center RCT, known as the STELVIO trial, combined high-resolution CT and the Chartis system to screen patients (*39*). In this study, 68 patients with no CV according to the Chartis system and an intact interlobular fissure according to high-resolution CT were randomly divided into patients receiving an EBV ($n = 34$) and patients receiving standard treatment ($n = 34$). After 6 months, FEV_1 increased by a mean of 26.5% in patients receiving an EBV and 3.6% in the control group ($p < 0.001$). Improvement in the forced vital capacity (FVC) and results on the 6MWT were also statistically and clinically significant. The combination of fissure analysis using CT and CV measurement with the Chartis system apparently improves the clinical benefit of EBV implantation.

However, the combination of high-resolution CT and the Chartis system in patient selection has its disadvantages. Gompelmann *et al*. reported that a number of patients with no CV and an incomplete interlobular fissure and patients with CV and a complete interlobular fissure can benefit from EBV implantation (*38*). Although a strategy combining both approaches can provide a clinical benefit, it would inevitably deprive some patients of the opportunity to benefit from treatment.

In a recent retrospective study ($n = 38$), de Oliveira *et al*. proposed new criteria for patient selection (*40*). The study indicated that TLVR would not exceed 350 mL after EBV implantation in patients with an interlobular fissure that was less than 75% complete ($n = 8$). A TLVR $\geq$ 350 mL was achieved in 19 of 21 patients with interlobular fissure integrity greater than 90% and in 7 of 10 patients of interlobular fissure integrity of 70-90%. The effectiveness of EBV implantation was closely correlated with an interlobular fissure integrity

of more than 75% (the previous standard was more than 90% completeness), and interlobular fissure integrity of more than 75% had an accuracy of 87.2% at predicting a TLVR $\geq$ 350 mL. Therefore, the study's authors contended that EBV implantation should be considered for all patients with interlobular fissure integrity greater than 75% and that EBV implantation should definitely be considered for all patients with interlobular fissure integrity greater than 90%. The authors also indicated that collateral ventilation should be assessed with Chartis in patients with interlobular fissure integrity of 75-90%.

Nevertheless, Schuhmann *et al*. indicated that the response rate was only 65% in patients with fissure integrity greater than 90% (*34*). Similar results were obtained in studies by Davey *et al*. and Klooster *et al*. (*31,39*). If the fissure is incomplete (< 90%), the chance of EBV implantation succeeding would be quite small according to Schuhmann *et al*., and this group of patients would not need to be examined with Chartis (*34*). Therefore, a strategy combining CT and Chartis can ensure a clinical benefit of EBV implantation and avoid useless treatment of unsuitable patients. The patient selection strategy advocated by de Oliveira *et al*. needs to be studied in more RCTs.

2.2.4. *Heterogeneity of emphysema*

Heterogeneity of emphysema is another possible predictor of the effectiveness of EBV implantation. Clinical evidence has not led to any definite conclusions regarding this predictor. The VENT study in the US and a retrospective study of 57 patients found greater improvement in patients with more heterogeneous emphysema (*18,41*). However, the VENT study in Europe found that the extent of heterogeneity had no significant impact on the success of EBV implantation in patients with an intact interlobular fissure and collapse of the target lobe (*19*). In a study by Herth *et al*., 14 of 20 patients (70%) with no CV and less heterogeneous emphysema had a TLVR $\geq$ 350 mL after treatment (*36*). Klooster *et al*. indicated that patients with no CV and an intact interlobular fissure had greater improvement if emphysema was heterogeneous rather than homogeneous, but the difference between the two was not statistically significant (*39*). Theoretically, more heterogeneous emphysema means non-target lobes on the same side are healthier than the target lobe. If the target lobe collapsed by atelectasis, a healthier lobe on the same side can benefit more from an improvement in respiratory dynamics. Patients with more heterogeneous emphysema should improve more after EBV implantation. Recent studies have not indicated significant differences between high and low heterogeneous emphysema. This may relate to the currently designated values for the threshold of heterogeneity (the average heterogeneity of emphysema in patients who received the minimal clinical benefit in the VENT study). Therefore, whether the heterogeneity

of emphysema can be a predictive index for EBV implantation and its threshold level should be studied further.

2.2.5. Other predictors

An EBV can be implanted in the upper or lower lobe of the left or right lung. Retrospective studies of the VENT results indicated that post-procedure lung function improvement did not differ significantly when an upper or lower lobe was treated (*42,43*). However, recent studies have found that each lobe plays a different role in lung functioning, with the lower lobe of the lung having more of an impact on FEV_1 than the upper lobe (*44,45*). Therefore, EBV implantation in the lower lobe may have more of a benefit, but this contention needs to be verified. Several studies have indicated that EBV implantation in the left lobe was more likely to achieve a TLVR than implantation in the right lobe (*40,42*). This may be because the left lobe is less likely to have collateral ventilation than the right lobe (*46*). In addition, the right lobe has two interlobular fissures while the left lobe has only one; thus, there is a greater likelihood of interlobular collateral ventilation occurring. A study by Davey *et al.* indicated that when the interlobular fissures were intact and there was no collateral ventilation, treatment of the left lobe resulted in better improvement in the FEV_1 than treatment of the right lobe did, but the difference was not significant (*31*). The sample in the study by Davey *et al.* was too small, and the issue of whether treatment of the left or right lobe affects the effectiveness of EBV implantation needs to be studied further.

In some studies, ventilation/perfusion scintigraphy of the lungs is routinely performed (*11-18*). The state of lung perfusion is usually consistent with the extent of damage (*47*), but in a few instances the state of lung perfusion and extent of emphysema may differ because local vascular inflammation has induced vascular remodeling, which can also lead to irregularities in pulmonary perfusion (*48,49*). Therefore, pulmonary perfusion should be assessed prior to the procedure to comprehensively assess the lungs. Lung perfusion is usually assessed using a combination of CT and single-photon emission computed tomography (SPECT). Every lung perfusion scintigram is craniocaudally divided into three equal parts. The upper part of regional perfusion is similar to the upper lobe of the lung, and the lower part is similar to that of the lower lobe (*50*). A series of studies found that BLVR would cause a decrease in target lung perfusion and increase ipsilateral non-target lobe and contralateral lung perfusion (*51-53*). Therefore, assessment of lobe perfusion before treatment may be an index of the success of EBV. A retrospective study of the VENT results found that baseline hypoperfusion of the target lobe improved significant results on the 6MWT after EBV implantation. However, in this study the hypoperfused lobe had more emphysema, so the

extent of emphysema in the target lobe may affect post-procedure results on the 6MWT (*54*). Thomsen *et al.* indicated that the degree of perfusion of the target lobe and its impact on post-procedure improvement in the 6MWT did not differ significantly, but patients with greater perfusion of the non-target lung on the same side had significant improvement in the 6MWT after treatment (*41*). Generally speaking, assessment of emphysema (heterogeneity) and pulmonary perfusion together may provide a more comprehensive assessment of the lobes and their state. Treating the affected lobe allows a "better" lobe on the same side to function better and can lead to greater benefits from EBV implantation. This strategy warrants further study with regard to patient selection.

2.3. Complications of valve implantation

The main complications of valve implantation are exacerbation of COPD, hemoptysis, pneumothorax, and valve displacement. Pneumothorax is the most common complication. Gompelmann *et al.* found that the more volume reduction in the target lobe, the higher the incidence of pneumothorax (*55*). Patients with pneumothorax benefit more from receiving EBVs. However, pneumothorax is a serious complication of EBV implantation, patients must be closely monitored for pneumothorax within 72-96 hours of the procedure; patients should be placed on bed rest for 48 hours and be given a cough suppressant since pneumothorax often occurs 4 days after EBV implantation (*56*). Experts in the treatment of postoperative pneumothorax have reached a consensus: all patients need to be closely observed, and patients with an expanding pneumothorax will need immediate insertion of a chest drain (*57*). Removal of one or all valves or immediate surgical intervention may be considered for patients with deteriorating clinical symptoms. IBV implantation and EBV implantation involve similar post-procedure complications.

EBVs have been implanted to treat severe emphysema for more than 10 years and are mainly used in patients with unilateral heterogeneous emphysema. EBV treatment is performed in one lobe only once in most patients. A recent retrospective study of patients with emphysema in both lungs received EBV treatment in one lung; if lung function failed to improve or declined again after improving, a second EBV treatment was performed in the opposite lung (*58*). The study indicated that patients receiving a 2-steps EBV treatment in both lungs could also benefit from the second procedure; there were no significant differences in post-procedure complications for patients receiving EBV treatment in one or both lungs although the latter had a longer hospital stay. Further RCTs need to be conducted to evaluate the effectiveness of this sequential EBV treatment in both lungs.

Ongoing RCTs of EBV implantation aim to optimize patient screening (LIBERATE study, NCT01796392), evaluate long-term outcomes (LIVE study, NCT01580215), to treat patients with mild to moderate COPD (REMODEL study, NCT01969734), and to treat patients with homogeneous emphysema (IMPACT study, NCT02025205). Ongoing RCTs of IBV implantation include complete occlusion of target lobe in one lung with implanted IBVs (EMPROVE study, NCT01812447; SVS study, NCT01989182) and an open-label study of IBV implantation in patients with no CV (NCT01902732).

3. Non-blocking BLVR

3.1. *LVRC*

LVRC (PneumRx/BTG, Camberley, UK) involves the use of nickel-titanium alloy coils 10-20 cm long. A delivery system is used to place the straightened coils in an affected lung. The coils regain their shape and compress lung tissue affected by emphysema; as the tissue is compressed, its volume is reduced, directing air to healthier portions of the lung, thus achieving a reduction in lung volume (*59*). LVRC can be used for treatment of bilateral or unilateral emphysema. For patients with bilateral emphysema, treatment usually involves 2 steps: treatment of the lung on one side and then treatment of the lung on the other side 1-4 months later. Whether patients have collateral ventilation does not need to be considered in LVRC, and LVRC can target the most severely damaged pulmonary segment for treatment instead of the entire lobe, thus leaving as much healthy lung tissue intact as possible. LVRC has obvious advantages over EBV implantation. However, the disadvantage of LVRC is that it is partially irreversible since removal of coils is difficult and is certainly not feasible in all cases.

Small early trials indicated the safety and effectiveness of LVRC (*60,61*). A prospective European multicenter single-arm study involving 60 patients with bilateral heterogeneous emphysema found that FEV_1, results on the 6MWT, and scores on the SGRQ improved significantly at the 1-year follow-up (*62*). A small-scale study by Klooster *et al*. suggested that LVRC might be equally effective in treating both homogeneous and heterogeneous emphysema (*63*). In the RESET study, 47 patients with homogeneous or heterogeneous emphysema were randomly assigned to either an LVRC treatment group or the control group (*64*). The treatment group consisted of 23 patients who underwent bilateral LVRC implantation. Three months after the procedure, lung function, exercise capacity, and quality of life improved significantly in comparison to the control group. There was no significant difference in the benefit received by patients with homogeneous or heterogeneous emphysema in that study. One year

after the procedure, patients were still found to benefit from the treatment (*65*). In a multicenter RCT, known as the REVOLENS trial, 100 patients with bilateral emphysema were assigned to receive LVRC treatment or standard care. After 6 months, significantly more patients in the treatment group (*n* = 50) had an improvement of 54 m in the 6MWT in comparison to the control group (*n* = 50) (36% of patients, *n* = 18 *vs*. 17% of patients, *n* = 9), although the absolute between-group difference in results on the 6MWT was only modest (21 m) (*66*). The study sample was carefully selected to include patients with a residual volume greater than 220% of the predicted volume, which represents a higher degree of expiratory air trapping and contrasts with the 150% predicted volume specified in inclusion criteria for most BLVR trials. A recent RCT (*n* = 315), known as the RENEW trial, required a residual volume of greater than 175% of the predicted volume. In comparison to standard care, implantation of LVRCs only resulted in a modest improvement in exercise capacity and slight improvement in lung function, with a higher likelihood of post-procedure complications. However, a subgroup analysis indicated that patients with homogeneous or heterogeneous emphysema and a residual volume of greater than 225% of the predicted volume had a significant improvement in lung function and quality of life because of LVRC implantation (*67*). Usually there are few choices for treatment of patients with homogeneous emphysema besides conventional treatment (more than 75% cannot undergo LVRS or some other BLVR), so LVRC offers a treatment option. Therefore, patients with a high degree of air trapping may be the main beneficiaries of LVRC treatment. Whether LVRC treatment is able to increase the long-term survival of patients needs to be verified by further studies.

The main complications of LVRC treatment include exacerbation of COPD, hemoptysis, transient chest pain, pneumonia, and pneumothorax; most complications occur within a few weeks after LVRC implantation, but mild hemoptysis may persist for a few months after the procedure (*60*).

3.2. *BTVA*

BTVA (Uptake Medical Corporation, Seattle, Wash., USA) delivers water heated by an endobronchial catheter to the affected lobe to induce an inflammatory response, leading to irreversible pulmonary parenchymal fibrosis, scar formation, and distal atelectasis, thus achieving a reduction in lung volume (*68*). Thus far, BTVA has only been used to treat patients with heterogeneous emphysema primarily in the upper lung regions. BTVA can treat the most affected segment of one lobe, regardless of collateral ventilation. However, this technique is irreversible.

A single-arm multicenter study of 44 patients with

upper lobe emphysema indicated that patients receiving unilateral BTVA had an improved FEV_1 of 140.8 mL ($p < 0.001$) after 6 months, and 58% of patients had 12% improvement in their FEV_1 (69). However, the inflammatory reaction causes most patients to develop complications such as a fever, cough, sputum, and hemoptysis in the 4 weeks after the procedure; the inflammatory response gradually subsides after 12 weeks but it prolongs hospitalization. Nevertheless, the inflammatory reaction seems to be necessary for the success of BTVA. Patients who develop an inflammatory reaction have a better clinical outcome than patients without respiratory adverse events after BTVA (70). Henne *et al.* wondered whether BTVA at a lower dose would reduce the incidence of complications and provide benefits similar to those of BTVA at a higher dose (71). Recently, the multicenter STEP-UP study compared 46 patients who received low-dose BTVA with 24 patients who received standard care (72). The study used 8.5 calories of vapor energy per gram of lung tissue to treat affected segments, in contrast to 10 calories per gram used in previous trials. In order to reduce post-procedure complications, the treatment was performed in two steps. The first procedure treated the most severely damaged pulmonary segment of a lobe, and the second procedure treated the remaining segments of the same lobe 3-4 months later. After 6 months, the trial group had significant changes in its FEV_1 (improvement of 14.7% in the BTVA group *vs.* the control group, $p < 0.0001$) and its scores on the SGRQ (reduction of 9.7 points in the BTVA group, $p = 0.0021$). Furthermore, the incidence of adverse events decreased significantly in comparison to that in previous BTVA trials. STEP-UP study is the only RCT involving BTVA. Further studies are needed to verify the long-term survival benefit of BTVA.

3.3. *BioLVR*

BioLVR is another irreversible BLVR technique using an emphysematous lung sealant system (Aeris Therapeutics, Woburn, Mass., USA). BioLVR involves injecting synthetic polymers to block the airways of affected regions in order to promote bronchial remodeling, scarring, and atelectasis, resulting in a reduction in target lung hyperinflation (73).

Previous studies indicated that BioLVR achieved a reduction in lung volume. Six months after BioLVR, patients had significant improvement in their FEV_1 and scores on the SGRQ, and patients with advanced heterogeneous emphysema generally tolerated the procedure (74). Another study indicated that BioLVR improved lung function and quality of life for patients with homogeneous emphysema (75). A study by Kramer *et al.* indicated that BioLVR is effective in treating both heterogeneous and homogeneous emphysema, and benefits in patients with heterogeneous or homogeneous

emphysema did not differ significantly 2 years after treatment (76,77). Magnussen *et al.* found that whether interlobular fissures were complete had no obvious effect on the effectiveness of BioLVR (73). In a recent RCT, known as the ASPIRE study, Come *et al.* compared patients undergoing BioLVR and a control group receiving standard care, and they found that 34 patients who underwent BioLVR had a significantly improved quality of life (FEV_1: 11.4 % *vs.* -2.1%, $p = 0.0037$; SGRQ: -11 *vs.* -4, $p = 0.026$) (78). Six months after treatment, these improvements were still evident, and more than 50% of patients who underwent BioLVR had a clinically significant improvement (improvement in $FEV_1 \geq 12$ % or improvement in scores on the SGRQ ≥ 4); however, 44% of treated patients had respiratory complications requiring hospitalization at the 90-day follow-up and two deaths were reported. The major complications of BioLVR are a fever, cough, chest pain, acute exacerbation of COPD, pneumonia, and hemoptysis. BioLVR needs to be evaluated further in clinical trials.

3.4. *ABS*

ABS is mainly used in patients with severe homogeneous emphysema. ABS provides a bypass so that gas trapped in an affected region of the lung can be released, thus reducing lung volume. Studies have indicated that ABS can improve pulmonary function and the symptom of dyspnea, but this improvement did not differ significantly between the treatment group and the control group (79,80). In 2011, a multicenter, double-blind, sham-controlled RCT, known as the EASE trial, randomly divided 315 patients with severe homogeneous emphysema into an ABS group ($n = 208$) and a sham surgery group ($n = 107$); follow-up assessments revealed no statistically significant differences in FEV_1, results on the 6MWT, or scores on the SGRQ for either group after 6 months (81). The trial did not achieve the expected primary endpoint (at the 6-month follow-up, FVC increased by at least 12% and mMRC fell by 1 point from the baseline). However, the trial indicated that ABS in the short term had certain curative effects. However, these effects gradually disappeared over time. This may be because ABS failed to open up a route for gas to escape because the ABS shifted, the respiratory tract was obstructed by secretions, or granulation tissue formed. Optimizing the design of the ABS and sustaining its effectiveness over the long term need to be explored further. ABS needs to bridge a vast divide to be ready for clinical use.

4. Conclusion

The high mortality and morbidity rate of LVRS has spurred the development of BLVR. Previous trials and follow-up data have indicated that BLVR can be used to
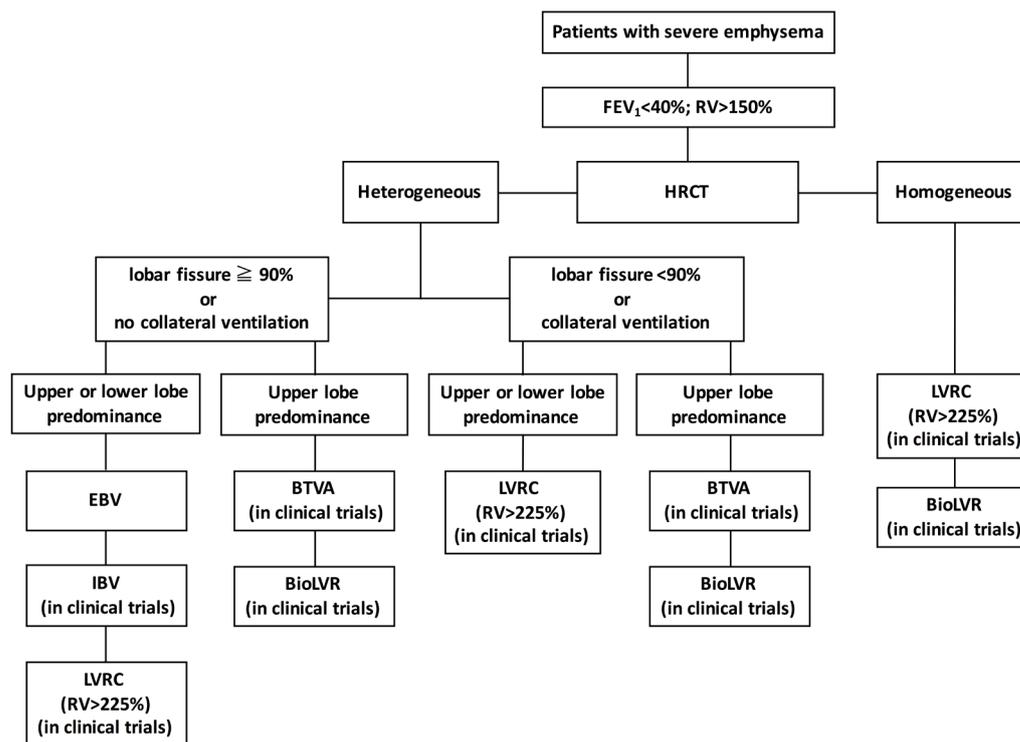
Figure 1. Recommended algorithm for bronchoscopic lung volume reduction in patients with severe emphysema in accordance with the distribution of emphysema and the presence or absence of collateral ventilation. BioLVR, biological lung volume reduction; BTVA, bronchoscopic thermal vapor ablation; EBV, endobronchial valve; FEV_1, forced expiratory volume over 1 second; IBV, intrabronchial valve; LVRC, lung volume reduction coil; RV, residual volume.

treat patients with severe emphysema. However, BLVR has yet to yield satisfactory results in terms of the improvement in pulmonary function, exercise capacity, and quality of life and the incidence of complications. The long-term benefit of BLVR needs to be studied further. More work is needed to define patient selection criteria for each individual technique. According to the research, the current options for BLVR to treat patients with emphysema are as shown in Figure 1. This algorithm is similar with those proposed by previous studies, but is modified based on the latest studies and clinical evidence (*82,83*). Future research will focus on devising new criteria for patient selection and improving patient benefit while expanding the pool of eligible patients. As imaging and clinical indicators are studied further, clinicians of the future may choose a different BLVR technique based on more accurate patient characteristics, achieving "precision medicine" for patients with emphysema.

In summary, BLVR is a minimally invasive treatment for severe emphysema, providing treatment options for patients who are unable to undergo LVRS or lung transplantation. This technique may be of great value in improving lung function, exercise capacity, and quality of life, and it has the potential to replace conventional surgery for patients with severe emphysema. Optimal patient selection and the proper selection of the BLVR technique in accordance with

patient characteristics are crucial to the success of BLVR. More multicenter, prospective RCTs need to be conducted in the future.

References

1. Vestbo J, Hurd SS, Agusti AG, Jones PW, Vogelmeier C, Anzueto A, Barnes PJ, Fabbri LM, Martinez FJ, Nishimura M, Stockley RA, Sin DD, Rodriguez-Roisin R. Global strategy for the diagnosis, management, and prevention of chronic obstructive pulmonary disease: GOLD executive summary. Am J Respir Crit Care Med. 2013; 187:347-365.
2. Murray CJ, Lopez AD. Measuring the global burden of disease. N Engl J Med. 2013; 369:448-457.
3. World Health Organization. Burden of COPD. *http://www.who.int/respiratory/copd/burden/en/* (accessed July 28, 2016).
4. Kemp SV, Polkey MI, Shah PL. The epidemiology, etiology, clinical features, and natural history of emphysema. Thorac Surg Clin. 2009; 19:149-158.
5. Brantigan OC, Mueller E. Surgical treatment of pulmonary emphysema. Am Surg. 1957; 23:789-804.

6.   Washko GR, Fan VS, Ramsey SD, Mohsenifar Z, Martinez F, Make BJ, Sciurba FC, Criner GJ, Minai O, Decamp MM, Reilly JJ, National Emphysema Treatment Trial Research Group. The effect of lung volume reduction surgery on chronic obstructive pulmonary disease exacerbations. Am J Respir Crit Care Med. 2008; 177:164-169.

7.   Fishman A, Martinez F, Naunheim K, Piantadosi S, Wise R, Ries A, Weinmann G, Wood DE, National Emphysema Treatment Trial Research Group. A randomized trial comparing lung-volume-reduction surgery with medical therapy for severe emphysema. N Engl J Med. 2003; 348:2059-2073.

8.   Hosenpud JD, Bennett LE, Keck BM, Edwards EB, Novick RJ. Effect of diagnosis on survival benefit of lung transplantation for end-stage lung disease. Lancet. 1998; 351:24-27.

9.   Stavem K, Bjortuft O, Borgan O, Geiran O, Boe J. Lung transplantation in patients with chronic obstructive pulmonary disease in a national cohort is without obvious survival benefit. J Heart Lung Transplant. 2006; 25:75-84.

10. Ingenito EP, Reilly JJ, Mentzer SJ, Swanson SJ, Vin R, Keuhn H, Berger RL, Hoffman A. Bronchoscopic volume reduction: A safe and effective alternative to surgical therapy for emphysema. Am J Respir Crit Care Med. 2001; 164:295-301.

11. Toma TP, Hopkinson NS, Hillier J, Hansell DM, Morgan C, Goldstraw PG, Polkey MI, Geddes DM. Bronchoscopic volume reduction with valve implants in patients with severe emphysema. Lancet. 2003; 361:931-933.

12. Snell GI, Holsworth L, Borrill ZL, Thomson KR, Kalff V, Smith JA, Williams TJ. The potential for bronchoscopic lung volume reduction using bronchial prostheses. Chest. 2003; 124:1073-1080.

13. Yim AP, Hwong TM, Lee TW, Li WW, Lam S, Yeung TK, Hui DS, Ko FW, Sihoe AD, Thung KH, Arifi AA. Early results of endoscopic lung volume reduction for emphysema. J Thorac Cardiovasc Surg. 2004; 127:1564-1573.

14. Venuta F, de Giacomo T, Rendina EA, Ciccone AM, Diso D, Perrone A, Parola D, Anile M, Coloni GF. Bronchoscopic lung-volume reduction with one-way valves in patients with heterogenous emphysema. Ann Thorac Surg. 2005; 79:411-416; discussion 416-417.

15. de Oliveira HG, Macedo-Neto AV, John AB, Jungblut S, Prolla JC, Menna-Barreto SS, Fortis EA. Transbronchoscopic pulmonary emphysema treatment: 1-month to 24-month endoscopic follow-up. Chest. 2006; 130:190-199.

16. Hopkinson NS, Toma TP, Hansell DM, Goldstraw P, Moxham J, Geddes DM, Polkey MI. Effect of bronchoscopic lung volume reduction on dynamic hyperinflation and exercise in emphysema. Am J Respir Crit Care Med. 2005; 171:453-460.

17. Wan IY, Toma TP, Geddes DM, Snell G, Williams T, Venuta F, Yim AP. Bronchoscopic lung volume reduction for end-stage emphysema: Report on the first 98 patients. Chest. 2006; 129:518-526.

18. Sciurba FC, Ernst A, Herth FJ, Strange C, Criner GJ, Marquette CH, Kovitz KL, Chiacchierini RP, Goldin J, McLennan G, Group VSR. A randomized study of endobronchial valves for advanced emphysema. N Engl J Med. 2010; 363:1233-1244.

19. Herth FJ, Noppen M, Valipour A, Leroy S, Vergnon JM, Ficker JH, Egan JJ, Gasparini S, Agusti C, Holmes-Higgin

D, Ernst A, International VENT Study Group. Efficacy predictors of lung volume reduction with Zephyr valves in a European cohort. Eur Respir J. 2012; 39:1334-1342.

20. Valipour A, Herth FJ, Burghuber OC, Criner G, Vergnon JM, Goldin J, Sciurba F, Ernst A, VENT Study Group. Target lobe volume reduction and COPD outcome measures after endobronchial valve therapy. Eur Respir J. 2014; 43:387-396.

21. Hopkinson NS, Kemp SV, Toma TP, Hansell DM, Geddes DM, Shah PL, Polkey MI. Atelectasis and survival after bronchoscopic lung volume reduction for COPD. Eur Respir J. 2011; 37:1346-1351.

22. Venuta F, Anile M, Diso D, Carillo C, De Giacomo T, D'Andrilli A, Fraioli F, Rendina EA, Coloni GF. Long-term follow-up after bronchoscopic lung volume reduction in patients with emphysema. Eur Respir J. 2012; 39:1084-1089.

23. Sterman DH, Mehta AC, Wood DE, *et al*. A multicenter pilot study of a bronchial valve for the treatment of severe emphysema. Respiration. 2010; 79:222-233.

24. Ninane V, Geltner C, Bezzi M, *et al*. Multicentre European study for the treatment of advanced emphysema with bronchial valves. Eur Respir J. 2012; 39:1319-1325.

25. Wood DE, Nader DA, Springmeyer SC, *et al*. The IBV Valve trial: A multicenter, randomized, double-blind trial of endobronchial therapy for severe emphysema. J Bronchology Interv Pulmonol. 2014; 21:288-297.

26. Eberhardt R, Gompelmann D, Schuhmann M, Heussel CP, Herth FJ. Complete unilateral *vs* partial bilateral endoscopic lung volume reduction in patients with bilateral lung emphysema. Chest. 2012; 142:900-908.

27. Kohn HN. Zur Histologie des indurierenden fibrinösen Pneumonie. Münch Med Wochenschr 1893; 40:42-45.

28. Lambert MW. Accessory bronchiolealveolar communications. J Pathol Bacteriol. 1955; 70:311-314.

29. Martin HB. Respiratory bronchioles as the pathway for collateral ventilation. J Appl Physiol. 1966; 2:1443-1447.

30. Gompelmann D, Eberhardt R, Herth FJ. Collateral ventilation. Respiration. 2013; 85:515-520.

31. Davey C, Zoumot Z, Jordan S, McNulty WH, Carr DH, Hind MD, Hansell DM, Rubens MB, Banya W, Polkey MI, Shah PL, Hopkinson NS. Bronchoscopic lung volume reduction with endobronchial valves for patients with heterogeneous emphysema and intact interlobar fissures (the BeLieVeR-HIFi study): A randomised controlled trial. Lancet. 2015; 386:1066-1073.

32. Koenigkam-Santos M, Puderbach M, Gompelmann D, Eberhardt R, Herth F, Kauczor HU, Heussel CP. Incomplete fissures in severe emphysematous patients evaluated with MDCT: Incidence and interobserver agreement among radiologists and pneumologists. Eur J Radiol. 2012; 81:4161-4166.

33. van Rikxoort EM, Goldin JG, Galperin-Aizenberg M, Abtin F, Kim HJ, Lu P, van Ginneken B, Shaw G, Brown MS. A method for the automatic quantification of the completeness of pulmonary fissures: Evaluation in a database of subjects with severe emphysema. Eur Radiol. 2012; 22:302-309.

34. Schuhmann M, Raffy P, Yin Y, Gompelmann D, Oguz I, Eberhardt R, Hornberg D, Heussel CP, Wood S, Herth FJ. Computed tomography predictors of response to endobronchial valve lung reduction treatment: Comparison with Chartis. Am J Respir Crit Care Med. 2015; 191:767-774.

35. Gompelmann D, Eberhardt R, Michaud G, Ernst A, Herth

FJ. Predicting atelectasis by assessment of collateral ventilation prior to endobronchial lung volume reduction: A feasibility study. Respiration. 2010; 80:419-425.

36. Herth FJ, Eberhardt R, Gompelmann D, Ficker JH, Wagner M, Ek L, Schmidt B, Slebos DJ. Radiological and clinical outcomes of using Chartis to plan endobronchial valve treatment. Eur Respir J. 2013; 41:302-308.

37. Shah PL, Herth FJ. Dynamic expiratory airway collapse and evaluation of collateral ventilation with Chartis. Thorax. 2014; 69:290-291.

38. Gompelmann D, Eberhardt R, Slebos DJ, Brown MS, Abtin F, Kim HJ, Holmes-Higgin D, Radhakrishnan S, Herth FJ, Goldin J. Diagnostic performance comparison of the Chartis System and high-resolution computerized tomography fissure analysis for planning endoscopic lung volume reduction. Respirology. 2014; 19:524-530.

39. Klooster K, ten Hacken NH, Hartman JE, Kerstjens HA, van Rikxoort EM, Slebos DJ. Endobronchial valves for emphysema without interlobar collateral ventilation. N Engl J Med. 2015; 373:2325-2335.

40. de Oliveira HG, de Oliveira SM, Rambo RR, de Macedo Neto AV. Fissure integrity and volume reduction in emphysema: A retrospective study. Respiration. 2016; 91:471-479.

41. Thomsen C, Theilig D, Herzog D, Poellinger A, Doellinger F, Schreiter N, Schreiter V, Schurmann D, Temmesfeld-Wollbrueck B, Hippenstiel S, Suttorp N, Hubner RH. Lung perfusion and emphysema distribution affect the outcome of endobronchial valve therapy. Int J Chron Obstruct Pulmon Dis. 2016; 11:1245-1259.

42. Liberator C, Shenoy K, Marchetti N, Criner G. The role of lobe selection on FEV_1 response in endobronchial valve therapy. COPD. 2016; 13:477-482.

43. Eberhardt R, Herth FJ, Radhakrishnan S, Gompelmann D. Comparing clinical outcomes in upper versus lower lobe endobronchial valve treatment in severe emphysema. Respiration. 2015; 90:314-320.

44. Matsuo K, Iwano S, Okada T, Koike W, Naganawa S. 3D-CT lung volumetry using multidetector row computed tomography: Pulmonary function of each anatomic lobe. J Thorac Imaging. 2012; 27:164-170.

45. Kitano M, Iwano S, Hashimoto N, Matsuo K, Hasegawa Y, Naganawa S. Lobar analysis of collapsibility indices to assess functional lung volumes in COPD patients. Int J Chron Obstruct Pulmon Dis. 2014; 9:1347-1356.

46. Herzog D, Hippenstiel S, Schürmann D, *et al*. Prevalence of interlobar collateral ventilation in COPD patients. Eur Respir J. 2014; 44 (Suppl 58):3714.

47. Hueper K, Vogel-Claussen J, Parikh MA, *et al*. Pulmonary microvascular blood flow in mild chronic obstructive pulmonary disease and emphysema. The MESA COPD Study. Am J Respir Crit Care Med. 2015; 192:570-580.

48. Harkness LM, Kanabar V, Sharma HS, Westergren-Thorsson G, Larsson-Callerfelt AK. Pulmonary vascular changes in asthma and COPD. Pulm Pharmacol Ther. 2014; 29:144-155.

49. Santos S, Peinado VI, Ramírez J, Melgosa T, Roca J, Rodriguez-Roisin R, Barberà JA. Characterization of pulmonary vascular remodelling in smokers and patients with mild COPD. Eur Respir J. 2002; 19:632-638.

50. Chandra D, Lipson DA, Hoffman EA, Hansen-Flaschen J, Sciurba FC, Decamp MM, Reilly JJ, Washko GR, National Emphysema Treatment Trial Research Group. Perfusion scintigraphy and patient selection for lung volume reduction surgery. Am J Respir Crit Care Med. 2010; 182:937-946.

51. Pizarro C, Ahmadzadehfar H, Essler M, Fimmers R, Nickenig G, Skowasch D. Volumetric and scintigraphic changes following endoscopic lung volume reduction. Eur Respir J. 2015; 45:262-265.

52. Pizarro C, Ahmadzadehfar H, Essler M, Tuleta I, Fimmers R, Nickenig G, Skowasch D. Effect of endobronchial valve therapy on pulmonary perfusion and ventilation distribution. PLoS One. 2015; 10:e0118976.

53. Brown MS, Kim HJ, Abtin FG, Strange C, Galperin-Aizenberg M, Pais R, Da Costa IG, Ordookhani A, Chong D, Ni C, McNitt-Gray MF, Tashkin DP, Goldin JG. Emphysema lung lobe volume reduction: Effects on the ipsilateral and contralateral lobes. Eur Radiol. 2012; 22:1547-1555.

54. Argula RG, Strange C, Ramakrishnan V, Goldin J. Baseline regional perfusion impacts exercise response to endobronchial valve therapy in advanced pulmonary emphysema. Chest. 2013; 144:1578-1586.

55. Gompelmann D, Herth FJ, Slebos DJ, Valipour A, Ernst A, Criner GJ, Eberhardt R. Pneumothorax following endobronchial valve therapy and its impact on clinical outcomes in severe emphysema. Respiration. 2014; 87:485-491.

56. Herzog D, Poellinger A, Doellinger F, Schuermann D, Temmesfeld-Wollbrueck B, Froeling V, Schreiter NF, Neumann K, Hippenstiel S, Suttorp N, Hubner RH. Modifying post-operative medical care after EBV implant may reduce pneumothorax incidence. PLoS One. 2015; 10:e0128097.

57. Valipour A, Slebos DJ, de Oliveira HG, Eberhardt R, Freitag L, Criner GJ, Herth FJ. Expert statement: Pneumothorax associated with endoscopic valve therapy for emphysema--potential mechanisms, treatment algorithm, and case examples. Respiration. 2014; 87:513-521.

58. Fiorelli A, D'Andrilli A, Anile M, Diso D, Poggi C, Polverino M, Failla G, Venuta F, Rendina EA, Santini M. Sequential bilateral bronchoscopic lung volume reduction with one-way valves for heterogeneous emphysema. Ann Thorac Surg. 2016; 102:287-294.

59. Klooster K, Ten Hacken NH, Slebos DJ. The lung volume reduction coil for the treatment of emphysema: A new therapy in development. Expert Rev Med Devices. 2014; 11:481-489.

60. Herth FJ, Eberhard R, Gompelmann D, Slebos DJ, Ernst A. Bronchoscopic lung volume reduction with a dedicated coil: A clinical pilot study. Ther Adv Respir Dis. 2010; 4:225-231.

61. Slebos DJ, Klooster K, Ernst A, Herth FJ, Kerstjens HA. Bronchoscopic lung volume reduction coil treatment of patients with severe heterogeneous emphysema. Chest. 2012; 142:574-582.

62. Deslee G, Klooster K, Hetzel M, Stanzel F, Kessler R, Marquette CH, Witt C, Blaas S, Gesierich W, Herth FJ, Hetzel J, van Rikxoort EM, Slebos DJ. Lung volume reduction coil treatment for patients with severe emphysema: A European multicentre trial. Thorax. 2014; 69:980-986.

63. Klooster K, Ten Hacken NH, Franz I, Kerstjens HA, van Rikxoort EM, Slebos DJ. Lung volume reduction coil treatment in chronic obstructive pulmonary disease patients with homogeneous emphysema: A prospective feasibility trial. Respiration. 2014; 88:116-125.

64. Shah PL, Zoumot Z, Singh S, Bicknell SR, Ross ET,

Quiring J, Hopkinson NS, Kemp SV. Endobronchial coils for the treatment of severe emphysema with hyperinflation (RESET): A randomised controlled trial. Lancet Respir Med. 2013; 1:233-240.

65. Zoumot Z, Kemp SV, Singh S, Bicknell SR, McNulty WH, Hopkinson NS, Ross ET, Shah PL. Endobronchial coils for severe emphysema are effective up to 12 months following treatment: Medium term and cross-over results from a randomised controlled trial. PLoS One. 2015; 10:e0122656.

66. Deslee G, Mal H, Dutau H, *et al*. Lung volume reduction coil treatment *vs*. usual care in patients with severe emphysema: The REVOLENS Randomized Clinical Trial. JAMA. 2016; 315:175-184.

67. Sciurba FC, Criner GJ, Strange C, *et al*. Effect of endobronchial coils *vs*. usual care on exercise tolerance in patients with severe emphysema: The RENEW Randomized Clinical Trial. JAMA. 2016; 315:2178-2189.

68. Gompelmann D, Heussel CP, Eberhardt R, Snell G, Hopkins P, Baker K, Witt C, Valipour A, Wagner M, Stanzel F, Egan J, Ernst A, Kesten S, Herth FJ. Efficacy of bronchoscopic thermal vapor ablation and lobar fissure completeness in patients with heterogeneous emphysema. Respiration. 2012; 83:400-406.

69. Snell G, Herth FJ, Hopkins P, Baker KM, Witt C, Gotfried MH, Valipour A, Wagner M, Stanzel F, Egan JJ, Kesten S, Ernst A. Bronchoscopic thermal vapour ablation therapy in the management of heterogeneous emphysema. Eur Respir J. 2012; 39:1326-1333.

70. Gompelmann D, Eberhardt R, Ernst A, Hopkins P, Egan J, Stanzel F, Valipour A, Wagner M, Witt C, Baker KM, Gotfried MH, Kesten S, Snell G, Herth FJ. The localized inflammatory response to bronchoscopic thermal vapor ablation. Respiration. 2013; 86:324-331.

71. Henne E, Kesten S, Herth FJ. Evaluation of energy in heated water vapor for the application of lung volume reduction in patients with severe emphysema. Respiration. 2013; 85:493-499.

72. Herth FJ, Valipour A, Shah PL, *et al*. Segmental volume reduction using thermal vapour ablation in patients with severe emphysema: 6-month results of the multicentre, parallel-group, open-label, randomised controlled STEP-UP trial. Lancet Respir Med. 2016; 4:185-193.

73. Magnussen H, Kramer MR, Kirsten AM, Marquette C, Valipour A, Stanzel F, Bonnet R, Behr J, Fruchter O, Refaely Y, Eberhardt R, Herth FJ. Effect of fissure integrity on lung volume reduction using a polymer sealant in advanced emphysema. Thorax. 2012; 67:302-308.

74. Herth FJ, Gompelmann D, Stanzel F, Bonnet R, Behr J, Schmidt B, Magnussen H, Ernst A, Eberhardt R. Treatment of advanced emphysema with emphysematous lung sealant (AeriSeal®). Respiration. 2011; 82:36-45.

75. Refaely Y, Dransfield M, Kramer MR, Gotfried M, Leeds W, McLennan G, Tewari S, Krasna M, Criner GJ. Biologic lung volume reduction therapy for advanced homogeneous emphysema. Eur Respir J. 2010; 36:20-27.

76. Kramer MR, Refaely Y, Maimon N, Rosengarten D, Fruchter O. Bilateral endoscopic sealant lung volume reduction therapy for advanced emphysema. Chest. 2012; 142:1111-1117.

77. Kramer MR, Refaely Y, Maimon N, Rosengarten D, Fruchter O. Two-year follow-up in patients treated with emphysematous lung sealant for advanced emphysema. Chest. 2013; 144:1677-1680.

78. Come CE, Kramer MR, Dransfield MT, *et al*. A randomised trial of lung sealant versus medical therapy for advanced emphysema. Eur Respir J. 2015; 46:651-662.

79. Choong CK, Cardoso PF, Sybrecht GW, Cooper JD. Airway bypass treatment of severe homogeneous emphysema: Taking advantage of collateral ventilation. Thorac Surg Clin. 2009; 19:239-245.

80. Cardoso PF, Snell GI, Hopkins P, Sybrecht GW, Stamatis G, Ng AW, Eng P. Clinical application of airway bypass with paclitaxel-eluting stents: Early results. J Thorac Cardiovasc Surg. 2007; 134:974-981.

81. Shah PL, Slebos DJ, Cardoso PFG, Cetti E, Voelker K, Levine B, Russell ME, Goldin J, Brown M, Cooper JD, Sybrecht GW. Bronchoscopic lung-volume reduction with Exhale airway stents for emphysema (EASE trial): Randomised, sham-controlled, multicentre trial. Lancet. 2011; 378:997-1005.

82. Shah PL, Herth FJ. Current status of bronchoscopic lung volume reduction with endobronchial valves. Thorax. 2014; 69:280-286.

83. Eberhardt R, Gompelmann D, Herth FJ, Schuhmann M. Endoscopic bronchial valve treatment: Patient selection and special considerations. Int J Chron Obstruct Pulmon Dis. 2015; 10:2147-2157.

Original Article

Proteomic characterization of histone variants in the mouse testis by mass spectrometry-based top-down analysis

Ho-Geun Kwak[1,2], Naoshi Dohmae[1,2,*]

[1] *Biomolecular Characterization Unit, RIKEN Center for Sustainable Resource Science, Hirosawa, Wako, Japan;*
[2] *Graduate School of Science and Engineering, Saitama University, Saitama, Japan.*

Summary	Various histones, including testis-specific histones, exist during spermatogenesis and some of them have been reported to play a key role in chromatin remodeling. Mass spectrometry (MS)-based characterization has become the important step to understand histone structures. Although individual histones or partial histone variant groups have been characterized, the comprehensive analysis of histone variants has not yet been conducted in the mouse testis. Here, we present the comprehensive separation and characterization of histone variants from mouse testes by a top-down approach using MS. Histone variants were successfully separated on a reversed phase column using high performance liquid chromatography (HPLC) with an ion-pairing reagent. Increasing concentrations of testis-specific histones were observed in the mouse testis and some somatic histones increased in the epididymis. Specifically, the increase of mass abundance in H3.2 in the epididymis was inversely proportional to the decrease in H3t in the testis, which was approximately 80%. The top-down characterization of intact histone variants in the mouse testis was performed using LC-MS/MS. The masses of separated histone variants and their expected post-translation modifications were calculated by performing deconvolution with information taken from the database. TH2A, TH2B and H3t were characterized by MS/MS fragmentation. Our approach provides comprehensive knowledge for identification of histone variants in the mouse testis that will contribute to the structural and functional research of histone variants during spermatogenesis.

Keywords: Testis-specific histones, top-down analysis, mass spectrometry

1. Introduction

Several histones have been detected in mammalian testes and testis-specific variants are specifically and highly expressed during spermatogenesis (*1-3*). Testis-specific histones (H1t, TH2A, TH2B, and H3t) are related to dynamic chromatin remodeling during the histone-to-transitional protein stage as well as their functional roles, such as fertility (*1-3*). For example, our recent study indicated that the lack of Th2a and Th2b encoding TH2A and TH2B, respectively, resulted in sterility in male mice, and the loss of TH2A and TH2B was linked

with cohesion release and histone replacement during spermatogenesis (*4*). Additionally, linker testis-specific histone H1t revealed that there was no influence on male mice fertility (*5*). There is some evidence that testis-specific histone H1t and H3t are linked with chromatin remodeling during spermatogenesis, but further research to investigate the relationship with testis-specific histone variants such as H3t is still needed (*3*).

Studies for characterization of testis-specific histones are essential to trace epigenetic activities of histone variants. Some studies on the characterization of individual testis-specific histones during spermatogenesis have been reported. Lu *et al*. discovered the mass value for TH2B from mice as well as those for different TH2B post-translational modifications (PTMs) present during spermatogenesis using Liquid chromatography (LC)-mass spectrometry (MS) with trypsin digestion (*6*). Additionally, studies have reported that LC-MS enabled characterization of TH2B expression patterns during mouse spermatogenesis (*4,7*). However, research

involving MS-based characterization of histone variants in mouse testes is limited in comparison to functional studies. The elucidation of comprehensive analytical approaches for functional research into testis-specific histone variants is imperative.

MS-based proteomic analysis has become a universal and powerful tool enabling the characterization of peptides and proteins. This method has conventionally relied upon a bottom-up strategy due to its excellent sensitivity. However, the digestion processes associated with active enzymes hinder extensive characterization of intact proteins, resulting in the loss of significant information pertaining to the sequencing of histone proteins due to the availability of only extremely short peptide sequences. For this reason, a top-down technique that enables characterization of intact proteins is used (8-11). LC in top-down strategies is generally utilized for the separation of intact proteins using reversed phase (RP) columns (C4, C8, and C18). In particular, columns designed for shorter alkyl groups are traditionally used in top-down approaches due to the intensive nature of the recovery techniques (8,10). Improvements in methods addressing the technical and structural challenges for relationships to intact-protein separation are feasible and necessary for the development of analytical sensitivity in columns (10,12). Likewise, ion-pairing reagents, such as trifluoroacetic acid (TFA), pentafluoropropionic acid, and heptafluorobutyric acid (HFBA), are useful in reducing the hydrophilicity of proteins and peptides through interactions with anions, resulting in enhanced resolution of RP columns. Shibue et al. reported that the efficiency of peptide separation was enhanced by strengthening the hydrophobicity of the reagent. Specifically, HFBA showed the most sensitive and intensive signals in results from RP chromatography when compared with other ion-pairing reagents (13).

Here, we report the comprehensive characterization of histone variants in mouse testes by MS-based proteomic analysis. The separation of histone variants in the mouse testis was performed by HPLC on the RP-column with HFBA as ion-pairing reagent. The top-down characterization of intact histone variants in the mouse testis was performed by LC-MS. Masses of separated histone variants and their expected PTMs were calculated by deconvolution based on the database. TH2A, TH2B and H3t were characterized by MS/MS fragmentation.

2. Materials and Methods

2.1. Materials

Trichloroacetic acid (TCA), hydrochloric acid (HCl), potassium chloride (KCl) magnesium acetate $(Mg(CH_3COO)_2)$ and dithiothreitol (DTT) were purchased from Wako Pure Chemicals (Osaka, Japan). Trizma base was from Sigma-Aldrich (St Luis, MO,

USA) and sulfuric acid (H_2SO_4) was obtained from Junsei Chemical Co. (Tokyo, Japan). HFBA (Thermo-Fisher Scientific, Waltham, MA, USA), TFA (Merck, Darmstadt, Germany) and acetonitrile (Thermo-Fisher Scientific, Waltham, MA, USA) were of HPLC reagent grade.

2.2. Extraction of histones from mouse testes

Mouse (BALB/c) testes combined with epididymides were purchased from Funakoshi Co. (Tokyo, Japan), and were homogeniged following separation. Whole histones in testis and epididymis were extracted using the TCA-precipitation method with minor modifications (14). In brief, all steps were carried out at 4°C. Testis (49.1 mg) and epididymis (50.4 mg) were suspended in hypertonic lysis buffer [10 mM Tris-Cl (pH 8.0), containing 1 mM KCl, 1.5 mM $Mg(CH_3COO)_2$, 1 mM DTT, and protease inhibitors] and then incubated for 30 min. Lysed cells were pelleted by centrifugation at 10,000× g for 10 min, re-suspended in 0.4 N H_2SO_4, and incubated for 30 min. To collect the supernatant containing histones, the nuclear debris in these samples was purified by centrifugation at 16,000× g for 10 min and the supernatant was precipitated by TCA and incubated for 30 min. The precipitated samples were pelleted by centrifugation at 16,000 × g for 10 min. After washing with acetone and drying at room temperature, samples were mixed with 100 μL MilliQ water.

2.3. Separation of histone variants

Histones, including testis histones, were separated by an Agilent 1100 series HPLC (Agilent Technologies, Snata Clara, CA, USA) using a WP300 C4 column (2.0 mm × 15.0 mm, 3-μm particle size; GL sciences, Tokyo, Japan) at room temperature. A 20-μL sample was injected and detected at a UV wavelength of 215 nm. HFBA was used as an ion-pairing reagent. The mobile phase A (5% acetonitrile with 0.1% HFBA) and B (90% acetonitrile with 0.1% HFBA) were delivered at a flow rate of 0.1 mL/min using the following gradient parameters: 0 min (to 5 min, 15% solvent B); 5 min (to 15 min, 15-48% solvent B); 15 min (to 25 min, 48% solvent B); 25 min (to 100 min, 48-62% solvent B); 100 min (to 120 min, 62-100% solvent B); 120 min (to 130 min, 100% solvent B); 130 min (to 135 min, 100-15% solvent B); 135 min (to 145 min, 15% solvent B). The fraction collector (Gilson, Middleton, WI, USA) was programmed to collect fractions at 1-min intervals from 30 min to 116 min.

2.4. Top-down analysis

Separated histones were analyzed by a Q-Exactive mass spectrometer (Thermo-Fisher Scientific, Bremen, Germany) using a linear gradient of 0-100% solvent
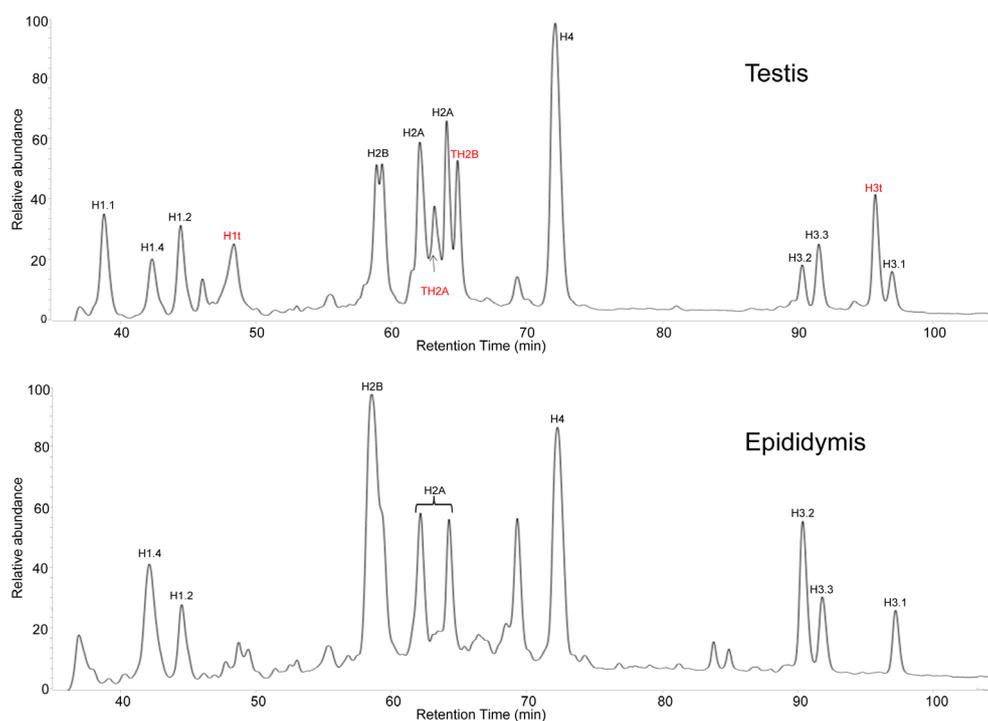
Figure 1. Chromatograms of histones in the mouse testis and epididymis. Histones from mouse testis (top) and epididymis (bottom) were separated using a C4 RP column with HFBA. Each signal was identified by PMF in advance (see Supporting Information).

B over 30 min (solvent A: 0.1% TFA; solvent B: 80% acetonitrile with 0.1% TFA). A flow rate of 300 nL/min was used with a 100 μm × 12 cm silica capillary column in-house packed with InertSustainSwift C18 (3-μm particle size; GL sciences, Tokyo, Japan). MS was directed using Xcalibur software version 3.0.63 (Thermo-Fisher Scientific, Bremen, Germany). A nanoelectrospray (Thermo-Fisher Scientific, Bremen, Germany) was applied with a 1.9 kV spray voltage and a capillary temperature of 275°C. MS data were obtained in the range of 400-2,000 *m/z* with a resolution of 35,000 (at 400 *m/z*). Q-Exactive data were deconvoluted using software (Thermo-Fisher Scientific, Bremen, Germany). MS/MS analysis was performed by higher-energy collisional dissociation (HCD) fragmentation. Three or four precursor ions representing the most abundant charge states were targeted in HCD mode from MS spectra. Precursor ion mass spectra were collected in the range of 400-2,000 *m/z* with a resolution of 70,000 (at 400 *m/z*).

2.4. *Data analysis*

Each histone variant fraction was identified by peptide-mass fingerprinting (PMF) in advance (Supporting Information). The sequences of histone variants and their modifications were searched against a database (NCBInr) and another study for H3t (*15*). Theoretical masses and MS/MS fragments were accomplished using the GPMAW 6.1 software (Lighthouse data, Odense, Denmark) and MS/MS spectra of TH2A,

TH2B and H3t were manually characterized. The mass values of histone variants with their modifications from MS spectra were calculated by deconvolution software (Protein deconvolution version 3.0, Thermo-Fisher Scientific, Bremen, Germany) with the following conditions; a resolution of 35,000 in the range of 400-2,000 *m/z* (at 400 *m/z*) and S/N threshold of 3.

3. Results

3.1. *Separation of histone variants by ion-pairing chromatography*

Figure 1 shows chromatograms of separated histones from mouse testis and epididymis. Several histones were separated from the sample on the WP300 C4 column using HFBA as an ion-pairing reagent. Separated fractions were identified by PMF in advance and data was searched against a protein database search (NCBInr) using the MASCOT search engine (Supplementary Table 1, see Supporting Information, *http://www.biosciencetrends. com/docindex.php?year=2016&kanno=5*). Here, we successfully separated each histone from the mouse testis and epididymis using an RP column with HFBA. We observed testis-specific histones in mouse testis; however, their concentrations were undetectable in the epididymis (Figure 1). Some somatic histone variants were increased in the epididymis. Specifically, signals denoting H2B and H3.2 remarkably increased in the epididymis as compared with the deficient levels of TH2B and H3t from the testis (Figure 1). The loss of H3t

in the mouse testis was compensated by somatic histone H3 variants in the epididymis (Figure 1 and Table 1). Interestingly, H3.2 mainly showed the proportional offset as 79.1% in the epididymis, as compared to H3t deficiency from the mouse testis (Table 1). In our results, we isolated H1t along with other H1 variants (H1.1, H1.2, and H1.4) from mouse testis. Additionally, H1.1 and H1t deficiency and increased levels of H1.4 were observed (Figure 1).

3.2. *MS-based identification of intact histone variants*

Separated intact histone variants from the mouse testis

Table 1. Quantification of H3 variants based on areas of peaks

Histone	Areas (Average ± S.D., %)	
	Testis	Epididymis
H3.2	16.5 ± 1.0	52.9 ± 0.2
H3.3	22.6 ± 0.04	26.5 ± 0.4
H3t	46.0 ± 0.8	ND
H3.1	14.8 ± 0.2	20.5 ± 0.3

ND: Not detected; Areas of H3 variants were calculated from the integrated peaks on chromatograms and were expressed as percentages relative to the total peak area. The data is shown as averages with SD (*n* = 3). H3.2 was mainly compensated in the epididymis as approximately 80% in comparison with the loss of H3t in the testis.

and epididymis were identified by a Q-Exactive mass spectrometer, followed by deconvolution of the data. Table 2 displays the list of somatic and testis-specific histones from the mouse testis. The observed masses of the intact histones were compared with their theoretical masses, which matched their known sequences and expected PTMs. Our results indicated that the deconvoluted masses of four testis-specific histones (H1t, TH2B, TH2A and H3t) were in agreement with their theoretical masses (~0.11 Da). Additionally, the monoisotopic masses of somatic histones from the mouse testis, such as, H2B variants (H2B1F, H2B1B, and H2B1C), H2A variants (H2A1, H2A2A, H2A3, H2A.X, and H2A.Z), H3 variants (H3.1, H3.2, and H3.3), and H4, were calculated with accuracy (Table 2).

We used a Q-Exactive mass spectrometer for the characterization of testis-specific histones (TH2A, TH2B andH3t) with each histone fragmented in HCD mode. Figure 2 shows an example of the TH2B characterization process. Larger masses observed in the MS spectrum were targeted as fragmentation sources. A total of 20 y and b ions associated with TH2B were generated in HCD mode, and these fragmented ions were matched in the MS/MS spectrum with the TH2B sequence. Similarly, the mapping of other testis-specific histones was conducted from the HCD fragmentation of precursor ions in the range of 400 *m/z*
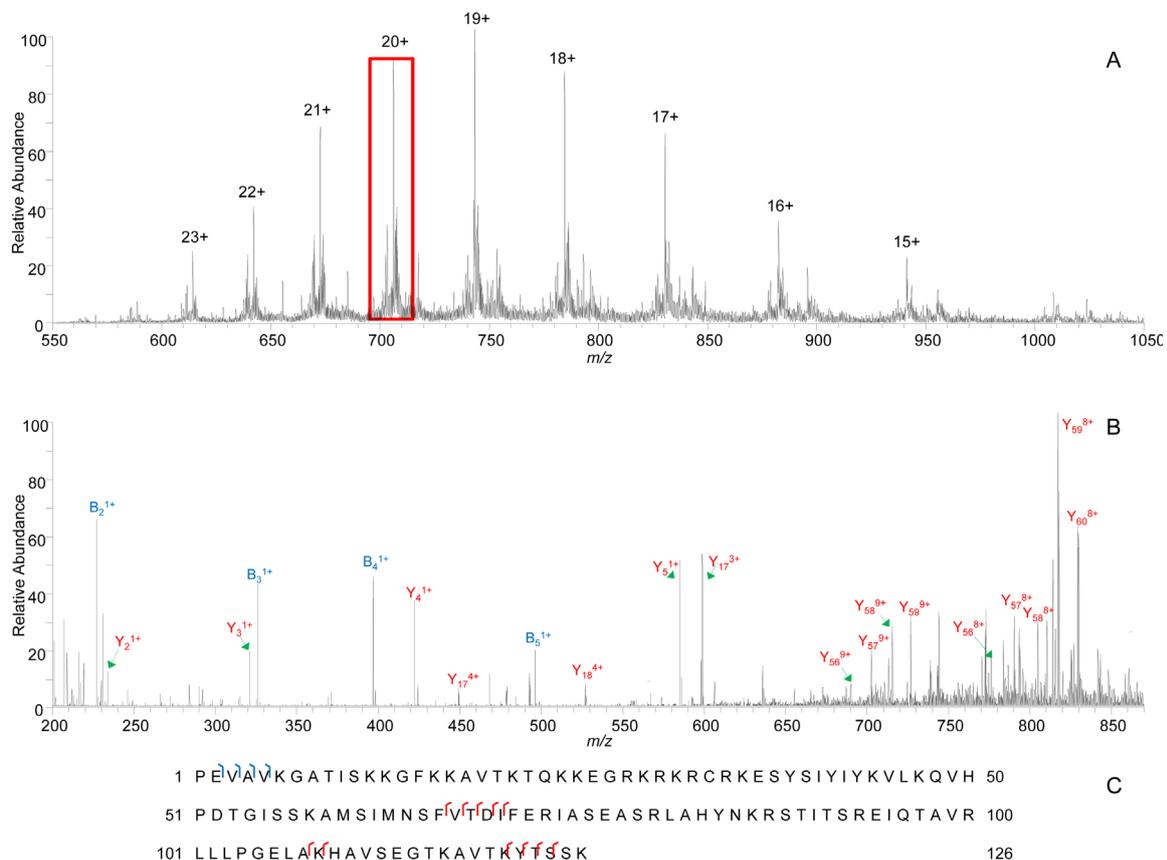

Figure 2. Top-down MS-based characterization of TH2B from mouse testis by HCD fragmentation. (A) MS spectrum of TH2B. Major precursor ions were targeted for MS/MS analysis. **(B)** HCD spectrum of precursor ions (z = 20) with matching b and y fragments. **(C)** Mapping HCD fragments of TH2B at the 20+ charge state.

Table 2. List of histone variant masses in the mouse testis

Histones	Accession	PTMs	Theoretical mass (Da)	Observed mass (Da)	ΔDa
H1t	Q07133	N-terminal acetylation	21438.12	21438.19	0.07
H2B1F	P10853	None	13796.53	13796.56	0.03
H2B1B	Q64475	None	13812.52	13812.55	0.03
H2B1C	Q6ZWY9	None	13766.52	13766.54	0.02
TH2B	P70696	None	14096.71	14096.79	0.08
H2A1	P22752	N-terminal acetylation	14037.92	14037.95	0.03
H2A2A	Q6GSS7	N-terminal acetylation	13997.86	13997.89	0.03
H2A3	Q8BFU2	N-terminal acetylation	14023.90	14023.92	0.02
H2A.Z	P0C0S6	None	13413.51	13413.48	0.03
H2A.X	P27661	N-terminal acetylation	15044.41	15044.44	0.03
TH2A	Q8CGP4	N-terminal acetylation	13958.83	13958.86	0.03
H4	P62806	N-terminal acetylation, Dimethylation	11299.38	11299.42	0.04
H3.1	P68433	5 methylation	15333.52	15333.63	0.11
H3.2	P84228	5 methylation	15317.54	15317.65	0.11
H3.3	P84244	4 methylation	15243.52	15243.64	0.12
H3t	·	4 methylation	15344.49	15344.60	0.11

Theoretical masses were calculated by the software based on reported sequence and their PTMs from the database and another study (H3t) (*15*). Observed masses are displayed as the most abundant form from the deconvoluted MS spectra.
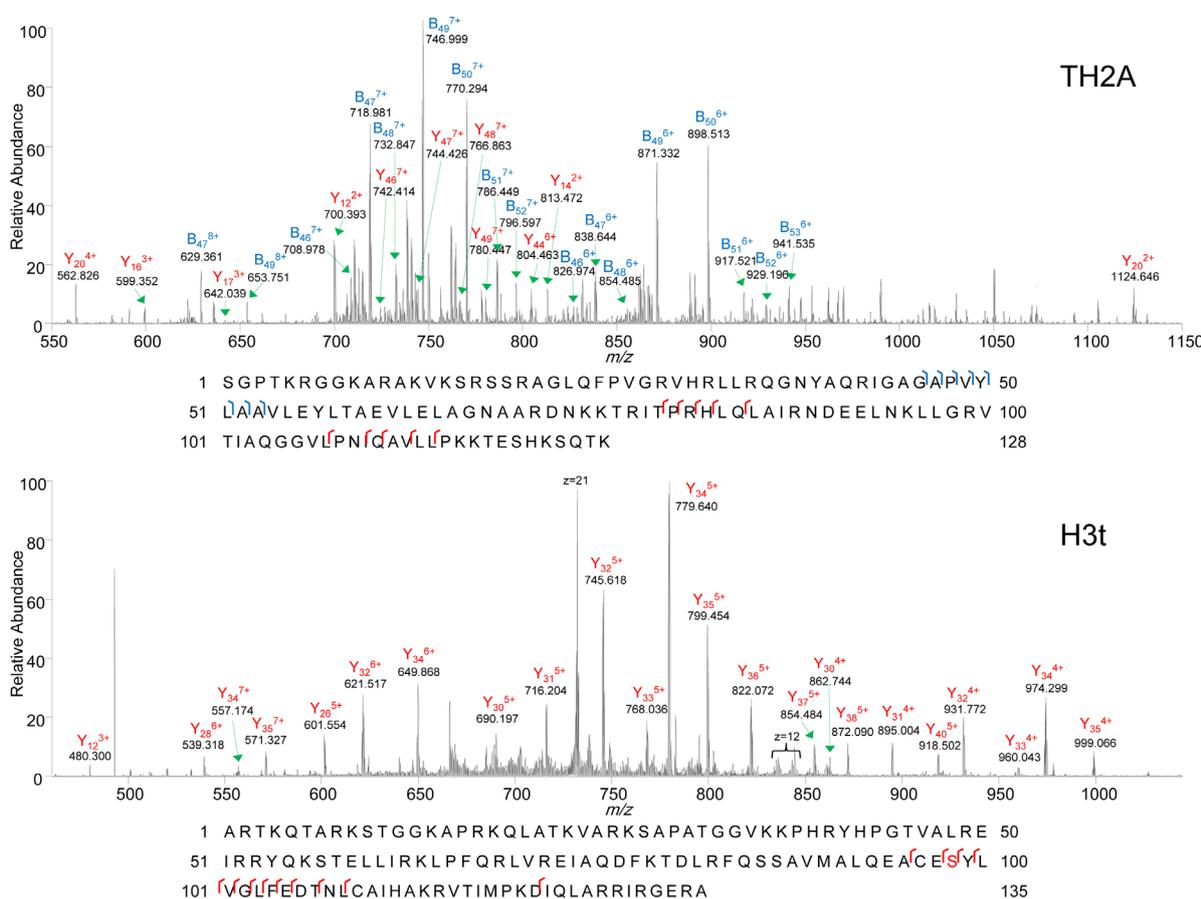

Figure 3. The mass spectra and sequences of TH2A and H3t. TH2A and H3t were characterized by HCD fragmentation. The sequences of histone variants were searched against the database (NCBInr) and another study (*15*).

to 2,000 *m/z*. Peaks in the 736.11 *m/z* (z = 19) range for TH2A and 732.13 *m/z* (z = 21) for H3t were selected for fragmentation, with the y- and b-ion fragments corresponding to TH2A and H3t sequences (Figure 3). We also found fragments of H1t, which were in agreement with y ions associated with its C-terminal region (data not shown).

3.3. *PTMs of testis-specific histone variants in mouse testis*

Figure 4 shows PTMs of histones in the mouse testis. Histone PTMs were calculated by deconvolution according to the MS spectra and our results revealed specific PTMs (methylation, acetylation and
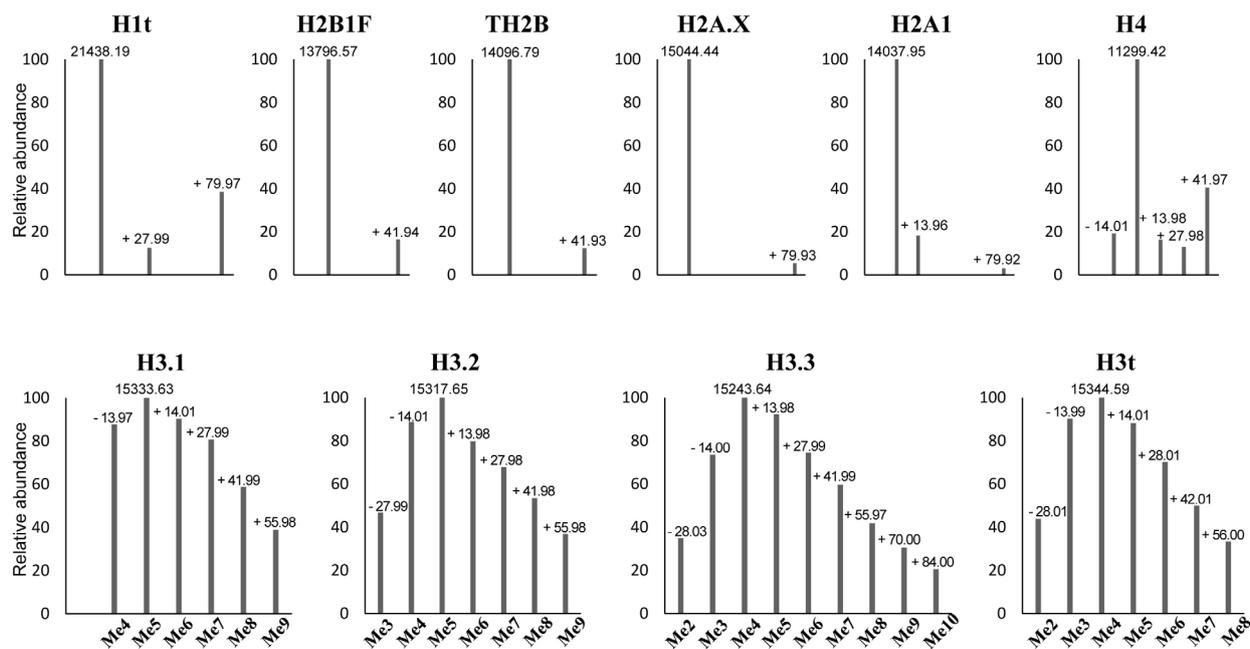
Figure 4. PTMs on histone variants from mouse testis. Me: methylation; The most abundant monoisotopic masses and mass differences were calculated using deconvolution. Acetylated N-termini of H1t, H2A1, H2A.X, and H4 (with dimethlyation) were observed as the most abundant masses. 5 methylated H3.1 and H3.2 and 4 methylated H3.3 and H3t histones were detected as the most abundant monoisotopic masses. +13.96 Da (monomethylation), +27.99 Da (dimethlyation), ~+41.93-+41.97 Da (trimethylation or acetylation), and ~+79.92-+79.97 Da (phosphorylation) were detected on H1t, H2B1F, TH2B, H2A.X, H2A1, and H4. The values of methylation of H4 and H3 variants were counted on the basis of their mass shifts from the most abundant masses. For example, the masses of -13.99 Da and +14.01 Da indicated trimethylation and 5 methlyation in H3t, respectively.

phosphorylation) on somatic and testis-specific histones (Figure 4). Here, we calculated changes in masses of ~13.96-14.01 Da for methylation from H2A1 and H4, ~27.98-27.99 Da for dimethylation from H1t and H4, ~41.93-41.97 for trimethylation or acetylation from H2B1F, TH2B, and H4, and ~79.92-79.97 Da for phosphorylation from H1t, H2A.X and H2A1 in the mouse testis (Figure 4). In addition, higher abundances of methylation were observed in H3 variants (Figure 4). 5 methylated H3.1 and H3.2 and 4 methylated H3.3 and H3t histones were detected as the most abundant monoisotopic masses by deconvolution and other methylations were also observed in H3 variants (Figure 4). The values of methylations of H3 variants were counted on the basis of their mass shifts from the most abundant masses. For example, the masses of -13.99 Da and +14.01 Da indicated trimethylation and 5 methlyation in H3t, respectively (Figure 4).

4. Discussion

Various histone variants as well as their PTMs are related to chromatin remodeling during spermatogenesis (*1-3*). To understand their structural patterns related to chromatin dynamics, an MS-based characterization process is required. Some studies have reported the MS-based characterization on individual histone variants (*4,6,7*). However, it is difficult to find the comprehensive identification of intact histones in the mouse testis. Here, we separated histone variants from the mouse testis and

conformed their replacement patterns in the epididymis. Each separated intact histone was identified using LC-MS/MS. Specifically, we conformed testis-specific histone's sequences by HCD fragmentation.

The separation of histone variants is an essential step for the structural research of histone proteins or their PTMs. We used HFBA as the ion-pairing reagent for histone separation in this study. Ion-pairing reagents play an important role in the RP-column separation of proteins and peptides in accordance with their hydrophobicity by causing interactions with protein side chains. Specifically, HFBA showed the best sensitivity and intensity in peptide-separation results when compared to other ion-pairing reagents (*13,16*). We successfully separated each testis-specific histone in this study. Moreover, our results showed a better separation efficiency, as compared to our previous research when we used TFA as the ion-pairing reagent (*4*).

Testis-specific histones, H1t, TH2A, TH2B and H3t, are abundant in mammalian testes and they gradually decrease during the histone-to-protamine stage by chromatin remodeling (*1-3*). The mouse epididymis is a tube connected to the testis where mature sperm is stored and transported (*2*). In this study, it was used to compare the histone dynamics between the testis and epididymis in mice. We observed the expression of testis-specific histones in the mouse testis and they were undetected in the mouse epididymis. To trace the transformed testis-specific histones as somatic types is also important to understand histone dynamics during spermatogenesis.

H1t is normally observed during spermatogenesis and somatic histone H1 variants are detected in H1t-deficient mice (*2,5,17*). An increased concentration of somatic histone H2B was observed in TH2B knock-out mice during spermatogenesis in our previous research (*4*). Our results showed compensated signals in the epididymis, as compared to the loss of testis-specific histones. Specifically, H3.2 was proportionally offset against the H3t deficiency in the epididymis. Histone H3t is highly expressed during spermatogenesis and observed at lower concentrations in somatic cells (*2,3,18*). However, the level of H3t was not observed in the mouse epididymis in this research. The relationship between H3t and other H3 variants in the testis has not been fully reported. Although further research concerning the compensatory nature of testis-specific histone expression is needed, our results indicating possible correlations between expression levels may provide unique and invaluable insight into the functional roles.

To characterize separated intact testis-specific histones, we used MS-based top-down analysis. Various histones including testis-specific histones and somatic histones coexist in the testis and some variants have similar sequences (*1*). For example, H3t shows only three different amino acids in its sequence in comparison with the canonical H3 (*15*). The MS-based top-down approach is suitable for comprehensive characterization of intact histones because the proteins' sequences and their PTMs are conserved (*8-11,19*). Previous research explored the use of proteomic analysis techniques and MS to identify the mass of TH2B (*4,6,7*); however, the results were not sufficiently comprehensive enough to verify MS-based characterization of testis-specific histones. In this study, we showed comprehensive analysis of histone variants in the mouse testis by the MS-based top-down approach. Additionally, we performed the characterization of testis-specific histones by sequencing using HCD fragmentation. HCD is similar to collision-induced dissociation (CID), and both fragmentation approaches are useful tools for identifying intact proteins with highly similar sequences. Moreover, HCD is more sensitive and allows for higher resolution of results relative to CID (*8,10*). Despite interest in functional and structural research of testis-specific histones, data associated with their MS-based characterization has been ambiguous. Our results presented successful sequence-based characterization of testis-specific histones from mice.

In this study, some PTMs on histone variants in the mouse testis were detected by MS-based top-down characterization. PTMs in male germ cells play a key role in biological activities related to chromatin remodeling, and can be found on histone proteins in the form of methylation, acetylation, phosphorylation, or ubiquitination (*2,3,20*). In particular, various mass shifts were observed from the most abundant monoisotopic masses of the H3 variants. PTMs as +14 Da (monomethylation), +28 Da (dimethylation) and +42 Da

(trimethylation or acetylation) are the general patterns on the N-terminal residues of histone H3 variants (*21*). These PTMs were also detected on H3 variants, including H3t, in our data. Several approaches have been undertaken to understand the novel markers and functions associated with histone PTMs during spermatogenesis (*22-24*). While further research to identify similar modifications (acetylation and trimethylation) and reduce variations between observed and theoretical values is still required, the data presented here provides valuable insight into MS-based characterizations of histone-specific PTMs.

In conclusion, we conducted MS-based top-down analysis to facilitate the comprehensive characterization of histone variants in the mouse testis. Histone variants were successfully separated on a reversed phase column with HFBA. Separated histone variants were characterized by an MS-based top-down approach. In this process, we found four testis-histone variants, H1t, TH2A, TH2B and H3t in the mouse testis when compared to the mouse epididymis and over-expressed H2B and H3 variants were detected in the epididymis. Specifically, approximately 80% of H3.2 was proportionally compensated in the epididymis, as compared to the decreased H3t from the testis. Moreover, our approach showed the masses of PTMs on the histone variant using deconvolution. These results provide information on histone variants in the mouse testis by comprehensive separation and characterization. Our work contributes to the structural and functional research of histone variants in mammalian testes.

Acknowledgements

References

1. Pradeepa MM, Rao RM. Chromatin remodeling during mammalian spermatogenesis: role of testis specific histone variants and transition proteins. Soc Reprod Fertil Suppl. 2007; 63:1-10.
2. Rathke C, Baarends WM, Awe S, Renkawitz-Pohl R. Chromatin dynamics during spermiogenesis. Biochim Biophys Acta. 2014; 1839:155-168.
3. Bao J, Bedford MT. Epigenetic regulation of the histone-to-protamine transition during spermatogenesis. Reproduction. 2016; 151:R55-R70.
4. Shinagawa T, Huynh LM, Takagi T, Tsukamoto D, Tomaru C, Kwak HG, Dohmae N, Noguchi J, Ishii S. Disruption of Th2a and Th2b genes causes defects in spermatogenesis. Development. 2015; 142:1287-1292.
5. Lin Q, Sirotkin A, Skoultchi AI. Normal spermatogenesis in mice lacking the testis-specific linker histone H1t. Mol Cell Biol. 2000; 20:2122-2128.
6. Lu S, Xie YM, Li X, Luo J, Shi XQ, Hong X, Pan YH, Ma X. Mass spectrometry analysis of dynamic post-translational modifications of TH2B during

spermatogenesis. Mol Hum Reprod. 2009; 15:373-378.

7. Montellier E, Boussouar F, Rousseaux S, *et a*l. Chromatin-to-nucleoprotamine transition is controlled by the histone H2B variant TH2B. Genes Dev. 2013; 27:1680-1692.

8. Zhou H, Ning Z, Starr AE, Abu-Farha M, Figeys D. Advancement in top-down proteomics. Anal Chem. 2012; 84:720-734.

9. Soldi M, Bremang M, Bonaldi T. Biochemical systems approaches for the analysis of histone modification readout. Biochim Biophys Acta. 2014; 1839:657-668.

10. Catherman AD, Skinner OS, Kelleher NL. Top down proteomics: facts and perspectives. Biochem Biophys Res Commun. 2014; 445:683-693.

11. Moradian A, Kalli A, Sweredoski MJ, Hess S. The top-down, middle-down, and bottom-up mass spectrometry approaches for characterization of histone variants and their post-translational modifications. Proteomics. 2014; 14:489-497.

12. Capriotti AL, Cavaliere C, Foglia P, Samperi R, Lagana A. Intact protein separation by chromatographic and/or electrophoretic techniques for top-down proteomics. J Chromatogr A. 2011; 1218:8760-8776.

13. Shibue M, Mant CT, Hodges RS. Effect of anionic ion-pairing reagent hydrophobicity on selectivity of peptide separations by reversed-phase liquid chromatography. J Chromatogr A. 2005; 1080:68-75.

14. Shechter D, Dormann HL, Allis DC, Hake SB. Extraction, purification and analysis of histones. Nat Protoc. 2007; 2:1445-1457.

15. Maehara K, Harada A, Sato Y, Matsumoto M, Nakayama KI, Kimura H, Ohkawa Y. Tissue-specific expression of histone H3 variants diversified after species separation. Epigenetics Chromatin. 2015; 8:35.

16. Feteke S, Veuthey JL, Guillarme D. New trends in reversed-phase liquid chromatographic separations of therapeutic peptides and proteins: theory and applications. J Pharm Biomed Anal. 2012; 69:9-27.

17. Drabent B, Saftig P, Bode C, Doenecke D. Spermatogenesis proceeds normally in mice without linker histone H1t. Histochem Cell Biol. 2000; 113:433-442.

18. Tachiwana H, Osakabe A, Kimura H, Kurumizaka H. Nucleosome formation with the testis-specific histone H3 variant, H3t, by human nucleosome assembly proteins *in vitro*. Nucleic Acids Res. 2008; 36:2208-2218.

19. Sidoli S, Lin S, Karch KR, Garcia BA. Bottom-up and middle-down proteomics have comparable accuracies in defining histone post-translational modification relative abundance and stoichiometry. Anal Chem. 2015; 87:3129-3133.

20. Govin J, Caron C, Lestrat C, Rousseaux S, Khochbin S. The role of histones in chromatin remodelling during mammalian spermiogenesis. Eur J Biochem. 2004; 271:3459-3469.

21. Thomas CE, Kelloher NL, Mizzen CA. Mass spectrometric characterization of human histone H3: a bird's eye view. J Proteome Res. 2006; 5:240-247.

22. Pentakota SK, Sandhya S, Sikarwar AP, Chandra N, Satyanarayana Rao MR. Mapping post-translational modifications of mammalian testicular specific histone variant th2b in tetraploid and haploid germ cells and their implications on the dynamics of nucleosome structure. J Proteome Res. 2014; 13:5603-5617.

23. Brunner AM, Nanni P, Mansuy IM. Epigenetic marking of sperm by post-translational modification of histones and protamines. Epigenetics Chromatin. 2014; 7:2.

24. Mishra LN, Gupta N, Rao SM. Mapping of post-translational modifications of spermatid-specific linker histone H1-like protein, HILS1. J Proteomics. 2015; 128:218-230.

Original Article

Polyphosphate-induced matrix metalloproteinase-13 is required for osteoblast-like cell differentiation in human adipose tissue derived mesenchymal stem cells

Nobuaki Ozeki[1],[*], Makio Mogi[2], Naoko Hase[1], Taiki Hiyama[1], Hideyuki Yamaguchi[1], Rie Kawai[1], Kazuhiko Nakata[1]

[1] *Department of Endodontics, School of Dentistry, Aichi Gakuin University, Nagoya, Aichi, Japan;*
[2] *Department of Integrative Education of Pharmacy, School of Pharmacy, Aichi Gakuin University, Nagoya, Aichi, Japan.*

Summary	Inorganic polyphosphate [Poly(P)] induces differentiation of osteoblastic cells. In this study, matrix metalloproteinase (MMP)-13 small interfering RNA (siRNA) was transfected into human adipose tissue-derived mesenchymal stem cells (hAT-MSC) to investigate whether MMP-13 activity induced by Poly(P) is associated with osteogenic differentiation. Real-time quantitative polymerase chain reaction, Western blotting, and an MMP-13 activity assay were used in this study. Poly(P) enhanced expression of mature osteoblast markers, such as osteocalcin (BGLAP) and osteopontin (SPP1), osterix (OSX), and bone sialoprotein (BSP), and increased alkaline phosphatase (ALP) activity and calcification capacity in hAT-MSCs. These cells also developed an osteogenic phenotype with increased expression of Poly(P)-induced expression of MMP-13 mRNA and protein, and increased MMP-13 activity. MMP-13 siRNA potently suppressed the expression of osteogenic biomarkers BGLAP, SPP1, OSX, BSP, and ALP, and blocked osteogenic calcification. Taken together, Poly(P)-induced MMP-13 regulates differentiation of osteogenic cells from hAT-MSCs.

Keywords: Adipose tissue, mesenchymal stem cells, osteogenic cells, matrix metalloproteinase-13

1. Introduction

Inorganic polyphosphate [Poly(P)] is a linear polymer consisting of tens to hundreds of orthophosphate residues linked by high-energy phosphoanhydride bonds. In mammals, Poly(P) is found in erythrocytes and cells of the brain, heart, lungs, and liver (*1-4*). The most researched and well-known role of Poly(P) is in the promotion of intracellular calcification (*5*). Because Poly(P) induces alkaline phosphate (ALP) activity and up-regulates osteocalcin (BGLAP) and osteopontin (SPP1) gene expression (*6*), Poly(P) is thought to play an important role in the maturation of bone-related immature cells, and may be involved in the construction of bone tissue by osteoblasts.

In addition to blood vessels and nerves, fibroblasts are a significant component of dental pulp tissue (*7*) and thus might represent a novel therapeutic target for treatment of pulpitis. We previously reported Poly(P) regulation of differentiation and proliferation in dental pulp fibroblast-like cells (DPFCs) and odontoblast-like cells (*8-10*). Recently, roles of Poly(P) have been suggested in apoptosis and modulation of the mineralization process in bone tissue (*11,12*).

Matrix metalloproteinases (MMPs) play central roles in cell proliferation, migration, differentiation, angiogenesis, apoptosis, and host defenses. Deregulation of MMPs has been implicated in many diseases including rheumatoid arthritis (RA), chronic ulcers, encephalomyelitis, and cancer (*13-15*). MMP-13 is highly overexpressed in pathological situations such as carcinomas, RA, and osteoarthritis (OA). Furthermore, MMP-13 may be involved in articular cartilage turnover and cartilage pathophysiology associated with OA. We previously reported that MMP-13 accelerates bone remodeling following development

of periradicular lesions (*16,17*), and presented evidence suggesting that MMP-13 plays a potentially unique physiological role in wound healing and regeneration of alveolar bone. Because alveolar bone tissue consists predominantly of osteoblasts, these cells may represent a potential target cell type for new therapeutic strategies to mitigate these disease states. Moreover, we have reported that the proinflammatory cytokine interleukin (IL)-1 induces MMP-13 activity in purified osteoblast-like cells derived from human stem cells (*16,17*).

Mesenchymal stem cells (MSCs) are multipotent cells in bone marrow and various other tissues, which are capable of differentiating into osteogenic cells, especially osteoblasts, as well as chondrogenic and adipogenic lineages by culturing in appropriate *in vitro* conditions (*18*). MSCs have been identified in adipose tissue, which are termed adipose tissue-derived MSCs (AT-MSCs) (*19-21*). Compared with bone marrow-derived MSCs (BMSCs), human AT-MSCs are easier to obtain, have relatively lower donor site morbidity, a higher yield at harvest, and can expand more rapidly *in vitro* than BMSCs (*22,23*). Moreover, the proliferation and differentiation potential of AT-MSCs are independent of age (*24,25*). Under appropriate conditions, AT-MSCs can be induced into an osteogenic lineage *in vitro* and can therefore be seeded in proper scaffolds as seed cells to repair bone defects. These advantages suggest that human AT-MSCs are a promising alternative source of seed cells for tissue engineering and regeneration.

We recently established a differentiation method for homogeneous α7 integrin-positive human skeletal muscle stem cell-derived osteoblast-like cells (*26*), and found that IL-1β induces MMP-13-regulated proliferation of these cells (*16,17*). These data suggest that MMP-13 plays a potentially unique physiological role in the regeneration of osteoblast-like cells. We previously reported that Poly(P) induces MMP-3-mediated proliferation of odontoblast-like cells derived from mouse induced pluripotent stem cells (*9*). Although it is known that Poly(P) induces differentiation of osteoblastic cells, the detailed mechanism of Poly(P)-induced differentiation in AT-MSCs remains to be elucidated.

In the current study, we employed purified osteoblast-like cells derived from human AT-MSCs (hAT-MSCs) as an appropriate cell model to examine the mechanism of Poly(P)-induced differentiation *in vitro*. We show, for the first time, that Poly(P)-induced MMP-13 regulates differentiation of osteoblast-like cells from hAT-MSCs.

2. Materials and Methods

2.1. *Materials*

Type-65 Poly(P) with an average chain length of 65 phosphate residues was prepared from sodium tripolyphosphate (Taihei Chemical Industrial Co., Ltd., Osaka, Japan). Concentrations of Poly(P) are shown in terms of phosphate residues (*27*). As a control, sodium phosphate buffer (pH 6.9) was used instead of Poly(P).

2.2. *Cell culture*

hAT-MSCs were obtained from Takara Bio Inc. (Shiga, Japan) and grown in growth medium (C-28010; Takara Bio Inc.) according to the manufacturer's protocols. hAT-MSCs were tested for cell morphology, proliferation potential, adherence rate, and viability. Furthermore, they were characterized by flow cytometric analysis of a comprehensive panel of markers, namely CD73, CD90, CD105, CD14, CD19, CD34, and CD45 (*28*). Adipogenic, osteogenic and chondrogenic differentiation assays were performed under each appropriate culture condition without antibiotics or antimycotics. Passage 6-9 cells were used in experiments. At 70% confluence, the medium was replaced with osteogenic differentiation medium (ODM) (C-28013; Takara Bio Inc.) or growth medium every 3 days up to 21 days. The first day the medium was replaced with osteogenic culture medium was defined as day 0.

2.3. *Cell proliferation assay and microscopic analysis*

Cell proliferation was evaluated using a bromodeoxyuridine (BrdU)-cell proliferation enzyme-linked immunosorbent assay (ELISA; Roche Applied Science, Mannheim, Germany) as described previously (*29,30*). In addition, cell proliferation was evaluated visually under a BZ-9000 microscope (Keyence, Osaka, Japan) using a BrdU immunohistochemistry kit (Abcam, Cambridge, UK) according to the manufacturer's instructions.

2.4. *Functional assay for assessment of the osteogenic phenotype*

To assess the phenotype of cultured cells, we measured ALP activity and calcification as markers of differentiation. ALP activity was determined using an ALP Staining Kit (Primary Cell Co., Ltd., Hokkaido, Japan). Mineralization from the Poly(P)-treated cells was quantified using an Alizarin red S (ARS) assay (Sigma-Aldrich, St. Louis, MO, USA). ARS staining was quantified using a previously reported method (*31*) and photographed under the BZ-9000 microscope and/ or an IN Cell Analyzer 2000 (GE Healthcare UK Ltd., Buckinghamshire, England).

2.5. *Real-time quantitative reverse transcription-polymerase chain reaction (qRT-PCR) analysis*

qRT-PCR was performed on all samples and standards

in triplicate with approximately 25 ng RNA, 0.25 mL Quantitect RT Mix (Qiagen Inc., Valencia, CA, USA), and 1.25 mL of 20× Primer/Probe Mix (human alkaline phosphatase[ALP; *ALPL*]: Hs01029144_m1; human osteocalcin [OC; *BGLAP*]: Hs00609452_g1; human osteopontin [OP; *SPP1*]: Hs00959010_m1; human osterix [*OSX*]: Hs00931793_m1; human bone sialoprotein [*BSP*]: Hs00173720_m1; human *MMP-1*: Hs00899658_m1; human *MMP-2*: Hs01548727_m1; human *MMP-3*: Hs00968305_m1; human MMP-9: Hs00234579_m1; human *MMP-13*: Hs0023392_m1). The standard curve method was used for relative quantification of gene expression with glyceraldehyde-3-phosphate dehydrogenase (GAPDH) and 18S rRNA as controls. Analysis was performed by the ΔΔ*Ct* method.

2.6. Western blot analysis

Cells were cultured for 6 h with or without Poly(P) and then lysed using cell lysis buffer (Cell Signaling Technology Japan, K.K., Tokyo, Japan). Proteins were separated on 12% SDS-polyacrylamide gels for Western blot analysis using anti-ALP, -OC, -OP, -OSX, -BSP, -MMP-13 and -β-tubulin polyclonal antibodies (sc-271431, sc-30044, sc-10593, sc-22538, sc-73634, sc-30073, and sc-9935, respectively; Santa Cruz Biotechnology, Inc., Santa Cruz, CA, USA). Visualization of blotted protein bands was performed using a Multi Gauge-Ver3.X (Fujifilm, Tokyo, Japan).

2.7. Measurement of MMP-13 activity

The protocol for measurement of MMP-13 activity has been described previously (*32,33*) and is now a commercially available MMP-13 activity assay kit (SensoLyte™ 520 MMP-13 assay kit; AnaSpec, San Jose, CA, USA).

2.8. Silencing of the MMP-13 gene by small interfering RNA (siRNA) transfection

Commercially available MMP-13 siRNA (sc-41559, Santa Cruz Biotechnology, Inc.) was transfected into cultured cells using an siRNA reagent system (sc-45064, Santa Cruz Biotechnology, Inc.) according to the manufacturer's protocol. GAPDH siRNA and a control siRNA without known homology to any vertebrate sequence (Thermo Scientific, Lafayette, CO, USA) were used as positive and negative controls, respectively.

2.9. Statistical analysis

Data presented in bar graphs are the means ± standard deviation (SD) of four to six independent experiments. Statistical significance was assessed using the Mann-Whitney *U*-test. A *p*-value of less than 0.05 was considered statistically significant.

3. Results

3.1. *Poly(P) alters hAT-MSC proliferation*

We first analyzed the effect of Poly(P) on the cell proliferation of hAT-MSCs using the BrdU-cell proliferation ELISA. As a result, we found that Poly(P) increased cell proliferation in a dose-independent manner. Poly(P) at a concentration of 0.2 mM was optimal to enhance cell growth ($p < 0.05$) (Figure 1). Both 0.1 and 0.5 mM Poly(P) resulted in potent inhibition of cell proliferation.

3.2. *Poly(P) induces osteogenic differentiation of hAT-MSCs*

We previously analyzed the effect of Poly(P) on cell proliferation of rat DPFCs, and found that 0.2 mM Poly(P) is an optimal concentration to enhance the cell growth, whereas more or less than 0.2 mM Poly(P) results in potent inhibition of cell proliferation (*10*).

To examine whether Poly(P) induced osteogenic characteristics in hAT-MSCs, the cells were cultured in the presence of 0.2 mM Poly(P) for 7 days. Both qRT-PCR and Western blotting revealed higher expression of osteogenic differentiation markers *ALPL*, *BGLAP*, *SPP1*, *OSX*, and *BSP* (Figure 2A-a, b).

The majority of Poly(P)-treated hAT-MSCs showed strong ALP expression, whereas control cells had undetectable ALP expression (Figure 2B-a, b). Extensive deposits of calcified matrix were observed in Poly(P)-treated hAT-MSC cultures, whereas calcified matrix was not apparent in control cell cultures (Figure 2C-a, b). Consistently, Poly(P) treatment induced a marked increase in ARS signals (Figure 2C-a, b). Taken
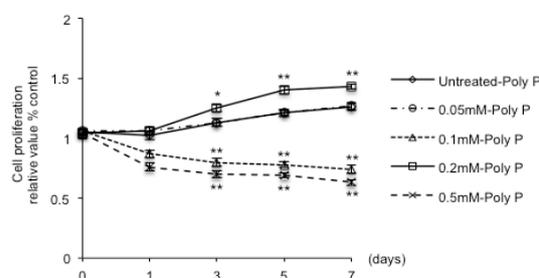
Figure 1. Optimization of Poly(P)-induced proliferation of hAT-MSCs. A BrdU-cell proliferation ELISA was employed to evaluate the proliferation of Poly(P)-treated cells and untreated (control) cells for up to 7 days. Cells were cultured in the absence or presence of the indicated concentrations of Poly(P) in triplicate wells. Data are the means ± SD. Differences between control and Poly(P)-treated groups were assessed by the Mann-Whitney U-test. *$p < 0.05$ and **$p < 0.01$ *vs.* control.

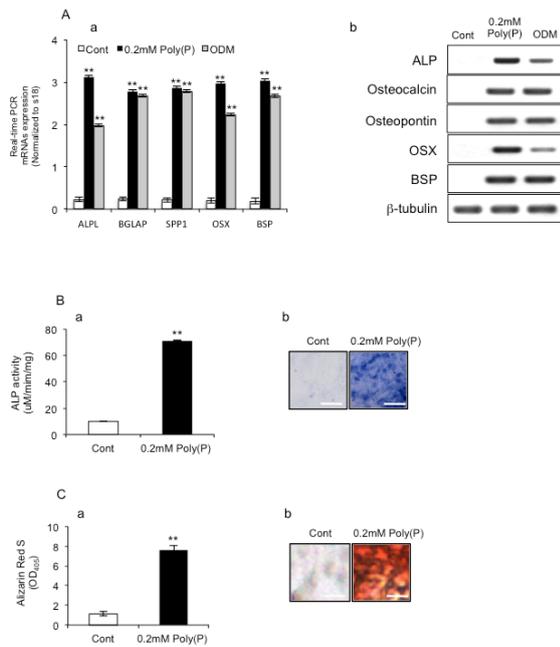**Figure 2. Expression of differentiation markers during osteogenic differentiation induced by Poly(P). (A-a)** hAT-MSCs were treated with Poly(P) for 7 days. Expression of osteogenic differentiation markers was assessed by qRT-PCR, including *ALPL, BGLAP, SPP1, OSX,* and *BSP* (**$p <$ 0.01 *vs.* control). Data are presented as the means ± SD and are representative of at least three independent experiments. Similar changes in the protein expression levels of these markers were observed in Western blot analyses **(A-b)**. ODM: osteogenic differentiation medium. ALP activity was measured in hAT-MSCs treated with or without Poly(P) **(B-a, b)**. ALP activity was measured by absorbance at 405 nm and normalized against total protein (**$p < 0.01$ *vs.* control). Scale bar: 100μm. **(C-a, b)** ARS staining of hAT-MSCs treated with Poly(P) (**$p < 0.05$ *vs.* control). Scale bar: 100 μm.

together, Poly(P) induced osteoblast-like cells from hAT-MSCs.

3.3. *Poly(P) induces expression of MMP-13 mRNA and activity of MMP-13 in hAT-MSCs*

MMP-13 induction by 0.2 mM Poly(P) was assessed using qRT-PCR to measure changes in MMP-13 mRNA expression. The levels of MMP-13 mRNA expression in Poly(P)-treated cells were significantly increased ($p < 0.05$) at days 3, 5, and 7 of culture (Figure 3A). Bone-associated cells also express other MMPs including MMP-1, MMP-2, MMP-3, and MMP-9 (*34-36*). However, we found no significant changes in their expression levels in hAT-MSCs treated with 0.2 mM Poly(P) (Figure 3B). Furthermore, MMP-13 activity was significantly increased ($p < 0.01$) at days 3, 5, and 7 following treatment of hAT-MSCs with Poly(P) for 24 h (Figure 3C), and no significant differences were found between Poly(P) treatments for 12 or 24 h.

　　MMP-13 activity is precisely regulated at the post-translational level as a precursor zymogen and by endogenous tissue inhibitors of metalloproteinases (TIMPs) (*37*). Although TIMP-2 and TIMP-3 are
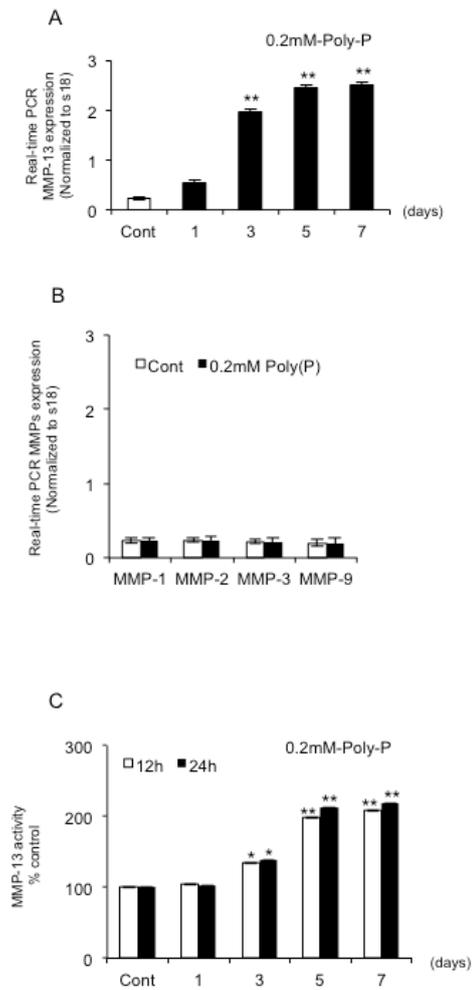

Figure 3. Evaluation of Poly(P)-induced MMP-13 mRNA expression and MMP-13 activity in hAT-MSCs. (A) qRT-PCR analysis of Poly(P)-induced MMP-13 mRNA in hAT-MSCs at 24 h. **(B)** Expression of other MMP mRNAs and proteins in hAT-MSCs. hAT-MSCs were treated with 0.2 mM Poly(P) prior to qRT-PCR analysis of MMP-1, MMP-2, MMP-3, and MMP-9 mRNA expression compared with the control (18S rRNA). Data are the means ± SD of four independent experiments. **(C)** Measurement of active MMP-13 released from cultured hAT-MSCs following treatment with 0.2 mM Poly(P). Cells were incubated in serum-free medium in the absence or presence of 0.2 mM Poly(P) for 12 or 24 h. Data are the means ± SD of at least three independent experiments (*$p <$ 0.05; **$p < 0.01$).

known to be induced by cytokines (*37*), we found that TIMP-1–3 proteins were constitutively expressed in all experimental conditions (data not shown).

3.4. *siRNA silencing of MMP-13 blocks osteogenic differentiation*

To examine whether the up-regulation of MMP-13 expression was associated with osteogenic differentiation, hAT-MSCs were transfected with MMP-13 siRNA or a control scrambled siRNA, and then treated with Poly(P) as described above. Transfection of MMP-13 siRNA abrogated the induction of osteogenic
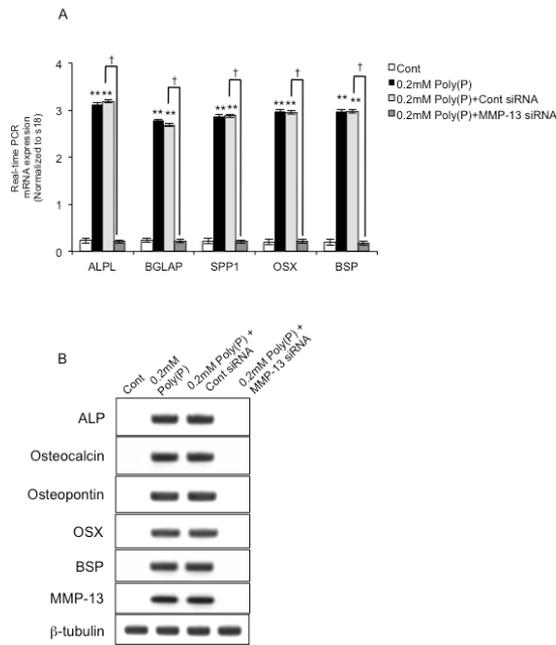
Figure 4. Effect of siRNA silencing on induction of osteogenic markers. (A) The expression of osteogenic marker mRNAs (*ALPL*, *BGLAP*, *SPP1*, *OSX*, and *BSP*) in Poly(P)-treated hAT-MSCs was assessed by qRT-PCR following culture in the presence of MMP-13 siRNA. Data are the means ± SD (n = 4). **$p < 0.01$ *vs.* control; †$p < 0.01$ as indicated. **(B)** Western blot analysis of osteogenic marker protein expression in these cells at 24 h after siRNA transfection. Poly(P)-treated hAT-MSCs were treated with MMP-13 siRNA, and then expression of ALP, OC, OP, OSX, BSP, and MMP-13 proteins was measured. No significant cross-reactivity with other proteins was observed for the antibodies used in the analyses. Images are representative of at least three independent experiments.

Figure 5. siRNA silencing of MMP-13 blocks osteogenic differentiation. (A-a, b) Effect of MMP-3 siRNA on the functional activities of hAT-MSCs. ALP activity was measured in control and MMP-13-depleted hAT-MSCs treated with 0.2 mM Poly(P). Data are presented as the means ± SD (n = 4) normalized against total protein, (**$p < 0.01$ *vs.* control; †$p < 0.05$ as indicated). Scale bar: 100 μm. **(B-a, b)** Effect of MMP-13 siRNA on the mineralization capacity of hAT-MSCs. Cells were prepared and mineralization was assessed by ARS staining with quantification performed by measuring absorbance at 405 nm. Data are the means ± SD (n = 4). *$p < 0.05$ *vs.* control; †$p < 0.05$ as indicated. Scale bar: 100 μm.

differentiation markers *ALPL*, *BGLAP*, *SPP1*, *OSX*, and *BSP* ($p < 0.05$, Figure 4A). Similar changes in the protein levels of each marker were observed in Western blot analyses (Figure 4B). Furthermore, MMP-13 siRNA blocked induction of ALP activity in Poly(P)-treated cells ($p < 0.01$, Figure 5A-a, b). Similarly, the induction of calcification was markedly suppressed ($p < 0.05$) by Poly(P) treatment of MMP-13-depleted cells (Figure 5B-a, b). Collectively, these data show that expression of MMP-13 is required for osteoblast-specific functions in hAT-MSCs.

4. Discussion

First, this study is the first report of Poly(P)-induced, MMP-13-mediated responses in the differentiation of hAT-MSCs. We demonstrated that Poly(P)-treated hAT-MSCs could be a novel *in vitro* model of bone tissue regeneration. Poly(P) at a concentration of 0.2 mM induced MMP-13 expression in hAT-MSCs (Figure 2A) and led to enhanced hAT-MSC differentiation into osteoblast-like cells (Figure 2A-C), although we were unable to precisely determine how many hAT-MSCs had differentiated. However, phenotypic
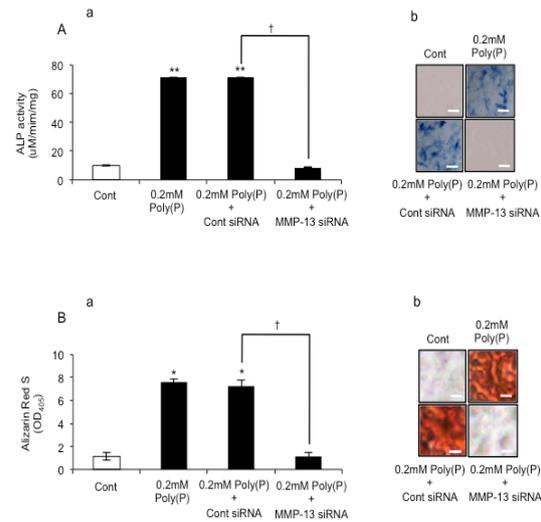
characterization based on calcification and the levels of *ALPL*, *BGLAP*, *SPP1*, *OSX*, and *BSP* suggested that a large proportion of the hAT-MSCs had differentiated into osteoblast-like cells (Figure 2A-a, b).

We have previously demonstrated that the inflammatory cytokine IL-1β or a cytokine mixture induces MMP-3-regulated cell proliferation and suppresses apoptosis in rat DPFCs (*38,39*). Moreover, we previously reported that Poly(P)-induced, MMP-3-mediated proliferation in rat DPFCs is mediated by a Wnt5 signaling cascade (*10*). Considering the effect of MMP-13 on osteogenic cell differentiation, the present findings suggest that targeting the *MMP-13* gene in these osteogenic cells may have utility in the treatment of periradicular lesions. Additionally, Poly(P)-treated hAT-MSCs could serve as an effective model to explore the pathophysiological mechanisms of wound healing. Furthermore, our current evidence suggests that Poly(P)-induced MMP-13 has previously unrecognized physiological functions in wound healing and bone tissue regeneration.

We showed that Poly(P)-induced cells acquired osteoblast-specific functions following differentiation from hAT-MSCs. Poly(P)-treated hAT-MSCs appeared to be predominantly osteoblasts. A major concern is that we were unable to identify the differentiated cells as osteoblasts because these cells also expressed specific osteoblastic markers including osteocalcin and osteopontin.

In conclusion, the current findings presented here support our previous reports (38,39) and indicate that MMP-13 may have a previously unrecognized physiological function in wound healing and bone tissue regeneration. Because Poly(P) induces MMP-13-regulated hAT-MSC differentiation into osteoblast-like cells, the use of Poly(P) represents a potentially superior therapeutic approach for treatment of periradicular lesions combined with root canal treatment.

Acknowledgements

References

1   Kornberg A, Rao NN, Ault-Riche D. Inorganic polyphosphate: A molecule of many functions. Annu Rev Biochem. 1999; 68:89-125.
2   Kumble KD, Kornberg A. Inorganic polyphosphate in mammalian cells and tissues. J Biol Chem. 1995; 270:5818-5822.
3   Leyhausen G, Lorenz B, Zhu H, Geurtsen W, Bohnensack R, Muller W E, Schroder HC. Inorganic polyphosphate in human osteoblast-like cells. J Bone Miner Res. 1998; 13:803-812.
4   Schroder HC, Kurz L, Muller WE, Lorenz B. Polyphosphate in bone. Biochemistry (Mosc). 2000; 65:296-303.
5   Shiba T, Nishimura D, Kawazoe Y, Onodera Y, Tsutsumi K, Nakamura R, Ohshiro M. Modulation of mitogenic activity of fibroblast growth factors by inorganic polyphosphate. J Biol Chem. 2003; 278:26788-26792.
6   Kawazoe Y, Shiba T, Nakamura R, Mizuno A, Tsutsumi K, Uematsu T, Yamaoka M, Shindoh M, Kohgo T. Induction of calcification in MC3T3-E1 cells by inorganic polyphosphate. J Dent Res. 2004; 83:613-618.
7   Teles JC. Study on the dentin-pulp complex. Rev Bras Odontol. 1967; 25:305-310.
8   Hiyama T, Ozeki N, Hase N, Yamaguchi H, Kawai R, Kondo A, Mogi M, Nakata K. Polyphosphate-induced matrix metalloproteinase-3-mediated differentiation in rat dental pulp fibroblast-like cells. Biosci Trends. 2016; 9:360-366.
9   Ozeki N, Hase N, Yamaguchi H, Hiyama T, Kawai R, Kondo A, Nakata K, Mogi M. Polyphosphate induces matrix metalloproteinase-3-mediated proliferation of odontoblast-like cells derived from induced pluripotent stem cells. Exp Cell Res. 2015; 333:303-315.
10   Ozeki N, Yamaguchi H, Hase N, Hiyama T, Kawai R, Kondo A, Nakata K, Mogi M. Polyphosphate-induced matrix metalloproteinase-3-mediated proliferation in rat dental pulp fibroblast-like cells is mediated by a Wnt5 signaling cascade. Biosci Trends. 2015; 9:160-168.
11   Kawano MM. Inorganic polyphosphate induces apoptosis specifically in human plasma cells. Haematologica. 2006; 91:1154A.
12   Orriss IR, Key ML, Brandao-Burch A, Patel JJ, Burnstock G, Arnett TR. The regulation of osteoblast function and bone mineralisation by extracellular nucleotides: The role of p2x receptors. Bone. 2012; 51:389-400.
13   Almeida M, Han L, Bellido T, Manolagas SC, Kousteni S. Wnt proteins prevent apoptosis of both uncommitted osteoblast progenitors and differentiated osteoblasts by beta-catenin-dependent and -independent signaling cascades involving Src/ERK and phosphatidylinositol 3-kinase/AKT. J Biol Chem. 2005; 280:41342-41351.
14   Paula-Silva FW, da Silva LA, Kapila YL. Matrix metalloproteinase expression in teeth with apical periodontitis is differentially modulated by the modality of root canal treatment. J Endod. 2010; 36:231-237.
15   Tseng WY, Huang YS, Chiang NY, Chou YP, Wu YJ, Luo SF, Kuo CF, Lin KM, Lin HH. Increased soluble CD4 in serum of rheumatoid arthritis patients is generated by matrix metalloproteinase (MMP)-like proteinases. PLoS One. 2013; 8:e63963.
16   Ozeki N, Kawai R, Yamaguchi H, Hiyama T, Kinoshita K, Hase N, Nakata K, Kondo A, Mogi M, Nakamura H. IL-1beta-induced matrix metalloproteinase-13 is activated by a disintegrin and metalloprotease-28-regulated proliferation of human osteoblast-like cells. Exp Cell Res. 2014; 323:165-177.
17   Ozeki N, Mogi M, Hase N, Hiyama T, Yamaguchi H, Kawai R, Kondo A, Nakata K. Wnt16 Signaling Is Required for IL-1beta-Induced Matrix Metalloproteinase-13-Regulated Proliferation of Human Stem Cell-Derived Osteoblastic Cells. Int J Mol Sci. 2016;17:221
18   Wong SP, Rowley JE, Redpath AN, Tilman JD, Fellous TG, Johnson JR. Pericytes, mesenchymal stem cells and their contributions to tissue repair. Pharmacol Ther. 2015; 151:107-120.
19   Minteer DM, Marra KG, Rubin JP. Adipose stem cells: Biology, safety, regulation, and regenerative potential. Clin Plast Surg. 2015; 42:169-179.
20   Zuk P A, Zhu M, Ashjian P, De Ugarte DA, Huang JI, Mizuno H, Alfonso ZC, Fraser JK, Benhaim P, Hedrick MH. Human adipose tissue is a source of multipotent stem cells. Mol Biol Cell. 2002; 13:4279-4295.
21   Zuk PA, Zhu M, Mizuno H, Huang J, Futrell JW, Katz AJ, Benhaim P, Lorenz H P, Hedrick MH. Multilineage cells from human adipose tissue: Implications for cell-based therapies. Tissue Eng. 2001; 7:211-228.
22   Cowan CM, Shi YY, Aalami OO, Chou YF, Mari C, Thomas R, Quarto N, Contag CH, Wu B, Longaker MT. Adipose-derived adult stromal cells heal critical-size mouse calvarial defects. Nat Biotechnol. 2004; 22:560-567.
23   De Ugarte DA, Morizono K, Elbarbary A, Alfonso Z, Zuk PA, Zhu M, Dragoo J L, Ashjian P, Thomas B, Benhaim P, Chen I, Fraser J, Hedrick MH. Comparison of multi-lineage cells from human adipose tissue and bone marrow. Cells Tissues Organs. 2003; 174:101-109.
24   Buschmann J, Gao S, Harter L, Hemmi S, Welti M, Werner CM, Calcagni M, Cinelli P, Wanner GA. Yield and proliferation rate of adipose-derived stromal cells as a function of age, body mass index and harvest site-increasing the yield by use of adherent and supernatant fractions? Cytotherapy. 2013; 15:1098-1105.

25 Ding DC, Chou HL, Hung WT, Liu HW, Chu TY. Human adipose-derived stem cells cultured in keratinocyte serum free medium: Donor's age does not affect the proliferation and differentiation capacities. J Biomed Sci. 2013; 20:59.

26 Ozeki N, Lim M, Yao CC, Tolar M, Kramer RH. Alpha7 integrin expressing human fetal myogenic progenitors have stem cell-like properties and are capable of osteogenic differentiation. Exp Cell Res. 2006; 312:4162-4180.

27 Tsutsumi K, Saito N, Kawazoe Y, Ooi HK, Shiba T. Morphogenetic study on the maturation of osteoblastic cell as induced by inorganic polyphosphate. PLoS One. 2014; 9:e86834.

28 Dominici M, Le Blanc K, Mueller I, Slaper-Cortenbach I, Marini F, Krause D, Deans R, Keating A, Prockop D, Horwitz E. Minimal criteria for defining multipotent mesenchymal stromal cells. The International Society for Cellular Therapy position statement. Cytotherapy. 2006; 8:315-317.

29 Mogi M, Togari A. Activation of caspases is required for osteoblastic differentiation. J Biol Chem. 2003; 278:47477-47482.

30 Ozeki N, Mogi M, Nakamura H, Togari A. Differential expression of the Fas-Fas ligand system on cytokine-induced apoptotic cell death in mouse osteoblastic cells. Arch Oral Biol. 2002; 47:511-517.

31 Gregory CA, Gunn WG, Peister A, Prockop DJ. An Alizarin red-based assay of mineralization by adherent cells in culture: Comparison with cetylpyridinium chloride extraction. Anal Biochem. 2004; 329:77-84.

32 Candelario-Jalil E, Taheri S, Yang Y, Sood R, Grossetete M, Estrada EY, Fiebich BL, Rosenberg GA. Cyclooxygenase inhibition limits blood-brain barrier disruption following intracerebral injection of tumor necrosis factor-alpha in the rat. J Pharmacol Exp Ther. 2007; 323:488-498.

33 Koyama Y, Tanaka K. Endothelins stimulate the production of stromelysin-1 in cultured rat astrocytes. Biochem Biophys Res Commun. 2008; 371:659-663.

34 Hayami T, Kapila YL, Kapila S. MMP-1 (collagenase-1) and MMP-13 (collagenase-3) differentially regulate markers of osteoblastic differentiation in osteogenic cells. Matrix Biol. 2008; 27:682-692.

35 Huang CY, Pelaez D, Dominguez-Bendala J, Garcia-Godoy F, Cheung HS. Plasticity of stem cells derived from adult periodontal ligament. Regen Med. 2009; 4:809-821.

36 Xu J, Wang W, Kapila Y, Lotz J, Kapila S. Multiple differentiation capacity of STRO-1+/CD146+ PDL mesenchymal progenitor cells. Stem Cells Dev. 2009; 18:487-496.

37 Visse R, Nagase H. Matrix metalloproteinases and tissue inhibitors of metalloproteinases: Structure, function, and biochemistry. Circ Res. 2003; 92:827-839.

38 Ozeki N, Yamaguchi H, Hiyama T, Kawai R, Nakata K, Mogi M, Nakamura H. IL-1beta-induced matrix metalloproteinase-3 regulates cell proliferation in rat dental pulp cells. Oral Dis. 2015; 21:97-105.

39 Yamaguchi H, Ozeki N, Kawai R, Tanaka T, Hiyama T, Nakata K, Mogi M, Nakamura H. Proinflammatory cytokines induce stromelysin-1-mediated cell proliferation in dental pulp fibroblast-like cells. J Endod. 2014; 40:89-94.

Original Article

MicroRNA-613 regulates the expression of brain-derived neurotrophic factor in Alzheimer's disease

Wei Li, Xu Li, Xin Xin, Peng-Cheng Kan, Yan Yan[*]

Department of Clinical Laboratory, Tianjin Huan Hu Hospital, Tianjin, China.

Summary	Alzheimer's disease (AD) is a neurodegenerative disorder characterized by progressive loss of memory and other cognitive functions and presents an increasing clinical challenge in terms of diagnosis and treatment. Brain-derived neurotrophic factor (BDNF) plays an important role in neuronal survival and proliferation. In the present study, the mRNA and protein expression level of BDNF was detected in serum, and cerebrospinal fluid (CSF) of patients with mild cognitive impairment (MCI), dementia of Alzheimer's type (DAT), and hippocampus in APP/PS1 mice. A significant decrease of BDNF mRNA and protein expression was observed in serum and CSF of patients and hippocampus in APP/PS1 mice compared with the corresponding controls. miR-613, which is predicted to target the 3'-UTR of BDNF, was also detected in patients and the mouse model. Opposite to the alteration of BDNF, miR-613 expression in serum, CSF and hippocampus were obviously increased compared to the controls. In conclusion, these findings showed that miR-613 may function in the development of AD and may provide new insights in diagnosis and treatment of AD.

Keywords: miRNAs, mild cognitive impairment, dementia of Alzheimer's type, APP/PS1 mice

1. Introduction

Alzheimer's disease (AD) is a progressive neurodegenerative disease leading to deteriorating cognitive and memory function, immobility, and eventually death in affected patients (*1*). It is predicted that AD will affect 1 in 85 people globally by 2050 (*2*), thus AD has become a global health problem, and will bring a heavy burden to society. Until now, the etiology and pathogenesis of AD have not been elucidated.

Brain-derived neurotrophic factor (BDNF) is a member of the neurotrophic factor family and is known to protect against neurotoxicity of the Aβ peptide and neural cell death by aggregation of Aβ and tau proteins (*3,4*). Previous research suggested that BDNF was decreased in the frontal cortex and hippocampus of patients with AD (*5*), and DNA methylation of BDNF

promoter is associated with the manifestation and clinical presentation of AD (*6*).

MicroRNAs (miRNAs) are small non-coding RNA molecules that regulate gene expression at the post transcriptional level. Recently, several miRNAs have been found to be related to AD pathogenesis by affecting the expression of function of AD-relevant molecules such as amyloid precursor protein (APP) (*7*), β-site amyloid precursor protein cleaving enzyme 1 (BACE1) (*8*) or Tau (*9,10*). Measurements of miRNAs in blood and cerebrospinal fluid (CSF) have become a novel diagnostic tool for various neurological diseases, including AD. miR-613, which was predicted to target BDNF in our study has neither been detected in patients with AD, nor been reported to be associated with AD.

In this study, we found that BDNF was significantly decreased in serum and CSF of patients with mild cognitive impairment (MCI) and dementia of Alzheimer's type (DAT), and also in hippocampus in APP/PS1 transgenic mice compared to the controls. Conversly, the expression of miR-613, which was predicted and confirmed to target 3'-UTR of BDNF, was increased in patients and APP/PS1 mice. This finding demonstrates that miR-613 may be a new biomarker for diagnosis of AD and helpful to explore new treatment strategies.

2. Materials and Methods

2.1. *Study population*

The present study was approved by the ethics committee of Huan Hu Hospital (Tianjin, China), and written informed consent was received from all the patients. Patients were diagnosed and characterized based on the National Institute of Neurological and Communicative Disorders and Stroke and the Alzheimer's Disease and Related Disorders Association (NINCDS-ADRDA) diagnostic criteria amendment, which was published by the National Institute on Aging and the Alzheimer's Association (NIA-AA) in April 2011 (*11*). A total of 32 MCI (22 females, 20 males, mean age 64.8 ± 7.2) and 48 DAT patients (26 females, 22 males, mean age 65.5 ± 6.8) were selected for the following study. 40 healthy individuals (22 females, 18 males, mean age 63.2 ± 6.3) were obtained from Physical examination center of Huan Hu Hospital and informed consent was also received from the participants. The serum and CSF samples were extracted from the patients, centrifuged at 12,000× g for 5 min at 4°C. Serum was stored at -80°C, and CSF samples were stored at -20°C for further analysis.

2.2. *Animals*

The 3-, 6- and 9-month-old APP/PS1 double-transgenic mice with C57BL/6J genetic background were purchased from Zhongke Biotechnology Co., Ltd (Beijing, China). The study protocols of animals were approved by Ethics Committee of Huan Hu Hospital of Tianjin in China. Non-transgenic mice (wild-type mice) were used as controls. Mice were anesthetized with ether and blood was taken by removing the eyes. After the mice were sacrificed, their brains were moved into a 35-mm dish. The cranial cavity and cerebral ventricles, which include lateral, third and fourth ventricles, were rinsed with PBS, and CSF was harvested with PBS, the washing solution was CSF-like fluid.

The hippocampus was isolated for further detection. There were 6 mice in each group. All the samples were stored in liquid nitrogen until required.

2.3. *Cell culture and transfection*

SH-SY5Y cells were cultured in Dulbecco's Modified Eagle Medium (DMEM, Gibco, USA) which contains 10% fetal bovine serum (FBS) at 37°C with 5% CO_2. Oligonucleotides and plasmids were transfected using LipofectamineTM 2000 reagent (Invitrogen, USA) according to the manufacturer's instructions.

2.4. *Plasmid construction and oligonucleotides*

The miR-613 sequence was amplified and inserted into pcDNA3 vector. miR-613 antisense oligonucleotides (ASO-miR-613) was used as the inhibitor of miR-613 and ASO-NC was used as control. EGFP coding region from the pEGFP-N2 vector was cloned into pcDNA3. The fragment of the 3'-UTR of BDNF (wild-type or mutant-type) was amplified and cloned into the pcDNA3-EGFP vector.

2.5. *Reverse transcription-quantitative polymerase chain reaction (RT-qPCR)*

Total RNA and miRNAs were isolated using Trizol reagent (Invitrogen) and mirVana miRNA isolation kit (Ambion, Austin, TX, USA). Then cDNA was obtained by using oligo-dT primers or stem-loop reverse transcriptase (RT) primers, respectively. β-actin and U6 were used as controls for BDNF and miR-613, respectively. PCR was performed under the following conditions: 94°C for 4 min followed by 40 cycles at 94°C for 1 min, 56°C for 1 min and 72°C for 1 min. Relative expression levels of the genes were calculated using the $2^{-\Delta\Delta Ct}$ method.

2.6. *Western blot analysis*

Total proteins in serum and CSF samples were extracted with protein lysis solution (Tiangen Biotech). Cell lysates were obtained with RIPA lysis buffer after transfection. Protein samples were separated by sodium dodecyl sulfate-polyacrylamide gel electrophoresis (SDS-PAGE), transferred to nitrocellulose membranes and blocked with 5% skimmed milk for 1 h at room temperature. The membranes were incubated with rabbit anti-human monoclonal anti-BDNF antibody (1:500, Abcam, Cambridge, MA, USA) or antibody against glyceraldehyde phosphate dehydrogenase (GAPDH) overnight at 4°C. A goat anti-rabbit polyclonal IgG secondary antibody (1:1,000, Abcam) was added for incubation with the membrane at room temperature for 2 h. Protein expression level was assessed by enhanced chemiluminescence and exposure to film (Fujifilm, Tokyo, Japan). The relative expression was determined as the ratio to the GAPDH.

2.7. *EGFP reporter assay*

SH-SY5Y cells were plated in 24-well plates. Cells were transiently transfected with pcDNA3-pri-613, pcDNA, ASO-miR-613, ASO-NC and reporter vectors bearing either BDNF 3'-UTR wild-type or BDNF 3'-UTR mutant-type. The RFP expression vector was used as the corresponding control. The intensity of fluorescence was detected with an F-4500 fluorescence spectrophotometer (Hitachi, Tokyo, Japan). EGFP fluorescence intensity was normalized to the RFP fluorescence intensity.

2.8. Statistical analysis

Data are expressed as the mean ± standard deviation. A two-tailed Student's *t*-test was performed for group comparisons and $p < 0.05$ was considered to be statistically significant.

3. Results

3.1. BDNF mRNA and protein expression levels were decreased in the serum and CSF of patients with MCI and DAT

BDNF was reported to be associated with cognitive impairment, especially immediate memory (*12*). To explore the role of BDNF in the pathogenesis of AD, RT-qPCR and Western blot analysis were performed to detect the mRNA and protein expression levels of BDNF. The experimental groups were divided into the MCI (*n* = 32) and DAT (*n* = 48) groups, and healthy participants (*n* = 40), respectively. Data demonstrated that BDNF mRNA expression in the serum and CSF of MCI and DAT groups were significantly reduced compared to the control group (Figure 1A and 1B). Relatively, the expression levels of BDNF were much lower in the DAT group compared to the MCI group. Similarly, the protein expression of BDNF in serum and CSF were significantly decreased in the MCI and DAT groups compared to that in the control group. Moreover, the expression levels of BDNF protein were lower in the DAT group than in the MCI group (Figure 1C and 1D). All of these findings suggest that BDNF mRNA and protein expression are reduced in the serum and CSF of patients with MCI and DAT and BDNF is
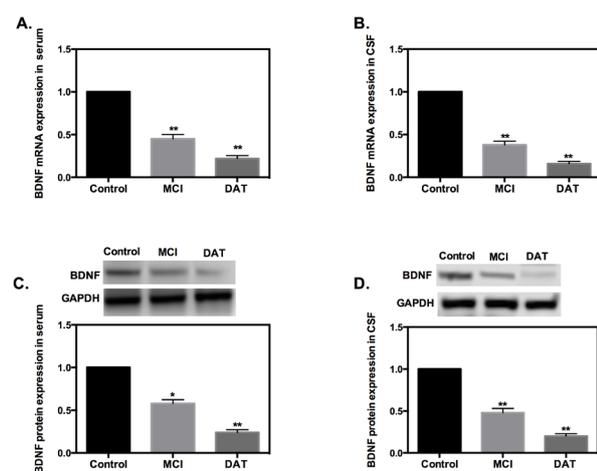
maybe related to the development of AD.

3.2. Expression levels of BDNF mRNA and protein were reduced in the serum, CSF-like fluid and hippocampus of transgenic mice

To further determine the crucial role of BDNF, we used APP/PS1 transgenic mice and also detected mRNA and protein levels of BDNF in the serum, CSF-like fluid and hippocampus of the animal model. The results suggested that the relative mRNA and protein expression of BDNF were significantly decreased in 3-, 6- and 9-month transgenic mice compared to the wild-type (WT) mice, respectively. Furthermore, the expression level of BDNF in the serum, CSF-like fluid and hippocampus of 6- and 9-month transgenic mice were much lower than that of the 3-month mice (Figure 2).

3.3. Bioinformatics prediction

We used miRanda, Targetscan and PicTar to predict the miRNAs which may target BDNF. Combining the results from these three bioinformatics softwares, we

Figure 1. Alterations of BDNF mRNA and protein levels in the serum and CSF of patients with MCI and DAT. RT-qPCR was used to detect the mRNA expression of BDNF in the serum and CSF **(A and B)** and Western blot was used to detect the protein levels of BDNF **(C and D)**. Compared to the control group, *$p < 0.05$ and **$p < 0.01$. The expression levels of control group were normalized to 1. MCI, mild cognitive impairment; DAT, dementia of Alzheimer's type.

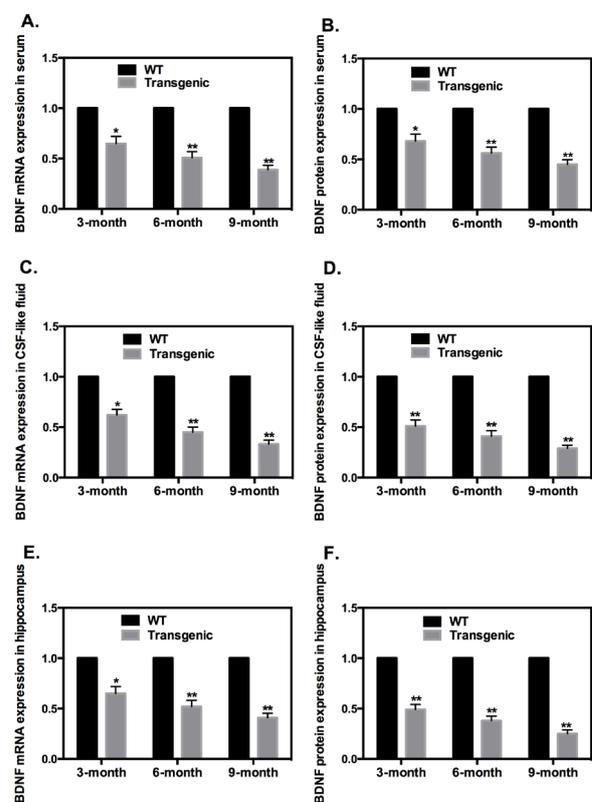**Figure 2. BDNF mRNA and protein expression were reduced in the serum, CSF-like fluid, and hippocampus tissues of APP/PS1 transgenic mice.** Expression levels of BDNF in the serum **(A and B)**, CSF-like fluid **(C and D)**, and hippocampus tissues **(E and F)** of mice. Compared to the WT group, *$p < 0.05$ and **$p < 0.01$. The expression levels of WT group were normalized to 1. WT, wild type mice; transgenic, transgenic mice.

selected 12 miRNAs. Considering that miR-613 has never been determined as a regulator in AD, then miR-613 was finally chosen for further study (Figure 3).

3.4. BMiR-613 directly targets the 3'-UTR of BDNF

To further determine whether or not miR-613 directly targets BDNF, an EGFP reporter analysis was performed. EGFP vectors bearing wild-type or mutant-type BDNF 3'-UTR were transfected into SH-SY5Y cells when miR-613 was over-expressed or inhibited. As shown in Figure 4, over-expression of miR-613
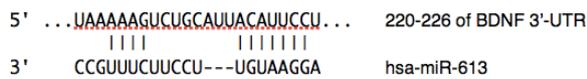

Figure 3. miR-613 could target the 3'-UTR of BDNF. The predicted sites of miR-613 binding to the 3'-UTR of BDNF are shown.
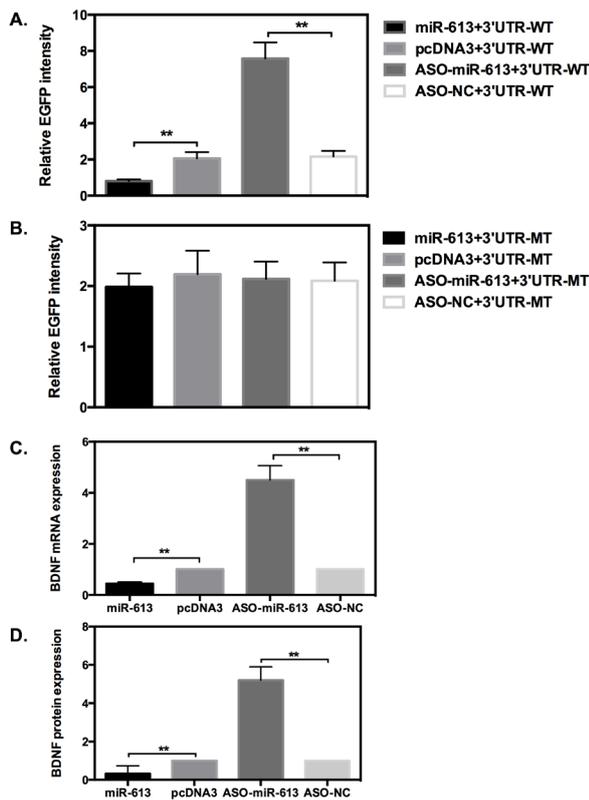

Figure 4. miR-613 could directly target BDNF and down-regulate its mRNA and protein expression in SH-SY5Y cells. (A) EGFP analysis was performed to detect the intensity of the wild-type 3'-UTR of BDNF when miR-613 was over-expressed or inhibited. **(B)** The intensity of the mutant-type 3'-UTR of BDNF when the expression level of miR-613 was changed. **(C)** RT-qPCR analysis was used to detect the mRNA expression of BDNF when miR-613 expression was altered. **(D)** Western blot analysis was used to detect the protein expression level of BDNF. $**p < 0.01$. miR-613, pcDNA3-pri-miR-613; ASO-miR-613, miR-613 inhibitor; WT, wild-type; MT, mutant-type. pcDNA3 and ASO-NC groups are the corresponding controls. The mRNA and protein expression of BDNF in control groups were normalized to 1.

decreased the intensity with wild-type 3'-UTR by almost 61%. While the EGFP intensity with mutant-type 3'-UTR was increased approximately 2.5-fold when miR-613 was inhibited (Figure 4A). However, the EGFP intensity with the mutant-type 3'-UTR was not affected when altering the expression level of miR-613 (Figure 4B). These data indicate that miR-613 can directly target BDNF by binding to the 3'-UTR.

We then explored whether or not miR-613 affects the expression of BDNF. RT-qPCR and Western blot analysis were examined and showed that miR-613 significantly reduced the mRNA and protein expression by 55% and 67%, respectively. However, the expression levels of BDNF were increased by 3.5- and 4.2-fold when miR-613 was inhibited (Figure 4C and 4D). This finding suggests that miR-613 negatively regulates the expression of BDNF in SH-SY5Y cells.

3.5. Expression levels of miR-613 were increased in patients with MCI and DAT, and also in APP/PS1 transgenic mice

Since miR-613 can directly target BDNF and down-regulates its expression both at the mRNA and
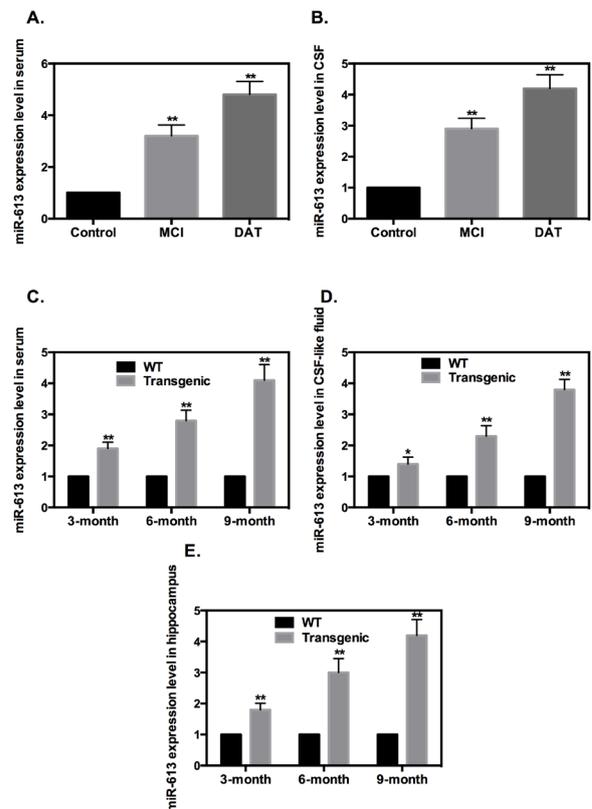
Figure 5. The expression level of miR-613 was significantly increased in the patients and animal models. (A and **B)** miR-613 expression level in the serum and CSF of patients with MCI and DAT. **(C)** miR-613 expression in the serum of transgenic mice and wild type mice. **(D)** The expression of miR-613 in the CSF-like fluid in animal models. **(E)** miR-613 expression level in the hippocampus tissues in transgenic and wild-type mice. Compared to the corresponding controls, $*p < 0.05$ and $**p < 0.01$.

protein level, we then investigated whether or not the expression level of miR-613 was changed in patients or transgenic mice. Accordingly, RT-qPCR was used and showed that miR-613 expression levels were significantly increased in serum and CSF of patients with MCI and DAT compared to healthy individuals, respectively (Figure 5A and 5B). Moreover, miR-613 mRNA expression was also remarkably increased in serum, CSF-like fluid, and hippocampus of APP/PS1 transgenic mice compared to wild-type mice (Figure 5C, 5D, and 5E).

4. Discussion

Accumulated evidence has shown that miRNAs are related to various diseases, including cancer, immune diseases, inflammation, and neurodegenerative diseases (*13-16*). Furthermore, numerous miRNAs have been determined to be associated with AD, such as miR-512 (*17*), miR-29c (*18*), and miR-155 (*19*). miR-613 is also reported to play a role in the pathogenesis and development of various cancers (*20-22*). However, there has been no data to suggest a link between miR-613 and AD. In the present study, we first detected a significant increase of miR-613 in body fluid of patients with MCI and AD and also in APP/PS1 transgenic mice. We also determined that miR-613 directly targets the 3'-UTR of BDNF and down-regulates its mRNA and protein expression.

BDNF is one of the neurotrophic factors that support differentiation (*23*), maturation (*24*), and survival of neurons in the nervous system (*25*) and shows a neuroprotective effect. Previous studies have indicated that the level of BDNF was reduced in many neurodegenerative diseases, such as Huntington's disease (*26*), multiple sclerosis (*27*), and Parkinson's disease (*28*). In this research, we found that BDNF is also significantly decreased in the body fluid of patients and an animal model. Biomarkers, which are the objective indicators of biological and pathological processes, were utilized to assess the risk or prognosis of disease, to guide clinical diagnosis or to monitor the intervention effect. CSF is in direct contact with the extracellular space of the brain and can directly reflect biochemical changes. Therefore, CSF is the preferred source of AD biomarkers. Because the process of obtaining CSF is traumatic, serum is also suitable for study. We detected BDNF and miR-613 expression levels in serum and CSF both in patients with MCI and DAT and transgenic mice, and also in hippocampus of an animal model. Results showed significant alterations of BDNF and miR-613 expression.

Furthermore, we identified that miR-613 directly targets BDNF. This conclusion is based on several experimental results. First, EGFP reporter assay showed that miR-613 significantly decreased the fluorescence intensity of wild-type 3'-UTR of BDNF, while miR-613 inhibitor increased the relative intensity of the 3'-UTR. However, the intensity of mutant-type 3'-UTR was not affected by alteration of miR-613 expression. Second, miR-613 decreased the expression of BDNF both at the mRNA and protein levels in SH-SY5Y cells. Third, both in body fluid of patients and the animal model, the expression of BDNF was negatively correlated to that of miR-613.

Moreover, we also found that the changes of BDNF and miR-613 were more obvious in patients with DAT than those with MCI. Meanwhile, the alteration of BDNF and miR-613 expression levels was more significant in 6- and 9-month transgenic mice than that in 3-month mice. These data suggested that BDNF and miR-613 may be related to the severity and progression of AD.

In conclusion, the present results indicated that BDNF mRNA and protein expression levels were decreased in patients with AD and transgenic mice. miR-613, which could directly target the 3'-UTR of BDNF, was inversely increased in patients and animal models. These findings demonstrated that miR-613 may be a new biomarker of AD pathogenesis and development, and may provide novel insights into the diagnosis and therapy of AD.

Acknowledgements

References

1. Alzheimer's Association. 2015 Alzheimer's disease facts and figures. Alzheimers Dement. 2015; 11:332-384.
2. Brookmeyer R, Johnson E, Ziegler- Graham K, Arrighi HM. Forecasting the global burden of Alzheimer's disease. Alzheimers Dement. 2007; 3:186-191.
3. Aicardi G, Argilli E, Cappello S, Santi S, Riccio M, Thoenen H, Canossa M. Induction of long-term potentiation and depression is reflected by corresponding changes in secretion of endogenous brain-derived neurotrophic factor. Proc Natl Acad Sci U S A. 2004; 101:15788-15792.
4. Poo MM. Neurotrophins as synaptic modulators. Nat Rev Neurosci. 2001; 2:24-32.
5. Ferrer I, Marín C, Rey MJ, Ribalta T, Goutan E, Blanco R, Tolosa E, Martí E. BDNF and full length and truncated TrkB expression in Alzheimer disease. Implications in therapeutic strategies. J Neuropathol Exp Neurol. 1999; 58:729-739.
6. Nagata T, Kobayashi N, Ishii J, Shinagawa S, Nakayama R, Shibata N, Kuerban B, Ohnuma T, Kondo K, Arai H, Yamada H, Nakayama K. Association between DNA methylation of the BDNF promoter region and clinical presentation in Alzheimer's disease. Dement Geriatr Cogn Dis Extra. 2015; 5:64-73.
7. Vilardo E, Barbato C, Ciotti M, Cogoni C, Ruberti F.

MicroRNA-101 regulates amyloid precursor protein expression in hippocampal neurons. J Biol Chem. 2010; 285:18344-18351.

8. Wang WX, Rajeev BW, Stromberg AJ, Ren N, Tang G, Huang Q, Rigoutsos I, Nelson PT. The expression of microRNA miR-107 decreases early in Alzheimer's disease and may accelerate disease progression through regulation of beta-site amyloid precursor protein-cleaving enzyme 1. J Neurosci. 2008; 28:1213-1223.

9. Absalon S, Kochanek DM, Raghavan V, Krichevsky AM. MiR-26b, upregulated in Alzheimer's disease, activates cell cycle entry, tau-phosphorylation, and apoptosis in postmitotic neurons. J Neurosci. 2013; 33:14645-14659.

10. Banzhaf-Strathmann J, Benito E, May S, Arzberger T, Tahirovic S, Kretzschmar H, Fischer A, Edbauer D. MicroRNA-125b induces tau hyperphosphorylation and cognitive deficits in Alzheimer's disease. EMBO J. 2014; 33:1667-1680.

11. Alzheimer's Association. 2011 Alzheimer's disease facts and figures. Alzheimers Dement. 2011; 7:208-244.

12. Zhang XY, Liang J, Chen da C. Xiu MH, Yang FD, Kosten TA, Kosten TR. Low BDNF is associated with cognitive impairment in chronic patients with schizophrenia. Psychopharmacology (Berl). 2012; 222:277-284.

13. Meng D, Li Z, Ma X, Fu L, Qin G. MicroRNA-1280 modulates cell growth and invasion of thyroid carcinoma through targeting estrogen receptor α. Cell Mol Biol (Noisy-le-grand). 2016; 62:1-6.

14. Wang W, Zhang Y, Zhu B, Duan T, Xu Q, Wang R, Lu L, Jiao Z. Plasma microRNA expression profiles in Chinese patients with rheumatoid arthritis. Oncotarget. 2015; 6:42557-42568.

15. Thome AD, Harms AS, Volpicelli-Daley LA, Standaert DG. microRNA-155 regulates Alpha-Synuclei-induced inflammatory response in models of Parkinson disease. J Neurosci. 2016; 36:2383-2390.

16. Mushtaq G, Greig NH, Anwar F, Zamzami MA, Choudhry H, Shaik MM, Tamargo IA, Kamal MA. miRNAs as circulating biomarkers for Alzheimer's disease and Parkinson's disease. Med Chem. 2016; 12:217-225.

17. Mezache L, Mikhail M, Garofalo M, Nuovo GJ. Reduced miR-512 and the elevated expression of its targets cFLIP and MCL1 localize to neurons with hyperphosphorylated Tau protein in Alzheimer disease. AppI Immunohistochem Mol Morphol. 2015; 23:615-623.

18. Zong Y, Yu P, Cheng H, Wang H, Wang X, Liang C, Zhu H, Qin Y, Qin C. miR-29c regulates NAV3 protein expression in a transgenic mouse model of Alzheimer's disease. Brain Res. 2015; 1624:95-102.

19. Song J, Lee JE. miR-155 is involved in Alzheimer's disease by regulating T lymphocyte function. Front Aging Neurosci. 2015; 7:61.

20. Li D, Li DQ, Liu D, Tang XJ. MiR-613 induces cell cycle arrest by targeting CDK4 in non-small cell lung cancer. Cell Oncol (Dordr). 2016; 39:139-147.

21. Zhang X, Zhang H. Diminished miR-613 expression as a novel prognostic biomarger for humal ovarian cancer. Eur Rev Med Pharmacol Sci. 2016; 20:837-841.

22. Zhong D, Zhang Y, Zeng YJ, Gao M, Wu GZ, Hu CJ, Huang G, He FT. MicroRNA-613 represses lipogenesis in HepG2 cells by downregulating LXRα. Lipids Health Dis. 2013; 12:32.

23. Binder DK, Scharfman HE. Brain-derived neurotrophic factor. Growth Factors. 2004; 22:123-131.

24. Acheson A, Conover JC, Fandl JP, DeChiara TM, Russell M, Thadani A, Squinto SP, Yancopoulos GD, Lindsay RM. A BDNF autocrine loop in adult sensory neurons prevents cell death. Nature. 1995; 374:450-453.

25. Huang EJ, Reichardt LF. Neurotrophins: Roles in neuronal development and function. Ann Rev Neurosci. 2001; 24:677-736.

26. Mughal MR, Baharani A, Chigurupati S, Son TG, Chen E, Yang P, Okun E, Arumugam T, Chan SL, Mattson MP. Electroconvulsive shock ameliorates disease processes and extends survival in huntingtin mutant mice. Hum Mol Genet. 2011; 20:659-669.

27. Sohrabji F, Lewis DK. Estrogen-BDNF interactions: Implications for neurodegenerative diseases. Front Neuroendocrinol. 2006; 27:404-414.

28. Scalzo P, Kummer A, Bretas TL, Cardoson F, Teixeira AL. Serum levels of brain-derived neurotrophic factor correlate with motor impairment in Parkinson's disease. J Neurol. 2010; 257:540-545.

The significance of low levels of LINC RP1130-1 expression in human hepatocellular carcinoma

Chaohui Xiao[1,2,*], Cheng Wang[3,*], Sijie Cheng[2], Chengcai Lai[4], Peirui Zhang[2], Zizheng Wang[1], Tao Zhang[1], Shaogeng Zhang[2,], Rong Liu[1,**]**

[1] *Departments of Surgical Oncology, Chinese People's Liberation Army (PLA) General Hospital, Beijing, China;*
[2] *Department of Hepatobiliary Surgery, Hospital 302 of the PLA , Beijing, China;*
[3] *Beijing 307 Hospital, Affiliated to Academy of Medical Sciences, Beijing, China;*
[4] *Beijing Institute of Microbiology and Epidemiology, State Key Laboratory of Pathogen and Biosecurity, Beijing, China.*

Summary   **Hepatocellular carcinoma (HCC) is the most common neoplasms. Little progress has been made in the diagnosis and treatment of HCC and its prognosis remains poor. Studies have increasingly found that long non-coding RNA (lncRNA) is involved in the regulation of the occurrence and development of HCC. To investigate the diagnostic and prognostic value of lncRNA in HCC, the current study examined 25 lncRNAs with differing levels of expression (according to the fold change) in microarray databases. Expression of LINC RP1130-1 was found to be markedly down-regulated in 51 HCC tissues compared to matching adjacent non-tumor liver tissues. The pattern of expression and clinical significance of LINC RP1130-1 were examined in HCC. The area under the receiver operating characteristic (ROC) curve was 0.74 for LINC RP1130-1. The expression of LINC RP1130-1 was associated with clinical stage, the number of tumors, portal vein tumor thrombus (PVTT), and microvascular invasion (MVI). More importantly, patients with a low level of LINC RP1130-1 expression had a shorter recurrence-free survival (RFS) ($n = 51$, $p < 0.05$) than those with a high level of LINC RP1130-1 expression. Taken together, these findings indicate that a low level of LINC RP1130-1 expression in patients with HCC may be a powerful tumor biomarker, with potential clinical use in diagnosing and predicting the prognosis for patients with HCC.**

         Keywords: LncRNA, hepatocellular carcinoma, biomarker

1. Introduction

Hepatocellular carcinoma (HCC) is the most common neoplasms, accounting for approximately 90% of liver cancer, and liver cancer is currently the second leading cause of cancer-related death worldwide (*1,2*). The main

risk factors for developing HCC are well-known and include cirrhosis, hepatitis B virus (HBV) or hepatitis C virus (HCV) infection, alcohol abuse, aflatoxin B1 ingestion, and non-alcoholic steatohepatitis. Major pathways with frequent mutations in HCC include the telomere maintenance pathway, the cell cycle pathway, the WNT-β-catenin pathway, the epigenetic remodeling pathway, and the chromatin remodeling pathway (*3-9*). Despite progress in the diagnosis and treatment of HCC, its prognosis still remains unfavorable. The median survival rate for curative therapy remains approximately 50% for 5 years. Recent studies have sought to ascertain the mechanisms underlying the initiation, propagation, and development of HCC in order to identify potential diagnostic biomarkers and therapeutic targets (*10-13*). Important work is to identify novel biomarkers for early diagnosis and evaluation of the prognosis of patients with HCC.

Long non-coding RNA (lncRNA) is RNA that is longer than 200 nucleotides in length and that does not code for proteins, although lncRNA can interact with proteins (*14,15*). lncRNA is not as well characterized as other small non-coding RNA such as microRNA, but lncRNAs play important roles in the regulation of a variety of cellular processes, including stem cell pluripotency, cell growth, cell proliferation, apoptosis, metabolism, and cancer cell migration(*16-21*). Functional lncRNA may be useful in cancer diagnosis and evaluation of prognosis and it may serve as a potential therapeutic target. Studies have reported that aberrant lncRNA expression affects tumor cell growth, apoptosis, invasion, and metastasis. The lncRNA MALAT1, a highly conserved LncRNA expressed in the nucleus, should allow prediction of lung cancer development, metastasis of prostate cancer, and presenting signs of esophageal squamous cell carcinoma (*22-24*). The lncRNA UCA1 plays a key role in human bladder cancer growth and tumorigenesis; UCA1may have crucial biological activity and it may serve as a new therapeutic target for bladder cancer (*25*). The lncRNA BANCR has been found to offer potential as a diagnostic marker of lung cancer (*26*), Zfas1 offers potential as a marker of breast cancer (*27*), and TUG1 offers potential as a diagnostic marker of bladder cancer (*28*). In addition, the lncRNAs PVT1 (*29*), HULC (*30*), HEIH (*31*), ATB (*32*), DANCR (*33*), and LINC00152 (*34*) have been found to be dys-regulated in conditions like HCC.

The present study examined microarray data from human lncRNA in public databases. The datasets GSE55191 (*www.ncbi.nlm.nih.gov/geo/query/acc.cgi?acc=GSE55191*) and GSE58043 (*www.ncbi.nlm.nih.gov/geo/query/acc.cgi?acc=GSE58043*) were obtained to analyze differences in levels of lncRNA expression in HCC and paired non-tumor tissues. Twenty-five lncRNAs with differing levels of expression (according to the fold change) in the datasets were examined (Figure 1A). The level of expression of these lncRNAs was determined in a normal human liver cell line LO2 and the HCC cell lines HepG2 and SMMC-7721 (Figure 1B). Four 4 lncRNAs that varied the most in their fold change in the HepG2 and SMMC-7721 cell lines and the LO2 cell line were consistent with the results from the microarray. As shown in Figure 1B, lncRNA L12, L17, L18, and L24 exhibited an impressive fold change (>10-fold). Expression of these lncRNAs was examined in 18 paired adjacent non-cancerous hepatic tissues (Figure 2). Results indicated that LINC RP1130-1 had the greatest difference in expression among the 4 lncRNAs. LINC RP1130-1 is located on gene RP11-30J20.1 (ENSG00000254101), which is the source of numerous lncRNA transcripts. The correlation between levels of LINC RP1130-1 expression and clinicopathological characteristics and recurrence-free survival (RFS) was examined in patients with HCC to determine whether
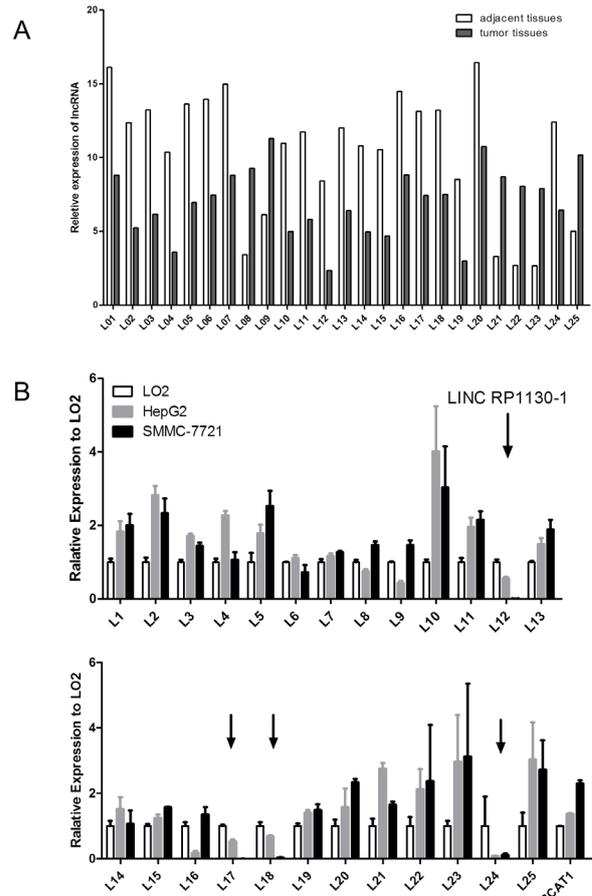
Figure 1. Twenty-five lncRNAs with differing levels of expression were identified from datasets (GSE55191 and GSE58043) and (A) the level of their expression in a normal human liver cell line (LO2) and HCC cell lines (HepG2 and SMMC-7721) and human HCC tissues was determined (B). L01-L25 respectively represent ASHG19A3A-012552, 018493, 054627, 006377, 051778, 024516, 054629, 054311, 054103, 053906, 015954, 040795, 014006, 021193, 025198, 033235, 043138, 044877, 047009, 053783, 054945, 027421, 044247, 029103, and 010811 in the datasets. "↓" represents 4 lncRNAs that were chosen to measure their level of expression. L12 represents LINC RP1130-1 (a positive control) and CCAT1 represents lncRNA CCAT1 (another positive control) that is reported to be consistently up-regulated in HCC cell lines. Gene numbers L17, L18, and L24 in the Ensembl database were respectively ENSG00000255723.1, ENSG00000251138.2, and ENSG00000269353.1.

LINC RP1130-1 could be a useful diagnostic and prognostic indicator in HCC.

2. Materials and Methods

2.1. *Clinical specimens and cell lines*

Data on 51 consecutive patients (42 males and 9 females) who underwent surgery for HCC at Hospital 302 in Beijing between August 2013 and April 2016 were collected from the records of the hospital's Department of Hepatobiliary Surgery. None of the patients had received preoperative chemotherapy or radiation therapy. All HCC diagnoses were confirmed histopathologically

Figure 2. Relative expression of 4 lncRNAs in 18 HCC tissues and paired adjacent non-cancerous hepatic tissues. *: $p < 0.05$, ***: $p < 0.001$.

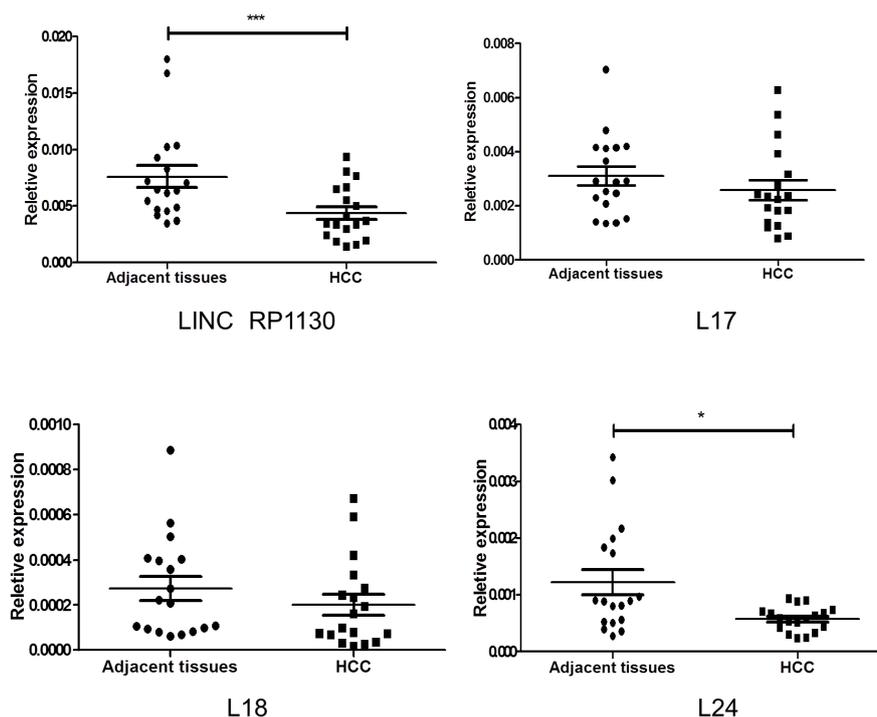by a clinical pathologist. Tumor tissues and adjacent non-tumor tissue specimens were collected from the patients after obtaining informed consent, in accordance with the institutional guidelines of the hospital's Ethics Committee. Resected tumor tissue and adjacent normal tissue specimens were immediately snap-frozen in liquid nitrogen and stored in a tissue bank until use. The experimental operators were blinded to the clinical data. The human cell lines used in this study were obtained from the Experimental Research Support Center of Hospital 302 in Beijing (Beijing, China) and included HepG2, LO2, Huh7, and SMMC-7721 cells. All of the cell lines were maintained in an atmosphere of 5% CO_2 and grown in DMEM medium (Thermo, Beijing, China) supplemented with 10% fetal bovine serum (Gibco, Beijing, China).

2.2. RNA preparation, reverse transcription, and quantitative real-time RT-PCR (qRT-PCR)

Total RNA from frozen HCC tissues and adjacent non-tumor tissue samples (n = 51) was extracted using TRIZOL reagent (Invitrogen Life Technologies, Carlsbad, CA, USA) according to the manufacturer's protocol. RNA integrity was evaluated using a NanoDrop ND-1000 spectrophotometer (NanoDrop Products, Wilmington, DE, USA), and cDNAs were synthesized from 50 ng of total RNA of each sample. Levels of LINC RP1130-1 expression were quantified with qRT-PCR performed on an ABI7500

system (Applied Biosystems, Foster City, CA, USA) using Maxima SYBR Green qRT-PCR master mix (Thermo Fisher Scientific, Waltham, MA, USA) according to the manufacturers' protocols. GAPDH expression was monitored as the endogenous control, and all samples were normalized to human GAPDH. All reactions were run in triplicate, using LINC RP1130-1-specific primers designed and synthesized by Sangon Biotech (Sangon, Shanghai, China). Their sequences were as follows: LINC RP1130-1 forward: 5'-ACCTCCCCACAAGCTGA-3', reverse: 5'- AACCGAATATTTGATGTCT-3'; GAPDH forward: 5'-CAGCCTCAAGATCATCAGCA-3' and reverse: 5'-TGTGGTCATGAGTCCTTCCA-3'. The amplification profile was 95°C for 5 min, followed by 40 cycles of denaturation at 95°C for 15 s, and annealing at 60°C for 30 s. The median of three reactions was used to calculate relative lncRNA expression (ΔCt = Ct median lncRNA - Ct median GAPDH). Fold changes in expression were calculated using the $2^{-\Delta\Delta Ct}$ method.

2.3. Statistical Analysis

All experiments were performed in triplicate and repeated at least three times. Data are expressed as the mean ± S.D. Statistically significant differences between HCC tissues and adjacent non-tumor tissue samples were determined using the Wilcoxon signed-rank test, and differences between cell lines were determined using the Student's t test. A receiver operating

characteristic (ROC) curve was plotted to determine how well the level of LINC RP1130-1 expression differentiated between HCC tissues and adjacent non-tumor tissues, and the cutoff value of 0.01 served as the level of expression sensitivity + specificity considered to be maximal. Associations between LINC RP1130-1 expression and clinicopathological characteristics were analyzed using a chi-squared test. Kaplan-Meier analyses were performed on the correlations between levels of LINC RP1130-1 expression and RFS. All statistical analyses were performed using SPSS for Windows software (ver. 16.0; SPSS Inc., Chicago, IL, USA). p values < 0.05 were considered significant.

3. Results

3.1. The level of LINC RP1130-1 expression decreased in HCC relative to that in adjacent non-tumor tissues

To assess the potential clinical significance of LINC RP1130-1, its level of expression in both HCC tissues and adjacent non-tumor tissue specimens was analyzed with qRT-PCR. LINC RP1130-1 expression decreased significantly relative to that in adjacent non-tumor

tissues (p < 0.001, Figure 3A, B, horizontal lines represent the median). LINC RP1130-1 expression was also examined with qRT-PCR in three HCC cell lines and the normal liver cell line. Results indicated that LINC RP1130-1 expression was lower in the HCC cell lines than in LO2 (p < 0.05, Figure 3C). ROC analysis was used to evaluate the ability of LINC RP1130-1 expression to differentiate between the tumor and control samples. The total area under the curve (AUC, representing accuracy of differentiation) was 0.74 for LINC RP1130-1 (Figure 3D), suggesting that the level of LINC RP1130-1 level has adequate sensitivity and specificity to differentiate between HCC tissues and adjacent non-tumor tissues.

3.2. LINC RP1130-1 expression is correlated with clinical stage, the number of tumors, PVTT, liver cirrhosis, and microvascular invasion in patients with HCC

To determine whether LINC RP1130-1 expression in HCC tissues is associated with clinicopathological parameters, the clinical stage, the number of tumors, and the presence of microvascular invasion were examined in samples from patients with HCC. As
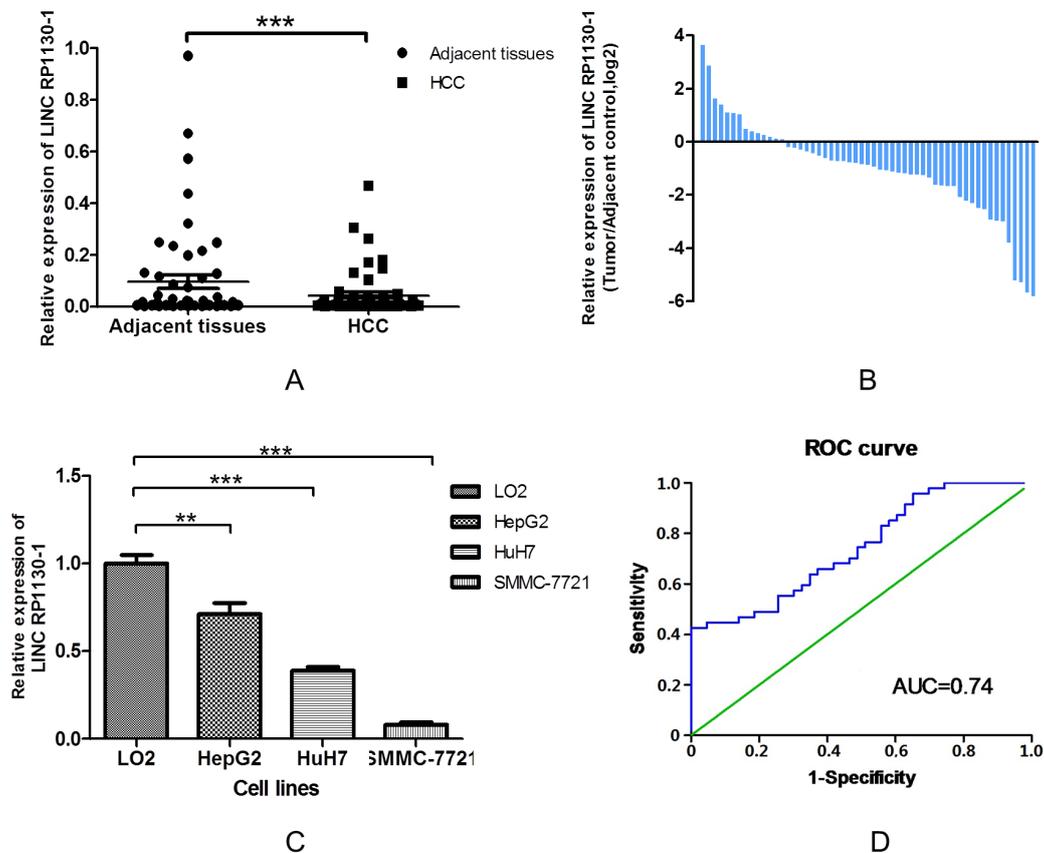
Figure 3. Relative level of LINC RP1130-1 expression in patients with hepatocellular carcinoma (HCC). (A). Relatively lower levels of LINC RP1130-1 expression were detected in HCC tissues than in adjacent non-tumor tissues from patients. **(B)**. Here, positive values for LINC RP1130-1 expression indicate a higher level of LINC RP1130-1 expression in tumor tissue than in non-tumor tissue and negative values indicate a lower level of LINC RP1130-1 expression in tumor tissue than in non-tumor tissue. **(C)**. The level of LINC RP1130-1 expression was lower in HCC cell lines than in LO2 (p < 0.05). **(D)**. The area under the receiver operating characteristic (ROC) curve was 0.74, distinguishing HCC from adjacent normal tissues. *: p < 0.05
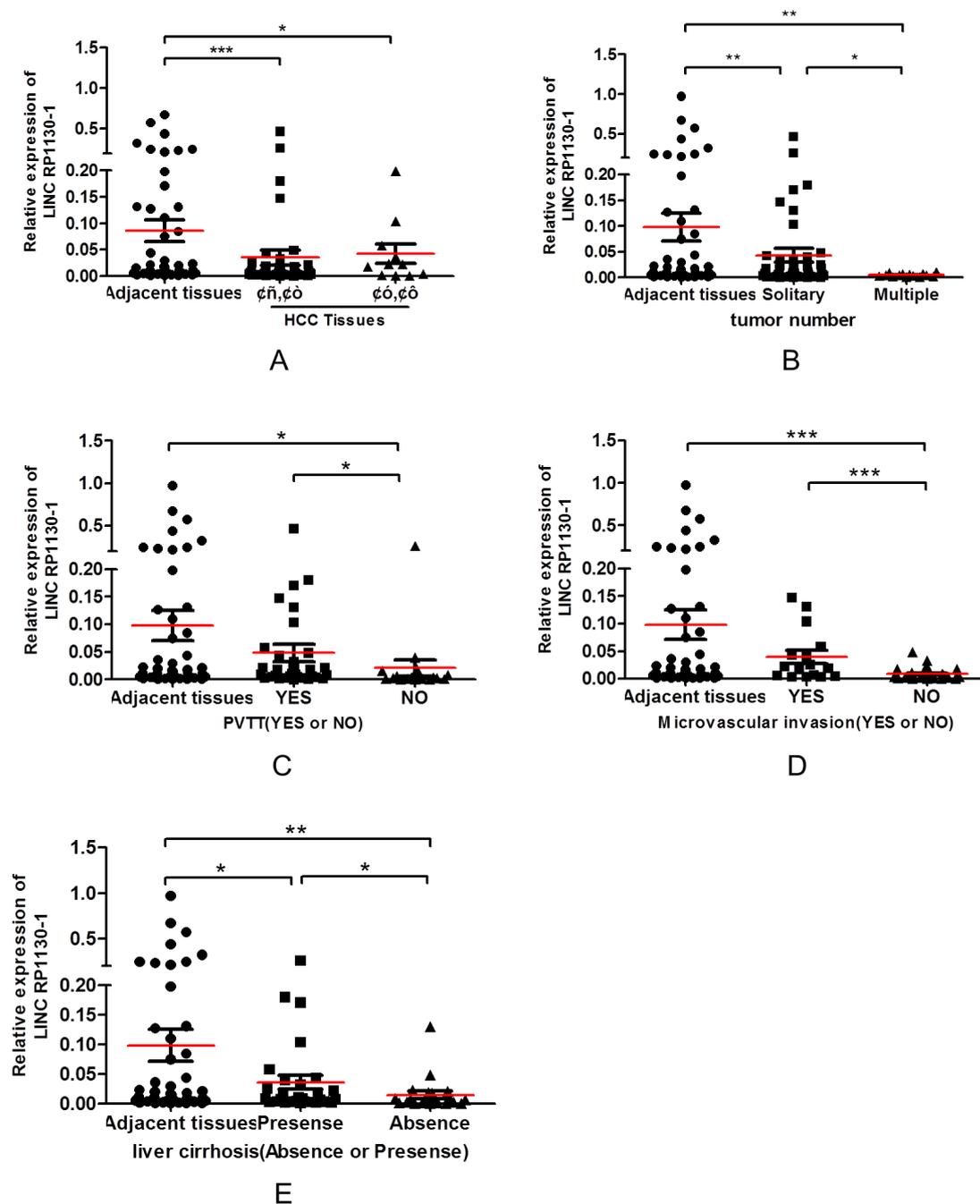
Figure 4. LINC RP1130-1 expression is associated with clinical stage, the number of tumors, PVTT, microvascular invasion, and liver cirrhosis. (A) LINC RP1130-1 expression in patients with stage I, II, III, or IV HCC was lower than in adjacent tissues. **(B)** LINC RP1130-1 expression was significantly higher in solitary HCC compared to multiple HCC. **(C)** LINC RP1130-1 expression changed markedly in patients with PVTT compared to patients without PVTT. **(D)** LINC RP1130-1 expression in patients with microvascular invasion differed significantly from that in patients without microvascular invasion. **(E)** Levels of LINC RP1130-1 expression in patients with liver cirrhosis were higher than those in patients without liver cirrhosis.

shown in Figure 4A, the level of LINC RP1130-1 expression was lower in tissue samples of clinical stage I and II HCC ($p < 0.001$) and clinical stage III and IV ($p < 0.05$) than in adjacent tissues. However, there was no significant difference in the level of expression in stage I, II, III, and IV. The level of LINC RP1130-1 expression was also lower in patients with multiple tumors than in those with solitary tumors (Figure 4B). In addition, the level of LINC RP1130-1 expression

differed markedly in patients with PVTT or MVI than in those without PVTT or MVI (Figure 4C, D). The level of LINC RP1130-1 expression also varied significantly in patients with liver cirrhosis and those without liver cirrhosis (Figure 4E). The level of LINC RP1130-1 expression in patients with PVTT, MVI, or cirrhosis was higher than that in patients without PVTT, MVI, or cirrhosis, but that level was still lower than the average level of expression in adjacent tissues.

Table 1. Association between LINC RP1130-1 and clinic pathological characteristics of patients with HCC[a]

Parameters	Total	LINC RP1130-1 expression		*p* value
		Low	High	
Gender				
Male	42	22	20	0.3
Female	9	3	6	
Age (years)				
< 60	36	19	17	0.406
≥ 60	15	6	9	
Tumor size (cm)				
<5 cm	23	11	12	0.877
≥5 cm	28	14	14	
AFP				
< 20	21	9	12	0.461
≥ 20	30	16	14	
Histological grade				
Well/moderate	2	2	0	0.141
Poorly	49	23	26	
Clinical stage				
I and II	40	23	17	0.021*
III and IV	11	2	9	
Number of tumors				
Solitary	44	24	20	0.048*
Multiple	7	1	6	
Alcohol consumption				
Yes	23	12	11	0.683
No	28	13	15	
Smoking status				
Yes	19	9	10	0.856
No	32	16	16	
HBV				
Yes	37	16	21	0.180
No	14	9	5	
Recurrence				
Yes	20	9	11	0.644
No	29	15	14	
PVTT				
Yes	33	12	21	0.014*
No	18	13	5	
Microvascular invasion				
Yes	19	18	1	< 0.001***
No	32	7	25	
Liver cirrhosis				
Absence	21	14	7	0.035*
Presence	30	11	19	

[a]: Table 1 summarizes the association between LINC RP1130-1 expression and the clinic pathologic features of patients with HCC. A low level of LINC RP1130-1 expression was found to significantly correlate with clinical stage ($p = 0.021$), the number of tumors ($p = 0.048$), PVTT ($p = 0.014$), liver cirrhosis ($p = 0.035$), and microvascular invasion ($p < 0.001$). However, LINC RP1130-1 expression was not significantly related to gender, age, tumor size, histological grade, alcohol consumption, smoking status, HBV, or recurrence ($p > 0.05$). The median level of LINC RP1130-1 expression served as the cutoff. *: $p < 0.05$, ***: $p < 0.001$.

3.3. Relationship between LINC RP1130-1 expression and RFS in patients with HCC

Patients were divided into 2 groups, those with a level of LINC RP1130-1 expression below the 50th percentile who were classified as having lower LINC RP1130-1 levels ($n = 26$). Patients with a level of LINC RP1130-1 expression above the 50th percentile were classified as having higher LINC RP1130-
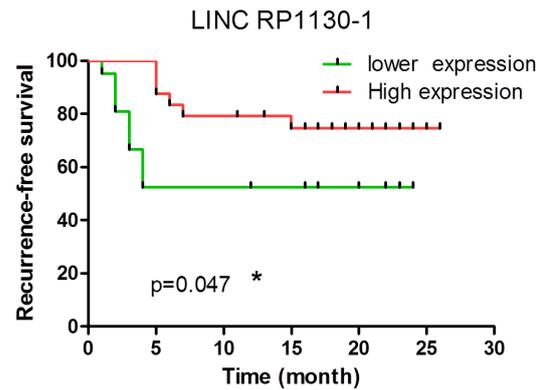

Figure 5. Kaplan-Meier curves for recurrence-free survival (RFS) in patients with HCC and a low or high level of LINC RP1130-1 expression

1 levels ($n = 25$). A second analysis yielded similar results, *i.e.* the level of LINC RP1130-1 expression was related to clinical stage, multiple tumors, and the presence of PVTT, MVI, or liver cirrhosis, but there was no significant correlation between LINC RP1130-1 expression and other clinicopathological features, including age, gender, tumor size, histological grade, alcohol consumption, smoking status, hepatitis B virus (HBV), and recurrence (Table 1). However, Kaplan-Meier analysis of the relationship between the level of LINC RP1130-1 expression and RFS indicated that patients with lower levels of LINC RP1130-1 expression had a significantly shorter RFS than patients with higher levels of expression ($p < 0.05$) (Figure 5).

4. Discussion

This study noted dys-regulation of LINC RP1130-1 in HCC tissues compared to matching adjacent non-tumor tissues. Results indicated that LINC RP1130-1 expression in HCC decreased significantly in both stage I and II ($p < 0.0001$) and in stage III and IV ($p < 0.05$). The AUC was 0.74 for LINC RP1130-1, indicating its specificity and sensitivity in the diagnosis of HCC, and patients with HCC and low levels of LINC RP1130-1 expression had a significantly shorter RFS ($p = 0.047$) than did patients with high levels of expression. Expression of LINC RP1130-1 differed significantly depending on the presence of PVTT or cirrhosis ($p < 0.05$), the number of tumors ($p < 0.05$), and microvascular invasion ($p < 0.001$). This suggests the prognostic value of LINC RP1130-1. Overall, LINC RP1130-1 may play an important role in the development and progression of HCC.

Numerous studies have found that factors, including the stage of HCC, the presence of PVTT or cirrhosis, and the number of tumors, have considerable significance in tumor recurrence. MVI is a sign of the invasive nature of HCC and is the most important predictor of HCC recurrence after surgery. Angiogenesis in tumor tissues

can lead to microvascular thrombus formation, which is a critical risk factor associated with intrahepatic metastasis of HCC. Recent studies have found that MVI is an independent risk factor for HCC recurrence and that microvascular thrombi tend to express different levels of lncRNA compared to tumor tissues. MVI has clinical significance in monitoring recurrence and guiding adjuvant therapy. Microvascular thrombi were difficult to detect in imaging tests and were always confirmed *via* a pathological examination after surgery. Thus, identifying a biomarker of MVI would greatly facilitate prediction of HCC recurrence. However, the current data indicated that levels of LINC RP1130-1 expression in patients without PVTT or MVI were lower than those in patients with PVTT or MVI, which was contrary to expectations. Samples were selected randomly instead of pairing patients with certain clinical indicators, which may have caused an uneven distribution of samples with specific characteristics and thus account for this unexpected result. As an example, only 7 patients had multiple tumors while the rest had solitary tumors. That said, the extent of intratumor heterogeneity may also account for this result. A recent study has shown that different subtypes of tumor cells with unique expression profiles were distributed within the same tumor lesions and that this distribution may change depending on the progression of tumor (*35*). The size of the clinical sample should be increased in subsequent experiments in order to verify the level of LINC RP1130-1 expression, especially in patients with PVTT or MVI. However, the level of LINC RP1130-1 expression consistently decreased in HCC, and it still should be able to serve as a potential biomarker of HCC.

HCC develops frequently when fibrosis is in an advanced stage, so eradicating HBV or HCV infection is a promising prophylactic therapy to prevent the occurrence of liver fibrosis and HCC (*36*). Numerous lncRNAs have been found to participate in the development and progression of liver cancer, but few studies have reported on the role of lncRNAs in the process of cirrhosis. Human hepatic stellate cells (HSCs) are closely related to cirrhosis. A recent study has reported that more than 3,600 lncRNAs are expressed at different levels in HSCs and that 400 lncRNAs are specifically expressed in HSC (*37*), suggesting that lncRNAs may play a key role in the progression of cirrhosis. The lncRNA HULC was found to be up-regulated in plasma samples from patients with HBV-related cirrhosis (*38*). The current study indicated that LINC RP-1130 tends to be expressed at lower levels in patients with cirrhosis than patients without cirrhosis, suggesting that some LncRNA expression profiles may change in patients with HCC and cirrhosis.

In conclusion, the current results are the first to indicate that LINC RP1130-1 levels were significantly lower in HCC tissues and that dysregulation of LINC RP1130-1 was correlated with PVTT and MVI in patients with HCC. Patients with HCC and low levels of LINC RP1130-1 expression had a significantly shorter RFS than did patients with high levels of expression. These findings indicate that LINC RP1130-1 may have potential as a diagnostic and prognostic biomarker for HCC.

References

1. Torre LA, Bray F, Siegel RL, Ferlay J, Lortet-Tieulent J, Jemal A. Global cancer statistics, 2012. CA Cancer J Clin. 2015; 65:87-108.
2. El-Serag HB. Hepatocellular carcinoma. N Engl J Med. 2011; 365:1118-1127.
3. Rogacki K, Kasprzak A, Stepinski A. Alterations of Wnt/beta-catenin signaling pathway in hepatocellular carcinomas associated with hepatitis C virus. Pol J Pathol. 2015; 66:9-21.
4. Raft MB, Jorgensen EN, Vainer B. Gene mutations in hepatocellular adenomas. Histopathology. 2015; 66:910-921.
5. Zucman-Rossi J, Villanueva A, Nault JC, Llovet JM. Genetic Landscape and Biomarkers of Hepatocellular Carcinoma. Gastroenterology. 2015; 149:1226-1239.e4.
6. Ding SL, Yang ZW, Wang J, Zhang XL, Chen XM, Lu FM. Integrative analysis of aberrant Wnt signaling in hepatitis B virus-related hepatocellular carcinoma. World J Gastroenterol. 2015; 21:6317-6328.
7. Xiong Y, Yuan J, Zhang C, Zhu Y, Kuang X, Lan L, Wang X. The STAT3-regulated long non-coding RNA Lethe promote the HCV replication. Biomed Pharmacother. 2015; 72:165-171.
8. Yao S, Johnson C, Hu Q, Yan L, Liu B, Ambrosone CB, Wang J, Liu S. Differences in somatic mutation landscape of hepatocellular carcinoma in Asian American and European American populations. Oncotarget. 2016. doi: 10.18632/oncotarget.9636.
9. Friemel J, Rechsteiner M, Bawohl M, Frick L, Mullhaupt B, Lesurtel M, Weber A. Liver cancer with concomitant TP53 and CTNNB1 mutations: A case report. BMC Clin Pathol. 2016; 16:7.
10. Buonaguro L, Consortium H. Developments in cancer vaccines for hepatocellular carcinoma. Cancer Immunol Immunother. 2016; 65:93-99.
11. Wu L, Shen F, Xia Y, Yang YF. Evolving role of radiopharmaceuticals in hepatocellular carcinoma treatment. Anticancer Agents Med Chem. 2016; 16:1155-1165.
12. Baldissera VD, Alves AF, Almeida S, Porawski M, Giovenardi M. Hepatocellular carcinoma and estrogen receptors: Polymorphisms and isoforms relations and implications. Med Hypotheses. 2016; 86:67-70.
13. Niu ZS, Niu XJ, Wang WH, Zhao J. Latest developments in precancerous lesions of hepatocellular carcinoma. World J Gastroenterol. 2016; 22:3305-3314.
14. Zou H, Shao CX, Zhou QY, Zhu GQ, Shi KQ, Braddock M, Huang DS, Zheng MH. The role of lncRNAs in hepatocellular carcinoma: Opportunities as novel targets for pharmacological intervention. Expert Rev Gastroenterol Hepatol. 2016; 10:331-340.
15. Huarte M. The emerging role of lncRNAs in cancer. Nat Med. 2015; 21:1253-1261.
16. Schmitt AM, Chang HY. Gene regulation: Long RNAs

wire up cancer growth. Nature. 2013; 500:536-537.

17. Jiang JF, Sun AJ, Xue W, Deng Y, Wang YF. Aberrantly expressed long noncoding RNAs in the eutopic endometria of patients with uterine adenomyosis. Eur J Obstet Gynecol Reprod Biol. 2016; 199:32-37.

18. Yan R, Wang K, Peng R, Wang S, Cao J, Wang P, Song C. Genetic variants in lncRNA SRA and risk of breast cancer. Oncotarget. 2016; 7:22486-22496.

19. Al-Tobasei R, Paneru B, Salem M. Genome-Wide Discovery of Long Non-Coding RNAs in Rainbow Trout. Plos One. 2016; 11:e0148940.

20. Yang Y, Wen L, Zhu H. Unveiling the hidden function of long non-coding RNA by identifying its major partner-protein. Cell Biosci. 2015; 5:59.

21. Casero D, Sandoval S, Seet CS, Scholes J, Zhu Y, Ha VL, Luong A, Parekh C, Crooks GM. Long non-coding RNA profiling of human lymphoid progenitor cells reveals transcriptional divergence of B cell and T cell lineages. Nat Immunol. 2015; 16:1282-1291.

22. Shen L, Chen L, Wang Y, Jiang X, Xia H, Zhuang Z. Long noncoding RNA MALAT1 promotes brain metastasis by inducing epithelial-mesenchymal transition in lung cancer. J Neurooncol. 2015; 121:101-108.

23. Wang D, Ding L, Wang L, Zhao Y, Sun Z, Karnes RJ, Zhang J, Huang H. LncRNA MALAT1 enhances oncogenic activities of EZH2 in castration-resistant prostate cancer. Oncotarget. 2015; 6:41045-41055.

24. Hu L, Wu Y, Tan D, Meng H, Wang K, Bai Y, Yang K. Up-regulation of long noncoding RNA MALAT1 contributes to proliferation and metastasis in esophageal squamous cell carcinoma. J Exp Clin Cancer Res. 2015; 34:7.

25. Wang Y, Chen W, Yang C, Wu W, Wu S, Qin X, Li X. Long non-coding RNA UCA1a(CUDR) promotes proliferation and tumorigenesis of bladder cancer. Int J Oncol. 2012; 41:276-284.

26. Jiang W, Zhang D, Xu B, Wu Z, Liu S, Zhang L, Tian Y, Han X, Tian D. Long non-coding RNA BANCR promotes proliferation and migration of lung carcinoma *via* MAPK pathways. Biomed Pharmacother. 2015; 69:90-95.

27. Askarian-Amiri ME, Crawford J, French JD, Smart CE, Smith MA, Clark MB, Ru K, Mercer TR, Thompson ER, Lakhani SR, Vargas AC, Campbell IG, Brown MA, Dinger ME, Mattick JS. SNORD-host RNA Zfas1 is a regulator of mammary development and a potential marker for breast cancer. RNA. 2011; 17:878-891.

28. Ji TT, Huang X, Jin J, Pan SH, Zhuge XJ. Inhibition of long non-coding RNA TUG1 on gastric cancer cell transference and invasion through regulating and controlling the expression of miR-144/c-Met axis. Asian Pac J Trop Med. 2016; 9:508-512.

29. Wang F, Yuan JH, Wang SB, Yang F, Yuan SX, Ye C, Yang N, Zhou WP, Li WL, Li W, Sun SH. Oncofetal long noncoding RNA PVT1 promotes proliferation and stem cell-like property of hepatocellular carcinoma cells by stabilizing NOP2. Hepatology. 2014; 60:1278-1290.

30. Lu Z, Xiao Z, Liu F, Cui M, Li W, Yang Z, Li J, Ye L, Zhang X. Long non-coding RNA HULC promotes tumor angiogenesis in liver cancer by up-regulating sphingosine kinase 1 (SPHK1). Oncotarget. 2016; 7:241-254.

31. Yang F, Zhang L, Huo XS, Yuan JH, Xu D, Yuan SX, Zhu N, Zhou WP, Yang GS, Wang YZ, Shang JL, Gao CF, Zhang FR, Wang F, Sun SH. Long noncoding RNA high expression in hepatocellular carcinoma facilitates tumor growth through enhancer of zeste homolog 2 in humans. Hepatology. 2011; 54:1679-1689.

32. Yuan JH, Yang F, Wang F, *et al*. A long noncoding RNA activated by TGF-beta promotes the invasion-metastasis cascade in hepatocellular carcinoma. Cancer cell. 2014; 25:666-681.

33. Yuan SX, Wang J, Yang F, Tao QF, Zhang J, Wang LL, Yang Y, Liu H, Wang ZG, Xu QG, Fan J, Liu L, Sun SH, Zhou WP. Long noncoding RNA DANCR increases stemness features of hepatocellular carcinoma by derepression of CTNNB1. Hepatology. 2016; 63:499-511.

34. Ji J, Tang J, Deng L, Xie Y, Jiang R, Li G, Sun B. LINC00152 promotes proliferation in hepatocellular carcinoma by targeting EpCAM *via* the mTOR signaling pathway. Oncotarget. 2015; 6:42813-42824.

35. Xue R, Li R, Guo H, Guo L, Su Z, Ni X, Qi L, Zhang T, Li Q, Zhang Z, Xie XS, Bai F, Zhang N. Variable Intra-Tumor Genomic Heterogeneity of Multiple Lesions in Patients With Hepatocellular Carcinoma. Gastroenterology. 2016; 150:998-1008.

36. Shirasaki T, Honda M, Shimakami T, Murai K, Shiomoto T, Okada H, Takabatake R, Tokumaru A, Sakai Y, Yamashita T, Lemon SM, Murakami S, Kaneko S. Impaired interferon signaling in chronic hepatitis C patients with advanced fibrosis *via* the transforming growth factor beta signaling pathway. Hepatology. 2014; 60:1519-1530.

37. Yang HI, Yuen MF, Chan HL, Han KH, Chen PJ, Kim DY, Ahn SH, Chen CJ, Wong VW, Seto WK, Group R-BW. Risk estimation for hepatocellular carcinoma in chronic hepatitis B (REACH-B): Development and validation of a predictive score. Lancet Oncol. 2011; 12:568-574.

38. Zhao J, Fan Y, Wang K, Ni X, Gu J, Lu H, Lu Y, Lu L, Dai X, Wang X. LncRNA HULC affects the differentiation of Treg in HBV-related liver cirrhosis. Int Immunopharmacol. 2015; 28:901-905.

Original Article

Ferulic acid prevents liver injury induced by Diosbulbin B and its mechanism

Chengwei Niu[1], Yuchen Sheng[2], Enyuan Zhu[1], Lili Ji[1,*], Zhengtao Wang[1]

[1] *Shanghai Key Laboratory of Complex Prescription, The MOE Key Laboratory for Standardization of Chinese Medicines, and The SATCM Key Laboratory for New Resources and Quality Evaluation of Chinese Medicines, Institute of Chinese Materia Medica, Shanghai University of Traditional Chinese Medicine, Shanghai, China;*
[2] *Center for Drug Safety Evaluation and Research, Shanghai University of Traditional Chinese Medicine, Shanghai, China.*

Summary	The rhizome of *Dioscorea bulbifera* Linn, traditionally used to treat thyroid disease and cancer in China, is reported to induce serious liver injury during clinical practice. Diosbulbin B (DB), a diterpene lactone, has been found to be the main toxic compound in *D. bulbifera*. The present study aims to investigate the protection of ferulic acid (FA) against DB-induced acute liver injury and its engaged mechanism. Mice were orally administered FA (20, 40, 80 mg/kg) once daily for 6 consecutive days; and then orally given DB (250 mg/kg) on the last day. Daily FA (40, 80 mg/kg) decreased DB (250 mg/kg)-induced increase in serum levels of alanine/aspartate aminotransferase (ALT/AST) and alkaline phosphatase (ALP). Histological evaluation showed that FA (80 mg/kg) ameliorated DB-induced hepatocellular degeneration and lymphocyte infiltration. Results of terminal dUTP nick-end labeling (TUNEL) staining assay showed that FA (80 mg/kg) decreased the DB-increased number of apoptotic hepatocytes. FA (40, 80 mg/kg) reduced DB-increased liver malondialdehyde (MDA) amount. FA (40, 80 mg/kg) decreased DB-increased serum levels of tumor necrosis factor alpha (TNF-α) and interferon-γ (IFN-γ), and liver myeloperoxidase (MPO) activity. FA (80 mg/kg) reversed the DB-induced decrease in expression of inhibitor of kappa B (IκB) and the increase in nuclear translocation of the p65 subunit of nuclear factor kappa B (NFκBp65). Taken together, our results demonstrate that FA prevents DB-induced acute liver injury *via* inhibiting intrahepatic inflammation and liver apoptosis.

Keywords: Hepatotoxicity, detoxification, inflammation, apoptosis, NFκB

1. Introduction

The rhizome of *Dioscorea bulbifera* Linn. is traditionally used to treat thyroid disease and cancer in China (*1*). However, *D. bulbifera* can cause severe hepatotoxicity in clinical practice, which seriously limits the anti-tumor activity of this medicinal herb (*2*). Our previous studies demonstrated that intake of *D. bulbifera* could result in severe liver injury such as liver swelling, fatty degeneration, and even animal death (*3-*

5). Diosbulbin B (DB), a diterpene lactone, was isolated from *D. bulbifera*, and showed significant antitumor activity in our previous reported study (*6*). However, our previous studies also showed that DB was the main hepatotoxic compound in *D. bulbifera*, and it caused oxidative stress-associated liver injury (*4,7*).

Ferulic acid (FA) is found in many Chinese medicinal herbs such as Angelica sinensis (Oliv) Diels (Angelica) and *Ligusticum chuanxiong* Hort. (Ligusticum) (*8*). FA exerts multiple biological activities such as antioxidant, and anti-inflammation (*9,10*) and it is known for treatment of Alzheimer's disease (*11*), cardiovascular disease (*12*), and cancer (*13*). In addition, FA is reported to have hepato-protective activity (*14,15*). Previous study in our lab has demonstrated that *A. sinensis* root prevented liver injury induced by *D. bulbifera* rhizome (*16*). As the main active compound in *A. sinensis*, we think that FA may prevent DB-induced liver injury

in mice. In addition, our previous study has already demonstrated that FA attenuated DB-induced liver injury in S180 tumor-bearing mice and further augmented DB-induced inhibition of tumor growth *in vivo* (*17*). The present study is designed to investigate protection by FA against acute liver injury induced by DB in mice and the potential underlying mechanism.

2. Materials and Methods

2.1. *Drugs and reagents*

DB (Figure1A) and FA (Figure 1B) were purchased from Shanghai Tauto Biotech Co., Ltd (Shanghai, China). Antibodies against inhibitor of kappa B (IκB), p65 subunit of nuclear factor kappa B (NFκBp65) and β-actin were all purchased from Cell Signaling Technology (Danvers, MA, USA). Peroxidase-conjugated goat anti-Rabbit IgG (H+L) was purchased from Jackson ImmunoResearch (West Grove, PA, USA). Nitrocellulose membranes were purchased from Bio-Rad (Hercules, CA, USA). Enhanced chemiluminescence detection system was obtained from Millipore Corporation (Billerica, MA, USA). Nuclear/Cytosol fractionation Kit was obtained from BioVision (Palo Alto, CA, USA). Enzyme linked immunosorbent assay (ELISA) Kits for determining tumor necrosis factor alpha (TNF-α) and interferon-γ (IFN-γ) were purchased from RapidBio (West Hills, CA, USA). Kits for detecting the activity of alanine/aspartate aminotransferase (ALT/AST), alkaline phosphatase (ALP), myeloperoxidase (MPO) and malondialdehyde (MDA) were purchased from Nanjing Jiancheng Bioengineering Institute (Nanjing, China).

2.2. *Experimental animals*

Specific pathogen free male ICR mice (18-22 g body weight) were obtained from the Shanghai laboratory animal center of Chinese Academy of Sciences (Shanghai, China). Animals were fed a standard laboratory diet and given free access to tap water, kept in a controlled room temperature (22 ± 1°C), humidity (65 ± 5 %), and a 12:12-h light/dark cycle. All animals received humane care in compliance with the institutional animal care guidelines approved by the Experimental Animal Ethical Committee of Shanghai University of Traditional Chinese Medicine.

2.3. *Treatment protocol*

Mice were divided into 6 groups. Mice in group 1 were used as control group. Mice in group 2 were orally administered DB (250 mg/kg, suspended in 0.5% sodium carboxyl methyl cellulose (CMC-Na)) only once on the sixth day. Mice in groups 3-5 were orally given FA suspended in 0.5% CMC-Na (20, 40 or 80 mg/kg per day) for six consecutive days, and DB was

orally given two hours after the final administration of FA. Mice in group 6 were given FA only, suspended in 0.5% CMC-Na (80 mg/kg per day), for six consecutive days. Twenty-four hours later after administration of DB, blood and liver samples were collected for further research (*16-18*).

2.4. *Assay for serum ALT, AST and ALP*

The blood samples collected from all groups of mice were kept at room temperature to coagulate for 2 h. Serum was then isolated and transferred to new tubes after centrifugation at 840 × g for 15 min. Serum ALT, AST and ALP levels were detected with kits according to the manufacturer's instructions.

2.5. *Histological observation*

The liver tissues were soaked in 10 % formalin, and embedded in paraffin. Samples were cut into five micrometer sections and stained with hematoxylin-eosin for further histological assessment of tissue damage.

2.6. *TdT-mediated biotin–dUTP nick-end labelling (TUNEL) assay*

For the detection of apoptosis, paraffin-embedded sections were stained with the TUNEL detection kit according to the manufacturer's protocol. The cells showing nuclear dark-brown staining were considered to be positive staining (apoptotic cells). The apoptotic hepatocytes were counted manually in at least nine randomly selected fields from each group using a light microscope at a magnification of ×200.

2.7. *Analysis of MDA amount*

MDA amount in liver was determined using an MDA detection kit according to the manufacturer's instructions. MDA amount is expressed as nmol/mg of protein.

2.8. *ELISA analysis*

Serum contents of TNF-α and IFN-γ were measured with ELISA kits according to the manufacturer's instructions.

2.9. *Analysis of MPO activity*

Liver MPO activity was determined using a MPO detection kit according to the manufacturer's instructions. MPO activity is expressed as units/g of protein.

2.10. *Extracting cytosol and nuclear proteins*

Cytosol and nuclear proteins were extracted according to the manufacturer's instructions. Protein concentration

was determined and normalized to equal protein concentrations.

2.11. Western blot analysis

Liver tissue was homogenized in ice-cold lysis buffer containing 50 mM Tris (pH 7.5), 150 mM NaCl, 1 mM EDTA, 20 mM NaF, 0.5% NP-40, 10% glycerol, 1 mM phenylmethylsulfonyl fluoride, 10 g/mL aprotinin, 10 g/mL leupeptin, 10 g/mL pepstatin A. The homogenate was centrifuged at 10,000 g for 20 min at 4°C. The supernatant was transferred to new tubes and protein concentration was assayed and normalized to equal protein concentrations. Protein samples were separated by sodium dodecyl sulfate-polyacrylamide gel electrophoresis (SDS-PAGE) and blots were incubated with primary and horseradish peroxidase (HRP)-conjugated secondary antibodies. The protein bands were quantified by ratios of integral optic density (IOD) following normalization to β-actin, and the results were expressed as percentage of control.

2.12. Statistical analysis

All experimental data were expressed as means ± standard error (S.E.). Significant differences were determined by One-Way ANOVA. $p < 0.05$ was considered as statistically significant difference.

3. Results

3.1. FA decreased DB-induced increase in serum levels of ALT, AST and ALP

Shown in Figure 1C and 1D, DB (250 mg/kg) are increased serum levels of ALT, AST and ALP as
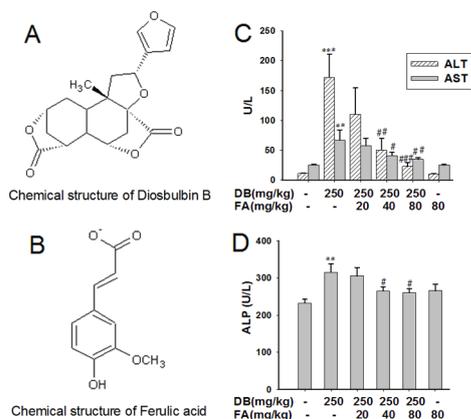

Figure 1. FA decreased the increased serum levels of ALT, AST and ALP induced by DB. Chemical structure of DB **(A)** and FA **(B)**; **(C)** ALT and AST; **(D)** ALP. Data are shown as means ± S.E. ($n = 10$). **$p < 0.01$, ***$p < 0.001$ versus control group, #$p < 0.05$, ##$p < 0.01$, ###$p < 0.001$ versus DB-treated group. ALP, alkaline phosphatase; ALT, alanine aminotransferase; AST, aspartate aminotransferase; DB, Diosbulbin B; FA, Ferulic acid.

compared with control. After treatment with FA (40, 80 mg/kg), DB-induced an increase in serum levels of ALT, AST and ALP, which were all decreased (p < 0.05, p < 0.01, p < 0.001). In addition, there were no significant differences in the serum levels of ALT, AST and ALP between control and FA (80 mg/kg)-treated mice ($p > 0.05$).

3.2. Histological evaluation of liver

As compared to control, the liver from the mice treated with DB showed serious liver damage, indicated by hepatocellular degeneration and lymphocyte infiltration (Figure 2B). After treatment with FA (20, 40, 80 mg/kg), all these phenomena were ameliorated (Figure 2C, 2D, and 2E), and FA at 80 mg/kg was the most effective. Livers from control (Figure 2A) and FA (80 mg/kg)-treated (Figure 2F) mice showed normal histology.

3.3. FA alleviated DB-induced cell apoptosis

As shown in Figure 3A-a and 3A-b, there were an increased number of brown (TUNEL-positive) apoptotic hepatocytes in DB (250 mg/kg)-treated mice as compared with control. After treatment with FA (80 mg/kg), the increased number of apoptotic cells was reduced (Figure 3A-c), but FA (80 mg/kg) alone had no effect on liver apoptosis. After counting the apoptotic hepatocytes, the results showed that FA (80 mg/kg) decreased the increased apoptotic hepatocytes induced by DB ($p < 0.01$) (Figure 3B).

3.4. FA decreased DB-induced increase of liver MDA amount

As shown in Figure 3C, DB increased liver amount of MDA ($p < 0.01$), whereas FA (40, 80 mg/kg) reduced the increased amount of MDA induced by DB ($p < 0.01$, $p < 0.001$).

3.5. FA reduced DB-induced increase in serum TNF-α and IFN-γ levels, and liver MPO activity

As shown in Figure 4A and 4B, DB increased serum levels of TNF-α and IFN-γ ($p < 0.01$, $p < 0.001$), whereas FA (20, 40, 80 mg/kg) reduced the increase in serum levels of TNF-α and IFN-γ induced by DB ($p < 0.05$, $p < 0.01$, $p < 0.001$). In addition, the results of Figure 4C showed that DB-induced increase in liver MPO activity was reduced in FA (40, 80 mg/kg)-treated mice ($p < 0.05$).

3.6. FA reversed DB-induced decrease in IκB expression and increase in NFκBp65 nuclear translocation
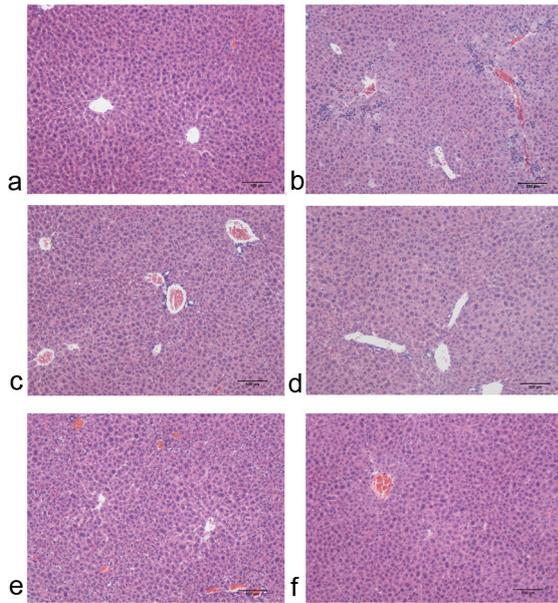
As shown in Figure 5A and 5C, FA (80 mg/kg) increased

Figure 2. Histological evaluation of liver. (a) Vehicle control; **(b)** DB (250 mg/kg); **(c)** DB (250 mg/kg) + FA (20 mg/kg); (d) DB (250 mg/kg) + FA (40 mg/kg); **(e)** DB (250 mg/kg) + FA (80 mg/kg), **(f)** FA (80 mg/kg). Liver sections were stained with hematoxylin-eosin (original magnification 100 ×). DB, Diosbulbin B; FA, Ferulic acid.
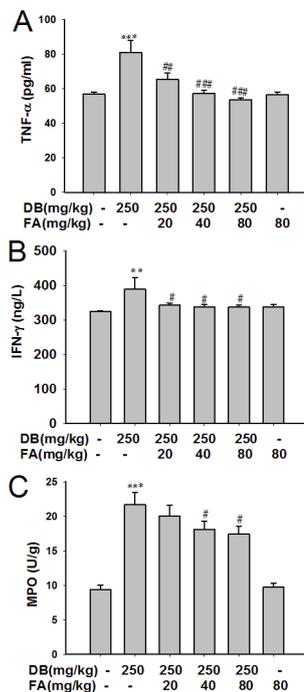

Figure 3. FA alleviated DB-induced liver apoptosis and DB-increased liver MDA amount. (A) Apoptosis was determined by TUNEL staining assay. Typical images were chosen from each group. **(a)** Vehicle control, **(b)** DB (250 mg/kg), **(c)** DB (250 mg/kg) + FA (80 mg/kg), **(d)** FA (80 mg/kg). (original magnification 200 ×). **(B)** Data are shown as means ± S.E., (n = 4). *p < 0.05 versus control, ##p < 0.01 versus DB-treated group. **(C)** FA decreased the increased liver MDA amount induced by DB. Data are shown as means ± S.E., (n = 9-10). **p < 0.01 versus control, ##p < 0.01, ###p < 0.001 versus DB-treated group. DB, Diosbulbin B; FA, Ferulic acid.

Figure 4. FA decreased DB-increased serum TNF-α and IFN-γ levels, and liver MPO activity. (A) Serum TNF-α; **(B)** Serum IFN-γ; **(C)** Liver MPO activity. Data are shown as means ± S.E., (n = 8-10). *p < 0.05, **p < 0.01, ***p < 0.001 versus control, #p < 0.05, ##p < 0.01 versus DB-treated group. DB, Diosbulbin B.
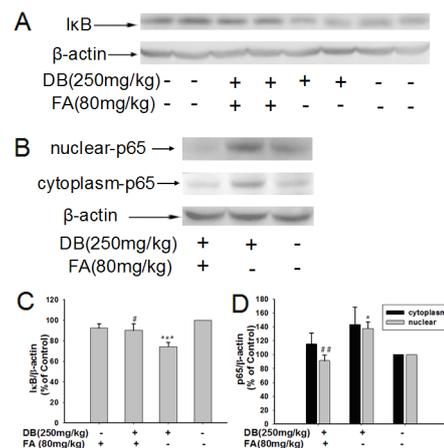
Figure 5. FA reversed DB-induced the decreased IκB expression and increased NFκBp65 nuclear translocation. (A) The expression of IκB in cytoplasm; **(B)** The expression of cytosol and nuclear NFκBp65 protein; **(C)** Quantitative densitometric analysis of IκB protein; **(D)** Quantitative densitometric analysis of NFκBp65 protein. The bands were normalized to basal β-actin expression and the vehicle control is set as 100%. Data are shown as means ± S.E., (n = 3-4). **p < 0.01, ***p < 0.001 versus control, #p < 0.05, ###p < 0.001 versus DB-treated group. DB, Diosbulbin B.

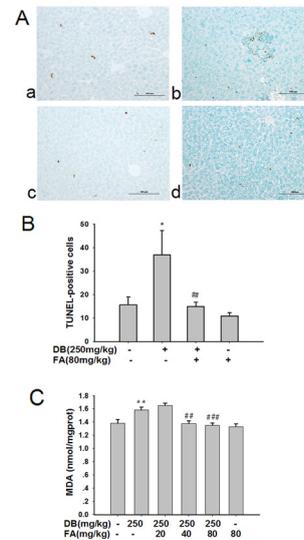the decreased expression of IκB protein induced by DB ($p < 0.05$). After treatment with DB (250 mg/kg), the nuclear expression of NFκBp65 protein was increased ($p < 0.05$) (Figure 5B and 5D). In contrast, FA (80 mg/kg) inhibited this increase of NFκBp65 protein in nucleus induced by DB ($p < 0.01$) (Figures 5B and 5D).

4. Discussion

The increased levels of serum ALT, AST and ALP are commonly used to indicate liver injury [19]. Our results of ALT, AST and ALP analysis demonstrate that FA can prevent DB-induced liver injury. In addition, such protection is further evidenced by histological evaluation of liver. Previous reports demonstrate that FA can attenuate ischemia/reperfusion or carbon tetrachloride-induced liver injury [14,15]. Meanwhile, in our previous study, FA can not only ameliorate DB-induced liver injury in tumor-bearing mice, but also increase the anticancer effect of DB [17]. The present study further evidenced the detoxification of FA against DB-induced acute liver injury, and the present and previous studies indicate the potential value for development of the combined application of DB with FA for cancer treatment.

Apoptosis is the process of programmed cell death, which may occur in various organisms including liver [20]. In situ detection of apoptosis by using TUNEL assay is a commonly used method to analyze the existence of apoptosis [21]. Our present results demonstrate that DB can induce hepatocyte apoptosis, whereas FA can prevent DB-induced apoptosis in liver. Our previous studies have already demonstrated that DB and *D. bulbifera* induced oxidative liver injury [3,4,7], and the present study is the first report concerning DB-induced liver apoptosis.

Oxidative stress plays an important role in drug-induced liver injury [22]. Reactive oxygen species (ROS) are very active and can react with lipid, and MDA is one of the main end products, thus MDA is often used as an indicator to assess oxidative injury [23]. Our previous studies have already demonstrated that DB and *D. bulbifera* can induce oxidative liver injury [3,4,7]. The present results demonstrate that FA can alleviate DB-induced liver oxidative injury *in vivo*.

TNF-α is a pro-inflammatory cytokine produced principally by activated macrophages, and previous reports demonstrated that TNF-α was involved in alcoholic hepatitis [24], and ischemia/reperfusion-induced liver injury [25]. IFN-γ is a cytokine that is critical for regulating innate and adaptive immunity, and it is also reported to be involved in various toxins-induced liver injuries such as acetaminophen and carbon tetrachloride [26,27]. MPO exists in neutrophils and its activity is generally used to assess the infiltration of neutrophils [28]. The increased MPO activity is found in carbon tetrachloride, α-naphthylisothiocyanate, and

trauma-hemorrhagic shock-induced liver injury [29-31]. The present study demonstrates that DB increases serum levels of TNF-α and IFN-γ, and elevates liver MPO activity, which indicates the occurrence of hepatic inflammation. Furthermore, FA can decrease those increased TNF-α, IFN-γ, and MPO activities, which suggests that FA can ameliorate DB-induced immunological liver injury.

It is well known that transcription factor NFκB plays a critical role in regulating host immune and inflammatory responses [32,33]. In un-stimulated cells, NFκB exists in cytoplasm associated with the inhibitory protein IκB [34]. The predominant form of NFκB is a heterodimer composed of p50 and p65 (Rel A) subunits, and NFκB is activated in response to primary (viruses, bacteria, UV) or secondary (inflammatory cytokines) pathogenic stimuli [32,35]. Stimulation induces the release of NFκB from IκB and translocation to the nucleus, where it binds to the DNA at specific κB sites, and thus initiates the expression of target genes such as TNF-α [36,37]. Our results demonstrate that FA reverses DB-induced translocation of p65 into the nucleus and decreased expression of cytosol IκB. Those results suggest that FA attenuates DB-induced immunological liver injury *via* inhibiting NFκB activation.

In conclusion, the present study demonstrates that FA, the major compound in *A. sinensis*, can prevent DB-induced liver injury, which may contribute to the detoxification of *A. sinensis* against liver injury induced by *D. bulbifera*, and provides strong experimental evidence of potential combined application of *A. sinensis* and *D. bulbifera* in the clinic. In addition, the amelioration of FA against DB-induced immunological liver injury *via* inhibiting NFκB activation may be the main mechanism involved in the protection of FA against DB-induced acute liver injury.

References

1. Gao H, Kuroyanagi M, Wu L, Kawahara N, Yasuno T, Nakamura Y. Antitumor-promoting constituents from Dioscorea bulbifera L. in JB6 mouse epidermal cells. Biol Pharm Bull. 2002; 25:1241-1243.
2. Liu JR. Two cases of toxic hepatitis caused by Dioscorea bulbifera L. Adverse Drug Reactions J. 2002; 2:129-130. (in Chinese)
3. Wang J, Ji L, Liu H, Wang Z. Study of the hepatotoxicity induced by Dioscorea bulbifera L. rhizome in mice. Biosci Trends. 2010; 4:79-85.
4. Wang JM, Liang QN, Ji LL, Liu H, Wang CH, Wang ZT. Gender-related difference in liver injury induced by Dioscorea bulbifera L. rhizome in mice. Hum Exp

Toxicol. 2011; 30:1333-1341.

5. Sheng YC, Ma YB, Deng ZP, Wang ZT. Cytokines as potential biomarkers of liver toxicity induced by Dioscorea bulbifera L. BioSci Trends. 2014; 8:32-37.

6. Wang JM, Ji LL, Branford-White CJ, Wang ZY, Shen KK, Liu H, Wang ZT. Antitumor activity of Dioscorea bulbifera L. rhizome *in vivo*. Fitoterapia. 2012; 83:388-394.

7. Ma YB, Niu CW, Wang JM, Ji LL, Wang ZT. Diosbulbin B-induced liver injury in mice and its mechanism. Hum Exp Toxicol. 2014; 33:729-736.

8. Ma ZC, Hong Q, Wang YG, Tan HL, Xiao CR, Liang QD, Cai SH, Gao Y. Ferulic acid attenuates adhesion molecule expression in gamma-radiated human umbilical vascular endothelial cells. Biol Pharm Bull. 2010; 33:752-758.

9. Ohnishi M, Matuo T, Tsuno T, Hosoda A, Nomura E, Taniguchi H. Antioxidant activity and hypoglycemic effect of ferulic acid in STZ-induced diabetic mice and KK-Ay mice. Biofactors. 2004; 21:315-319.

10. Sudheer AR, Muthukumaran S, Devipriya N, Devaraj H, Menon VP. Influence of ferulic acid on nicotine-induced lipid peroxidation, DNA damage and inflammation in experimental rats as compared to N-acetylcysteine. Toxicology. 2008; 243:317-329.

11. Yan JJ, Cho JY, Kim HS, Kim KL, Jung JS, Huh SO, Suh HW, Kim YH, Song DK. Protection against beta-amyloid peptide toxicity *in vivo* with long-term administration of ferulic acid. Br J Pharmacol. 2001; 133:89-96.

12. Alam MA, Sernia C, Brown L. Ferulic acid improves cardiovascular and kidney structure and function in hypertensive rats. J Cardiovasc Pharmacol. 2013; 61:240-249.

13. Prabhakar MM, Vasudevan K, Karthikeyan S, Baskaran N, Silvan S, Manoharan S. Anti-cell proliferative efficacy of ferulic acid against 7, 12-dimethylbenz (a) anthracene induced hamster buccal pouch carcinogenesis. Asian Pac J Cancer Prev. 2012; 13:5207-5211.

14. Kim HY, Park J, Lee KH, Lee DU, Kwak JH, Kim YS, Lee SM. Ferulic acid protects against carbon tetrachloride-induced liver injury in mice. Toxicology 2011; 282:104-111.

15. Kim HY, Lee SM. Ferulic acid attenuates ischemia/reperfusion-induced hepatocyte apoptosis *via* inhibition of JNK activation. Eur J Pharm Sci. 2012; 45:708-715.

16. Niu CW, Wang JM, Ji LL, Wang ZT. Protection of Angelica sinensis (Oliv) Diels against hepatotoxicity induced by Dioscorea bulbifera L. and its mechanism. Biosci Trends. 2014; 8:253-259.

17. Wang JM, Sheng YC, Ji LL, Wang ZT. Ferulic acid prevents liver injury and increases the anti-tumor effect of diosbulbin B *in vivo*. J Zhejiang Univ Sci B. 2014; 15:540-547.

18. Niu CW, Sheng YC, Yang R, Lu B, Bai QY, Ji LL, Wang ZT. Scutellarin protects against the liver injury induced by diosbulbin B in mice and its mechanism. J Ethnopharmacol. 2015; 164:301-308.

19. Panda V, Ashar H, Srinath S. Antioxidant and hepatoprotective effect of Garcinia indica fruit rind in ethanol-induced hepatic damage in rodents. Interdiscip Toxicol. 2012; 5:207-213.

20. Guicciardi ME, Gores GJ. Apoptosis as a mechanism for liver disease progression. Semin Liver Dis. 2012; 30:402-410.

21. Loo DT. In situ detection of apoptosis by the TUNEL assay: An overview of techniques. Methods Mol Biol.

2011; 682:3-13.

22. Stephens C, Andrade RJ, Lucena MI. Mechanisms of drug-induced liver injury. Curr Opin Allergy Clin Immunol. 2014; 14:286-292.

23. Kalender Y, Kaya S, Durak D, Uzun FG, Demir F. Protective effects of catechin and quercetin on antioxidant status, lipid peroxidation and testis-histoarchitecture induced by chlorpyrifos in male rats. Environ Toxicol Pharmacol. 2012; 33:141-148.

24. Yin M, Wheeler MD, Kono H, Bradford BU, Gallucci RM, Luster MI, Thurman RG. Essential role of tumor necrosis factor alpha in alcohol-induced liver injury in mice. Gastroenterology. 1999; 117:942-952.

25. Rüdiger HA, Clavien PA. Tumor necrosis factor alpha, but not Fas, mediates hepatocellular apoptosis in the murine ischemic liver. Gastroenterology. 2002; 122:202-210.

26. Shi YD, Zhang L, Jiang R, Chen WY, Zheng WP, Chen L, Tang L, Li L, Li L, Tang W, Wang Y, Yu Y. Protective effects of nicotinamide against acetaminophen-induced acute liver injury. Int Immunopharmacol. 2012; 14:530-537.

27. Cho BO, Ryu HW, So Y, Jin CH, Baek JY, Park KH, Byun EH, Jeong IY. Hepatoprotective effect of 2,3-dehydrosilybin on carbon tetrachloride-induced liver injury in rats. Food Chem. 2013; 138:107-115.

28. Amanzada A, Malik IA, Nischwitz M, Sultan S, Naz N, Ramadori G. Myeloperoxidase and elastase are only expressed by neutrophils in normal and in inflamed liver. Histochem Cell Biol. 2011; 135:305-315.

29. Luyendyk JP, Flanagan KC, Williams CD, Jaeschke H, Slusser JG, Mackman N, Cantor GH. Tissue factor contributes to neutrophil CD11b expression in alpha-naphthylisothiocyanate-treated mice. Toxicol Appl Pharmacol. 2012; 250:256-262.

30. Deng X, Wu K, Wa J, Li L, Jiang R, Jia M, Jing Y, Zhang L. Aminotriazole attenuated carbon tetrachloride-induced oxidative liver injury in mice. Food Chem Toxicol. 2012; 50:3073-3078.

31. Liu FC, Yu HP, Hwang TL, Tsai YF. Protective effect of tropisetron on rodent hepatic injury after trauma-hemorrhagic shock through p38 MAPK-dependent hemeoxygenase-1 expression. PLoS One. 2012; 7:e53203.

32. Baeuerle PA, Henkel T. Function and activation of NF-kappa B in the immune system. Annu Rev Immunol. 1994; 12:141-179.

33. Baeuerle PA, Baltimore D. NF-kappa B: Ten years after. Cell. 1996; 87:13-20.

34. Thompson JE, Phillips RJ, Erdjument-Bromage H, Tempst P, Ghosh S. I kappa B-beta regulates the persistent response in a biphasic activation of NF-kappa B. Cell. 1995; 80:573-582.

35. Thanos D, Maniatis T. NF-kappa B: A lesson in family values. Cell. 1995; 80:529-532.

36. Traenckner EB, Pahl HL, Henkel T, Schmidt KN, Wilk S, Baeuerle PA. Phosphorylation of human I kappa B-alpha on serines 32 and 36 controls I kappa B-alpha proteolysis and NF-kappa B activation in response to diverse stimuli. EMBO J. 1995; 14:2876-2883.

37. Scherer DC, Brockman JA, Chen Z, Maniatis T, Ballard DW. Signal-induced degradation of I kappa B alpha requires site-specific ubiquitination. Proc Natl Acad Sci U S A. 1995; 92:11259-11263.

Reversal of the multidrug resistance of human ileocecal adeno-carcinoma cells by acetyl-11-keto-β-boswellic acid *via* down-regulation of P-glycoprotein signals

Xia Xue[1], Fang Chen[1], Anxin Liu[2], Deqing Sun[1], Jing Wu[1], Feng Kong[3], Yun Luan[3], Xianjun Qu[4], Rongmei Wang[1,*]

[1] *Department of Pharmacy, the Second Hospital of Shandong University, Ji'nan, Shandong, China;*
[2] *Care Ward, Rizhao Hospital of TCM, Rizhao, Shandong, China;*
[3] *Central Laboratory, the Second Hospital of Shandong University, Ji'nan, Shandong, China;*
[4] *Department of Pharmacology, School of Basic Medical Sciences, Capital Medical University, Beijing, China.*

Summary
Multidrug resistance (MDR) represents a clinical obstacle to cancer chemotherapy since it causes cancer recurrence and metastasis. Acetyl-11-keto-β-boswellic acid (AKBA), an active ingredient derived from the plant *Boswellia serrata*, has been found to inhibit the growth of a wide variety of tumor cells, including glioma, colorectal cancer, leukemia, human melanoma, hepatocellular carcinoma, and prostate cancer cells. However, the actions of AKBA in multidrug-resistant cancer cells have not been fully elucidated. The current study examined the reversal of MDR by AKBA in a human ileocecal adenocarcinoma cell line with vincristine-induced resistance, HCT-8/VCR. A 3-[4, 5-dimethylthiazol-2-yl]-2,5-diphenyl-tetrazolium bromide (MTT) assay indicated that cytotoxicity increased drastically and the IC$_{50}$ of VCR in HCT-8/VCR cells decreased in the presence of AKBA. AKBA had a maximum "fold reversal" of MDR (FR) of 9.19-fold. In addition, HCT-8/VCR cells treated with AKBA and VCR exhibited a higher percentage of apoptotic tumor cells according to flow cytometry. The reversal of MDR by AKBA was evident in an intracellular increase in Rhodamine (Rh123), indicating that the activity of P-glycoprotein (P-gp) was blocked. Furthermore, AKBA inhibited the expression of P-gp and decreased levels of expression of multidrug resistance gene 1 in HCT-8/VCR cells. The current results indicated that AKBA might be a potential agent to reverse MDR in human ileocecal adenocarcinoma.

Keywords: Multidrug resistance (MDR), acetyl-11-keto-β-boswellic acid (AKBA), P-glycoprotein (P-gp), reversal of multidrug resistance

1. Introduction

Acquired multidrug resistance (MDR) has emerged as a major obstacle to effective chemotherapy (*1*). P-glycoprotein (P-gp) is encoded by multidrug resistance gene 1 (MDR1) and is a member of the ATP-binding cassette (ABC) superfamily (*2*). High levels of P-gp expression have been linked to the efflux of

chemotherapeutic drugs in cancer cells. Inhibition of P-gp-mediated drug efflux is an effective way to overcome cancer drug resistance (*3*). However, no agents targeting P-gp have been approved for clinical use (*4*). Therefore, agents to overcome drug resistance must be promptly identified in order to treat malignancies.

Acetyl-11-keto-β-boswellic acid (AKBA), a pentacyclic triterpene extracted from the fragrant gum resin of the *Boswellia serrata* tree, has been found to be effective against inflammatory diseases such as rheumatoid arthritis (*5*), ulcerative colitis (*6*), and trinitrobenzene sulphonic acid-induced colitis (*7*). Recently, AKBA was reported to exhibit antitumor action in several human cell lines, including malignant glioma (*8*), colon cancer (*9*), prostate cancer (*10*), and leukemia

(*11*) cell lines. In addition, AKBA has been found to suppress nuclear factor-κB and STAT3-related pathways (*12,13*). However, whether AKBA can modulate acquired MDR in tumors has yet to be determined.

The current study examined the reversal of MDR in HCT-8/VCR cells by AKBA. HCT-8/VCR is a human ileocecal adenocarcinoma cell line with vincristine-induced resistance. The ability of AKBA to reverse MDR is evident in an increase in the intracellular accumulation of VCR and inhibition of the expression of P-gp. Therefore, AKBA might be a potential agent to reverse MDR in human ileocecal adenocarcinoma.

2. Materials and Methods

2.1. *Drugs*

AKBA (Sigma-Aldrich, St. Louis, USA) was dissolved in dimethylsulfoxide (DMSO, Sigma-Aldrich) at 20 mM as a stock solution. Dilutions of all of the reagents were freshly prepared before each experiment.

2.2. *Cell lines and cell culture*

The human ileocecal adenocarcinoma cell line HCT-8 and its MDR counterpart HCT-8/VCR were purchased from Keygen Biotech (Nanjing, China). Cancer cells were maintained in RPMI-1640 (GIBCO, NY, USA) supplemented with 10% (v/v) heat-inactivated fetal bovine serum (GIBCO) and penicillin-streptomycin (100 IU/mL to 100 μg/mL) at 37°C in a humidified atmosphere (5% CO_2-95% air). Cells were harvested by brief incubation in trypsin 0.25% (w/v) and 0.53mM EDTA in PBS. HCT-8/VCR cells were maintained in a complete RPMI-1640 medium containing 1 mg/mL of vincristine (VCR, Wanle, Shenzhen, China) at 37°C in a humidified atmosphere of 5% CO_2. The cells were cultured for 2 weeks in drug-free medium prior to their use in experiments.

2.3. *Determination of P-gp*

P-gp expression was determined with a Western blot analysis as described elsewhere (*14*). A mouse monoclonal antibody against amino acids 1040-1280 of *MDR1* of human origin (sc-13131, Santa Cruz, CA, USA) was used to determine the expression of P-gp in HCT-8 and HCT-8/VCR cells. P-gp bands were quantified with densitometry using an electrophoresis image analysis system (FR980, Furi Science & Technology, China).

2.4. *Assay of cytotoxicity and reversal of MDR*

To test for reversal of P-gp-mediated MDR by AKBA, the cytotoxicity of AKBA to HCT-8/VCR and HCT-8 cells was first measured with an MTT assay (*15*). Briefly,

HCT-8/VCR and HCT-8 cells (1×10^4/well) were seeded in 96-well plates. After incubation for 12 h, the cells were treated with various concentrations of AKBA for 24 h, 48 h, and 72 h. Cell viability was assessed by adding 20 μL of MTT reagent (5 mg/mL, Sigma-Aldrich) and incubating cells for 4 h. Light absorbance of the solution was measured at 570 nm on a plate reader (TECAN, Austria).

The reversal of MDR by AKBA was then detected using the same method. Cells seeded in 96-well plates were treated with varying concentrations of VCR in the absence or presence of various concentrations of AKBA (1.25 μM, 2.5 μM, and 5 μM) for 72 h. IC_{50} values (the concentration resulting in 50% inhibition of cell growth) were calculated for VCR. The "fold reversal"of MDR (FR) was calculated by fitting data for ¼ the IC50 of VCR alone/the IC50 of VCR in the presence of AKBA. Experiments were performed in triplicate with three samples. Control cultures included an equivalent amount of DMSO (as the solvent control), which does not modulate the growth or drug sensitivity of these cells at the concentrations used in this study. In all of the experiments, verapamil (Wanle, Shenzhen, China) served as a positive control agent.

2.5. *Annexin V/FITC and 7-AAD staining analysis*

HCT-8/VCR and HCT-8 cells were seeded in 6-well plates (1.5×10^5 per well) and treated with VCR alone or treated with a combination of AKBA and VCR for 24 h. Cells were harvested and washed with cold PBS. The cell surface phosphatidylserine in apoptotic cells was quantitatively estimated using Annexin V/FITC and 7-AAD apoptosis detection kits according to manufacturer's instructions (Becton Dickinson, CA, USA). Cell apoptosis was analyzed on a FACScan flow cytometry system (Becton Dickinson) (*16*). Experiments were performed in triplicate with three samples.

2.6. *Rh123 accumulation*

The effect of AKBA on P-gp activity was assessed by measuring the intracellular accumulation of Rh123 (*17*). HCT-8/VCR cells were seeded into 96-well plates at a density of 1×10^4/well. Cells were pretreated with AKBA (1.25 μM, 2.5 μM, or 5 μM) for 90 min and were then incubated with 200 nM of Rh123 in culture medium in the dark at 37°C in 5% CO_2 for another 90 min. The cells were washed twice with ice-cold PBS. The MFI associated with Rh123 was measured using a multilabel counter with excitation/emission wavelengths of 485/535 nm.

2.7. *Real-time RT-PCR for MDR1 mRNA detection*

Real-time RT-PCR was performed to determine the level of expression of MDR1 mRNA. HCT-8/VCR

cells were seeded in 6-well plates and treated with various concentrations of AKBA for 24 h. Total RNA was extracted using the RNAeasy kit according to the manufacturer's instructions (Sangon, Shanghai, China). RNA quality was determined based on the ratio of A260/A280 (1.8-2). The concentration of total RNA was measured by detecting absorbance at 260 nm (A260) (*18*). Then, reverse transcription (RT) was performed with 2 μg of extracted RNA using the First Strand cDNA Synthesis Kit (Toyobo, Osaka, Japan) according to the supplied protocol. A 25-μL mixture for PCR included 2× SYBR Green real-time PCR Master Mix (Toyobo, Japan), 2 μg of the cDNA template, and 0.3 μM of each primer. The thermal profile of the reaction was as follows: 3 min at 95°C, followed by 40 cycles consisting of 20 s at 95°C, 30 s at 60°C, and 30 s at 70°C. The fold-change in the level of expression of MDR1 mRNA was calculated using the $2^{-\Delta\Delta CT}$ method. Experiments were performed in triplicate with three samples.

The following primers (Genecore Biotech, Guangzhou, China) were used for the specific amplification of MDR1 (forward: 5′-AGACATGACCAGGTATGCCTAT-3′ and reverse: 5′-AGCCTAT CTCCTGTCGCATTA-3′). The expression of GAPDH (forward: 5′-GAGGGGCCATCCACAGTCTT-3′ and reverse: 5′-TTCATTGACCTCAACTACAT-3′) served as an internal control.

2.8. Western blot analysis

HCT-8/VCR cells were treated with 1.25 μM, 2.5 μM, or 5 μM AKBA in cell growth medium for 48 h. Cells were harvested, lysed, and centrifuged as described previously. Supernatants were collected and protein concentration was determined using the Bradford assay (*19*). Samples containing 50 μg of protein were subjected to 10% SDS-PAGE and electro-transferred to nitrocellulose membranes that were blocked with 3% non-fat milk/0.1% Tween 20/TBS, 100 mM NaCl in 10 mM Tris, pH 7.5, incubated with anti-P-gp antibody (sc-13131, Santa Cruz, CA, USA) for 1 h at room temperature followed by horseradish-peroxidase-conjugated secondary antibody for another 1 h at room temperature. Protein bands were detected with ECL.

2.9. Statistical analysis

Data are expressed as the mean ± S.D. Data were analyzed using the Student's *t*-test. *p*-values below 0.05 were considered to be statistically significant.

3. Results

3.1. *High levels of P-gp expression in the HCT-8/VCR cell line*
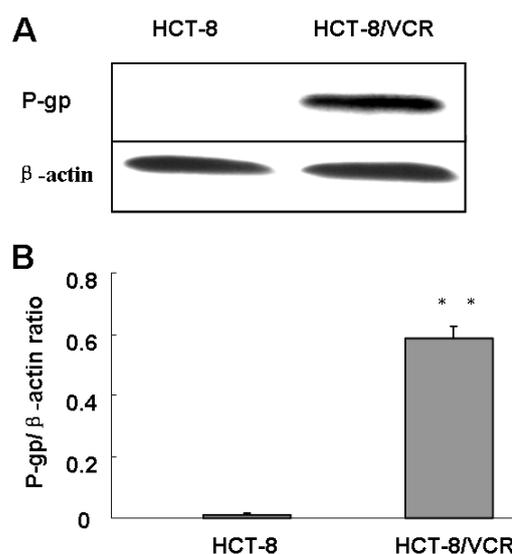
Western blot analysis was used to determine the

Figure 1. The expression of P-gp in HCT-8 and HCT-8/VCR cells. (A) Levels of P-gp in HCT-8 and HCT-8/VCR cells were estimated using Western blot analysis. **(B)** P-gp bands were quantified using densitometry. Bars indicate the mean ± S.D. *n* = 3). **p < 0.01 compared to HCT-8 cells.

expression of P-gp in multidrug-resistant HCT-8/VCR and parental HCT-8 cells (Figure 1A). Results indicated that drug-sensitive HCT-8 cells had markedly lower levels of P-gp when probed using an anti-P-gp monoclonal antibody, while drug-resistant HCT-8/VCR cells exhibited a stronger signal corresponding to P-gp (Figure 1B). These results indicated that HCT-8/VCR was an MDR cell line characterized by over-expression of P-gp.

3.2. *Effects of AKBA on proliferation of HCT-8 and HCT-8/VCR cells*

The effects of AKBA on HCT-8/VCR and parental HCT-8 cell proliferation were examined. As shown in Figures 2A and 2B, AKBA at concentrations ranging from 2.5 μM to 5 μM weakly inhibited HCT-8/VCR and HCT-8 cell proliferation, but significant differences in inhibition of cell proliferation were noted at higher concentrations (10 μM to 60 μM). Therefore, lower concentrations of AKBA (2.5 μM to 5 μM) were selected and short periods of incubation in were used in experiments to examine reversal of MDR.

3.3. *Effects of AKBA on sensitivity to VCR*

To assess the synergistic effects of AKBA on VCR-induced cytotoxicity, an MTT assay was performed first to determine the "fold reversal"of MDR in HCT-8/VCR and HCT-8 cells. Incubation with VCR at concentrations ranging from 8 to 256 μg/mL weakly inhibited HCT-8/VCR cell proliferation, but HCT-8 cells were sensitive to VCR at all concentrations. As shown in Table 1, VCR-induced cytotoxicity drastically

increased and the IC50 of VCR in HCT-8/VCR cells decreased in the presence of AKBA. AKBA at a concentration of 2.5 µM had a "fold reversal"of MDR (FR) of 8.20-fold and AKBA at a concentration of 5 µM had an FR of 9.19-fold.

The synergistic effects of AKBA on VCR were also evident in the induction of apoptosis. As indicated by the flow cytometry results shown in Figure 2, annexin V-positive cells increased significantly with 24 h of incubation in the presence of VCR and AKBA compared to VCR alone. At AKBA concentrations from 2.5-5 µM, the percentage of apoptotic HCT-8/VCR

Figure 2. Effects of P-gp on the proliferation of HCT-8 and HCT-8/VCR cells. HCT-8 **(A)** and HCT-8/VCR **(B)** cells were treated with various concentrations of AKBA for 24, 48, and 72 h. Viable cell numbers were evaluated with an MTT assay and were denoted as a percentage of untreated controls at the corresponding time point. Data are expressed as the mean ± S.D. from three independent experiments.

cells increased from 7.24% to a maximum of 22.22% (Figures 3B-3D). However, 2.5-5 µM of AKBA alone had almost no effect on apoptosis of HCT-8/VCR cells. The percentage of apoptotic HCT-8/VCR cells was 0.23% and 0.31% (Figures 3E and 3F).

3.4. Increased accumulation of Rh123

To further assess the role of AKBA in regulating P-gp expression, the transport activity of P-gp was examined by measuring the intracellular accumulation of Rh-123. As shown in Figure 4A, the fluorescence intensity of Rh-123 increased markedly in HCT-8/VCR cells treated with AKBA in comparison to cells in the control group. The average Rh123 accumulation MFI in 1.25µM AKBA group was $1,627 \pm 82$, compared to 536 ± 26 in control group. Incubation of HCT-8/VCR cells with 2.5 µM of AKBA resulted in Rh123 accumulation of $2,071 \pm 67$. AKBA at a concentration of 5 µM completely restored Rh123 accumulation in HCT-8/VCR cells, with an MFI $2,514 \pm 92$. The intracellular accumulation of Rh-123 increased significantly in the presence of AKBA in comparison to the control group (Figure 4B, $**p < 0.01$).

3.5. AKBA decreased P-gp expression in HCT-8/VCR cells

Levels of P-gp and MDR1 mRNA in HCT-8/VCR cells were also examined. As shown in Figure 5A, the level of MDR1 mRNA decreased significantly after 24 h of treatment with AKBA according to RT-PCR. Further examination indicated that the level of P-gp expression also markedly decreased as a result of AKBA and was accompanied by a notable decrease in P-gp in HCT-8/VCR cells treated with 2.5 µM or 5 µM of AKBA (Figure 5B, $^{\#\#}p < 0.01$).
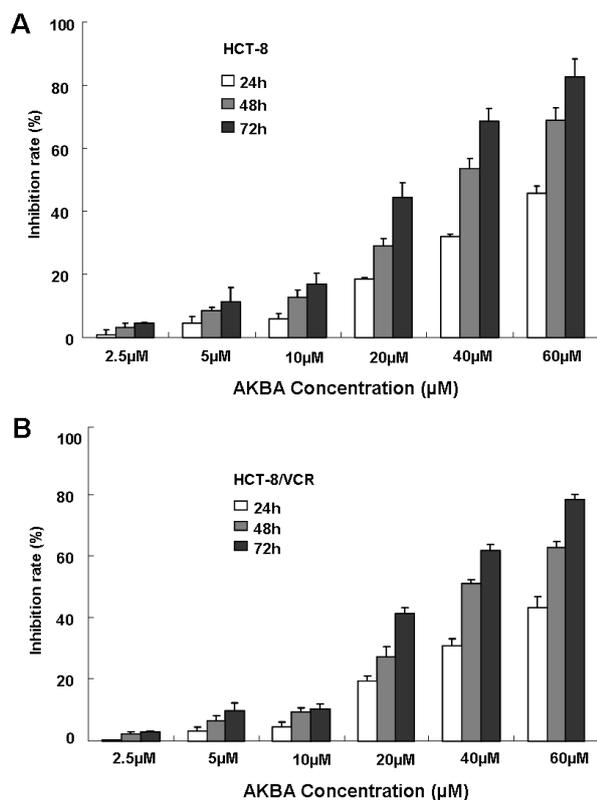
4. Discussion

The development of resistance to chemotherapeutic agents remains a major challenge to chemotherapy to treat ileocecal adenocarcinoma. Chemotherapeutic agents such as vincristine sulphate, 5-fluorouracil, and

Table 1. Effects of AKBA on the sensitivity of HCT-8/VCR and HCT-8 cells to VCR

Treatment	HCT-8/VCR		HCT-8	
	IC_{50} (µg/mL)	FR	IC_{50} (µg/mL)	FR
VCR alone	99.2 ± 3.58		18.66 ± 1.97	
VCR + 5 µg/mL of verapamil	$15.2 \pm 1.34**$	6.53	15.37 ± 1.25	1.21
VCR + 1.25 µM of AKBA	$21.4 \pm 0.89**$	4.63	15.89 ± 1.13	1.17
VCR+2.5 µM of AKBA	$12.1 \pm 0.75**$	8.20	14.23 ± 1.07	1.31
VCR+5 µM of AKBA	$10.8 \pm 0.56**$	9.19	16.27 ± 0.84	1.15

he effects of AKBA on the sensitivity of HCT-8/VCR cells to VCR were examined using an MTT assay. Cells were treated with varying concentrations of VCR in the presence of AKBA for 72 h. IC_{50} values for VCR were calculated and the "fold reversal" of MDR (FR) was compared. Data are the mean ± S.D. from three independent experiments. $**p < 0.01$ *vs.* VCR alone, untreated group.
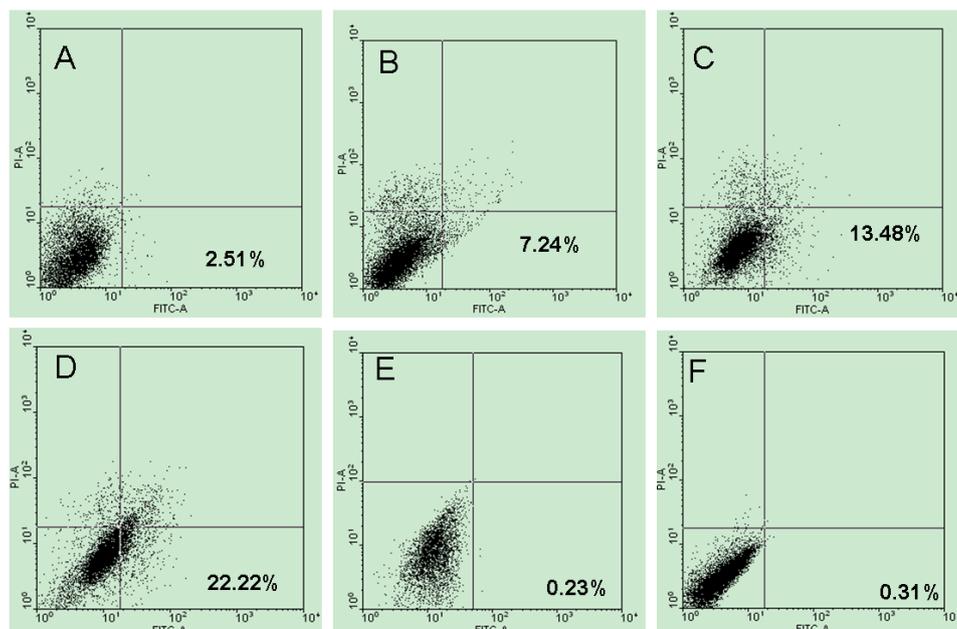
Figure 3. Detection of apoptotic cells with flow cytometric analysis after Annexin V/7-AAD staining. HCT-8/VCR cells were exposed to VCR and increasing concentrations of AKBA for 24 h. Cells were harvested and stained with AnnexinV/7-AAD. **(A)** Vehicle control; **(B)** VCR 20 μg/mL; **(C)** VCR 20 μg/mL + AKBA 2.5 μM; **(D)** VCR 20 μg/mL + AKBA 5 μM; **(E)** AKBA 2.5 μM **(F)** AKBA 5 μM.
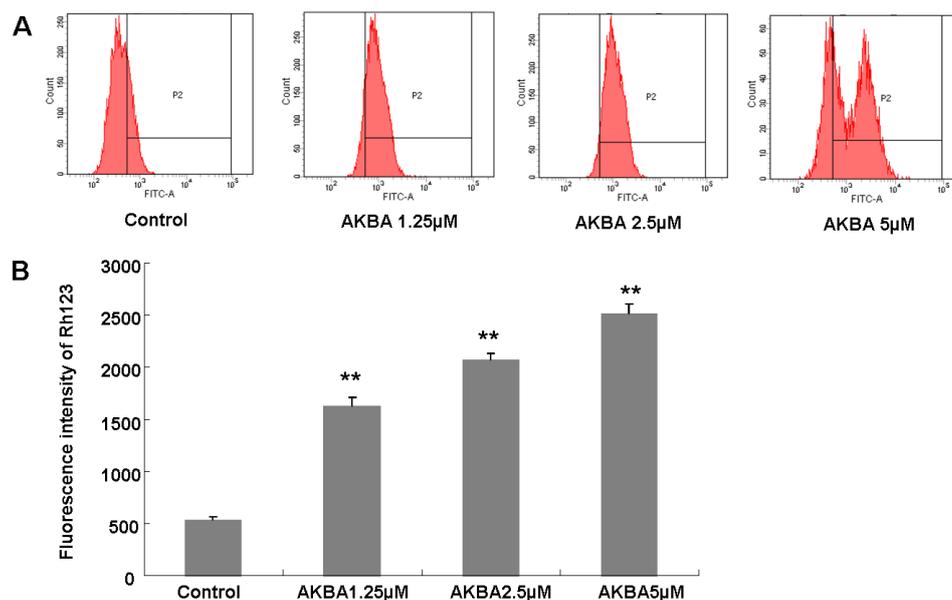

Figure 4. Effect of AKBA on accumulation of Rhodamine 123 (Rh-123) in HCT-8/VCR cells. HCT-8/VCR cells were cultured in RPMI 1640 supplemented with 200 nm of Rh-123 for 30 min at 37°C. At the end of incubation, the cells were washed twice with PBS to remove the free Rh-123 and kept in dye-free medium. **(A)** The fluorescence intensity of Rhodamine 123 in cells was measured with FACS. **(B)** Quantification of Rh-123 fluorescence intensity. Data are expressed as the mean ± S.D. from three independent experiments. $**p < 0.01$ compared to the control group.

capecitabine have been used in chemotherapy to treat ileocecal adenocarcinoma (*20*). However, cancer cells become resistant when these chemotherapeutic agents are used for a prolonged period. MDR has multiple causes, including (*i*) upregulation of drug efflux pumps (*21*), (*ii*) increased signaling *via* AKT (*22*), and (*iii*) decreased apoptosis (*23,24*). A key cause of MDR is enhanced expression of drug efflux proteins mediated by members of the superfamily of ABC transporters. Four members of ABC family function as drug efflux pumps: P-glycoprotein (P-gp/MDR1/ABCB1), multidrug resistance-associated protein 1 (MRP1/ABCC1), breast cancer resistance protein (BCRP/ABCG2), and lung resistance protein (LRP) (*25*). P-gp is known to interact with over 300 compounds and why it is able to achieve this has not yet been revealed
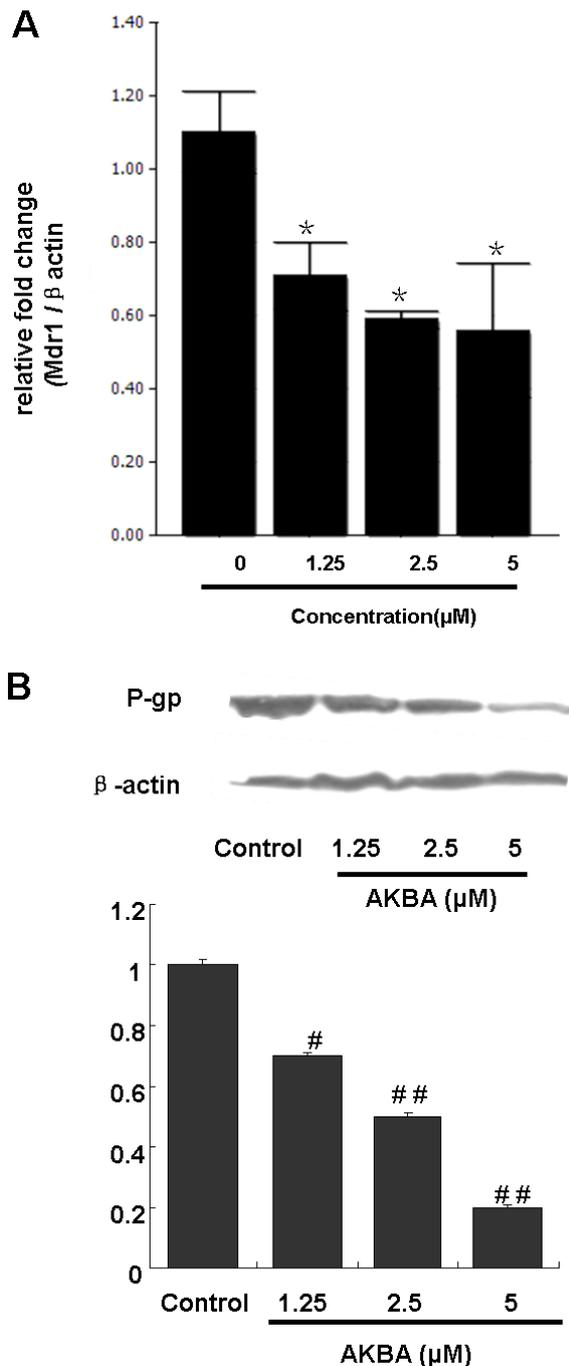
Figure 5. RT-PCR (A) and Western blot (B) analysis of P-gp in HCT-8/VCR cells after treatment with different concentrations of AKBA. Total cell proteins were separated with 10% SDS-PAGE, transferred to nitrocellulose filters, and incubated with anti-P-gp antibody. Immunoreactive proteins were visualized using ECL. Decreases in Mdr1 levels **(A)** and P-gp expression **(B)** in HCT-8/VCR cells after treatment with different concentrations of AKBA were detected. HCT-8/VCR cells were exposed to AKBA for the indicated time. Total RNA or proteins was extracted for P-gp or MDR1 analysis. **(A)** Decrease in MDR1 mRNA in HCT-8/VCR cells exposed to AKBA for 24 h. Levels of MDR1 mRNA were detected with a real-time PCR assay. Data are expressed as the mean ± S.D. from three independent experiments. $^*p < 0.05$, $^{**}p < 0.01$ compared to untreated controls. **(B)** Decrease in P-gp expression in HCT-8/VCR cells exposed to AKBA for 48 h. Data are expressed as the mean ± S.D. from three independent experiments. $^#p < 0.05$, $^{##}p < 0.01$ compared to the untreated controls.

(*26*). P-gp prevents the intracellular accumulation of anticancer drugs by an efflux mechanism. Furthermore, a range of agents have been developed to reverse the MDR phenotype and restore drug sensitivity to cancer cells (*27*). However, most agents to reverse MDR have proven to be intrinsically toxic or to decrease the pharmacokinetic effects of accompanying anticancer drugs (*28*). Therefore, new effective compounds that can increase the sensitivity of resistant cells to chemotherapeutic agents must quickly be identified.

Previous studies by the current authors indicated that orally administered AKBA resulted in an inhibition of intestinal tumorigenesis in APC$^{Min/+}$ mice. AKBA treatment significantly reduced polyp number and size and the degree of cytological dysplasia in the small intestine and colon (*29*). These effects might be produced by the inhibition of the Wnt/β-catenin and NF-κB/cyclooxygenase-2 signaling pathways. Moreover, numerous studies have indicated that NF-κB plays a critical role in resistance to chemotherapeutic agents (*30*). Inhibition of the transcription activity of NF-κB causes a decrease in the anti-apoptotic proteins Bcl-2 and Bcl-(XL), and this appears to be a synergistic effect. Combining NF-κB inhibitors with conventional chemotherapeutics might overcome the drug resistance of cancer cells. In addition, previous Western blotting results have indicated a decrease in NF-κB-p65RelA and its active form p-NF-κB Ser536 in intestinal polyps from mice treated with AKBA. AKBA reduced levels of NF-κB-p65RelA by 51.8% and p-NF-κB Ser536 by 48.6% in the small intestine and colon. The inhibitory effect of AKBA on COX-2, 5-LO, and TNF-α in intestinal polyps is also evident in Western blotting. Therefore, the hypothesis was that AKBA could be a potential agent to reverse MDR.

In the current study, AKBA markedly reversed MDR in HCT-8/VCR, a human ileocecal adenocarcinoma cell line with vincristine-induced resistance, according to an MTT assay and flow cytometry. AKBA had a maximum FR of MDR of 9.19-fold. In addition, the reversal of MDR by AKBA was evident in an intracellular increase in Rh123, indicating that the activity of P-gp was blocked. Furthermore, AKBA inhibited the expression of P-gp and decreased the levels of MDR1 gene expression in HCT-8/VCR cells. These results indicated that AKBA might be a potential agent to reverse MDR in human ileocecal adenocarcinoma. The mechanism of AKBA as a P-gp inhibitor has yet to be studied. In the current study, the inhibition of P-gp was evident both at the level of biosynthesis and also at the level of activity. Accumulating evidence suggests that P-gp, a member of the ATP-binding cassette superfamily, exports structurally diverse hydrophobic compounds from cells through a process driven by ATP hydrolysis (*31*). Efflux occurs depending on the energy produced by ATP hydrolysis when substrates bind with nucleotide-binding domains (NBDs) (*32*).

In the current study, AKBA probably blocked the activity of P-gp by inhibiting ATPase. That said, the exact regulatory mechanism is unclear and warrants further study. Furthermore, AKBA has been studied for its inhibition of Wnt/β-catenin signaling pathways. Previous studies found that the Wnt/β-catenin signal pathway was constitutively activated in cancer cells with doxorubicin-induced MDR. Specific knockdown of β-catenin by RNAi-mediated depletion eliminated MDR1 transcription and expression, resulting in a complete reversal of P-gp-dependent efflux function and restoration of sensitivity to doxorubicin-induced cytotoxicity (*33*). Therefore, the suppression of Wnt/β-catenin signaling by AKBA might be related to the inhibition of P-gp activity and function. However, the precise mechanisms by which AKBA reverses MDR need to be explored.

Acknowledgements

References

1. Xi G, Hayes E, Lewis R, Ichi S, Mania-Farnell B, Shim K, Takao T, Allender E, Mayanil CS, Tomita T. CD133 and DNA-PK regulate MDR1 *via* the PI3K-or Akt-NF-κB pathway in multidrug-resistant glioblastoma cells *in vitro*. Oncogene. 2015; 35:1-10.

2. Teodori E1, Dei S, Martelli C, Scapecchi S, Gualtieri F. The functions and structure of ABC transporters: Implications for the design of new inhibitors of Pgp and MRP1 to control multidrug resistance (MDR). Curr Drug Targets. 2006; 77:893-909.

3. Ye P, Xing H, Lou F, Wang K, Pan Q, Zhou X, Gong L, Li D. Histone deacetylase 2 regulates doxorubicin (Dox) sensitivity of colorectal cancer cells by targeting ABCB$_1$ transcription. Cancer Chemother Pharmacol. 2016; 77:613-621.

4. Kadioglu O, Saeed ME, Valoti M, Frosini M, Sgaragli G, Efferth T. Interactions of human P-glycoprotein transport substrates and inhibitors at the drug binding domain: Functional and molecular docking analyses. Biochem Pharmacol. 2016; 104:42-51.

5. Abdel-Tawab M, Werz O, Schubert-Zsilavecz M. *Boswellia serrata*: An overall assessment of *in vitro*, preclinical, pharmacokinetic and clinical data. Clin Pharmacokinet. 2011; 50:349-369.

6. Takada Y, Ichikawa H, Badmaev V, Aggarwal BB. Acetyl-11-keto-β-boswellic acid potentiates apoptosis, inhibits invasion, and abolishes osteoclastogenesis by suppressing NF-κB and NF-κB-regulated gene expression. J Immunol. 2006; 176:3127-3140.

7. Syrovets T, Buchele B, Krauss C, Laumonnier Y, Simmet T. Acetyl-boswellic acids inhibit lipopolysaccharide-mediated TNF-α induction in monocytes by direct interaction with IκB kinases. J Immunol. 2005; 174:498-506.

8. Hostanska K, Daum G, Saller R. Cytostatic and apoptosis-inducing activity of boswellic acids toward malignant cell lines *in vitro*. Anticancer Res. 2002; 22:2853-2862.

9. Liu JJ, Nilsson A, Oredsson S, Badmaev V, Zhao WZ, Duan RD. Boswellic acids trigger apoptosis *via* a pathway dependent on caspase-8 activation but independent on Fas/Fas ligand interaction in colon cancer HT-29 cells. Carcinogenesis. 2002; 23:2087-2093.

10. Lu M, Xia L, Hua H, Jing Y. Acetyl-keto-β-boswellic acid induces apoptosis through a death receptor 5-mediated pathway in prostate cancer cells. Cancer Res. 2008; 68:1180-1186.

11. Hostanska K, Daum G, Saller R. Cytostatic and apoptosis-inducing activity of boswellic acids toward malignant cell lines *in vitro*. Anticancer Res. 2002; 22:2853-2862.

12. Catanzaro D, Rancan S, Orso G, Dall'Acqua S, Brun P, Giron MC, Carrara M, Castagliuolo I, Ragazzi E, Caparrotta L, Montopoli M. *Boswellia serrata* preserves intestinal epithelial barrier from oxidative and inflammatory damage. PLoS One. 2015; 105:e0125375.

13. Kunnumakkara AB, Nair AS, Sung B, Pandey MK, Aggarwal BB. Boswellic acid blocks signal transducers and activators of transcription 3 signaling, proliferation, and survival of multiple myeloma *via* the protein tyrosine phosphatase SHP-1. Mol Cancer Res. 2009; 7:118-128.

14. Park EJ, Shin JW, Seo YS, Kim DW, Hong SY, Park WI, Kang BM. Gonadotropin-releasing hormone-agonist induces apoptosis of human granulosa-luteal cells *via* caspase-8, 9 and -3, and poly-(ADP-ribose)-polymerase cleavage. Biosci Trends. 2011; 5:120-128.

15. Shi YQ, Qu XJ, Liao YX, Xie CF, Cheng YN, Li S, Lou HX. Reversal effect of a macrocyclic bisbibenzyl plagiochin E on multidrug resistance in adriamycin-resistant K562/A02 cells. Eur J Pharmacol. 2008; 584:66-71.

16. Wang G, Chen H, Huang M, Wang N, Zhang J, Zhang Y, Bai G, Fong WF, Yang M, Yao X. Methyl protodioscin induces G2/M cell cycle arrest and apoptosis in HepG2 liver cancer cells. Cancer Lett. 2006; 241:102-109.

17. Sun LR, Li X, Cheng YN, Yuan HY, Chen MH, Tang W, Ward SG, Qu XJ. Reversal effect of substituted 1,3-dimethyl-1H-quinoxalin-2-ones on multidrug resistance in adriamycin-resistant K562/A02 cells. Biomed Pharmacother. 2009; 63:202-208.

18. Xue X, Qu XJ, Gao ZH, Sun CC, Liu HP, Zhao CR, Cheng YN, Lou HX. Riccardin D, a novel macrocyclic bisbibenzyl, induces apoptosis of human leukemia cells by targeting DNA topoisomerase II. Invest New Drugs. 2012; 30:212-222.

19. Zhang XF, Pan QZ, Pan K, Weng DS, Wang QJ, Zhao JJ, He J, Liu Q, Wang DD, Jiang SS, Zheng HX, Lv L, Chen CL, Zhang HX, Xia JC. Expression and prognostic role of ubiquitination factor E4B in primary hepatocellular carcinoma. Mol Carcinog. 2016; 55:64-76.

20. Wu S, Guo Z, Hopkins CD, Wei N, Chu E, Wipf P,

Schmitz JC. Bis-cyclopropane analog of disorazole C1 is a microtubule-destabilizing agent active in ABCB1-overexpressing human colon cancer cells. Oncotarget. 2015; 6:40866-40879.

21. Seebacher NA, Richardson DR, Jansson PJ. Glucose modulation induces reactive oxygen species and increases P-glycoprotein-mediated multidrug resistance to chemotherapeutics. Br J Pharmacol. 2015; 172:2557-2572.

22. Mao Z, Zhou J, Luan J, Sheng W, Shen X, Dong X. Tamoxifen reduces P-gp-mediated multidrug resistance *via* inhibiting the PI3K/Akt signaling pathway in ER-negative human gastric cancer cells. Biomed Pharmacother. 2014; 68:179-183.

23. Sui H, Zhou LH, Zhang YL, Huang JP, Liu X, Ji Q, Fu XL, Wen HT, Chen ZS, Deng WL, Zhu HR, Li Q. Evodiamine suppresses ABCG2 mediated drug resistance by inhibiting p50/NF-κB pathway in colorectal cancer. J Cell Biochem. 2016; 117:1471-1481.

24. Lee YY, Jeon HK, Hong JE, *et al.* Proton pump inhibitors enhance the effects of cytotoxic agents in chemoresistant epithelial ovarian carcinoma. Oncotarget. 2015; 6:35040-35050.

25. Vasiliou V, Vasiliou K, Nebert DW. Human ATP-binding cassette ABC transporter family. Hum Genomics. 2009; 3:281-290.

26. Callaghan R. Providing a molecular mechanism for P-glycoprotein; why would I bother? Biochem Soc Trans. 2015; 43:995-1002.

27. Ye S, Zhang J, Shen J, Gao Y, Li Y, Choy E, Cote G, Harmon D, Mankin H, Gray NS, Hornicek FJ, Duan Z. NVP-TAE684 reverses multidrug resistance (MDR) in human osteosarcoma by inhibiting P-glycoprotein (PGP1) function. Br J Pharmacol. 2016; 173:613-626.

28. Previs RA, Armaiz-Pena GN, Lin YG, Davis AN, Pradeep S, Dalton HJ, Hansen JM, Merritt WM, Nick AM, Langley RR, Coleman RL, Sood AK. Dual metronomic chemotherapy with Nab-paclitaxel and topotecan has potent antiangiogenic activity in ovarian cancer. Mol Cancer Ther. 2015; 14:2677-2686.

29. Liu HP, Gao ZH, Cui SX, Wang Y, Li BY, Lou HX, Qu XJ. Chemoprevention of intestinal adenomatous polyposis by acetyl-11-keto-β-boswellic acid in APC$^{Min/+}$ mice. Int J Cancer. 2013; 132:2667-2681.

30. Nabekura T, Hiroi T, Kawasaki T, Uwai Y. Effects of natural nuclear factor-κ B inhibitors on anticancer drug efflux transporter human P-glycoprotein. Biomed Pharmacother. 2015; 70:140-145.

31. Jones PM, George AM. Opening of the ADP-bound active site in the ABC transporter ATPase dimer: Evidence for a constant contact, alternating sites model for the catalytic cycle. Proteins. 2009; 75:387-396.

32. Matsunaga T, Kose E, Yasuda S, Ise H, Ikeda U, Ohmori S. Determination of P-Glycoprotein ATPase activity using luciferase. Biol Pharm Bull. 2006; 29:560-564.

33. Xia Z, Guo M, Liu H, Jiang L, Li Q, Peng J, Li JD, Shan B, Feng P, Ma H. CBP-dependent Wnt/β-catenin signaling is crucial in regulation of MDR1 transcription. Curr Cancer Drug Targets. 2015; 15:519-532.

Original Article

Effects of Bu-Shen-Ning-Xin Decoction on immune cells of the spleen and bone marrow in ovariectomized mice

Xuemin Qiu[1,2,3,4], Yuyan Gui[1,2,3,4], Na Zhang[1,2,3,4], Yingping Xu[1,2,3,4], Dajin Li[1,2,3,4,*], Ling Wang[1,2,3,4,*]

[1] *Obstetrics and Gynecology Hospital, Fudan University, Shanghai, China;*
[2] *Shanghai Key Laboratory of Female Reproductive Endocrine Related Diseases, Shanghai, China;*
[3] *Laboratory for Reproductive Immunology, Hospital & Institute of Obstetrics and Gynecology, IBS, Fudan University Shanghai Medical College, Shanghai, China;*
[4] *The Academy of Integrative Medicine of Fudan University, Shanghai, China.*

Summary   **Osteoimmunology is a new discipline that focuses on the interaction between the bones and the immune system. Immune cells play an important role in bone metabolism. The aim of this study was to illustrate the effect of Bu-Shen-Ning-Xin Decoction (BSNXD) on lymphocytes in the spleen and bone marrow to explore the potential role on the bone. C57BL/6 mice were divided into four groups: sham, ovariectomized (OVX), OVX+BSNXD, and OVX+ estrogen. The sham and OVX groups were treated with saline, the OVX+BSNXD group was treated with BSNXD, and the OVX+ estrogen group was treated with estrogen. After mice were sacrificed, the spleens and bones were collected, and the lymphocytes in the spleen and bone marrow were analyzed. We found that BSNXD lessened the extent of the increase of CD4^{+} and CD8^{+} T cells by ovariectomy. BSNXD increased the numbers of CTLA-4^{+} regulatory T cells (Tregs), but had no effect on Foxp3^{+} Tregs, which is a different finding than the OVX+ estrogen group. BSNXD decreased the proportion of CD19^{+} and B220^{+} B cells in the spleen and bone marrow. In contrast, these numbers were both increased in the OVX group. BSNXD had no influence on the percentage of γδ T cells. However, it increased the proportion of NK cells in the spleen and bone marrow. BSNXD lessened the extent of the increase of monocytes by ovariectomy. *In vitro* experiment, we found Tregs can decrease osteoclastogenesis when co-cultured with osteoclast precursor cells. This study suggests that BSNXD changes the immune environment and immune cells have a role in bone metabolism in OVX mice.**

Keywords: Traditional Chinese medicine, ovariectomy, T cells, regulatory T cells

1. Introduction

Postmenopausal osteoporosis (PMO) occurs after 5-7 years of menopause. Estrogen deficiency is the primary reason for the rapid and sustained increase in the rate of bone loss. Estrogen replacement therapy (ERT) is a widely used therapy to treat PMO. Many studies have suggested that estrogen can act directly on bone cells, lymphocytes, and may influence bone metabolism through immunoregulatory and anti-inflammatory activities (*1-6*). In our previous study, we found estrogen enhances the function of CD4^{+}CD25^{+}Foxp3^{+} regulatory T cells (Tregs), which can suppress osteoclast differentiation and bone resorption *in vitro* (*7*). In the present study, estrogen was used as a positive control.

Bu-Shen-Ning-Xin Decoction (BSNXD) is composed of traditional Chinese medicinal compounds that are used to treat women with PMO in clinical, and the composition of prescription, the main effective components, function of BSNXD was introduced in Table 1 (*8-18*). We have done many researches on the effects of BSNXD on bone, previously (*19,20*). BSNXD ameliorated the osteoporotic phenotype of ovariectomized mice without affecting the serum

Table 1. The composition of herbal formula Bu-Shen-Ning-Xin Decoction (BSNXD)

Pinyin Name	Common name	Latin name	Content	Main constituents	Biological activity
Gan di huang/ Sheng di huang	Dried Rehmannia Root	Radix Rehmanniae Exsiccata	15 g	iridoid glycosides, monosaccharides, amino acids	Immune regulation, promoting adrenal cortex and sex glands functioning, stimulating bone marrow, enhancing blood coagulation process, improving kidney and heart functioning, diuresis, lowering blood pressure, inhibiting gastric secretions, anti-tumor, inhibiting epithelial cell proliferation, anti-oxidative and anti-aging (*8*).
Zhi mu	Common Anemarrhena Rhizome	*Anemarrhena asphodeloides* Bunge	15 g	xanthones, steroidal compound	Resistant to microbial action, sympathetic – adrenal function, fall blood sugar function, antipyretic, antitumor (*9*).
Huang bo	Bark of Chinese Corktree	*Phellodendron amurense* Rupr	9 g	berberine, jatrorrhizine, magnoflorine, phellodendrine	Antibacterial, antifungal, suppression of cough, lower blood pressure, trichomonad resistance, anti-hepatitis, anti-ulcer, immunomodulatory (*10*).
Gou qi zi	Barbary Wolfberry Fruit	Fructus Lycii barbari	15 g	carotenoids, flavonoids, polysaccharides	Immunomodulatory, anti-oxidant, anti-stress, neuro-protective, anti-tumor, liver/eyes/male-fertility/glycemia level and hyperlipidemia/blood pressure effects (*11-13*).
Chang pu	Rhizoma Acori Tatarinowii	Acorus tatarinowii	12 g	cal-amendiol, acorenone, shyobunone, acorone, acoragermacrone, acolamone, isoacolamone	Antifungal, central nervous system/cardiovascular system/digestive system effects (*14*).
Xian ling pi/ Yin yang huo	Shorthorned Epimedium	*Epimedium brevicornum* Maxim	12 g	icariin, total flavonoids of epimedium (TFE)	Sexual function/cardiovascular system/ immune function/respiratory system effect, anti-virus (*15*).
Suan zao ren	Spina Date Seed	*Ziziphus jujuba* Mill. var. *spinosa*	9 g	jujuboside, betulinic acid, ascorbic acid	Sedative and hypnotic, radioprotective, protection from anoxia and reoxygenation damage, central nervous system, protective effects on cardiac cells, anti-neoplastic, enhancing immunity, protective against ischemic cerebral damages, tonify liver, sedative heart, restrain sweat, generate saliva (*16*).
Bu gu zhi	Malaytea Scurfpea Fruit	*Psoralea corylifolia* Linn.	12 g	volatile oil, coumarin, flavones, monoterpene phenols, lipid compounds, resins, stigmasteroids	Cardiovascular system/white blood cells/skin conditions effects, anti-cancer, estrogen-like effects (*17*).
Ze xie	Oriental Waterplantain Rhizome	*Alisma plantago-aquatica* Linn	12 g	alisol, alisol A monoacetate, alisol B monoacetate, alisol C monoacetate, alismol, alismoxide	Lipid-lowering, liver protection, cardiovascular/ diuretic/lipid metabolism effect (*18*).

estrogen concentration or uterus (*21*); BSNXD modulates mesenchymal stem cell differentiation into osteoblasts (*22*); BSNXD inhibits osteoclastogenesis by abrogating the RANKL-induced NFATc1 and NF-κB signaling pathways through selective estrogen receptors (*23*); BSNXD suppresses osteoclastogenesis *via* increasing dehydroepiandrosterone to prevent postmenopausal osteoporosis (*24*). However, how BSNXD affects immune cells and whether immune cells participate in the effect of BSNXD on bone metabolism is still unclear.

The interaction between immune cells and bone has attracted many attentions, and osteoimmunology is a new discipline that focuses on the influence of immune cells on bone cell function. In the previous work, though we have gotten some development on bone metabolism, but we know little about immune cells on the process of BSNXD treatment. Many immune cells were found can influence bone metabolism, for example, Receptor

activator of NF-kB ligand (RANKL), a tumor necrosis factor (TNF) family member that is expressed on activated T cells, is one of the key differentiation and survival factors for osteoclasts and provides a potential link between normal immune responses and bone metabolism (*25*). In the present study, we detected the changes of T cells, regulatory T cells, B cells, and even innate immune cells, such as NK cells, γδ T cells, and monocytes to explore whether immune cells participate in the effect of BSNXD on bone metabolism.

2. Materials and Methods

2.1. *Media and reagents*

Fetal bovine serum (FBS) and phenol red-free minimum essential media (MEM) were purchased from Gibco (Grand Island, NY, USA). Minimum essential media and 17-β-estradiol (E2) were purchased from Sigma-Aldrich

Co (Saint Louis, MO, USA). Flow cytometry antibodies fluorescein isothiocyanate (FITC)-conjugated anti-CD4, PE-conjugated anti-CD19/CD14/CD62L/B220/Foxp3/ anti-cytotoxic T lymphocyte antigen-4 (anti-CTLA-4), APC-conjugated anti-CD25, and their corresponding isotypes were obtained from eBioscience (San Diego, CA, USA). E2 and Leukocyte Acid Phosphatase Kit were purchased from Sigma-Aldrich Co (Saint Louis, MO, USA). Cell strainers were purchased from Becton Dickinson Labware, Franklin Lakes, NJ, USA). Regulatory T cell Isolation Kits were from Miltenyi Biotec (Bergisch Gladbach, Germany). The M-CSF was supplied by R&D Systems (Minneapolis, MN, USA), and RANKL was obtained from Peprotech (Rocky Hill, NJ, USA).

2.2. BSNXD and BSNXD serum preparation

BSNXD was obtained from the pharmacy of the Hospital of Obstetrics and Gynecology, Fudan University, Shanghai, China. BSNXD was formulated in accordance with traditional Chinese medicine theory and the clinical experience of the authors. BSNXD crude herbs were taken together, and then dissolved in double distilled water. BSNXD solution was intragastric administration to C57BL/6 mice, 7 days later, mice were sacrificed and heart blood was collected. Heart blood was solidification under the normal temperature for a half hour, and blood serum was collected for future use.

2.3. Mice

C57BL/6 mice (6-8 weeks) were purchased from the Laboratory Animal Facility of the Chinese Academy of Sciences (Shanghai, China). Housing and handling was in accordance with the guidelines of the Chinese Council for Animal Care. The mice were divided into 4 groups and treated by oral administration: sham group treated with saline ($n = 15$), OVX (ovariectomized) group treated with saline ($n = 15$), OVX+BSNXD group treated with BSNXD (total raw herbs 1 g/mL, $n = 15$), and OVX+ estrogen group treated with 17-β-estradiol (100 μg/kg/day orally, $n = 15$). After 12 weeks, the spleens and bones were collected for flow cytometry analysis of splenocytes and cells in the bone marrow.

2.4. Flow cytometry analysis

Splenocytes and bone marrow cells (1×10^6) were incubated for 30 minutes on ice with the indicated antibodies, washed, and resuspended in PBS containing 1% bovine serum albumin and 0.1% sodium azide. The non-specific signal was estimated by incubation with rat FITC- and PE-conjugated IgG isotype controls. Labeled cells were analyzed with a flow cytometer (Becton Dickinson, Palo Alto, CA, USA). Data are expressed as the percentage of positive cells.

2.5. Regulatory T cell's separation and purification

Spleens were harvested from mice 6 to 8 weeks old, gently cut into small pieces and passed through cell strainers. Red blood cells were lysed. To purify $CD4^+CD25^+$ T cells, cells were labelled with magnetic-activated cell sorting (MACS) beads by CD4 negative selection and CD25 positive selection. $CD4^+CD25^+$ T cells were selected on an LS column in a magnetic field, and flushed out by a plunger. The purity of the $CD4^+CD25^+$ T cells population varied from 90% to 95%.

2.6. Osteoclast culture and TRAP staining in vitro

Bone marrow-derived monocyte/macrophage precursor cells (BMMs) of 10-week-old mouse femurs were cultured in MEM without phenol red supplemented with FBS in the presence of 10 ng/mL M-CSF for 2 days and then differentiated into osteoclasts using 50 ng/ml RANKL and 10 ng/mL M-CSF for 3 days.

To estimate the effect of Tregs on osteoclastogenesis *in vitro*, the cells were exposed to BSNXD (10% serum) or estrogen (10^{-9} M) or solvent control with or without Tregs in presence of RANKL stimulation for 72 hours.

Then, osteoclastogenesis was calculated by TRAP staining by means of the Leukocyte Acid Phosphatase Kit. TRAP-positive multinucleated cells ($TRAP^+$ MNCs; more than five nuclei) were counted under microscope. Results from at least six independent experiments are shown.

2.7. Statistical analysis

All values are expressed as the mean ± standard error of the mean (S.E.M.). Data were analyzed by using SPSS and the variance was evaluated by using one-way analyses of variance (ANOVA). $p < 0.05$ was considered statistically significant.

3. Results

3.1. BSNXD improves the proportion of T cells in the spleen of ovariectomized mice

Activated T cells participate in osteoclast maturation by secreting RANKL. In this study, we assessed the proportion of $CD4^+$ and $CD8^+$ T cell subsets. We found that both $CD4^+$ and $CD8^+$ T cells were increased in the OVX group, but the cells were both decreased in the OVX+BSNXD and OVX+ estrogen groups ($p < 0.05$, Figure 1).

3.2. BSNXD increases $CTLA-4^+$ Tregs in the spleen of ovariectomized mice

$Foxp3^+$ Tregs are a T cell subset that inhibits immune responses. We assessed the percentage of $Foxp3^+$ and
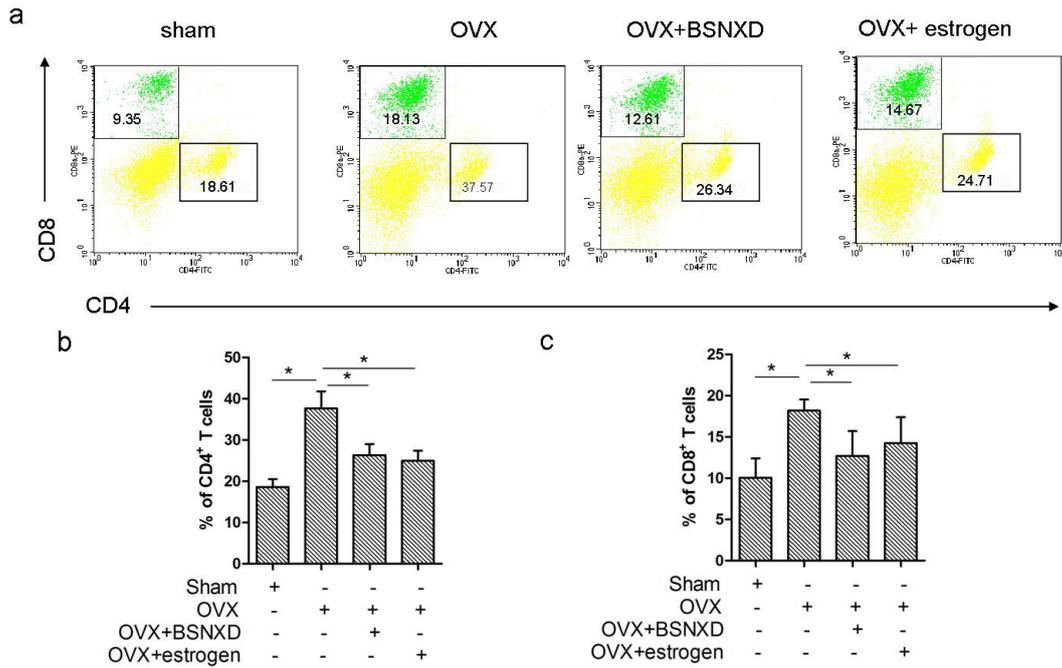
Figure 1. Proportion of T cells in the spleen of ovariectomized mice. (a) Flow cytometry of CD4^{+} and CD8^{+} T cells from each group. **(b, c)** Frequency of CD4^{+} and CD8^{+} T cells in mice as in **a**. *$p < 0.05$. Data are representative of at least three experiments.
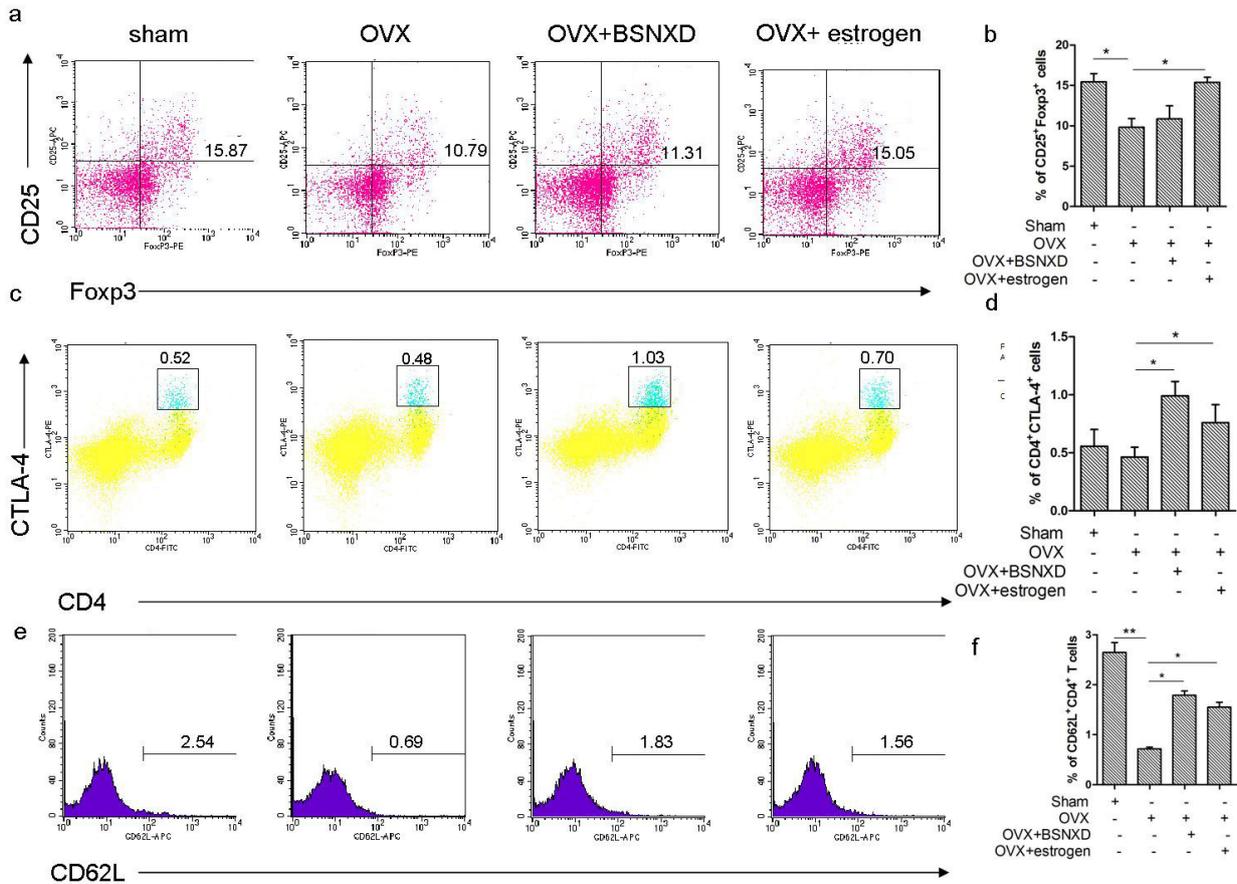
Figure 2. Regulatory T cells in the OVX mice. (a) Expression of CD25 and Foxp3 on CD4^{+}CD25^{+} T cells from each group. **(b)** Frequency of CD4^{+}Foxp3^{+} T cells in mice as in **a**. **(c)** Expression of CD4 and CTLA-4 on CD4^{+}CD25^{+} T cells from each group. **(d)** Frequency of CD4^{+} CTLA-4^{+} T cells in mice as in **c**. **(e)** Analysis of CD62L expression on CD4^{+} T cells from each group. **(f)** Frequency of CD4^{+} CD62L^{+} T cells in mice as in **e**. *$p < 0.05$. Data are representative of at least three experiments.

Figure 3. Proportion of B cells in the spleen and bone marrow of OVX mice. (a) Expression of CD19 on lymphocytes from each group. **(b)** Frequency of CD19^{+} B cells in mice as in **a**. **(c)** Expression of CD19 on bone marrow lymphocytes from each group. **(d)** Frequency of CD19^{+} B cells in the bone marrow of mice as in **c**. **(e)** Expression of B220 on splenocytes from each group. **(f)** Frequency of B220^{+} B cells in mice as in **e**. *$p < 0.05$. Data are representative of at least three experiments.

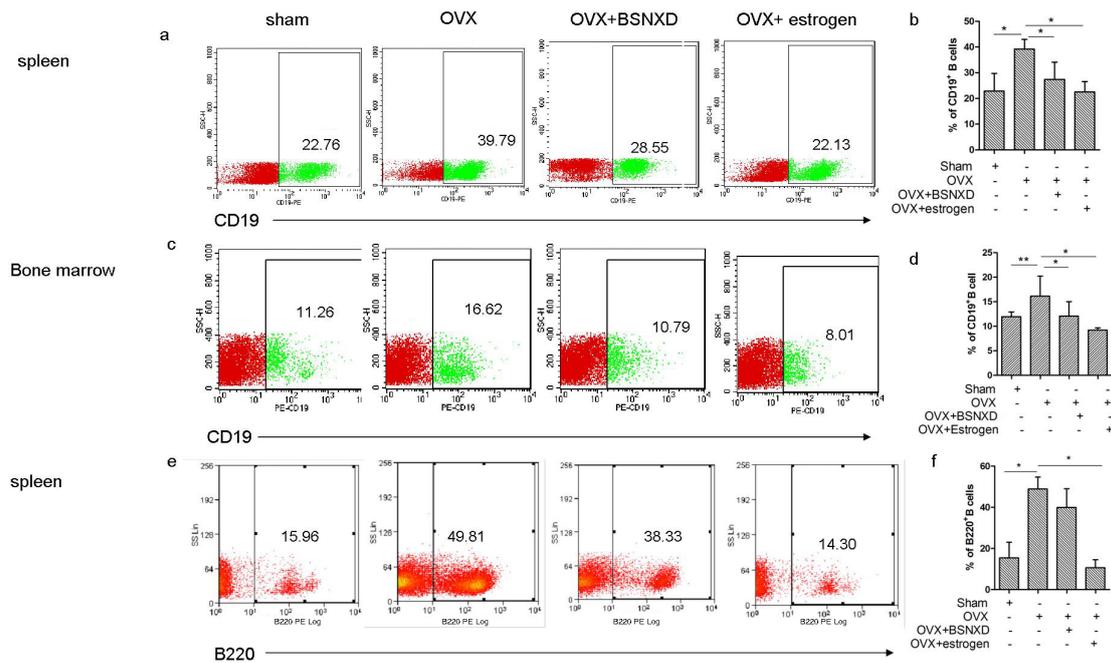CTLA-4^{+} Tregs. We found that Foxp3^{+} Tregs were decreased in the OVX group, but there was no change in the percentage of CTLA-4^{+} Tregs compared with the sham group. Compared with the OVX group, CTLA-4^{+} Tregs were increased, but Foxp3^{+} Tregs did not change in the OVX+BSNXD group ($p < 0.05$). Compared with the OVX group, both CTLA4^{+} and Foxp3^{+} Tregs were increased in the OVX+ estrogen group ($p < 0.05$, Figure 2a, b, c, d).

CD62L (L-selectin) is a cell adhesion molecule expressed on lymphocytes and acts as a "homing receptor". CD62L is also expressed on central memory T cells that have encountered antigen to enable them to localize to secondary lymphoid organs. Compared with the sham group, CD62L was decreased in the OVX group, while it was increased after treatment with BSNXD or estrogen ($p < 0.05$, Figure 2e, f).

3.3. BSNXD decreases the proportion of B cells in the spleen and bone marrow

B cells produce RANKL and OPG, which increases after T-cell stimulation, and they are the major source of OPG in the bone marrow (26). Compared with the sham group, both CD19^{+} and B220^{+} B cells in the spleen were increased in the OVX group, but the cells decreased after BSNXD and estrogen treatments ($p < 0.05$, Figure 3a, b, e, f). The same phenomenon was found in the lymphocytes of the bone marrow; BSNXD and estrogen treatments lessened the extent of the increase by ovariectomy ($p < 0.05$, Figure 3c, d).

3.4. BSNXD has no effect on γδ T cells in the spleen and bone marrow

To analyze the influence of γδ T cells on the bone (27), we assessed the percentage of γδ T cells in the spleen. Compared with the sham group, splenic γδ T cells were decreased in the OVX group, but the percentage did not change in the OVX+BSNXD and OVX+ estrogen groups ($p > 0.05$, Figure 4a, b).

3.5. BSNXD increases NK cell numbers in the spleen and bone marrow

Natural killer (NK) cells are bone marrow-derived cells that play a crucial role in the immune defense against viral infections. NK cells trigger osteoclast apoptosis in a dose-dependent manner that results in decreased bone erosion (28). Compared with the sham group, the percentage of splenic NK cells decreased in the OVX group, but the percentage was increased in the OVX+BSNXD and OVX+ estrogen groups ($p < 0.05$, Figure 4c, d). Though there was no difference in the numbers of bone marrow lymphocytes in the sham and OVX groups, BSNXD and estrogen treatments increased the proportion of NK cells ($p < 0.05$, Figure 4e, f).

3.6. BSNXD decreases the proportion of mononuclear cells in the spleen and bone marrow

Osteoclasts originate from mononuclear cells and can be induced by M-CSF and RANKL. The proportion of
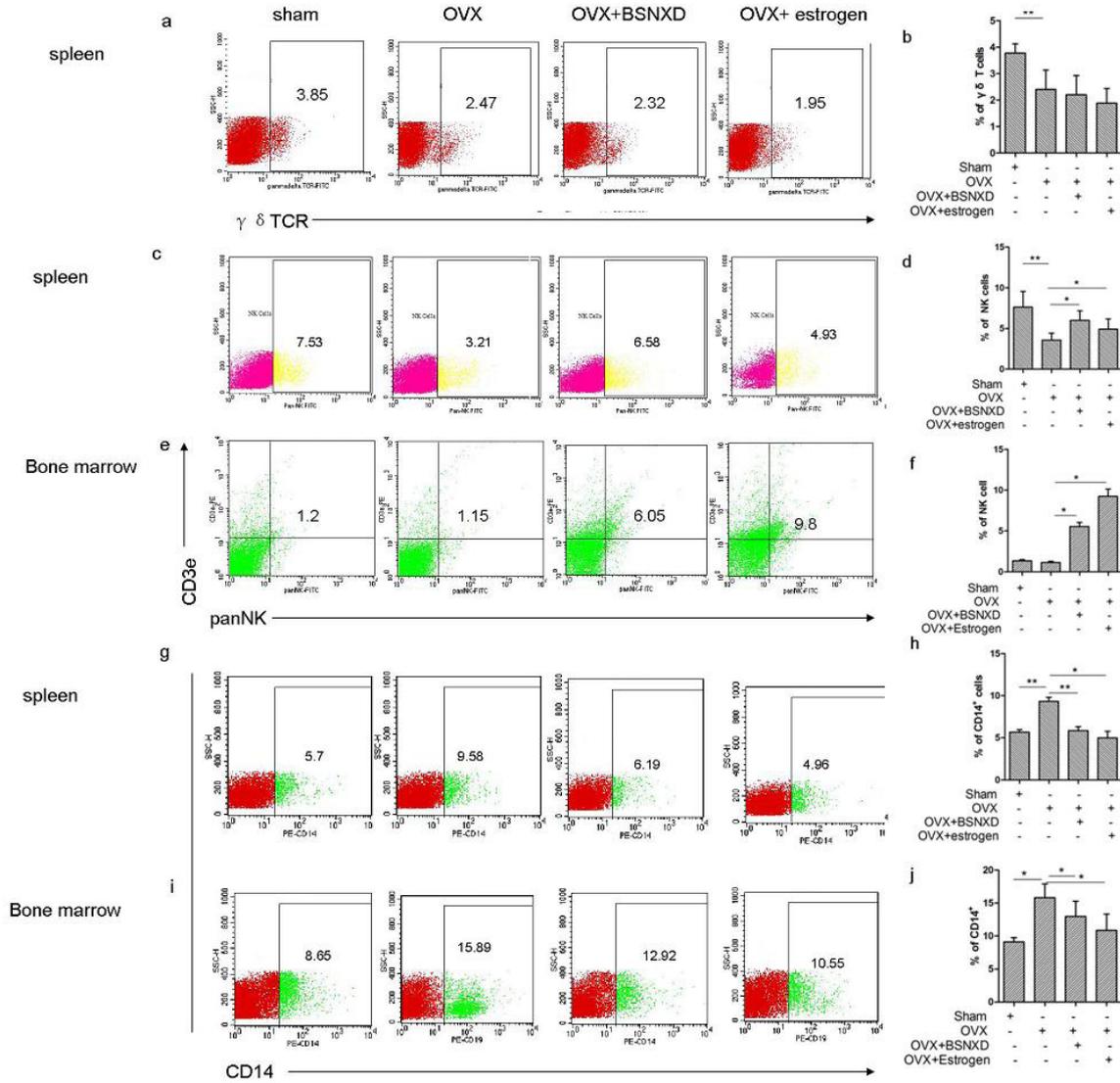
Figure 4. Innate immune cells in the spleen and bone marrow of ovariectomized mice. (a) Analysis of the γδ TCR on lymphocytes from the spleen of each group. **(b)** Frequency of γδ T cells in mice as in **a**. **(c)** Analysis of CD3e and panNK on splenocytes from each group. **(d)** Frequency of CD3e+ panNK+ NK cells in mice as in **c**. **(e)** Analysis of CD3e and panNK on bone marrow lymphocytes from each group. **(f)** Frequency of CD3e+ panNK+ NK cells in the bone marrow of mice as in **e**. **(g)** Expression of CD14 on lymphocytes from the spleen of each group. **(h)** Frequency of CD14+ monocytes in mice as in **g**. **(i)** Expression of CD14 on bone marrow lymphocytes from each group. **(j)** Frequency of CD14+ monocytes in the bone marrow of mice as in **i**. *$p < 0.05$. Data are representative of at least three experiments.

CD14+ cells was increased in the OVX group suggesting that there was an increase in osteoclast production. However, it was decreased in the OVX+BSNXD and OVX+ estrogen groups ($p < 0.05$, Figure 4g, h). Similarly, in the bone marrow, the proportion of CD14+ cells was decreased after BSNXD or estrogen treatments ($p < 0.05$, Figure 4i, j).

3.7. *Tregs decreases osteoclastogenesis*

In order to explore the role of Tregs on osteoclast differentiation, we cultured bone marrow monocytes with or without Tregs, and estrogen was also used as a positive control. Compared with control group, BSNXD

serum (10%) and estrogen treatment decreased TRAP+ multinucleate cells (MNC), and there were less TRAP+ MNC when Tregs were added to cell culture system. ($p < 0.05$). There was no difference in osteoclastogenesis between BSNXD serum group and estrogen group ($p > 0.05$, Figure 5).

4. Discussion

Immune cells participate in many physiological activities and their role on the bone has attracted much attention. In this study, we analyzed the changes of the percentage of immune cells in the spleen and bone marrow after BSNXD treatment using estrogen as
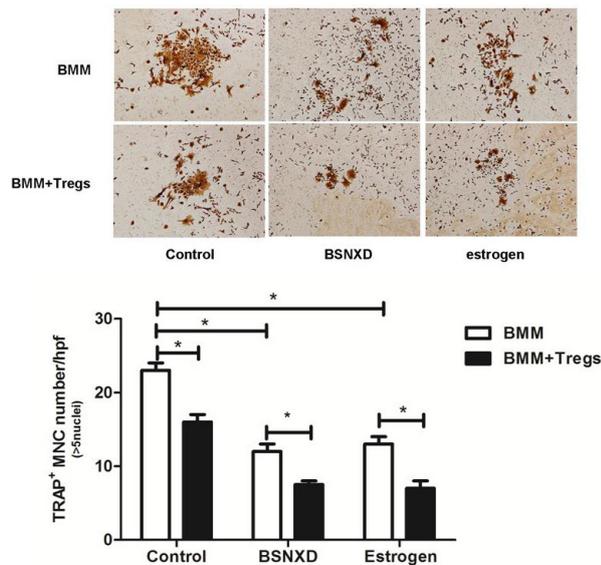
Figure 5. Effect of Tregs on osteoclast differentiation.
CD4$^+$CD25$^+$ regulatory T cells were collected through magnetic cell sorting (MACS) by CD4 negative selection and CD25 positive selection and then added to the bone marrow monocyte monoculture system with or without BSNXD serum/estrogen. 3days later, osteoclastogenesis was calcuated by TRAP staining. Brown: osteoclast. *p < 0.05, Data are representative of at least three experiments.

the positive control. We found that both BSNXD and estrogen treatments affected the proportion of immune cells *in vivo*.

4.1. The activation of CD4$^+$ and CD8$^+$ T cells and osteoporosis

T cells produce a number of mediators that influence osteoclast differentiation. Activated T cells produce factors, including RANKL, that strongly stimulate osteolysis, consistent with the association between inflammation and bone loss. However, T cells (particularly naive T cells) also mediate anti-osteoclastogenic activities. T cells can be divided into two major functional compartments: cytotoxic T cells (CTLs) that express CD8 and T helper cells that express CD4. Based on the importance of T cells on the bone, we assessed the proportion of T cells in the spleen. Lymphocytes express estrogen receptors, and in humans, estrogen loss is reported to cause a decline in T cell subsets. Conversely, ovariectomy increases T cell activation and TNF secretion in mice (*29-32*). In our study, we found that ovariectomy increased the proportion of T cells, and BSNXD treatment can reverse this effect. We found an increase in the proportion of CD8$^+$ T cells in the OVX group, which is consistent with the status prior to surgery. Interestingly, Pietschmann *et al.* found that CD8$^+$ T cells bearing markers suggestive of cell senescence are significantly increased in elderly patients with osteoporotic fractures (*33*). Some investigators focused on the CD4/CD8 T cell ratio, which is significantly higher in osteoporotic patients. The total

lymphocyte and T cell counts are unchanged compared with controls, and young normal control subjects have CD4/CD8 ratios that are similar to the elderly non-osteoporotic subjects (*34*).

4.2. Protection of Tregs on bone

Tregs suppress immune responses to maintain immune homeostasis and tolerance towards self-antigens (*35*). Tregs reduce joint destruction in an arthritis model by elevating the production of osteoclast-inhibiting cytokines. Tregs directly inhibit osteoclast formation through the transmembrane protein CTLA-4. Further studies on CTLA-4 activity can help explain the direct influence of Tregs on osteoclasts (*36*). In the present study, ovariectomy induced a decrease in CTLA-4$^+$ Tregs. However, after BSNXD and estrogen treatments, CTLA-4$^+$ Tregs were increased, suggesting a potential inhibitory role of BSNXD and estrogen on osteoclast maturation. Foxp3 is the transcriptional factor for Tregs and many studies have been conducted on the interaction between Foxp3$^+$ Tregs and the bone (*37,38*). In this study, we found that estrogen increased the numbers of Foxp3$^+$ Tregs. In contrast, BSNXD had no effect on the numbers of Foxp3$^+$ Tregs, suggesting that BSNXD and estrogen act through different pathways.

CD62L retains cells in the lymph nodes and its downregulation facilitates the emigration of effector T cells. In this present study, ovariectomy induced a decrease in CD62L. However, BSNXD treatment increased CD62L, suggesting that T cell activation was inhibited, which is consistent with the data shown in Figure 1. BSNXD inhibited T cell activation by increasing the proportion of CTLA-4$^+$ Tregs.

4.3. The controversial role of B cells on bone

Ovariectomy, which causes significant bone loss, increases B220$^+$ pre-B cell numbers, and estrogen deficiency is associated with an increase in bone marrow B220$^+$ B cells, which is not found in humans (*39*). In fact, in human males made hypogonadal and selectively replaced with either estrogen or testosterone, estrogen is associated with an increase in the percentage of bone marrow CD19$^+$ B cells (*40-43*). In our study, we found that ovariectomy induced an increase in CD19$^+$ and B220$^+$ B cells, but BSNXD treatment decreased B cell numbers in the BSNXD+OVX group. Though, the influence of B cells on the bone is controversial, their abundance in the bone marrow suggests they have some influence on the bone mass.

4.4. The participation of γδ T cells, NK cells, and monocytes on bone metabolism

The T cell-derived proinflammatory cytokines tumor necrosis factor (TNF)-α and interleukin (IL)-17 trigger

bone erosion by increasing the stimulation of osteoclast formation and activity. Recent studies in animal models of rheumatoid arthritis (RA) have implicated that γδ T cells are the major producers of pathogenic IL-17, and activated γδ T cells inhibit osteoclast differentiation and resorptive activity *in vitro* (*27*). Though we found a decrease in γδ T cells in the OVX group, we did not observe a change after BSNXD and estrogen treatments.

Activated NK cells are present in inflammatory sites associated with enhanced bone erosion. NK cells may participate in inducing apoptosis of osteoclasts that have matured and attached to the bone, which decreases bone resorption (*44-46*). Osteoclast precursors are derived from multipotent precursors of the monocyte-macrophage lineage (*47,48*). BSNXD and estrogen treatments increased the proportion of NK cells and monocytes in the OVX group.

4.5. *The difference between BSNXD and estrogen*

In the present study, we compared BSNXD with estrogen, and we found they are similar in most of effects on immune cells, but there are also some differences. The most interesting thing is the difference on the expression of Foxp3, CTLA-4 in Treg cells, of which BSNXD increases CTLA-4 expression, but estrogen increases the Foxp3 expression, suggesting a different modulation on regulatory T cells. *In vitro* experiment, Tregs decreased osteoclastogenesis, especially in BSNXD serum and estrogen group. In previous research, we also found there are some differences between BSNXD and estrogen on the effect of regulating mesenchymal stem cell differentiation: BSNXD increases MSCs differentiation to osteoblast and decreases MSCs differentiation to adipocyte; while, estrogen increases MSCs differentiation to osteoblast without affecting adipocyte differentiation (*49*).

5. Conclusion

In conclusion, the present study showed that BSNXD regulates the proportion of immune cells in the spleen and bone marrow. Regulatory T cells participate in the process of bone protecting. These findings place osteoimmunology in a position of unique clinical significance. BSNXD plays a different role from estrogen on immune cells to regulate the bone metabolism of OVX mice. The link between ovariectomy-induced bone loss and the change in the proportion of immune cells remains to be clarified.

Acknowledgements

References

1. Jochems C, Islander U, Erlandsson M, Verdrengh M, Ohlsson C, Carlsten H. Osteoporosis in experimental postmenopausal polyarthritis: The relative contributions of estrogen deficiency and inflammation. Arthritis Res Ther. 2005; 7:837-843.
2. Grahnemo L, Jochems C, Andersson A, Engdahl C, Ohlsson C, Islander U, Carlsten H.Possible role of lymphocytes in glucocorticoid-induced increase in trabecular bone mineral density. J Endocrinol. 2015; 224:97-108.
3. Verthelyi D. Sex hormones as immunomodulators in health and disease. Int Immunopharmacol. 2001; 1:983-993.
4. Arlt W, Hewison M. Hormones and immune function: Implications of aging. Aging Cell. 2004; 3:209-216.
5. Baeza I, de Castro NM, Alvarado C, Alvarez P, Arranz L, Bayón J, de la Fuente M. Improvement of Immune Cell Functions in Aged Mice Treated for Five Weeks with Soybean Isoflavones. Ann N Y Acad Sci. 2007; 1100:497-504.
6. Keller ET, Zhang J, Yao Z, Qi Y. The impact of chronic estrogen deprivation on immunologic parameters in the ovariectomized rhesus mon-key (Macaca mulatta) model of menopause. J Reprod Immunol. 2001; 50:41-55.
7. Luo C, Wang L, Sun C, Li Dj. Estrogen enhances the functions of CD4 [+]CD25^{+}Foxp3^{+} regulatory T cells that suppress osteoclast differentiation and bone resorption *in vitro*. Cell Mol Immunol. 2010; 8:50-58.
8. Zhu HF, Wan D, Chen Y, Xu XY, Chen L, He ZG. Effects of Rehmannia root decoction serum on cell proliferation and EPO expression in cultured human umbilical vein endothelial cells. Zhongguo Zhong Yao Za Zhi. 2008; 33:1579-1582. (in Chinese)
9. Ma C, Wang L, Tang Y, Fan M, Xiao H, Huang C. Identification of major xanthones and steroidal saponins in rat urine by liquid chromatography-atmospheric pressure chemical ionization mass spectrometry technology following oral administration of of Rhizoma Anemarrhenae decoction. Biomed Chromatogr. 2008; 22:1066-1083.
10. Talbott SM, Talbott JA, Pugh M. Effect of Magnolia officinalis and Phellodendron amurense (Relora®) on cortisol and psychological mood state in moderately stressed subjects. J Int Soc Sports Nutr. 2013; 10:37.

11. Chen Z, Lu J, Srinivasan N, Tan BK, Chan SH. Polysaccharide-protein complex from *Lycium barbarum* L. is a novel stimulus of dendritic cell immunogenicity. J Immuno. 2009; 182:3503-3509.

12. Chen Z, Soo MY, Srinivasan N, Tan BK, Chan SH. Activation of macrophages by polysaccharide-protein complex from *Lycium barbarum* L. Phytother Res. 2009; 23:1116-1122.

13. Lin CL, Wang CC, Chang SC, Inbaraj BS, Chen BH. Antioxidative activity of polysaccharide fractions isolated from Lycium barbarum Linnaeus. Int J Biol Macromol. 2009; 45:146-151.

14. Liu YX, Si MM, Lu W, Zhang LX, Zhou CX, Deng SL, Wu HS. Effects and molecular mechanisms of the antidiabetic fraction of Acorus calamus L. on GLP-1 expression and secretion *in vivo* and *in vitro*. J Ethnopharmacol. 2015; 166:168-175.

15. Xu Z, Feng S, Shen S, Wang H, Yuan M, Liu J, Huang Y, Ding C. The antioxidant activities effect of neutral and acidic polysaccharides from Epimedium acuminatum Franch. on Caenorhabditis elegans. Carbohydr Polym. 2016; 144:122-130.

16. Fang XSh, Hao JF, Zhou HY, Zhu LX, Wang JH, Song FQ. Pharmacological studies on the sedative-hypnotic effect of Semen Ziziphi spinosae (Suanzaoren) and Radix et Rhizoma Salviae miltiorrhizae (Danshen) extracts and the synergistic effect of their combinations. Phytomedicine. 2010; 17:75-80.

17. Yin FZ, Li L, Lu TL, Li WD, Cai BC, Yin W. Quality Assessment of Psoralea fructus by HPLC Fingerprint Coupled with Multi-components Analysis. Indian J Pharm Sci. 2015; 77:715-22.

18. Li S, Jin S, Song C, Chen C, Zhang Y, Xiang Y, Xu Y, Feng Y, Wan Q, Jiang H. The metabolic change of serum lysophosphatidylcholines involved in the lipid lowering effect of triterpenes from Alismatis rhizoma on high-fat diet induced hyperlipidemia mice. J Ethnopharmacol. 2016; 177:10-18.

19. Gui YY, Qiu XM, Xu YP, Li DJ, Wang L. Bu-Shen-Ning-Xin Decoction Suppresses Osteoclastogenesis *via* increasing DHEA to Prevent Postmenopausal Osteoporosis. BioSci Trends. 2015; 9:169-181.

20. Wang L, Qiu XM, Gui YY, Xu YP, Gober HJ, Li DJ. Bu-Shen-Ning-Xin Decoction Ameliorated the Osteoporotic Phenotype of Ovariectomized Mice without Affecting the Serum Estrogen Concentration or Uterus. Drug Des Devel Ther. 2015; 9:5019-5031.

21. Wang L, Wang YD, Wang WJ, Li DJ. Differential regulation of dehydroepiandrosterone and estrogen on bone and uterus in ovariectomized mice. Osteoporos Int. 2009; 20:79-92.

22. Qiu XM, Wang L, Gui YY, Xu YP, Li DJ. BSNXD modulates mesenchymal stem cell differentiation into osteoblasts in a postmenopausal osteoporotic mouse model. Int J Clin Exp Pathol. 2015; 8:4408-4417.

23. Wang L, Qiu XM, Gui YY, Xu YP, Gober HJ, Li DJ. Bu-Shen-Ning-Xin Decoction: Inhibiting Osteoclastogenesis by Abrogation of RANKL-induced NFATc1 and NF-κB Signaling Pathways *via* Selective Estrogen Receptors. Drug Des Devel Ther. 2015; 9:3755-3766.

24. Gui Y, Qiu X, Xu Y, Li D, Wang L. Bu-Shen-Ning-Xin Decoction Suppresses Osteoclastogenesis *via* increasing dehydroepiandrosterone to Prevent Postmenopausal Osteoporosis. BioSci Trends. 2015; 9:169-181.

25. Arron JR and Choi Y. Bone versus immune system.

Nature. 2000; 408:535-536.

26. Li Y, Terauchi M, Vikulina T, Roser-Page S, Weitzmann MN. B Cell Production of Both OPG and RANKL is Significantly Increased in Aged Mice. Open Bone J. 2014; 6:8-17.

27. Pappalardo A, Thompson K. Activated γδ T cells inhibit osteoclast differentiation and resorptive activity *in vitro*. Clin Exp Immunol. 2013; 174:281-291.

28. Feng S, Madsen SH, Viller NN, Neutzsky-Wulff AV, Geisler C, Karlsson L, Söderström K. Interleukin-15-activated natural killer cells kill autologous osteoclasts *via* LFA-1, DNAM-1 and TRAIL, and inhibit osteoclast-mediated bone erosion *in vitro*. Immunology. 2015; 145:367-379.

29. Pawelec G, Barnett Y, Forsey R, Frasca D, Globerson A, McLeod J, Caruso C, Franceschi C, Fülöp T, Gupta S, Mariani E, Mocchegiani E, Solana R. T cells and aging, January 2002 update. Front Biosci. 2002; 7:d1056-183.

30. Safadi FF, Dissanayake IR, Goodman GG, Jago RA, Baker AE, Bowman AR, Sass DA, Popoff SN, Epstein S. Influence of estrogen deficiency and replacement on T-cell populations in rat lymphoid tissues and organs. Endocrine. 2000; 12:81-88.

31. Cenci S, Weitzmann MN, Roggia C, Namba N, Novack D, Woodring J, Pacifici R. Estrogen deiciency induces bone loss by enhancing T-cell production of TNF-α. J Clin Invest. 2000; 106:1229-1237,

32. D'Amelio P, Grimaldi A, Di Bella S, Brianza SZ, Cristofaro MA, Tamone C, Giribaldi G, Ulliers D, Pescarmona GP, Isaia G. Estrogen deiciency increases osteoclastogenesis up-regulating T cells activity: A key mechanism in osteoporosis. Bone. 2008; 43:92-100.

33. Balakrishnan B, Indap MM, Singh SP, Krishna CM, Chiplunkar SV. Turbo methanol extract inhibits bone resorption through regulation of T cell function. Bone. 2014; 58:114-125.

34. Erben RG, Harti G, Graf H. Ovariectomy does not alter CD4^{+}/CD8^{+} ratio in peripheral blood T-lymphocytes in the rat. Horm Metab Res. 1998; 30:50-54.

35. Maloy KJ, Powrie F. Regulatory T cells in the control of immune pathology. Nat Immunol. 2001; 2:816-822.

36. Axmann R, Herman S, Zaiss M, Franz S, Polzer K, Zwerina J, Herrmann M, Smolen J, Schett G. CTLA-4 directly inhibits osteoclast formation. Ann Rheum Dis. 2008; 67:1603-1609.

37. Liu JC, Zhou CH, Zhang X, Chen Y, Xu BL, Cui L, Xu DH. Effect of 1,25-Dihydroxyvitamin D3 on Regulatory T Cells in Ovariectomized Mice. Biomed Environ Sci. 2014; 27:779-785.

38. Lai N, Zhang Z, Wang B, Miao X, Guo Y, Yao C, Wang Z, Wang L, Ma R, Li X, Jiang G. Regulatory effect of Traditional Chinese Medicinal Formula Zuo-Gui-Wan on the Th17/Treg paradigm in mice with bone loss induced by estrogen deficiency. J Ethnopharmacol. 2015; 166:228-239.

39. Sato T, Shibata T, Ikeda K and Watanabe K. Generation of bone-resorbing osteoclasts from B220^{+} cells: Its role in accelerated osteoclastogenesis due to estrogen deficiency. J Bone Miner Res. 2001; 16:2215-2221.

40. Tyagi AM, Srivastava K, Sharan K, Yadav D, Maurya R, Singh D. Daidzein prevents the increase in CD4^{+}CD28 null T cells and B lymphopoesis in ovariectomized mice: A key mechanism for anti-osteoclastogenic effect. PLoS One. 2011; 6:e21216.

41. Bernardi AI, Andersson A, Grahnemo L, Nurkkala-

Karlsson M, Ohlsson C, Carlsten H, Islander U. Effects of lasofoxifene and bazedoxifene on B cell development and function. Immun Inflamm Dis. 2014; 2:214-225.

42. Erlandsson MC, Jonsson CA, Lindberg MK, Ohlsson C, Carlsten H. Raloxifene- and estradiol-mediated effects on uterus, bone and B lymphocytes in mice. J Endocrinol. 2002; 175:319-327.

43. Grimaldi CM, Cleary J, Dagtas AS, Moussai D, Diamond B. Estrogen alters thresholds for B cell apoptosis and activation. J Clin Invest. 2002; 109:1625-1633.

44. Stubelius A, Erlandsson MC, Islander U, Carlsten H. Immunomodulation by the estrogen metabolite 2-methoxyestradiol. Clin Immunol. 2014; 153:40-48.

45. Hao S, Zhao J, Zhou J, Zhao S, Hu Y, Hou Y. Modulation of 17β-estradiol on the number and cytotoxicity of NK cells *in vivo* related to MCM and activating receptors. Int Immunopharmacol. 2007; 7:1765-1775.

46. Stopińska-Głuszak U, Waligóra J, Grzela T, Głuszak M, Jóźwiak J, Radomski D, Roszkowski PI, Malejczyk J. Effect of estrogen/progesterone hormone replacement therapy on natural killer cell cytotoxicity and immunoregulatory cytokine release by peripheral blood mononuclear cells of postmenopausal women. J Reprod Immunol. 2006; 69:65-75.

47. Thongngarm T, Jenkins JK, Ndebele K, Mcmurray RW. Estrogen and progesterone modulate monocyte cell cycle progression and apoptosis. Am J Reprod Immunol. 2003; 49:129-138.

48. Hodson LJ, Chua AC, Evdokiou A, Robertson SA, Ingman WV. Macrophage phenotype in the mammary gland fluctuates over the course of the estrous cycle and is regulated by ovarian steroid hormones. Biol Reprod. 2013; 89:65.

49. Qiu XM, Wang L, Gui YY, Xu YP, Li DJ. BSNXD modulates mesenchymal stem cell differentiation into osteoblasts in a postmenopausal osteoporotic mouse model. Int J Clin Exp Pathol. 2015; 8:4408-4417.

Original Article

Tao-Hong-Si-Wu Decoction ameliorates steroid-induced avascular necrosis of the femoral head by regulating the HIF-1α pathway and cell apoptosis

Jian Wu[1],*, Li Yao[1], Bing Wang[1], Zhen Liu[2], Keyong Ma[1]

[1] *Department of Joint Surgery, The First People's Hospital of Lianyungang, Lianyungang, Jiangsu, China;*
[2] *Department of Rehabilitation, The First People's Hospital of Lianyungang, Lianyungang, Jiangsu, China.*

Summary　　The aim of this study was to corroborate the hypothesis that Tao-Hong-Si-Wu Decoction (THSWD) affects steroid-induced avascular necrosis of the femoral head (SANFH) by regulating the hypoxia-inducible factor 1α (HIF-1α) pathway. Forty-eight New Zealand rabbits were randomly divided into a normal control group (NC group), a model group (SANFH group), a THSWD group, and a dimethyloxalylglycine group (DMOG group). Rabbits in the SANFH group were injected with both horse serum and methylprednisolone. Rabbits in the THSWD group were gavaged with THSWD in addition to receiving the same treatment as the SANFH group. Rabbits in the DMOG group were injected with extra DMOG in conjunction with the same treatment as the SANFH group. Rabbits in the NC group received the same amount of normal saline. Eight weeks after steroid treatment, the femoral heads of rabbits were removed to examine HIF-1α, vascular endothelial growth factor (VEGF), caspase-3, and bcl-2. Results indicated that THSWD significantly promoted the expression of HIF-1α and VEGF in the femoral head tissue of rabbits and markedly inhibit the apoptosis of osteocytes, chondrocytes, and bone marrow cells. In addition, THSWD suppressed caspase-3 expression and induced bcl-2 expression in femoral head tissues. In conclusion, THSWD can suppress SANFH by regulating the HIF-1α pathway and cell apoptosis.

Keywords: Tao-Hong-Si-Wu Decoction, avascular necrosis of the femoral head, HIF-1α, VEGF, caspase-3, bcl-2

1. Introduction

Steroid-induced avascular necrosis of the femoral head (SANFH) is an aseptic and ischemic condition that may result from long-term use of glucocorticoids. This condition is primarily characterized by the necrosis of bone marrow and trabecular bones (*1*). As suggested by a Chinese epidemiologic study, SANFH accounts for approximately 24.1% of all cases of osteonecrosis of the femoral head (ONFH) (*2*). Thus far, the mechanism underlying SANFH has not been not clear (*3*), but

the general consensus is that several pathways may interrupt the bone microcirculation process and affect the supply of essential nutrients. As a result, deaths of both osteocytes and fat cells may occur, resulting in further damage to bone structures (*4*). As SANFH progresses, bone collapse and osteoarthritis may also occur, and patients are likely to experience intolerable pain and ankylosis (*4,5*). SANFH affects patients with the condition directly and it also has a long-term impact on the health care system (*6*). An estimated four out of five patients may experience femoral head collapse if osteonecrosis occurs due to inappropriate treatment (*1*).

Most approaches used to preserve the joint focus on preventing collapse primarily by supporting the underlying subchondral bone (*7*) and there is debate as to whether these approaches are effective over the long term (*8*). Since a large proportion of patients with SANFH are adolescents who usually need additional surgery, identifying molecular and genetic pathways

that are associated with SANFH may assist clinicians to determine the optimal timing of surgery and to devise preventive interventions for articular surface collapse (*4*).

Hypoxia-inducible factors (HIFs) are a class of DNA-binding transcription factors that is able to activate a series of hypoxia-related genes under certain circumstances and trigger an adaptive response in order to decrease oxygen tension. Researchers have identified approximately 100 HIFs, including vascular endothelial growth factor (VEGF), hemexygenase-1, and glucose transporter protein-1 (*9*). As previous studies have suggested, VEGF promotes the development of new blood vessels and activated VEGF stimulates angiogenesis, erythropoiesis, and cell proliferation and survival (*10,11*). Furthermore, Riddle *et al*. reported that VEGF plays significant roles in angiogenic-osteogenic coupling in the process of osteanagenesis as a target of HIF-1α (*12*). A study by Li *et al*. found that deferoxamine stimulates angiogenesis and bone repair in SANFH by up-regulating the expression of HIF-1α (*8*). All of these findings indicate that activated HIF-1α pathways have positive effects on angiogenesis, osteanagenesis, and cell protection. Therefore, HIF-1α pathways could presumably be targeted in patients with SANFH. Caspase-3 is an apoptosis-related protein that may cleave cellular substrates and lead to apoptosis (*13*). Recent studies have suggested that the pathophysiology of SANFH is likely to be associated with the apoptosis of osteoblasts and osteocytes, which is mediated by nitric oxide (NO) (*14,15*). In addition, Weinstein *et al*. noted the marked apoptosis of osteocytes in specimens obtained from patients with SANFH (*16*).

Tao-Hong-Si-Wu Decoction (THSWD) is a traditional Chinese medication that consists of four basic herbs: Radix Rehmanniae Praeparata (shu di huang), Radix Angelicae Sinensis (dang gui), Rhizoma Ligustici (Chuan xiong), and Radix Paeoniae Alba (bai shao). THSWD also contains two additional ingredients, Semen Prunus and Flos Carthami Tinctorii. A wide range of benefits of THSWD have been identified since its introduction, including stimulation of blood circulation, neuroprotection, and facilitation of angiogenesis (*17-19*). A combination of a recombinant tissue-type plasminogen activator and THSWD resulted in a decreased infarct size, it stimulated cerebral blood circulation, and it enhanced neuron function in patients who had suffered a cerebral embolic stroke (*20*). THSWD has been used to treat rabbits in a model of SANFH, resulting in reduced blood viscosity, increased regeneration of local micro-vessels, improved local blood supply, and facilitation of the recovery of the necrotic femoral head (*21,22*). THSWD appears to be closely associated with regulation of HIF-1α, and HIF-1α is reported to prevent the occurrence of SANFH (*1,23*). However, few systematic studies have consolidated the aforementioned findings, and whether THSWD affects SANFH *via* the HIF-1α signaling pathway is still debated.

The current study sought to explore the effects of THSWD in a model of SANFH by detecting the level of VEGF expression and clarifying the role of the HIF-1α pathway. This study also detected the rate of cell apoptosis and it examined the level of expression of the apoptosis-related proteins caspase-3 and Bcl-2 in order to determine whether THSWD influences cell apoptosis in a model of SANFH. This study represents an intriguing approach that links HIF-1α to SANFH and it also reveals potential clues to managing patients with SANFH in clinical practice.

2. Materials and Methods

2.1. *Lentivirus transduction and creation of a model of SANFH*

A fragment containing HIF-1α was cloned into a pCDH vector. This vector was, together with other packaging plasmids, co-transfected into cells using the Lipofectamine LTX kit (Invitrogen, CA), and the viral particles therein were collected 48 h after transfection.

A total of 48 healthy New Zealand rabbits weighing between 2.0 and 2.5 kg were housed at the Experimental Animal Center of The First People's Hospital of Lianyungang at a temperature of 25 ± 3°C and all rabbits were fed normally. All experimental protocols were approved by the Medical Animal Studies Committee of The First People's Hospital of Lianyungang, China.

Rabbits ate and drank freely with a normal 12 h-light and 12 h-dark cycle. After rabbits were given an initial adaptation period of seven days, they were randomly divided into 4 groups: a SANFH group (*n* = 12), a THSWD group (*n* = 12), a vector group (*n* =12), and an HIF-1α group (*n* = 12). Rabbits in the SANFH group were injected with horse serum (Sigma, USA) *via* the ear vein at a dose of 10 mg/kg. After 3 weeks, horse serum was injected again *via* the ear vein at a decreased dose of 6 mg/kg. After 2 weeks, methylprednisolone (Sigma) was injected into rabbits intraperitoneally at a daily dose of 45 mg/kg for 3 consecutive days. Penicillin was also injected intraperitoneally accompanied with the injection of hormones in order to prevent infection. Rabbits in the THSWD group were gavaged with THSWD at a concentration of 0.75 g/mL, 20 μg/g once a day in addition to receiving the same treatment as the SANFH group. Rabbits in the vector group were injected with Lentivirus, and an empty vector (5.5 ×10^{11} vp/mL, 25 μL per side) was injected into the collapsed portion of the femoral head in addition to receiving the same treatment as the SANFH group. Rabbits in the HIF-1α group were injected with Lentivirus, and an HIF-1α fragment (5.5 × 10^{11} vp/mL, 25 μL per side) was injected into the collapsed portion of the femoral head in addition to receiving the same treatment as the SANFH group.

No rabbits died during creation of the model and

Table 1. HIF-1α, VEGF, and β-actin primers for RT-PCR

Gene	Forward	Reverse	Length
HIF-1α	5'-GCTTGCTCATCAGTTGCC-3'	5'-GCCTTCATTTCATCTTCAATATCC-3'	706 bp
VEGF	5'-TGCACCCACGACAGAAGGGGA-3'	5'-TCACCGCCTTGGCTTGTCACAT-3'	360 bp
β-actin	5'-CCCATTGAACACGGCATT-3'	5'-GGTACGACCAGAGGCATACA-3'	250 bp

HIF-1α: Hypoxia-inducible factor 1α; VEGF: vascular endothelial growth factor; RT-PCR: reverse transcription-polymerase chain reaction.

SANFH was verified using hematoxylin and eosin (HE) staining. Rabbits in each group were sacrificed after eight weeks and their femoral heads were examined using both RT-PCR and immunohistochemical analysis.

2.2. Immunohistochemistry (IHC)

IHC was performed to detect the expression of HIF-1α, VEGF, caspase-3, and bcl-2 proteins. IHC was performed in triplicate for each sample and femoral head tissues in the NC control group served as controls. All tissue samples were incubated with primary antibodies against HIF-1α (1:500), VEGF (1:400), caspase-3 (1:500), and bcl-2 (1:500) overnight at 4°C and then incubated with a secondary antibody biotinylated with goat anti-mouse IgG (1:900) for 30 minutes. Phosphate buffer saline (PBS) solutions served as the negative controls in order to replace the primary antibodies and all antibodies were purchased from Santa Cruz. Six random fields were chosen for each sample (× 200) in order to record the number of positive cells. Another 10 random fields were then chosen and positive staining was determined based on the integrated optical density (IOD). IHC results were analyzed by two independent researchers using the software Image-Pro Plus 6.0.

2.3. RNA isolation and RT-PCR

Total RNA from tissues was isolated using the TRIzol reagent (Invitrogen, Germany) according to the manufacturer's instructions. The ReverTra Ace qPCR RT Kit (Toyobo, Japan) was used to transcribe total RNA into cDNA, and RT-PCR was performed with the THUNDERBIRD SYBR® qPCR Mix (Toyobo, Japan) using the CFX96 Touch Real-Time PCR Detection System (Bio-Rad). The corresponding primer sequences are listed in Table 1. The level of expression of the target gene was normalized to that of β-actin and was calculated using the $2^{-\Delta\Delta CT}$ method. The corresponding experiment was replicated three times.

2.4. Intra-artery ink perfusion

Intra-artery ink perfusion assay was performed to visualize and assess the blood supply in the femoral head of rats. Rats were intraperitoneally administered pentobarbital sodium and then the inferior vena cava and abdominal aorta were immediately exposed and ligated. One tube used to infuse ink was inserted into the distal abdominal aorta and another tube for drainage was inserted into the inferior vena. Heparinized saline (25,000 units in 250 mL 0.9% sodium chloride) was used to wash the inferior vena, and then the abdominal aorta was infused with 10% gelatin/Indian ink (20 g gelatin in 100 mL Indian ink and 100 mL water) using a pressure of 90 mmHg. The above procedures were continued until the toes and lower legs were uniformly black. Samples were harvested and stained using HE. The ratio of perfusion was calculated with the software Image-Pro Plus 6.0 (Media Cybernetics, Silver Spring, MD), and the ratio of perfusion was defined as the area of the inked artery with respect to the area of the entire artery.

2.5. Quantification of microvessel density (MVD)

MVD was used to determine the state of angiogenesis, which was quantified by IHC with anti-CD31 antibody as previous described (24). A single endothelial cell or endothelial cell cluster that was clearly separated from adjacent microvessels was considered to be a microvessel.

2.6. Transferase-mediated dUTP nick end labeling (TUNEL) assay

A TUNEL detection kit (Promega, China) was used to evaluate apoptosis according to the manufacturer's instructions. Cells that were colored brown or that contained brown-yellow nuclei or brown-yellow granules in their cytoplasm were classified as TUNEL-positive cells. TUNEL-positive cells were observed under a fluorescent microscope (Nikon, Japan) at 200×. The corresponding rate of apoptosis was calculated as the number of TUNEL-positive cells divided by the total number of cells. Calculations were obtained by three independent researchers.

2.7. Statistical analysis

All statistical analysis was performed with the software SPSS 21.0 (Chicago, USA). Continuous data are expressed as the mean ± standard deviation (S.D.). A *t*-test or one-way analysis of variance (ANOVA) was used to compare groups and a *p*-value of less than 0.05 was considered to indicate statistical significance.
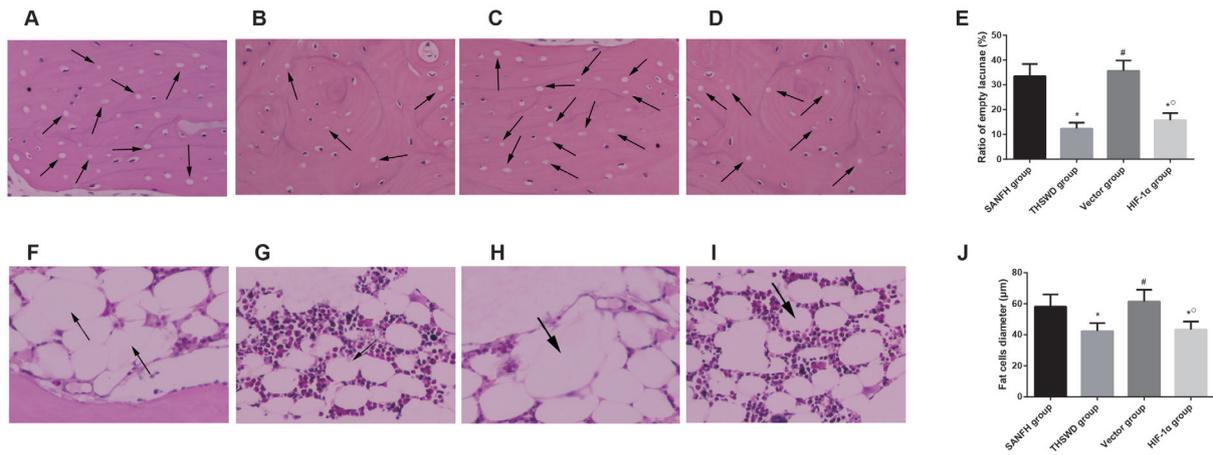
Figure 1. Histopathological observations (200×). Empty lacunae were observed in the SANFH group **(A)**, THSWD group **(B)**, vector group **(C)**, and HIF-1α group **(D)**. Comparison of the ratio of empty lacunae among the four groups **(E)**. The diameter of fat cells was measured in the marrow of the SANFH group **(F)**, THSWD group **(G)**, vector group **(H)**, and HIF-1α group **(I)**. Comparison of the diameter of fat cells among the four groups **(J)**. SANFH: avascular necrosis of the femoral head, THSWD: Tao-Hong-Si-Wu Decoction. Data are presented as the mean ± S.D. *$p < 0.05$ *vs.* the SANFH group, #$p < 0.05$ *vs.* the THSWD group, °$p < 0.05$ *vs.* the vector group.
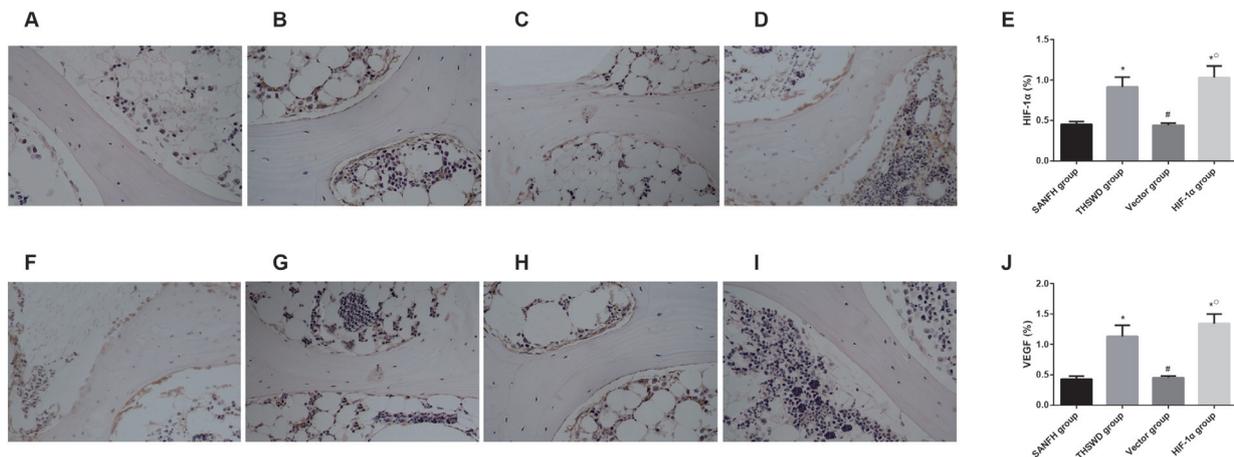
Figure 2. Immunohistochemical staining of HIF-1α and VEGF (200×). Immunohistochemical staining of HIF-1α in the SANFH group **(A)**, THSWD group **(B)**, vector group **(C)**, and HIF-1α group **(D)**. Semi-quantitative analysis of HIF-1α in the four groups **(E)**. Immunohistochemical staining of VEGF in the SANFH group **(F)**, THSWD group **(G)**, vector group **(H)**, and HIF-1α group **(I)**. Semi-quantitative analysis of VEGF in the four groups **(J)**. Data are presented as the mean ± S.D. *$p < 0.05$ *vs.* the SANFH group, #$p < 0.05$ *vs.* the THSWD group, °$p < 0.05$ *vs.* the vector group.

3. Results

3.1. *THSWD and HIF-1α played protective roles in the process of SANFH*

As shown in Figure 1A-E, rats in the SANFH and vector groups displayed obvious osteonecrosis, which was evident as pyknosis and empty lacunae in bone cells. The ratio of empty lacunae in the THSWD and HIF-1α groups was significantly lower than that in the SANFH and vector groups ($p < 0.05$). In addition, the cellular structure of some fat cells collapsed, whereas the diameter of fat cells in the THSWD and HIF-1α groups was significantly smaller than the diameter of those cells in the SANFH and vector groups ($p < 0.05$, Figure 1F-J).

3.2. *THSWD promoted HIF-1α and VEGF expression in femoral head tissues*

Levels of HIF-1α and VEGF expression were measured using IHC and RT-PCR in order to assess whether THSWD was able to affect the HIF-1α pathway. As suggested by the eight-week IHC analysis (Figure 2), the HIF-1α group exhibited higher levels of HIF-1α and VEGF expression than the other groups. The THSWD group had increased levels of HIF-1α and VEGF expression in comparison to the SANFH and vector groups ($p < 0.05$). Similarly, RT-PCR results indicated that the level of expression of HIF-1α mRNA in the THSWD and HIF-1α groups was markedly higher than that in the SANFH and vector groups ($p < 0.05$; Figure 3A). A similar trend in VEGF expression is shown in

Figure 3B ($p < 0.05$). Therefore, results indicated that the HIF-1α pathway is regulated by THSWD.

3.3. *Angiogenesis was regulated by THSWD and HIF-1α*

The results of intra-arterial ink perfusion are shown in Figure 4. Few capillaries that formed a sparse network

were identified in the medullary cavity of rats in the SANFH and vector groups. The perfusion ratios in the THSWD and HIF-1α groups were significantly higher than those in the SANFH and vector groups ($p < 0.05$). MVD is shown in Figure 5, indicating immunostaining for CD31. Both the THSWD and HIF-1α groups exhibited significantly larger numbers of microvessels in subchondral bone in comparison to the SANFH and vector groups ($p < 0.05$).

3.4. *THSWD inhibited the apoptosis of osteocytes, chondrocytes, and bone marrow cells*

The average rate of apoptosis in the four groups was calculated once the corresponding treatment had been administered for eight weeks. Apoptosis of osteocytes, chondrocytes, and bone marrow cells was examined. As shown in Figure 6, the number of TUNEL-positive cells in the THSWD and HIF-1α groups was significantly lower than the number of those cells in the SANFH and vector groups ($p < 0.05$). These findings suggested that

Figure 3. Levels of expression of HIF-1α (A) and VEGF (B) mRNA were measured in femoral head tissues using RT-PCR. Data are presented as the mean ± S.D. *$p < 0.05$ *vs.* the SANFH group, #$p < 0.05$ *vs.* the THSWD group, °$p < 0.05$ *vs.* the vector group.
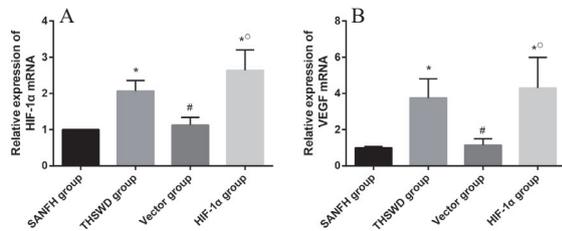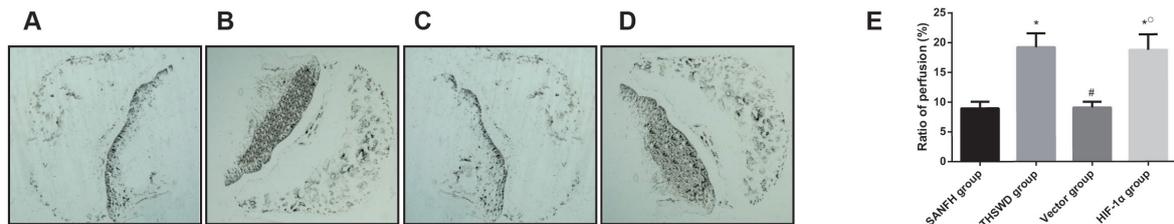

Figure 4. Results of intra-arterial ink perfusion in the SANFH group (A), THSWD group (B), vector group (C), and HIF-1α group (D), and a comparison of the perfusion ratio among the four groups (200×). Data are presented as the mean ± S.D. *$p < 0.05$ *vs.* the SANFH group, #$p < 0.05$ *vs.* the THSWD group, °$p < 0.05$ *vs.* the vector group.

Figure 5. Immunohistochemical staining using antibodies against CD31 in the SANFH group (A), THSWD group (B), vector group (C), and HIF-1α group (D) and a comparison of microvessel density among the four groups (200×). Data are presented as the mean ± S.D. *$p < 0.05$ *vs.* the SANFH group, #$p < 0.05$ *vs.* the THSWD group, °$p < 0.05$ *vs.* the vector group

Figure 6. The apoptosis of osteocytes, chondrocytes, and bone marrow cells in the SANFH group (A), THSWD group (B), vector group (C), and HIF-1α group (D) was determined with a TUNEL assay, and the quantitative results were analyzed (200×). Data are presented as the mean ± S.D. *$p < 0.05$ *vs.* the SANFH group, #$p < 0.05$ *vs.* the THSWD group, °$p < 0.05$ *vs.* the vector group.
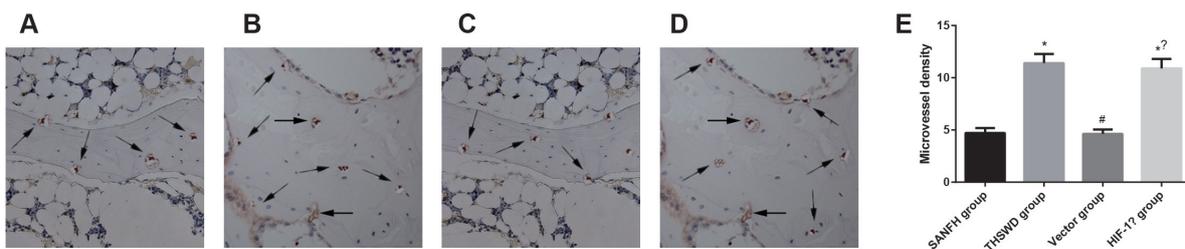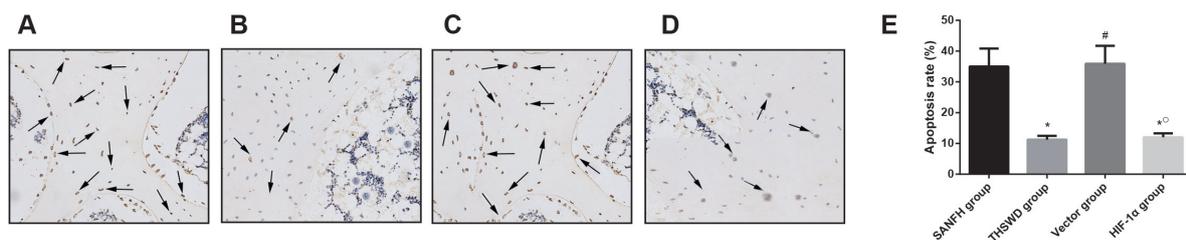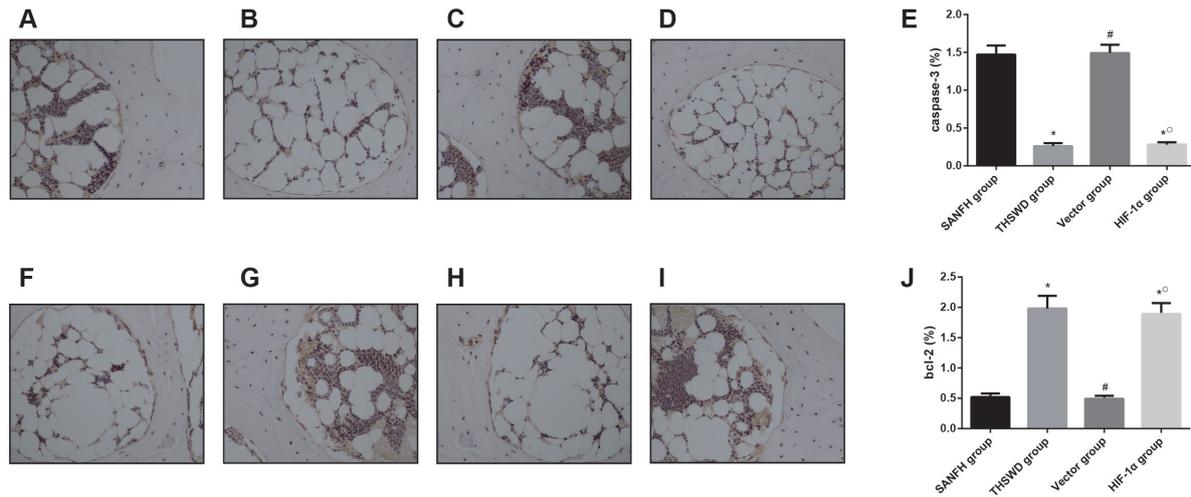
Figure 7. Immunohistochemical staining of caspase-3 and bcl-2 (200×). Immunohistochemical staining of caspase-3 in the SANFH group **(A)**, THSWD group **(B)**, vector group **(C)**, and HIF-1α group **(D)**. Semi-quantitative analysis of caspase-3 in the four groups **(E)**. Immunohistochemical staining of bcl-2 in the SANFH group **(F)**, THSWD group **(G)**, vector group **(H)**, and HIF-1α group **(I)**. Semi-quantitative analysis of bcl-2 in the four groups **(J)**. Data are presented as the mean ± S.D. *$p < 0.05$ *vs.* SANFH group, #$p < 0.05$ *vs.* THSWD group, ○$p < 0.05$ *vs.* vector group.

both THSWD and HIF-1α can suppress early apoptosis in steroid-associated osteonecrosis.

3.5. *THSWD inhibited caspase-3 expression and induced bcl-2 expression in femoral head tissues*

IHC was performed to assess the levels of expression of apoptosis-related proteins such as caspase-3 and bcl-2 in femoral head tissues. Figure 7A-E shows that immunoreactivity to caspase-3 was weak in the THSWD and HIF-1α groups but significantly stronger in the SANFH and vector groups ($p < 0.05$). The THSWD and HIF-1α groups exhibited strong immunoreactivity to bcl-2 while the SANFH and vector groups exhibited relatively weak immunoreactivity ($p < 0.05$, Figure 7F-J). Therefore, THSWD and HIF-1α were able to suppress the progression of SANFH by influencing the expression of apoptosis-related proteins.

4. Discussion

SANFH is a condition often found in young and middle-aged populations, and excessive or long-term usage of steroids accounts for most cases of SANFH (*25*). Steroid hormones regulate the metabolism of sugar, fat, and proteins and also affect oxidative stress, cell proliferation, and apoptosis (*26*). The current study attempted to establish a link between THSWD and HIF-1α/VEGF pathways in order to clarify whether THSWD is able to regulate the apoptosis of bone cells.

Although the mechanisms SANFH are unclear, the consensus view is that the final result of SANFH is an interruption of bone microcirculation (*27*), mainly through disruption of angiogenesis and limiting of the penetration of new vessels into necrotic bone (*1*). Regular angiogenesis is thus crucial to ameliorating SANFH,

since angiogenesis is closely correlated with increased circulation of oxygen and nutrients in bone tissues (*28*). HIF-1α is a key regulatory factor that restores the intracellular oxygen concentration, and HIF-1α has been found to play a critical role in manipulating angiogenesis in stem cells (*29*). The significance of HIF-1α is also evident from the fact that administration of ethyl 3,4-dihudroxybenzoate (EDHB) deters the progression of SANFH because it inhibits the functioning of HIF prolyl hydroxylase and it stabilizes HIF-1α expression (*1,30,31*). A target gene of HIF-1α, VEGF, also plays a major role in encouraging the angiogenesis-osteogenesis coupling process (*32-34*). VEGF improves angiogenesis by activating a variety of signal pathways. One such pathway is the MEK/ERK pathway, which is crucial to the proliferation of endothelial cells (*35*).

In addition, steroids may accelerate osteonecrosis by facilitating the apoptosis of osteoblasts and osteocytes, thereby partially contributing to bone cell death (*14,36-38*). Bcl-2 and caspase-3 are typical apoptosis-related factors. Bcl-2 was found to be up-regulated and caspase-3 was found to be down-regulated during the development of SANFH (*39*). Intriguingly, HIF-1α appears to regulate numerous pro-apoptotic proteins (*e.g.* BNIP3 and NOXA) and anti-apoptotic proteins (*e.g.* Bcl-2, Bcl-xl and Bid) as well (*40,41*). Since the HIF-1α signaling pathway has been found to be involved in regulation of the morphology/function of bone cells and osteoblasts (*42*), HIF-1α presumably plays a major role in the progression of SANFH.

THSWD was first described in the traditional Chinese medical text "YiZongJinJian" (*The Golden Mirror of Medical Orthodoxy*). In response to the negative effects of SANFH, THSWD excels at limiting the aggregation of platelets, increasing blood viscosity, and altering blood stasis (*43,44*). Three components of THSWD, *i.e.*

danggui, chuan xiong, and bai shao, have been found to improve microcirculation and to facilitate microvessel regeneration. These effects are specifically evident in the form of increased blood/plasma viscosity, repair/limited aggregation of blood cells, and a decrease in plasma fibrinogen levels (*45*). THSWD is adept at restoring a necrotic femoral head, and this restoration starts at the interface between the necrotic bone and normal bone. The new bone tissues that form cover the surface of necrotic bone trabeculae and thereby form a dense mass. Fibrous granulation tissues form within this mass and bone resorption spreads to the necrotic portion of bone. Despite restoration reaching a certain stage, collapse of the femoral head can occur because of poor blood circulation (*46*). A key potential action of THSWD is that it may improve blood flow in microcirculation, and this action has been enhanced by modifying both HIF-1α and TNF-α (*23*). These contentions ultimately imply that THSWD might promote osteogenesis and angiogenesis by elevating HIF-1α.

The current study used the traditional Chinese medicine THSWD to specifically treat SANFH, and this study filled a gap in research with solid evidence that THSWD molecularly modified HIF/VEGF signaling to ameliorate symptoms of SANFH. Moreover, this study lifted the mysterious veil surrounding traditional Chinese medicine and it suggested that THSWD is beneficial to patients with SANFH by facilitating angiogenesis and suppressing cell apoptosis. These findings suggest that certain molecules within THSWD might play a crucial role in alleviation of micro-circulatory disturbances, and extraction of these molecules should be the next priority. The extracts can be concentrated and made into pills, since pills would be a convenient and highly efficient form of administration.

In conclusion, levels of HIF-1α and VEGF expression were elevated when THSWD was given. THSWD inhibited the apoptosis of bone cells and the transference of HIF-1α in order to regulate the transcription of VEGF. These findings suggest that THSWD might ameliorate SANFH by regulating HIF-1α signaling and inhibiting the apoptosis of bone cells. Nevertheless, these conclusions should be investigated further in clinical trials in order to justify use of THSWD as an effective treatment for SANFH.

References

1. Fan L, Li J, Yu Z, Dang X, Wang K. Hypoxia-inducible factor prolyl hydroxylase inhibitor prevents steroid-associated osteonecrosis of the femoral head in rabbits by promoting angiogenesis and inhibiting apoptosis. PloS One. 2014; 9:e107774.
2. Cui L, Zhuang Q, Lin J, Jin J, Zhang K, Cao L, Lin J, Yan S, Guo W, He W, Pei F, Zhou Y, Weng X. Multicentric epidemiologic study on six thousand three hundred and ninety five cases of femoral head osteonecrosis in China. Int Orthop. 2016; 40:267-276.
3. Fotopoulos V, Mouzopoulos G, Floros T, Tzurbakis M. Steroid-induced femoral head osteonecrosis in immune thrombocytopenia treatment with osteochondral autograft transplantation. Knee Surg Sports Traumatol Arthrosc. 2015; 23:2605-2610.
4. Powell C, Chang C, Gershwin ME. Current concepts on the pathogenesis and natural history of steroid-induced osteonecrosis. Clin Rev Allergy Immunol. 2011; 41:102-113.
5. Alves EM, Angrisani AT, Santiago MB. The use of extracorporeal shock waves in the treatment of osteonecrosis of the femoral head: A systematic review. Clin Rheumatol. 2009; 28:1247-1251.
6. Kerachian MA, Seguin C, Harvey EJ. Glucocorticoids in osteonecrosis of the femoral head: A new understanding of the mechanisms of action. J Steroid Biochem Mol Biol. 2009; 114:121-128.
7. Jones LC, Hungerford DS. Osteonecrosis: Etiology, diagnosis, and treatment. Curr Opin Rheumatol. 2004; 16:443-449.
8. Li J, Fan L, Yu Z, Dang X, Wang K. The effect of deferoxamine on angiogenesis and bone repair in steroid-induced osteonecrosis of rabbit femoral heads. Exp Biol Med (Maywood). 2015; 240:273-280.
9. Masoud GN, Li W. HIF-1alpha pathway: Role, regulation and intervention for cancer therapy. Acta Pharm Sin B. 2015; 5:378-389.
10. Shen X, Wan C, Ramaswamy G, Mavalli M, Wang Y, Duvall CL, Deng LF, Guldberg RE, Eberhart A, Clemens TL, Gilbert SR. Prolyl hydroxylase inhibitors increase neoangiogenesis and callus formation following femur fracture in mice. J Orthop Res. 2009; 27:1298-1305.
11. Tsai CC, Chen YJ, Yew TL, Chen LL, Wang JY, Chiu CH, Hung SC. Hypoxia inhibits senescence and maintains mesenchymal stem cell properties through down-regulation of E2A-p21 by HIF-TWIST. Blood. 2011; 117:459-469.
12. Riddle RC, Khatri R, Schipani E, Clemens TL. Role of hypoxia-inducible factor-1alpha in angiogenic-osteogenic coupling. J Mol Med (Berl). 2009; 87:583-590.
13. Xu X, Wen H, Hu Y, Yu H, Zhang Y, Chen C, Pan X. STAT1-caspase 3 pathway in the apoptotic process associated with steroid-induced necrosis of the femoral head. J Mol Histol. 2014; 45:473-485.
14. Calder JD, Buttery L, Revell PA, Pearse M, Polak JM. Apoptosis – a significant cause of bone cell death in osteonecrosis of the femoral head. J Bone Joint Surg Br. 2004; 86:1209-1213.
15. Youm YS, Lee SY, Lee SH. Apoptosis in the osteonecrosis of the femoral head. Clin Orthop Surg. 2010; 2:250-255.
16. Zhang C, Zou YL, Ma J, Dang XQ, Wang KZ. Apoptosis associated with Wnt/beta-catenin pathway leads to steroid-induced avascular necrosis of femoral head. BMC Musculoskelet Disord. 2015; 16:132.
17. Han L, Ji Z, Chen W, Yin D, Xu F, Li S, Chen F, Zhu G, Peng D. Protective effects of tao-Hong-si-wu decoction on memory impairment and hippocampal damage in animal model of vascular dementia. Evid Based Complement Alternat Med. 2015; 2015:195835.
18. Li L, Yang N, Nin L, Zhao Z, Chen L, Yu J, Jiang Z, Zhong Z, Zeng D, Qi H, Xu X. Chinese herbal medicine formula tao hong si wu decoction protects against cerebral ischemia-reperfusion injury *via* PI3K/Akt and

the Nrf2 signaling pathway. J Nat Med. 2015; 69:76-85.

19. Xu X, Wang S, Chen W, Chen G. Effects of taohong siwu decoction II in the chick chorioallantoic membrane (CAM) assay and on B16 melanoma in mice and endothelial cells ECV304 proliferation. J Tradit Chin Med. 2006; 26:63-67.

20. Yen TL, Ong ET, Lin KH, Chang CC, Jayakumar T, Lin SC, Fong TH, Sheu JR. Potential advantages of Chinese medicine Taohong Siwu Decoction (桃红四物汤) combined with tissue-plasminogen activator for alleviating middle cerebral artery occlusion-induced embolic stroke in rats. Chin J Integr Med. 2014. DOI: 10.1007/s11655-014-1847-x

21. Qi ZX, Du CB. Local microcirculation changes in rabbits with glucocorticoid-induced avascular necrosis of femoral head following Taohong Siwudecoction treatment. Journal of Clinical Rehabilitative Tissue Engineering Research. 2008; 12:2104-2107.

22. Qi ZX, Cao Y. Comparative study of different methods for the treatment of glucocorticoid induced necrosis of the femoral head. China Journal of Orthopaedics and Traumatology. 2002;2:17-18. (in Chinese)

23. Wu CJ, Chen JT, Yen TL, Jayakumar T, Chou DS, Hsiao G, Sheu JR. Neuroprotection by the Traditional Chinese Medicine, Tao-Hong-Si-Wu-Tang, against Middle Cerebral Artery Occlusion-Induced Cerebral Ischemia in Rats. Evid Based Complement Alternat Med. 2011; 2011:803015.

24. Weidner N, Semple JP, Welch WR, Folkman J. Tumor angiogenesis and metastasis – correlation in invasive breast carcinoma. N Engl J Med. 1991; 324:1-8.

25. Wang J, Kalhor A, Lu S, Crawford R, Ni JD, Xiao Y. iNOS expression and osteocyte apoptosis in idiopathic, non-traumatic osteonecrosis. Acta Orthop. 2015; 86:134-141.

26. Yu Q, Guo W, Shen J, Lv Y. Effect of glucocorticoids on lncRNA and mRNA expression profiles of the bone microcirculatory endothelial cells from femur head of Homo sapiens. Genom Data. 2015; 4:140-142.

27. Mont MA, Cherian JJ, Sierra RJ, Jones LC, Lieberman JR. Nontraumatic osteonecrosis of the femoral head: Where do we stand today? A Ten-Year Update. J Bone Joint Surg Am. 2015; 97:1604-1627.

28. Stegen S, van Gastel N, Carmeliet G. Bringing new life to damaged bone: The importance of angiogenesis in bone repair and regeneration. Bone. 2015; 70:19-27.

29. Mutijima E, De Maertelaer V, Deprez M, Malaise M, Hauzeur JP. The apoptosis of osteoblasts and osteocytes in femoral head osteonecrosis: Its specificity and its distribution. Clin Rheumatol. 2014; 33:1791-1795.

30. Baay-Guzman GJ, Bebenek IG, Zeidler M, Hernandez-Pando R, Vega MI, Garcia-Zepeda EA, Antonio-Andres G, Bonavida B, Riedl M, Kleerup E, Tashkin DP, Hankinson O, Huerta-Yepez S. HIF-1 expression is associated with CCL2 chemokine expression in airway inflammatory cells: Implications in allergic airway inflammation. Respir Res. 2012; 13:60.

31. Chu PW, Beart PM, Jones NM. Preconditioning protects against oxidative injury involving hypoxia-inducible factor-1 and vascular endothelial growth factor in cultured astrocytes. Eur J Pharmacol. 2010; 633:24-32.

32. Zhang W, Yuan Z, Pei X, Ma R. *In vivo* and *in vitro* characteristic of HIF-1alpha and relative genes in ischemic femoral head necrosis. Int J Clin Exp Pathol. 2015; 8:7210-7216.

33. Drescher W, Schlieper G, Floege J, Eitner F. Steroid-related osteonecrosis – an update. Nephrol Dial Transplant. 2011; 26:2728-2731.

34. Weinstein RS, Wan C, Liu Q, Wang Y, Almeida M, O'Brien CA, Thostenson J, Roberson PK, Boskey AL, Clemens TL, Manolagas SC. Endogenous glucocorticoids decrease skeletal angiogenesis, vascularity, hydration, and strength in aged mice. Aging Cell. 2010; 9:147-161.

35. Yin D, Liu Z, Peng D, Yang Y, Gao X, Xu F, Han L. Serum Containing Tao-Hong-Si-Wu Decoction Induces Human Endothelial Cell VEGF Production *via* PI3K/Akt-eNOS Signaling. Evid Based Complement Alternat Med. 2013; 2013:195158.

36. Weinstein RS, Jilka RL, Parfitt AM, Manolagas SC. Inhibition of osteoblastogenesis and promotion of apoptosis of osteoblasts and osteocytes by glucocorticoids. Potential mechanisms of their deleterious effects on bone. J Clin Invest. 1998; 102:274-282.

37. Samara S, Dailiana Z, Chassanidis C, Koromila T, Papatheodorou L, Malizos KN, Kollia P. Expression profile of osteoprotegerin, RANK and RANKL genes in the femoral head of patients with avascular necrosis. Exp Mol Pathol. 2014; 96:9-14.

38. Tsuji M, Ikeda H, Ishizu A, Miyatake Y, Hayase H, Yoshiki T. Altered expression of apoptosis-related genes in osteocytes exposed to high-dose steroid hormones and hypoxic stress. Pathobiology. 2006; 73:304-309.

39. Tian L, Dang XQ, Wang CS, Yang P, Zhang C, Wang KZ. Effects of sodium ferulate on preventing steroid-induced femoral head osteonecrosis in rabbits. J Zhejiang Univ Sci B. 2013; 14:426-437.

40. Chen MH, Ren QX, Yang WF, Chen XL, Lu C, Sun J. Influences of HIF-lalpha on Bax/Bcl-2 and VEGF expressions in rats with spinal cord injury. Int J Clin Exp Pathol. 2013; 6:2312-2322.

41. Sowter HM, Ratcliffe PJ, Watson P, Greenberg AH, Harris AL. HIF-1-dependent regulation of hypoxic induction of the cell death factors BNIP3 and NIX in human tumors. Cancer Res. 2001; 61:6669-6673.

42. Zuo GL, Zhang LF, Qi J, Kang H, Jia P, Chen H, Shen X, Guo L, Zhou HB, Wang JS, Zhou Q, Qian ND, Deng LF. Activation of HIFa pathway in mature osteoblasts disrupts the integrity of the osteocyte/canalicular network. PloS One. 2015; 10:e0121266.

43. Han L, Peng DY, Xu F, Wang N, Liu D, Li YB, Tan QL. Study on antithrombotic effects of Taohong Siwu decoction. Journal of Anhui TCM College. 2010; 29:47-49. (in Chinese)

44. Han L, Xu F, Zhang XB, Xu J, Dai M, Peng DY, Liu QY. The experimental researches of blooding-quickening and stasis-transforming actions of TaoHong Siwu decoction. Journal of Anhui TCM College. 2007; 26:36-38. (in Chinese)

45. Liu JG, Shi DZ. Study of Chinese Herbal Drugs in Affecting Hemorheology Promoting Blood Circulation and Removing Blood Stasis. Chin J Hemorheol. 2004;133-137. (in Chinese)

46. Brody AS, Strong M, Babikian G, Sweet DE, Seidel FG, Kuhn JP. John Caffey Award paper. Avascular necrosis: Early MR imaging and histologic findings in a canine model. AJR Am J Roentgenol. 1991; 157:341-345.

Commentary

Chinese non-governmental organizations involved in HIV/AIDS prevention and control: Intra-organizational social capital as a new analytical perspective

Danni Wang[1,2,3], Guangliang Mei[2], Xiaoru Xu[2], Ran Zhao[2], Ying Ma[2], Ren Chen[2,*], Xia Qin[2], Zhi Hu[1,2,*]

[1] *Department of Epidemiology and Biostatistics, School of Public Health, Anhui Medical University, Hefei, China;*
[2] *School of Health Services Management, Anhui Medical University, Hefei, China;*
[3] *Department of Preventive Medicine, Bengbu Medical College, Bengbu, China.*

Summary   **HIV/AIDS is a major public health and social problem worldwide, and non-governmental organizations (NGOs) have played an irreplaceable role in HIV/AIDS prevention and control. At the present time, however, NGOs have not fully participated in HIV/AIDS prevention and control in China. As an emerging focus on international academic inquiry, social capital can provide a new perspective from which to promote the growth of NGOs. The Joint United Nations Program on HIV/AIDS (UNAIDS) recommends creating regional policies tailored to multiple and varying epidemics of HIV/AIDS. In order to provide evidence to policymakers, this paper described the basic information on NGOs and their shortage of social capital. This paper also compared the actual NGOs to "government-organized non-governmental organizations" (GONGOs). Results indicated that i) Chinese NGOs working on HIV/AIDS are short of funding and core members. GONGOs received more funding, had more core members, and built more capacity building than actual NGOs; ii) Almost half of the NGOs had a low level of trust and lacked a shared vision, networks, and support. The staff of GONGOs received more support from their organization than the staff of actual NGOs. Existing intra-organizational social capital among the staff of NGOs should be increased. Capacity building and policymaking should differentiate between actual NGOs and GONGOs. The relationship between social capital and organizational performance is a topic for further study.**

Keywords: *Non-governmental organization (NGOs), intra-organizational social capital (ISC), HIV/AIDS, China*

1. Introduction

In China, non-governmental organizations (NGOs) have played an irreplaceable role in HIV/AIDS prevention and control. They act as service providers and are involved in education, service delivery, and provision of other services (*1,2*). There are two main types of NGOs

in China, namely, actual NGOs and "government-organized" NGOs (GONGOs). Actual NGOs are organizations created at the grassroots level and tend to be small, lack capacity, and lack political and financial resources. GONGOs are government sponsored and tend to be large, with more professional staff, and a bureaucratic structure; examples of GONGOs include the Family Planning Associations, Women's Federation, Red Cross, Youth League, trade unions, and various academic associations (*3*). Recognized as an important social force to promote health (*4-6*), NGOs have increasingly filled a positive and significant role in the response to AIDS (*7-9*). Specifically, their flexibility and favor among HIV/AIDS patients has made them a more accessible provider for HIV/AIDS services, and

has helped the Chinese government meet their demands (*10*). Despite their active involvement, many challenges lay ahead for the future development of NGOs. HIV/AIDS-related NGOs face challenges in terms of human, financial, and technical resources (*11*). An absence of good relationships among members of an organization and a lack of external resources have threatened the development of NGOs and diminished their successful response to HIV/AIDS (*12,13*).

Understood as "features of a social organization, such as networks, norms, and trust, that facilitate coordination and cooperation for mutual benefit" (*14*), social capital can be an individual or a collective asset that resides in the relationships among individuals, groups, or organizations. NGOs serve as places for the generation of social capital. Most of the studies on social capital in NGOs have focused either on the role of NGOs in fostering civic engagement (*15*) or on the ways that NGOs build social capital for individuals associated with the organization (*16*). Previous studies seldom focused on the development of organizational social capital in NGOs (*17-19*). Intra-organizational social capital (ISC) represents the relationships among members of the organization that can serve as a basis to improve the capacity of the organization, perform committed actions, and create value (*20-22*), and these relationships can be simply understood as relationships among members of an organization. Several studies have found that drawing on ISC can promote the development of an organization and they have explained the role of ISC in resource mobilization, resulting in an improved and more effective organization (*20-23*).

The Joint United Nations Program on HIV/AIDS (UNAIDS) recommends creating regional policies tailored to multiple and varying epidemics of HIV/AIDS (*24*). HIV/AIDS-related NGOs in China need to be surveyed in order to determine what is needed to implement those policies and to provide evidence for decision-makers. This paper describes the basic information on NGOs and ISC residing in these NGOs. This paper also compares actual NGOs and GONGOs. ISC could be used to provide a brand new view and frame of reference for the study of NGOs taking part in HIV/AIDS prevention and control.

2. Methodology of a cross-sectional survey of Chinese NGOs involved in HIV/AIDS

Identification and selection of the study sample. NGOs working on HIV/AIDS were chosen based on the prevalence of HIV/AIDS and availability of resources. NGOs were selected from eight provinces in China: Hunan, Sichuan, and Yunnan were considered areas of high prevalence; Anhui, Hubei, Shandong, and Jilin were considered areas of moderate prevalence; and Gansu was considered an area of low prevalence (*25*). NGOs were included in the study if they were:

i) organizations listed as social organizations working on HIV/AIDS according to the local CDC and *ii*) the organization had been in operation for a year or longer.

Participants in this study. To conveniently and rapidly obtain information, core members of the organizations were surveyed. Core members would have extensive knowledge of the organization's operation and management procedures. Core members were defined as the founder, chief, or administrator of the organization or a member playing a leading role in the organization. Respondents consisted of 327 core members from 212 organizations in eight provinces. Organizations were allowed to have multiple core members participate in the survey. Ninety-one organizations had multiple members (206 members in total) participate in the survey and 121 organizations had only one member (121 members in total) participate. Responses from multiple core members of one organization were averaged to provide a single response for analysis, resulting in a total of 212 responses.

Survey components. The survey consisted of two parts: a questionnaire asking about basic information on the NGO and the 16-item ISC Tool. The questionnaire consisted of six questions: the organization's name, the number of years it was in operation, the number of core members, the amount of organizational funding it received in the past year, the type of organization, and the scope of its work. The ISC Tool was developed by the current authors based on previous research (*26,27*). ISC was defined as networks, trust, support, and a shared vision among members of an NGO. Social capital may enable people and institutions to gain access to resources like social services, volunteers, or funding. The 16-item ISC Tool consisted of four dimensions (social networks, trust, support, and a shared vision) (Table 1). Responses were measured on a 5-point Likert scale ranging from 1 (strongly disagree) to 5 (strongly agree).

3. Organizational characteristics and social capital of HIV/AIDS-related NGOs

Validity and reliability of the ISC Tool. Four factors were extracted with eigenvalues above 1.0: trust (EV = 7.04), a shared vision (EV = 2.31), social networks and ties (EV = 1.30), and support (EV = 1.05). After a promax (oblique) rotation was performed, the four factors explained 73.07% of the total variance. This finding indicates that the four specific factors closely coincided with the original dimensions. The coefficient of reliability (Cronbach's α) was used to evaluate internal reliability. The internal consistency had an overall Cronbach's α of 0.89, and Cronbach's α for the four factors ranged from 0.68 to 0.91. The ISC Tool is a valid and reliable scale to measure ISC for civil society organizations (CSOs) involved in HIV/AIDS programs in China.

Table 1. The Intra-organizational Social Capital Tool (ISC Tool)

Items	Disagree			Agree	
Social networks and ties					
1. Core members contact each other frequently in private.	1	2	3	4	5
2. Core members and general staff contact each other frequently in private.	1	2	3	4	5
3. General members contact each other frequently in private.	1	2	3	4	5
Trust					
4. You believe that members of the organization will keep their promises.	1	2	3	4	5
5. You believe that members of the organization are honest.	1	2	3	4	5
6. You believe that the volunteers will cooperate and work effectively.	1	2	3	4	5
7. You believe that the core members can lead the organization effectively.	1	2	3	4	5
8. If you were busy and needed to re-allocate your work, you would be able to entrust it to your colleagues.	1	2	3	4	5
Support					
9. The organization offers training for members.	1	2	3	4	5
10. The organization provides material support when members need it.	1	2	3	4	5
11. The organization provides emotional support when members need it.	1	2	3	4	5
Shared vision					
12. The members of the organization know the meaning of HIV/AIDS-related terminology they routinely encounter.	1	2	3	4	5
13. The members of the organization readily communicate.	1	2	3	4	5
14. The members of the organization share a set of norms.	1	2	3	4	5
15. The members of the organization approve of the way the organization operates.	1	2	3	4	5
16. The members of the organization identify with the strategies and aims of the organization.	1	2	3	4	5

Organizational characteristics of NGOs. A total of 327 core members from 212 organizations in 8 provinces participated in the survey (Table 2). The 212 NGOs included 134 actual NGOs (63.2%) and 78 GONGOs (36.8%). Results for the 212 NGOs indicated that the organizations had been in operation an average of 7 years (interquartile range (IQR): 5-9), organizations had an average of 4 core members (IQR: 3-5), and received an average of $7,670 (IQR: $3,068-$18,408) in funding in the past year (2014). One hundred and ninety-nine NGOs (93.9%) provided educational services, 165 (77.8%) provided delivery services, 71 (33.5%) provided antiretroviral treatment, 82 (38.7%) built capacity, 129 (60.9%) provided care and support to people living with HIV/AIDS (PLWHA), and 175 (82.6%) implemented interventions (Table 3).There were significant differences between actual NGOs and GONGOs in the number of core members, funding, and the percentage of organizations that built capacity. Compared to actual NGOs, GONGOs had more core members, received more funding, and built more capacity.

Amount of social capital in NGOs. The mean component score was used as the cut-off point to divide social capital into a large amount of social capital (component score ≥ 0) and a small amount of social capital (component score < 0) (*26*). Based on the cut-off points for the four dimensions of social capital, 125 NGOs (59.0%) had a high level of trust, 116 (54.7%) had a shared vision, 112 (52.8%) had extensive social networks, and 120 (56.6%) had a high level of support. Compared to actual NGOs, GONGOs had a greater amount of support from higher organizations, with a *p*

Table 2. HIV/AIDS-related NGOs and participants in this study

Province	No. of NGOs (%)	No. of participants (%)
Hunan	13 (6.1)	13 (4.0)
Sichuan	28 (13.2)	61 (18.7)
Yunnan	63 (29.7)	103 (31.5)
Anhui	30 (14.2)	39 (11.9)
Hubei	13 (6.1)	22 (6.7)
Shandong	16 (7.5)	21 (6.4)
Jilin	25 (11.8)	34 (10.4)
Gansu	24 (11.3)	34 (10.4)
Overall	212 (100)	327 (100)

≤ 0.1. There were no statistically significant differences between actual NGOs and GONGOs in terms of the other dimensions of social capital. The staff of GONGOs received more support from their organization than the staff of actual NGOs. In conclusion, almost half of the NGOs had a low level of trust and lacked a shared vision, networks, and support. The staff of GONGOs received more support from their organizations than the staff of actual NGOs.

4. Lessons and issues for practice and development

Many NGOs form spontaneously in China (*1*). Of the organizations studied here, 63.2% were actual NGOs. Most actual NGOs do not have legal status while GONGOs do. Before legally registering with the Ministry of Civil Affairs, an "NGO" must obtain sponsorship from a relevant government ministry or bureau, the leader of which will be personally responsible for any misconduct by the NGO (*12*). Legal status as

Table 3. Characteristics and social capital among HIV/AIDS-related NGOs (*n* = 212)

Variables	Overall (*n* = 212)	Grass-roots (*n* = 134)	GONGOs (*n* = 78)	Z/χ²	*p* value
Characteristic					
No. of years in operation	7 (5-9)	7 (5-9)	7 (4-9)	- 0.28	0.78
No. of core members	4 (3-5)	3 (2-5)	5 (3-6)	- 2.57	0.01
Funding (USD)	$7,670; $ (3,068-18, 408)	$5,296; $ (1,182-12,716)	$13,389; $ (4,862-37,773)	- 4.77	< 0.01
Scope of work					
Education (Yes)	199 (93.9%)	124 (92.5%)	75 (96.2%)	0.58	0.45
Service delivery (Yes)	165 (77.8%)	105 (78.4%)	60 (76.9%)	0.06	0.81
Antiviral treatment (Yes)	71 (33.5%)	45 (33.6%)	26 (33.3%)	0.00	0.97
Capacity building (Yes)	82 (38.7%)	39 (29.1%)	43 (55.1%)	14.08	< 0.01
Care and support (Yes)	129 (60.9%)	76 (56.7%)	53 (67.9%)	2.61	0.11
Interventions	175 (82.6%)	111 (82.8%)	64 (82.1%)	0.02	0.89
Social capital					
Trust (High)	125 (59.0%)	82 (61.2%)	43 (55.1%)	0.75	0.39
Shared vision (High)	116 (54.7%)	72 (53.7%)	44 (56.4%)	0.14	0.71
Social networks and ties (High)	112 (52.8%)	71 (53.0%)	41 (52.6%)	0.00	0.95
Support (High)	120 (56.6%)	70 (52.2%)	50 (64.1%)	2.83	0.09

an NGO is important because unregistered NGOs are typically unable to manage their own finances and bank accounts, making it difficult for them to mobilize large-scale resources (*28*). Over the past few years, registration restrictions for NGOs have been loosened in China (*13*). However, without reform of the registration process most NGOs will face difficulties functioning as professional organizations and will be unable to structurally and financially increase the scale of the services they provide (*1*). The current study's findings indicate that GONGOs with legal status and governmental backing are likely to have more annual funding and more core members. Unsurprisingly, more GONGOs focus on capacity building than actual NGOs. Since they are not registered with the Ministry of Civil Affairs, true NGOs have difficulty applying for grants and thus often encounter financial difficulties when providing regular services, much less building capacity (*12*).

According to a previous study, NGOs working on HIV/AIDS receive financial support from three places: *i*) the government; *ii*) international programs; and *iii*) corporate or individual donations. A previous study in China revealed that NGOs working on HIV/AIDS had an annual budget of $7,000 in 2009 (*1*). The current study found that most of the organizations studied lacked adequate funding, and the average amount of financial support received in 2014 was only about 50,000 RMB ($7,670), so funding has not increased in five years. In June 2014, the Global Fund to Fight AIDS concluded its support for operations in China and a project entitled the "Fund for Social Organizations Participating in HIV/AIDS Prevention and Control" was established by the Chinese Government in June 2015 (*2*). These particular events explain why the studied NGOs had such a low annual budget in 2014. In 2014, the Chinese NGOs working on HIV/AIDS were faced with an absence of previous funds and no new

funds to replace them.

The shortage of professional social workers and public health specialists in NGOs is also an important obstacle to the development of NGOs (*12*). Sufficient numbers of paid, professional staff are essential to the effective long-term functioning and stability of NGOs (*29*). The staff of NGOs varies in composition, so the current study examined the number of core members in these NGOs instead of full-time/part-time members and volunteers. In a study by Kelly *et al.*, NGOs in Africa had an average of 5 full-time staff, those in Central/Eastern Europe & Central Asia had an average of 5, those in Latin America had an average of 5, and those in the Caribbean had an average of 2.5 (*11*). The current study found that NGOs only had an average of 4 core members. The current authors developed a scale to assess social capital in NGOs involved in HIV/AIDS prevention programs in China. The social capital assessed was ISC, which represents relationships based on networks, trust, support, and a shared vision among members of an NGO. Social capital may enable people and institutions to gain access to resources like social services, volunteers, or funding. ISC is one factor that influences how NGOs function and the ISC Tool is an important instrument with which to study and enhance the third sector (*16*). The ISC Tool had good internal consistency and construct validity. This Tool will facilitate the study of NGOs' specific strategies to build capacity to respond to the Chinese HIV/AIDS epidemic.

The current results indicated that *i*) Chinese NGOs working on HIV/AIDS are short of funding and core members. GONGOs had more core members, received more funding, and built more capacity than actual NGOs; *ii*) Almost half of the NGOs had a low level of trust and lacked a shared vision, networks, and support. The staff of GONGOs received more support

from their organization than the staff of actual NGOs. These results indicate the potential benefit of increasing the existing social capital among the staff of NGOs, perhaps by fostering relationship through joint activities or further training in teamwork for an organization's staff. Capacity building and policymaking should differentiate actual NGOs and GONGOs. NGOs have long-term, reciprocal, trust-based relationships with communities and other organizations that extend beyond the networks of their individual staff (*16*). Further studies are need to evaluate trust, cooperation, and reciprocity between NGOs and the government, the private sector, and media organizations and to identify deep-rooted opposition and ways to deal with it. Another topic for future study is the relationship between social capital and organizational performance.

Acknowledgements

References

1. Li H, Kuo NT, Liu H, Korhonen C, Pond E, Guo H, Smith L, Xue H, Sun J. From spectators to implementers: Civil society organizations involved in AIDS programmes in China. Int J Epidemiol. 2010; 39 Suppl 2:ii65-ii71.

2. Notification on establishment of a fund for social organizations participating in HIV/AIDS prevention and control. National Health and Family Planning Commission of China. *http://www.nhfpc.gov.cn/jkj/s3586/201507/2aa0 e3f7bd794711a2af08c10a8d4789.shtml* (accessed July 25, 2015) (in Chinese).

3. Yu ZY. The effects of resources, political opportunities and organisational ecology on the growth trajectories of AIDS NGOs in China. VOLUNTAS. 2016;1-22.

4. The People's Daily: Giving full attention to social organizations and promoting innovations in social governance. *http://opinion.people.com.cn/n/2014/0415/ c1003-24894914.html* (accessed March 20, 2015) (in Chinese).

5. Poutiainen C, Berrang-Ford L, Ford J, Heymann J. Civil society organizations and adaptation to the health effects of climate change in Canada. Public Health. 2013; 127:403-409.

6. Marta M, Camila R. Civil society organizations in the prevention of sexually transmitted infections among female sex workers, in Portugal. *http://www.scielo.br/ scielo.php?pid=S0104-12902014000100077&script=sci_ arttext&tlng=en* (accessed March 27, 2015).

7. Coutinho A, Roxo U, Epino H, Muganzi A, Dorward E, Pick B. The expanding role of civil society in the global HIV/AIDS response: What has the president's emergency program for AIDS relief's role been? J Acquir Immune Defic Syndr. 2012; 60 Suppl 3:S152-S157.

8. Peersman G, Ferguson L, Torres MA, Smith S, Gruskin S. Increasing civil society participation in the national HIV response: The role of UNGASS reporting. J Acquir Immune Defic Syndr. 2009; 52 Suppl 2:S97-S103.

9. Kakietek J, Geberselassie T, Manteuffel B, Ogungbemi K, Krivelyova A, Bausch S, Rodriguez-Garcia R, Bonnel R, N'Jie N, Fruh J, Gar S. It takes a village: Community-based organizations and the availability and utilization of HIV/AIDS-related services in Nigeria. AIDS Care. 2013; 25 Suppl 1:S78-S87.

10. Bhan A, Singh JA, Upshur RE, Singer PA, Daar AS. Grand challenges in global health: Engaging civil society organizations in biomedical research in developing countries. PLoS Med. 2007; 4:e272.

11. Kelly JA, Somlai AM, Benotsch EG, Amirkhanian YA, Fernandez MI, Stevenson LY, Sitzler CA, McAuliffe TL, Brown KD, Opgenorth KM. Programmes, resources, and needs of HIV-prevention nongovernmental organizations (NGOs) in Africa, Central/Eastern Europe and Central Asia, Latin America and the Caribbean. AIDS Care. 2006; 18:12-21.

12. Cai R. Global Funds freeze for China: Time to consider the role of NGOs in the country. *http://www.bmj.com/ rapid-response/2011/11/03/global-funds-freeze-china-time-consider-role-ngos-country* (accessed July 8, 2016).

13. Kaufman J. HIV, sex work, and civil society in China. J Infect Dis. 2011; 204 Suppl 5:S1218-S1222.

14. Putnam RD. Social capital and public affairs. Bulletin of the American Academy of Arts and Sciences. 1994; 47:5-19. *http://www.jstor.org/stable/3824796?seq=1#page_ scan_tab_contents* (accessed July 8, 2016).

15. Passey A, Lyons M. Nonprofits and social capital: Measurement through organizational surveys. Nonprofit Management & Leadership. 2006; 16:481-495. *http:// onlinelibrary.wiley.com/doi/10.1002/nml.122/pdf* (accessed July 8, 2016).

16. Schneider JA. Organizational social capital and nonprofits. Nonprofit and Voluntary Sector Quarterly. 2009; 38:643-662. *http://nvs.sagepub.com/content/38/4/643.full.pdf* (accessed July 8, 2016).

17. Mondal AH. Social capital formation: The role of NGO rural development programs in Bangladesh. Policy Sci. 2000; 33:459-475.

18. Muriisa RK, Jamil I. Addressing HIV/AIDS challenges in Uganda: Does social capital generation by NGOs matter? Sahara J. 2011; 8:2-12.

19. MacIntyre LM, Waters CM, Rankin SH, Schell E, Laviwa J, Luhanga MR. How community trust was gained by an NGO in Malawi, Central Africa, to mitigate the impact of HIV/AIDS. J Transcult Nurs. 2013; 24:263-270.

20. Leana C, Van-Buren HJ. Organizational social capital and employment practices. Acad Manage Rev. 1999; 24:538-555.

21. Rhys A. Organizational social capital, structure and performance. Human Relations. 2010; 63:583-608.

22. Erlan B, Naim K. The role of organizational social capital in increasing organizational performance in public organizations: Evidence from Kyrgyz National Police (KNP). Int J of Publ Admin. 2012; 35:976-988.

23. Pablo R, Ricardo M, Job R. Intra-organizational social capital in business organizations: A theoretical model with a focus on servant leadership as antecedent. Ramon Llull J of Applied Ethics. 2010; 1:43-59.

24. UNAIDS 2016-2021 Strategy: On the fast-track to end AIDS. *http://www.unaids.org/sites/default/files/media_ asset/20151027_UNAIDS_PCB37_15_18_EN_rev1.pdf*

(accessed July 27, 2016).

25. 2015 China AIDS Response Progress Report. National Health and Family Planning Commission of China. *http://www.unaids.org/sites/default/files/country/documents/CHN_narrative_report_2015.pdf* (accessed February 3, 2016).

26. Ma Y, Qin X, Chen RL, Li NN, Chen R, Hu Z. Impact of individual-level social capital on quality of life among AIDS patients in China. PloS One. 2012; 7:e48888.

27. Hu FY, Niu L, Chen R, Ma Y, Qin X, Hu Z. The association between social capital and quality of life among type 2 diabetes patients in Anhui province, China: A cross-sectional study. BMC Public Health. 2015; 15:786.

28. Niu CX. A survey of grassroots NGOs involved in China's HIV/AIDS prevention and control. ZhongGuo Xing KeXue. 2005; 14:8-17 (in Chinese).

29. Crane SF, Carswell JW. A review and assessment of non-governmental organization-based STD/AIDS education and prevention projects for marginalized groups. Health Educ Res. 1992; 7:175-194.

BioScience Trends

Guide for Authors

1. Scope of Articles

BioScience Trends is an international peer-reviewed journal. BioScience Trends devotes to publishing the latest and most exciting advances in scientific research. Articles cover fields of life science such as biochemistry, molecular biology, clinical research, public health, medical care system, and social science in order to encourage cooperation and exchange among scientists and clinical researchers.

2. Submission Types

Original Articles should be well-documented, novel, and significant to the field as a whole. An Original Article should be arranged into the following sections: Title page, Abstract, Introduction, Materials and Methods, Results, Discussion, Acknowledgments, and References. Original articles should not exceed 5,000 words in length (excluding references) and should be limited to a maximum of 50 references. Articles may contain a maximum of 10 figures and/or tables.

Brief Reports definitively documenting either experimental results or informative clinical observations will be considered for publication in this category. Brief Reports are not intended for publication of incomplete or preliminary findings. Brief Reports should not exceed 3,000 words in length (excluding references) and should be limited to a maximum of 4 figures and/or tables and 30 references. A Brief Report contains the same sections as an Original Article, but the Results and Discussion sections should be combined.

Reviews should present a full and up-to-date account of recent developments within an area of research. Normally, reviews should not exceed 8,000 words in length (excluding references) and should be limited to a maximum of 100 references. Mini reviews are also accepted.

Policy Forum articles discuss research and policy issues in areas related to life science such as public health, the medical care system, and social science and may address governmental issues at district, national, and international levels of discourse. Policy Forum articles should not exceed 2,000 words in length (excluding references).

Case Reports should be detailed reports of the symptoms, signs, diagnosis, treatment, and follow-up of an individual patient. Case reports may contain a demographic profile of the patient but usually describe an unusual or novel occurrence. Unreported or unusual side effects or adverse interactions involving medications will also be considered. Case Reports should not exceed 3,000 words in length (excluding references).

News articles should report the latest events in health sciences and medical research from around the world. News should not exceed 500 words in length.

Letters should present considered opinions in response to articles published in BioScience Trends in the last 6 months or issues of general interest. Letters should not exceed 800 words in length and may contain a maximum of 10 references.

3. Editorial Policies

Ethics: BioScience Trends requires that authors of reports of investigations in humans or animals indicate that those studies were formally approved by a relevant ethics committee or review board.

Conflict of Interest: All authors are required to disclose any actual or potential conflict of interest including financial interests or relationships with other people or organizations that might raise questions of bias in the work reported. If no conflict of interest exists for each author, please state "There is no conflict of interest to disclose".

Submission Declaration: When a manuscript is considered for submission to BioScience Trends, the authors should confirm that 1) no part of this manuscript is currently under consideration for publication elsewhere; 2) this manuscript does not contain the same information in whole or in part as manuscripts that have been published, accepted, or are under review elsewhere, except in the form of an abstract, a letter to the editor, or part of a published lecture or academic thesis; 3) authorization for publication has been obtained from the authors' employer or institution; and 4) all contributing authors have agreed to submit this manuscript.

Cover Letter: The manuscript must be accompanied by a cover letter signed by the corresponding author on behalf of all authors. The letter should indicate the basic findings of the work and their significance. The letter should also include a statement affirming that all authors concur with the submission and that the material submitted for publication has not been published previously or is not under consideration for publication elsewhere. The cover letter should be submitted in PDF format. For example of Cover Letter, please visit http://www.biosciencetrends.com/downcentre.php (Download Centre).

Copyright: A signed JOURNAL PUBLISHING AGREEMENT (JPA) form must be provided by post, fax, or as a scanned file before acceptance of the article. Only forms with a hand-written signature are accepted. This copyright will ensure the widest possible dissemination of information. A form facilitating transfer of copyright can be downloaded by clicking the appropriate link and can be returned to the e-mail address or fax number noted on the form (Please visit Download Centre). Please note that your manuscript will not proceed to the next step in publication until the JPA Form is received. In addition, if excerpts from other copyrighted works are included, the author(s) must obtain written permission from the copyright owners and credit the source(s) in the article.

Suggested Reviewers: A list of up to 3 reviewers who are qualified to assess the scientific merit of the study is welcomed. Reviewer information including names, affiliations, addresses, and e-mail should be provided at the same time the manuscript is submitted online. Please do not suggest reviewers with known conflicts of interest, including participants or anyone with a stake in the proposed research; anyone from the same institution; former students, advisors, or research collaborators (within the last three years); or close personal contacts. Please note that the Editor-in-Chief may accept one or more of the proposed reviewers or may request a review by other qualified persons.

Language Editing: Manuscripts prepared by authors whose native language is not English should have their work proofread by a native English speaker before submission. If not, this might delay the publication of your manuscript in BioScience Trends.

The Editing Support Organization can provide English proofreading, Japanese-English translation, and Chinese-English translation services to authors who want to publish in BioScience Trends and need assistance before submitting a manuscript. Authors can visit this organization directly at http://www.iacmhr.com/iac-eso/support.php?lang=en. IAC-ESO was established to facilitate manuscript preparation by researchers whose native language is not English and to help edit works intended for international academic journals.

4. Manuscript Preparation

Manuscripts should be written in clear, grammatically correct English and submitted as a Microsoft Word file in a single-column format. Manuscripts must be paginated and typed in 12-point Times New Roman font with 24-point line spacing. Please do not embed figures in the text. Abbreviations should be used as little as possible and should be explained at first mention unless the term is a well-known abbreviation (*e.g.* DNA). Single words should not be abbreviated.

Title Page: The title page must include 1) the title of the paper (Please note the title should be short, informative, and contain the major key words); 2) full name(s) and affiliation(s) of the author(s), 3) abbreviated names of the author(s), 4) full name, mailing address, telephone/fax numbers, and e-mail address of the corresponding author; and 5) conflicts of interest (if you have an actual or potential conflict of interest to disclose, it must be included as a footnote on the title page of the manuscript; if no conflict of

interest exists for each author, please state "There is no conflict of interest to disclose"). Please visit Download Centre and refer to the title page of the manuscript sample.

Abstract: The abstract should briefly state the purpose of the study, methods, main findings, and conclusions. For article types including Original Article, Brief Report, Review, Policy Forum, and Case Report, a one-paragraph abstract consisting of no more than 250 words must be included in the manuscript. For News and Letters, a brief summary of main content in 150 words or fewer should be included in the manuscript. Abbreviations must be kept to a minimum and non-standard abbreviations explained in brackets at first mention. References should be avoided in the abstract. Key words or phrases that do not occur in the title should be included in the Abstract page.

Introduction: The introduction should be a concise statement of the basis for the study and its scientific context.

Materials and Methods: The description should be brief but with sufficient detail to enable others to reproduce the experiments. Procedures that have been published previously should not be described in detail but appropriate references should simply be cited. Only new and significant modifications of previously published procedures require complete description. Names of products and manufacturers with their locations (city and state/country) should be given and sources of animals and cell lines should always be indicated. All clinical investigations must have been conducted in accordance with Declaration of Helsinki principles. All human and animal studies must have been approved by the appropriate institutional review board(s) and a specific declaration of approval must be made within this section.

Results: The description of the experimental results should be succinct but in sufficient detail to allow the experiments to be analyzed and interpreted by an independent reader. If necessary, subheadings may be used for an orderly presentation. All figures and tables must be referred to in the text.

Discussion: The data should be interpreted concisely without repeating material already presented in the Results section. Speculation is permissible, but it must be well-founded, and discussion of the wider implications of the findings is encouraged. Conclusions derived from the study should be included in this section.

Acknowledgments: All funding sources should be credited in the Acknowledgments section. In addition, people who contributed to the work but who do not meet the criteria for authors should be listed along with their contributions.

References: References should be numbered in the order in which they appear in the text. Citing of unpublished results, personal communications, conference abstracts, and theses in the reference list is not recommended but these sources may be mentioned in the text. In the reference list, cite the names of all authors when there are fifteen or fewer authors; if there are sixteen or more authors, list the first three followed by *et al.* Names of journals should be abbreviated in the style used in PubMed. Authors are responsible for the accuracy of the references. Examples are given below:

Example 1 (Sample journal reference):
Inagaki Y, Tang W, Zhang L, Du GH, Xu WF, Kokudo N. Novel aminopeptidase N (APN/CD13) inhibitor 24F can suppress invasion of hepatocellular carcinoma cells as well as angiogenesis. Biosci Trends. 2010; 4:56-60.

Example 2 (Sample journal reference with more than 15 authors):
Darby S, Hill D, Auvinen A, *et al.* Radon in homes and risk of lung cancer: Collaborative analysis of individual data from 13 European case-control studies. BMJ. 2005; 330:223.

Example 3 (Sample book reference):
Shalev AY. Post-traumatic stress disorder: diagnosis, history and life course. In: Post-traumatic Stress Disorder, Diagnosis, Management and Treatment (Nutt DJ, Davidson JR, Zohar J, eds.). Martin Dunitz, London, UK, 2000; pp. 1-15.

Example 4 (Sample web page reference):
Ministry of Health, Labour and Welfare of Japan. Dietary reference intakes for Japanese. *http://www.mhlw.go.jp/houdou/2004/11/h1122-2a.html* (accessed June 14, 2010).

Tables: All tables should be prepared in Microsoft Word or Excel and should be arranged at the end of the manuscript after the References section. Please note that tables should not in image format. All tables should have a concise title and should be numbered consecutively with Arabic numerals. If necessary, additional information should be given below the table.

Figure Legend: The figure legend should be typed on a separate page of the main manuscript and should include a short title and explanation. The legend should be concise but comprehensive and should be understood without referring to the text. Symbols used in figures must be explained.

Figure Preparation: All figures should be clear and cited in numerical order in the text. Figures must fit a one- or two-column format on the journal page: 8.3 cm (3.3 in.) wide for a single column, 17.3 cm (6.8 in.) wide for a double column; maximum height: 24.0 cm (9.5 in.). Please make sure that the symbols and numbers appeared in the figures should be clear. Please make sure that artwork files are in an acceptable format (TIFF or JPEG) at minimum resolution (600 dpi for illustrations, graphs, and annotated artwork, and 300 dpi for micrographs and photographs). Please provide all figures as separate files. Please note that low-resolution images are one of the leading causes of article resubmission and schedule delays. All color figures will be reproduced in full color in the online edition of the journal at no cost to authors.

Units and Symbols: Units and symbols conforming to the International System of Units (SI) should be used for physicochemical quantities. Solidus notation (*e.g.* mg/kg, mg/mL, $mol/mm^2/min$) should be used. Please refer to the SI Guide www.bipm.org/en/si/ for standard units.

Supplemental data: Supplemental data might be useful for supporting and enhancing your scientific research and BioScience Trends accepts the submission of these materials which will be only published online alongside the electronic version of your article. Supplemental files (figures, tables, and other text materials) should be prepared according to the above guidelines, numbered in Arabic numerals (*e.g.*, Figure S1, Figure S2, and Table S1, Table S2) and referred in the text. All figures and tables should have titles and legends. All figure legends, tables and supplemental text materials should be placed at the end of the paper. Please note all of these supplemental data should be provided at the time of initial submission and note that the editors reserve the right to limit the size and length of Supplemental Data.

5. Submission Checklist

The Submission Checklist will be useful during the final checking of a manuscript prior to sending it to BioScience Trends for review. Please visit Download Centre and download the Submission Checklist file.

6. Online Submission

Manuscripts should be submitted to BioScience Trends online at http://www.biosciencetrends.com. The manuscript file should be smaller than 5 MB in size. If for any reason you are unable to submit a file online, please contact the Editorial Office by e-mail at office@biosciencetrends.com.

7. Accepted Manuscripts

Proofs: Galley proofs in PDF format will be sent to the corresponding author via e-mail. Corrections must be returned to the editor (proof-editing@biosciencetrends.com) within 3 working days.

Offprints: Authors will be provided with electronic offprints of their article. Paper offprints can be ordered at prices quoted on the order form that accompanies the proofs.

Page Charge: Page charges will be levied on all manuscripts accepted for publication in BioScience Trends ($140 per page for black white pages; $340 per page for color pages). Under exceptional circumstances, the author(s) may apply to the editorial office for a waiver of the publication charges at the time of submission.

(*Revised February 2013*)

JOURNAL PUBLISHING AGREEMENT (JPA)

Manuscript No.:

Title:

Corresponding Author:

The International Advancement Center for Medicine & Health Research Co., Ltd. (IACMHR Co., Ltd.) is pleased to accept the above article for publication in BioScience Trends. The International Research and Cooperation Association for Bio & Socio-Sciences Advancement (IRCA-BSSA) reserves all rights to the published article. Your written acceptance of this JOURNAL PUBLISHING AGREEMENT is required before the article can be published. Please read this form carefully and sign it if you agree to its terms. The signed JOURNAL PUBLISHING AGREEMENT should be sent to the BioScience Trends office (Pearl City Koishikawa 603, 2-4-5 Kasuga, Bunkyo-ku, Tokyo 112-0003, Japan; E-mail: **office@biosciencetrends.com**; Tel: **+81-3-5840-8764**; Fax: **+81-3-5840-8765**).

1. Authorship Criteria

As the corresponding author, I certify on behalf of all of the authors that:
1) The article is an original work and does not involve fraud, fabrication, or plagiarism.
2) The article has not been published previously and is not currently under consideration for publication elsewhere. If accepted by BioScience Trends, the article will not be submitted for publication to any other journal.
3) The article contains no libelous or other unlawful statements and does not contain any materials that infringes upon individual privacy or proprietary rights or any statutory copyright.
4) I have obtained written permission from copyright owners for any excerpts from copyrighted works that are included and have credited the sources in my article.
5) All authors have made significant contributions to the study including the conception and design of this work, the analysis of the data, and the writing of the manuscript.
6) All authors have reviewed this manuscript and take responsibility for its content and approve its publication.
7) I have informed all of the authors of the terms of this publishing agreement and I am signing on their behalf as their agent.

2. Copyright Transfer Agreement

I hereby assign and transfer to IACMHR Co., Ltd. all exclusive rights of copyright ownership to the above work in the journal BioScience Trends, including but not limited to the right 1) to publish, republish, derivate, distribute, transmit, sell, and otherwise use the work and other related material worldwide, in whole or in part, in all languages, in electronic, printed, or any other forms of media now known or hereafter developed and the right 2) to authorize or license third parties to do any of the above.

I understand that these exclusive rights will become the property of IACMHR Co., Ltd., from the date the article is accepted for publication in the journal BioScience Trends. I also understand that IACMHR Co., Ltd. as a copyright owner has sole authority to license and permit reproductions of the article.

I understand that except for copyright, other proprietary rights related to the Work (*e.g.* patent or other rights to any process or procedure) shall be retained by the authors. To reproduce any text, figures, tables, or illustrations from this Work in future works of their own, the authors must obtain written permission from IACMHR Co., Ltd.; such permission cannot be unreasonably withheld by IACMHR Co., Ltd.

3. Conflict of Interest Disclosure

I confirm that all funding sources supporting the work and all institutions or people who contributed to the work but who do not meet the criteria for authors are acknowledged. I also confirm that all commercial affiliations, stock ownership, equity interests, or patent-licensing arrangements that could be considered to pose a financial conflict of interest in connection with the article have been disclosed.

Corresponding Author's Name (Signature):

Date:

BioScience Trends (www.biosciencetrends.com)

Pearl City Koishikawa 603, 2-4-5 Kasuga, Bunkyo-ku, Tokyo 112-0003, Japan; E-mail: office@biosciencetrends; Tel: +81-3-5840-8764; Fax: +81-3-5840-8765